POLITECNICO DI TORINO

Department of Environment, Land

and Infrastructure Engineering

Performance of plant-produced sustainable bituminous mixtures containing RAP and recycled waste plastics

Master's Degree in Civil Engineering

Supervisors:

Prof. Orazio Baglieri

Prof. Davide Dalmazzo

Dott. Ing. Joseph Nicolas La Macchia

Candidate:

Luca Cosimo Perrone

Academic Year 2025-2026

Ai miei angeli custodi,

Preziosa, Cesare e Cosimo,

che questo traguardo

vi possa far sorridere

ovunque voi siate…

Abstract

In recent decades, environmental sustainability and circular economy principles have become central elements of contemporary society, significantly influencing the infrastructure sector.

Within this framework, several standards and regulations have been developed worldwide to encourage the use of alternative and reclaimed materials in the asphalt industry. In Italy, the Ministerial Decree 05/08/2024 introduced the "Minimum Environmental Criteria" (Criteri Ambientali Minimi, C.A.M.) to guide the road sector towards more sustainable practices by mandating minimum percentages of recovered, recycled, or by-product materials in new asphalt mixtures.

In this perspective, the growing use of reclaimed materials in the production of bituminous mixtures for road pavements is gaining relevance: among these, RAP (Reclaimed Asphalt Pavement) and recycled plastics play a leading role.

The present thesis aims to investigate the mechanical properties of plant-produced sustainable mixtures containing 50% RAP and different dosages of a polymeric compound derived from hard recycled waste plastics, added through the hybrid modification method. Four mixtures in total were examined: three hybrid-modified mixtures differing in polymeric compound content (0.3%, 0.5%, and 0.7% by total mixture weight), and a wet-modified reference mixture containing a polymer-modified binder (PmB).

The experimental activity involved the analysis of volumetric and performance-related indicators - such as air voids at different numbers of gyrations, workability, voids in mineral aggregate, and voids filled with binder - followed by a mechanical characterisation including indirect tensile stiffness, strength, and fatigue tests on cylindrical specimens having diameter of 150 mm and compacted at 120 gyrations.

Moreover, fatigue performance was corroborated through four-point bending tests on prismatic specimens at 10 Hz and 20°C in accordance with the requirements of BS EN 12697-24. For each testing condition, a minimum of eight replicates were tested to ensure data repeatability.

The results were compared with those obtained from previous laboratory-scale investigations involving the same materials.

Although some production issues resulted in a reduced bio-based rejuvenator dosage compared to the design composition, meaningful conclusions were derived. Plant-produced mixtures were characterised by lower workability and reduced fatigue resistance compared to the laboratory-scale outcomes, due to the decreased rejuvenator content.

Overall, hybrid-modified mixtures resulted in higher stiffness, strength, and fatigue performance compared to the wet-modified reference mixture. However, higher polymeric compound contents do not necessarily imply higher performance.

The experimental results confirmed the validity of the hybrid modification method to combine satisfactory mechanical performance and several environmental benefits.

Nevertheless, further investigation with higher rejuvenator dosages is advisable to broaden and consolidate the current body of knowledge.

Summary

List of Tables

List of Figures

1. Sustainable bituminous mixtures

1.1. Introduction

In a global context marked by a growing focus on environmental issues, the design and construction of road infrastructures must be based on innovative solutions capable of combining appropriate techniques with environmental and economic sustainability.

Within this framework, bituminous conglomerate plays a particularly important role, as it represents a significant field of research and experimentation and is one of the most widely used materials in the sector.

The use of Reclaimed Asphalt Pavement (RAP), that is, constituted by the milled asphalt recovered during existing pavements maintenance and the incorporation of recycled rigid plastics, known as Plastic Waste Materials (PWM), within bituminous mixtures reduce the consumption of virgin aggregates and bituminous binder.

Moreover, this is accompanied by a decrease in the emissions associated with their extraction processes and by the valorisation of materials that would otherwise be destined for disposal, thus contributing to the reduction of the overall environmental impact of the sector.

However, it becomes essential to recognise that a massive use of reclaimed materials also introduces specific challenges linked to the aging condition of the bituminous binder. As bitumen ages, it undergoes oxidative reactions that progressively modify its chemical structure and rheological behaviour. These transformations lead to increased stiffness, reduced elasticity, and, more generally, a deterioration of its mechanical performance.

To mitigate these effects, several products specifically engineered and classified as rejuvenators are employed to partially restore the properties of aged binders.

In conclusion, the adoption of such solutions, supported by experimental evidence and by a regulatory framework that is progressively evolving, aims to demonstrate how sustainability can become a cornerstone in the design of road infrastructures. Alongside this, there is the opportunity to develop innovative materials and more efficient roads, promoting construction models that are increasingly responsible and aware.

1.2. RAP material

1.2.1. Definition and use worldwide

As stated in the introduction, RAP is mainly composed of bituminous mixtures removed from existing infrastructures and, to a lesser extent, from mixtures discarded or rejected during production processes. Since it consists of valuable non-renewable resources—namely about 95% by weight of aggregates and 5% by weight of aged bituminous binder—it can be reused in new mixtures, reducing the demand for virgin aggregates and bitumen.

The percentage of RAP reused has gradually increased in many countries around the world. Currently, a considerable amount of this recycled material is employed in the production of Hot Mix Asphalt (HMA) and Warm Mix Asphalt (WMA), which represent the ideal use of aggregates derived from RAP [1].

The first virtuous example of RAP use in bituminous mixture formulations, up to 40% of the total mixture weight, was introduced in South Africa as early as 2009. About a decade later, in-plant recycling with the same RAP percentages became established as a widespread industrial practice [2].

Continuing along the timeline, already in 2013, the Japanese road sector had developed an efficient RAP recycling system, managing to reuse 99% by weight of the total amount produced. This result was favoured by the relatively small size of the country, the limited availability of natural resources, and the restricted space available for waste disposal [3].

Moving overseas, the latest annual survey by the National Asphalt Pavement Association (NAPA) reported that, in 2018, the U.S. asphalt industry reused over 99% by weight of the available RAP, confirming it as the most recycled material in the United States [4].

In the Old Continent, the European Asphalt Pavement Association (EAPA) monitors all European activities related to asphalt, including the reuse and/or recycling of RAP. Below, in Table 1, the values obtained by considering the estimated data from the U.S. survey on RAP use in 2018, as well as the European average results of the collected data, are reported.

Considered Quantities	USA	EUROPE
Total production of HMA and WMA	389.3×10^6 Tons	297.9×10^6 Tons
Total RAP accepted in facilities of plants	101.1×10^6 Tons	49.5×10^6 Tons
RAP used in HMA/WMA mixtures	81.3%	51.4%
RAP used in CMA mixtures	0.297%	3.81%
RAP used as aggregates for unbound layers	6.33%	17.0%
RAP used for other purposes	1.98%	2.00%
RAP landfilled	≈0.00%	9.63%

Table 1. Comparison of the uses of Reclaimed Asphalt Pavement (RAP) in the USA and Europe: data from (NAPA, 2019) and (EAPA, 2018)

Overall, Europe disposes of a very large amount of RAP compared to the United States. Therefore, the percentages reported in Table 1 highlight that European countries could make greater use of the potential of recycled aggregates.

1.2.2. Production techniques

Hot Mix Asphalt (HMA) mixtures can be produced using two main types of plants: batch plants (also referred to as discontinuous plants) and continuous plants (drum plants).

Both allow the production of the same mixture with the same characteristics, with the only difference lying in the production process: batch plants enable the dosing and therefore the feeding of the mixing drum with each component separately, thus producing a specific quantity of the required mixture. Continuous plants, instead, do not involve operational interruptions, as the name itself suggests, since the components are added in such a way as to ensure a continuous flow of the final bituminous conglomerate [5].

Figure 1 schematically illustrates the typical operating procedures of both plant types.

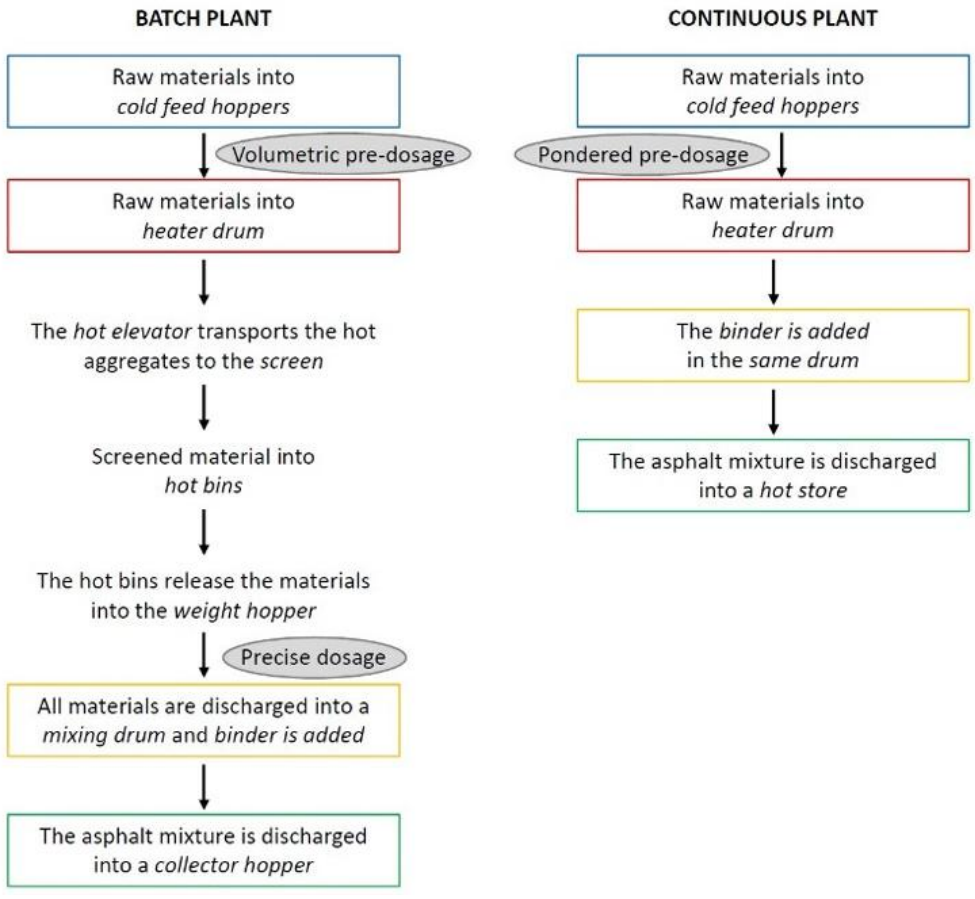

Figure 1. Typical operating procedures of batch plants (left) and continuous plants (right) (source: "The Challenges of Using Reclaimed Asphalt Pavement for New Asphalt Mixtures: A Review" Tarsi [1])

The batch plant offers greater flexibility in mixture design, as it allows the introduction of different types and sizes of aggregates into the cold feeding bins. Moreover, during production, the aggregates are screened a second time and weighed after being heated and dried, ensuring that their moisture content does not affect the weight of the material. Consequently, in a batch plant the constituent materials undergo a higher number of screening and control operations.

The continuous plant, on the other hand, provides higher productivity and, being a simpler system compared to the batch plant, allows a reduction in maintenance costs. However, it presents the disadvantage of having to weigh the aggregates before the heating and drying phases; therefore, knowledge of the material's moisture content becomes a key factor in ensuring proper production. In general, the consistency of the characteristics of the incoming materials to a plant represents a fundamental requirement for maintaining bituminous mixture production with the minimum number of variations and delays.

With regard to RAP, from a plant-engineering perspective, it cannot be incorporated in the same way as virgin aggregates: in fact, since it contains on average 5% by weight of aged bituminous binder generally coating the surface of the aggregates, it cannot be heated by the burner's direct flame, as its combustion would generate an excessive amount of blue smoke. Therefore, it can only be heated through conduction or by contact with hot virgin aggregates. Furthermore, another aspect to be considered concerns an increase in mixing times, since RAP is characterised by a moisture content of 7–8%, which contributes to lowering the temperature [6].

Therefore, to incorporate RAP into the previously described production processes, it is possible to follow one of the following three methods:

1. Addition of cold RAP at a specific stage of the production process.
2. Pre-heating of RAP in a separate dryer.
3. Use of a combined dryer to heat RAP and virgin materials simultaneously.

The first two methods can be applied to batch plants, while the third is mainly used in continuous plants [7].

As mentioned, the first method of RAP incorporation involves introducing the recycled aggregates at ambient temperature; subsequently, they will be dried by encountering the overheated virgin aggregates, which will transfer heat to them. In this case, RAP aggregates can be introduced at three different stages of bituminous mixture production: at the base of the hot elevators, in the weighing hopper, or in the mixer.

If this occurs at the base of the hot elevator, the suction system of the mixing tower removes the steam generated, reducing process emissions. If the aggregates contained in the RAP need to be further screened, this procedure would limit the

maximum RAP content to relatively low percentages (10–15%) to prevent the heated aggregates from clogging the screens due to the softening of the aged binder.

Conversely, directing the overheated virgin aggregates and the cold RAP directly into the hot bins, without passing through the screens, allows the RAP content to be increased up to 40% by weight [8].

The second method requires a separate dryer to pre-heat the RAP to a temperature lower than that of the virgin aggregates, allowing the introduction of more than 70% RAP by weight of the total mixture. This incorporation method requires an upgrade of the plant, since the milled material must be conveyed into a dedicated heated storage bin equipped with its own weighing hopper. Consequently, the disadvantages of this method include the high initial investment.

Finally, the production of bituminous mixtures containing RAP in a continuous plant allows the introduction of higher percentages of recycled aggregates compared to batch plants, since the RAP is pre-heated. However, it is not possible to exceed a RAP content of 50% by weight of the total mixture, as the plant may generate higher emissions due to the contact between the recycled aggregates and the burner flame [1].

1.2.3. Disadvantages of RAP use and performance limitations

Despite the advantages discussed so far regarding the use of recycled aggregates and the feasibility of producing bituminous mixtures containing high percentages of RAP (generally above 40% by weight and, in some cases, even up to 100% by weight), in Hot Mix Asphalt (HMA) mixtures its content is usually limited to around 15–30% by weight.

The reasons for such caution can be attributed to the quality of the recycled aggregates, the technology of the production plant (discussed in the previous paragraph), the mix-design methodology, and the performance of the final mixture.

Each of these aspects significantly affects the possibility of increasing the percentage of recycled material without compromising durability, workability, and compliance with technical specifications. Therefore, the following paragraphs provide concise, yet detailed analyses of the aspects mentioned above.

1. Quality of recycled aggregates. The first aspect to analyse concerns the quality and homogeneity of the recycled aggregates and of the stockpiles. In fact, the removed bituminous conglomerate often presents a high content of fine particles, because of milling and crushing operations. This fraction may limit the maximum RAP content, since it can compromise the gradation curve of the final mixture, and it also contains a higher amount of aged binder due to its greater specific surface [8].

The quality of the milled material depends on operational factors, such as the machine used for milling, the operating speed, and the milling depth; the latter is particularly relevant, as the material taken from the same layer presents more homogeneous properties (aggregate type, gradation curve, binder characteristics and content) [9].

To increase the consistency of the material, it is therefore advisable to keep the millings from individual maintenance operations in separate stockpiles, preventing contamination with different layers.

However, in industrial practice, separate storage is often impractical due to the limited space available at production plants and the small quantities coming from individual construction sites. For these reasons, screening, crushing, and fractioning operations are recommended. Thus, accurate RAP management, combined with adequate control and characterization procedures, is essential to ensure performance and reliability of mixtures containing recycled material [10].

2. Mix-Design methodology. Although bituminous mixtures incorporating RAP must meet the same performance criteria as mixtures containing only virgin aggregates, the traditional mix-design methodology requires modification to account for the characteristics of this material in terms of aggregate gradation and properties and content of the aged binder [11].

   The binder contained in RAP governs the rheological properties and the overall composition of the final blended binder, which includes both aged and virgin components, and consequently influences the characteristics of the bituminous mixture. Most road agencies and national specifications assume complete blending between aged and virgin binder; however, this is in contrast with what has been demonstrated experimentally.

   Thus, this aspect represents one of the main limitations in designing mixtures with high RAP contents. Increasing the percentage of RAP may also require the use of softening and/or rejuvenating agents to restore the properties of the aged binder. The introduction of such agents represents an additional variable in the mix design, requiring the selection of compatible products and the definition of an appropriate dosage [12].

3. Performance of the final mixture. Increasing the RAP content in bituminous mixtures tends to raise the stiffness of the final conglomerate, and this is mainly linked to the properties of the aged binder. A higher modulus may reduce resistance to fatigue cracking, thermal shocks, and crack propagation. However, when properly assessed, the presence of aged binder can improve resistance to moisture damage and reduce susceptibility to permanent deformation [13].

Therefore, in the mix design of mixtures with high RAP contents, the use of softer binders and rejuvenating agents must be balanced to mitigate the increase in stiffness without excessively softening the resulting binder, in order to limit rutting phenomena. Moreover, the use of incompatible agents or excessive doses of additives may lead to flushing phenomena, such as the migration of binder towards the surface of the bituminous layer.

1.2.4. Economic and environmental aspects

When addressing environmental issues, the use of recycled materials in bituminous pavements preserves non-renewable resources, reducing aggregate extraction and the use of virgin bitumen, while also decreasing the amount of material destined for landfill.

The consumption of land required to dispose of milled material is indeed an aspect to consider: in 2018, in the United States, only a very small percentage of RAP was landfilled, allowing an estimated saving of about 46.7 million cubic metres of landfill space in a single year [14].

However, to fully assess the environmental benefits deriving from the incorporation of recycled materials into bituminous mixtures, it is necessary to consider and quantify atmospheric emissions and energy consumption throughout the entire life cycle of road infrastructures.

Independently of RAP use, the production of bituminous mixtures mainly releases carbon dioxide (CO_2), methane (CH_4), and nitrous oxide (N_2O), originating from the extraction of raw materials, transport, production, laying, and compaction of the mixtures themselves. Generally, greenhouse gas emissions are expressed as CO_2-equivalent emissions, since the greater the energy required for a product, the greater the fuel consumed and the carbon dioxide emitted [15].

The use of RAP for the production of bituminous mixtures would allow a reduction of 18 kg of CO_2 and an energy saving of about 20% per tonne of laid mixture, according to a study by Zaumanis et al., [11].

Vidal et al. analysed the Life Cycle Assessment (LCA) of pavements from the construction phase to their end of life. They highlighted that the stages with the greatest environmental impact are the extraction of raw materials and the production of the final mixture. In quantitative terms, the use of 15% RAP results in a reduction of the impact on climate change of about 13% and a decrease in the impact on fossil resource depletion of about 14% [16].

Setting aside environmental benefits, the use of RAP also offers significant advantages from an economic perspective. A detailed analysis conducted by NAPA shows that the United States saved 2.8 billion dollars in 2018 thanks to the replacement of virgin aggregates with recycled materials. In fact, 4.1 million tonnes of virgin binder and 78 million tonnes of virgin aggregates were saved.

These savings must be evaluated while considering the additional costs associated with RAP processing, testing, and the use of rejuvenating agents. In this context, the study by Zaumanis et al. [11] estimated the cost per tonne of bituminous mixtures containing RAP by varying its percentage.

As shown in Figure 2, the analysis examines a mixture with a total binder content of 5.7% (of which 5.1% is aged binder from RAP and 0.6% is rejuvenating agent) and different RAP contents: it emerged that the cost per tonne of a mixture composed entirely of RAP may be 50–70% lower than that of a mixture containing only virgin materials [11].

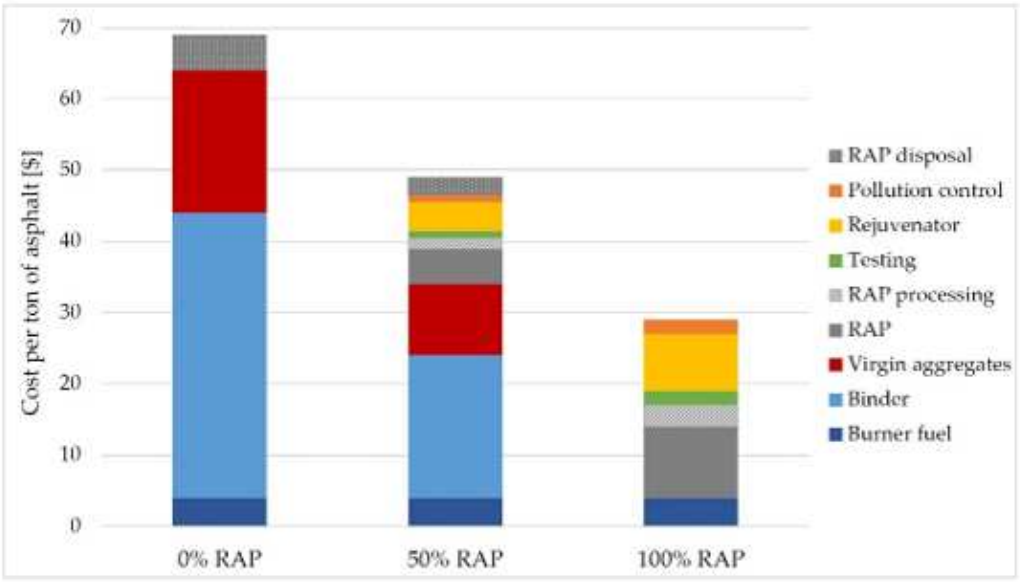

Figure 2. Costs of recycled Hot Mix Asphalt mixtures as a function of RAP content (source: Zaumanis et al., 2014)

1.3. Recycled plastics

1.3.1. The global plastic crisis

Plastic has been one of the greatest industrial revolutions of all time; its light weight, durability, workability and low production cost have driven its widespread adoption across all manufacturing sectors, from packaging to construction.

However, the same factors that contributed to its success are now at the core of one of the most pressing environmental challenges. Global plastic production continues to rise, and with it the amount of waste generated each year.

On a global scale, one of the main players in the sector is China. In 2017, the country introduced the policy known as National Sword, marking a shift in national priorities and increasing attention toward environmental protection. With the implementation of this policy, China closed its borders to the import of plastic waste from abroad—approximately 45% of the world's plastic waste, amounting to around 111 million tonnes per year. However, the actual outcome did not match the intended one, as much of this waste was dispersed into the environment rather than being properly managed in suitable landfills [17].

Currently, it is estimated that only 9% of global plastic is recycled each year, while more than 80% ends up in landfills or in the natural environment. Between 4 and 12 million tonnes of plastic waste reach the oceans annually [18], [19].

This trend is also reflected in the United States. In 2018, according to the Environmental Protection Agency (EPA), plastic accounted for 35.4 million tonnes of waste, compared to 31.4 million tonnes in 2010, highlighting the increasing consumption of this material. Of these 35.4 million tonnes, only 8.4% was recycled, while 5.6 million tonnes were incinerated and 26.8 million tonnes were sent to landfill.

Figure 3. Production and management of plastic waste in the United States from 1960 to 2017 (EPA, 2020)

Considering the critical situation just outlined, it becomes necessary to reflect on what future developments might look like. The analysis presented in the *Global Plastics Outlook: Policy Scenarios to 2060*, published by the OECD in June 2022, holds relevance in this context. This report is based on simulations carried out using the OECD's dynamic general equilibrium model, ENV-Linkages, which has been expanded to include 14 categories of polymers and both primary and secondary (recycled) plastic production.

Model projections suggest that, under current policies, global plastic use will almost triple, rising from 460 million tonnes in 2019 to 1,231 million tonnes in 2060. The main driver behind this increase is economic growth, along with the associated rise in global population.

Virgin plastics are projected to remain dominant in the coming decades, reaching about 88% of total use in 2060, while recycled plastics, despite growing more rapidly, are expected to account for only 12% of overall consumption. At the same time, plastic waste is anticipated to almost triple, rising from 353 million tonnes in 2019 to 1,014 million tonnes in 2060, with short-lived products such as packaging, consumer goods, and textiles continuing to generate roughly two thirds of all waste.

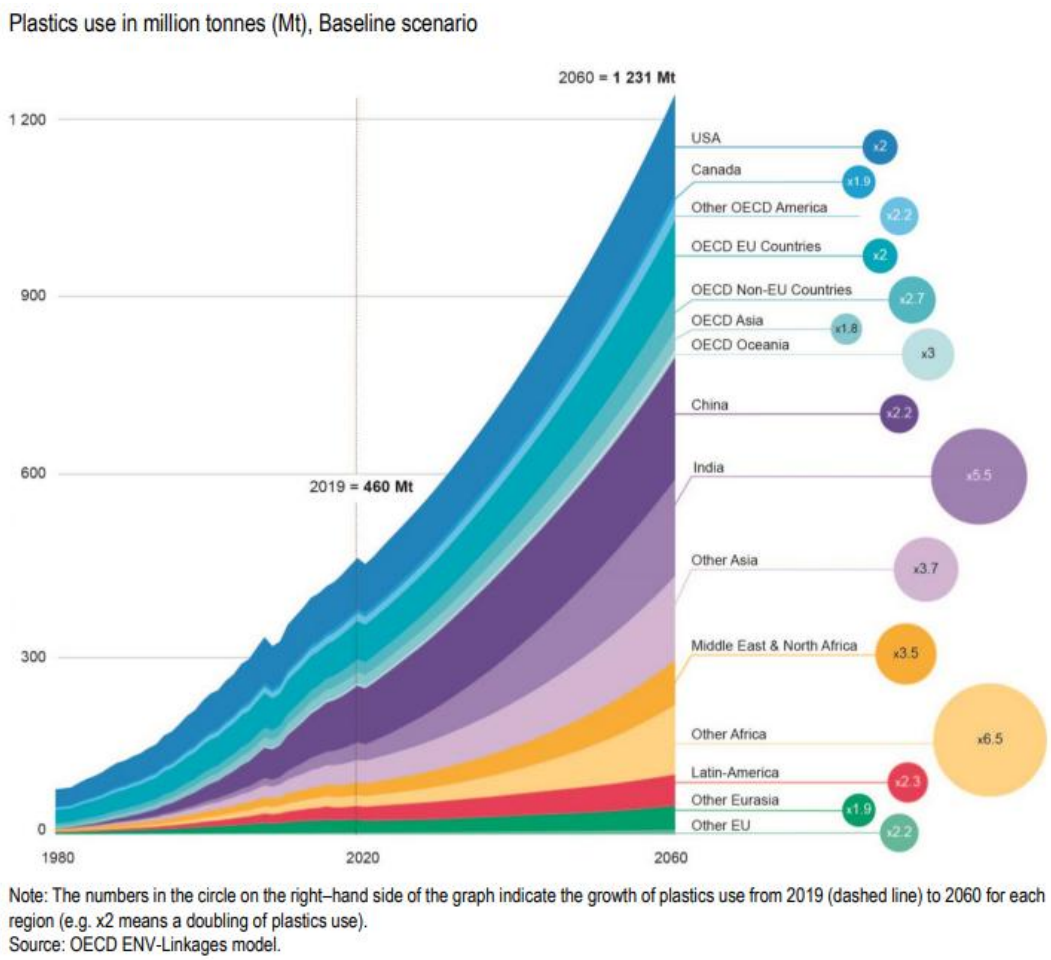

Figure 4. Projection of global plastic use in 2060 (OECD, 2022)

Plastic waste generated by the construction and transport sectors will also remain significant, particularly considering the rapid economic development occurring in many emerging and developing economies. A substantial share of global plastic waste will be produced in non-OECD countries (65%), especially in emerging economies in Asia and Africa, where plastic waste is projected to grow at the fastest rates.

Recycling is expected to surpass all other waste-management methods, with recycling rates increasing from 9% in 2019 to 17% in 2060. However, even with this improvement, recycling will still represent a smaller share compared to incineration (18%) and controlled landfill disposal (50%).

Among the environmental consequences, greenhouse-gas emissions associated with the plastic life cycle are expected to more than double, increasing from 1.8 gigatonnes of carbon-dioxide equivalent to 4.3 gigatonnes. A range of other life-cycle impacts—such as ozone formation, acidification, and human toxicity—are also projected to more than double.

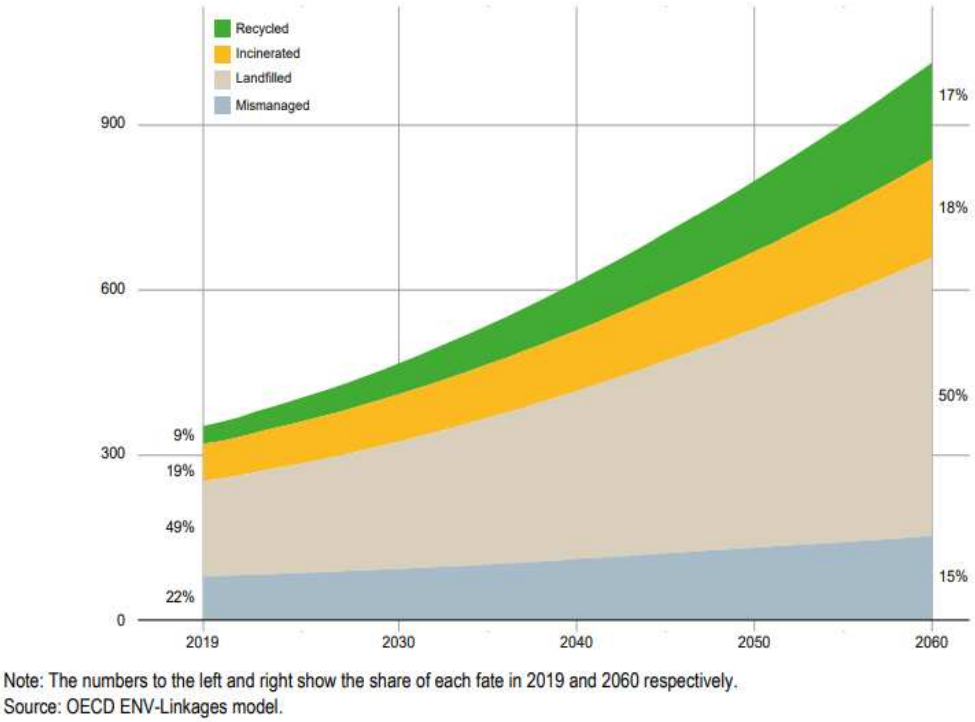

Figure 5. Projection of global plastic waste management (OECD, 2022)

1.3.2. The different types of plastics and their recycling

Considering the data presented so far, the importance of proper waste management and recycling becomes evident. It is essential to understand that this is a rather complex process; in fact, seven different types of plastics are currently identified, each with very distinct chemical compositions, and classified through resin identification codes. For clarity, these categories are listed in Table 2 [20].

Number	Types of Plastics	Application/Uses	Melting Point (°C)	Melting Point (°F)
1	Polyethylene Terephalate (PET)	Bottles for water and soda; Food packaging; Food containers	>250	>482
2	High Density Polyethylene (HDPE)	Plastic mailing envelopes; Flexible pipes; Plastic chairs/stools; Toys and playground equipment; Plastic bags; Shampoo bottles	130 but can vary in grade	266 but can vary in grade
3	Polyvinyl Chloride (PVC)	Pipes; Electric cables; Construction material; Sign boards; Vinyl flooring	100-260	212-500
4	Low Density Polyethylene (LDPE)	Trays and containers; Plastic wraps; Plastic bags; Juice and milk containers	110-120	230-248
5	Polypropylene (PP)	Plastic hinges; Piping system; Plastic Chairs; Reusable plastic containers; Plastic moldings	160-165	320-330
6	Polystyrene (PS)	Food packaging; CD and DVD casing; Disposable utensils; License plate frames; Foam beverage cups	Glass Transition at 100	Glass Transition at 212
7	Other (Polycarbonate – PC; Polylactide – PLCA; Acrylonitrile Butadiene Styrene – ABS; Nylon; Fiberglass; Acrylic)	Baby bottles; Car parts; Water cooler bottles; Food containers	Based on grade and plastic type	

Table 2. Different types of plastics (NAPA – IS 142, 2020)

Among the various strategies for recovering plastic waste, its use in road infrastructure represents a particularly interesting solution, given the vast extent of the road network and the constant need for maintenance.

In this application, the melting point is a crucial characteristic: if recycled plastics are intended to modify the bituminous binder, they must melt and become part of the binder itself. However, most asphalt mixtures are produced at temperatures below 170 °C. Some plastics may not melt even under the typical operating conditions of an asphalt-mixing plant, preventing their blending with the binder or their coating of the aggregates.

Another extremely important aspect to consider is the potential impact these plastics may have on human health. For example, when polyvinyl chloride (PVC) is heated, it can generate polychlorinated dibenzo-p-dioxins (PCDDs) and dibenzofurans (PCDFs) in the exhaust gases of asphalt-mixing plants. These dioxins are harmful to human health, thus the use of PVC in bituminous mixtures should be avoided for safety reasons.

Therefore, it should be emphasised that not all types of plastic waste are suitable for being incorporated into asphalt mixtures.

1.3.3. Methods for incorporating plastics into bituminous mixtures

To better understand the different methodologies used to incorporate plastic waste into bituminous mixtures, it is important to consider the main properties of polymeric materials, such as melting point (discussed in the previous section), fume emissions, particle size and shape, density, and Melt Flow Index (MFI) [21].

Regarding the size and shape of plastic particles, these characteristics influence their dispersion within the mixture and, consequently, the homogeneity of the final product. Typically, plastics are used in the form of pellets, flakes, shreds, or powders.

Parameters such as density and Melt Flow Index (MFI) are crucial to ensure good dispersion, compatibility, and workability of the material. In fact, the density of the polymer should not differ excessively from that of bitumen, to avoid segregation phenomena and to ensure proper interaction between the two phases.

High MFI values indicate low plastic viscosity, which can help improve the mixture's resistance to permanent deformation, while at the same time reducing workability. It is therefore essential to identify plastics with suitable MFI values, capable of ensuring a balance between crack resistance and good dispersion within the binder [22], [23].

Depending on their melting point, plastics can be incorporated into road pavements through three different methods: wet, dry, or hybrid [24].

1. Wet method. In this process, recycled plastics are added directly to the bituminous binder, where they act as polymer modifiers or, in some cases, as partial substitutes for bitumen. To obtain a plastic-modified binder

(PMB), adequate mechanical mixing is required, typically performed using a shear mixer. This method is particularly suitable for plastics with a low melting point, such as LLDPE, LDPE, and HDPE, which can melt at typical bitumen processing temperatures, generally between 150 and 160 °C.

Typically, the amount of recycled plastic used in this method ranges from 2% to 8% by weight of the bituminous binder [25].

However, this method presents several significant challenges, mainly related to the poor compatibility between the polymer and the bituminous binder. This often requires the use of chemical stabilizing additives to limit polymer migration within the binder. Moreover, the difference in density between the materials compromises storage stability, promoting phase separation and reducing binder homogeneity in the absence of continuous agitation [26].

All these factors make the incorporation of plastics through the wet method a highly complex and costly operation.

2. Dry process. It introduces recycled plastics directly into the bituminous mixture, where they can assume different roles and, importantly, act as a partial substitute for the lithic fraction. Plastics with a high melting point—above the typical production temperatures of bituminous mixtures, usually around 200 °C—are particularly suitable for replacing part of the aggregate skeleton, as they maintain adequate thermal stability and integrate effectively into the mixture's structure.

   Plastics can also function as mixture modifiers, a role applicable to most polymers such as PE, PP, PET, and PS, with the exception of PVC, as previously noted in Section 1.3.2. In this method, the dosage of recycled plastic generally ranges between 0.2% and 1% by weight of the aggregates [25].

3. Hybrid method. It represents an intermediate approach between the dry and wet processes, and its distinctiveness lies in the behaviour of low-melting-point plastics when they encounter the hot bituminous binder. In this technique, recycled plastics are added directly into the mixture, as in the dry process, but their lower melting temperature causes them to partially soften or melt during mixing. This partial melting allows the polymers to disperse within the binder phase while still retaining a fraction of their solid structure, creating a dual contribution: they behave both as modifiers of the bituminous matrix and as partial substitutes for the lithic fraction. This dual role enhances the mixture's mechanical response, especially under repeated loading, and can improve resistance to rutting and fatigue. At the same time, the presence of a partially solid plastic phase helps maintain mixture stability without requiring the complete dissolution of the polymer into the binder.

The hybrid method is also considered promising from an operational standpoint. Low-melting plastics can be incorporated without significantly altering production temperatures, and their partial melting reduces the risk of agglomeration that sometimes affects the dry process.

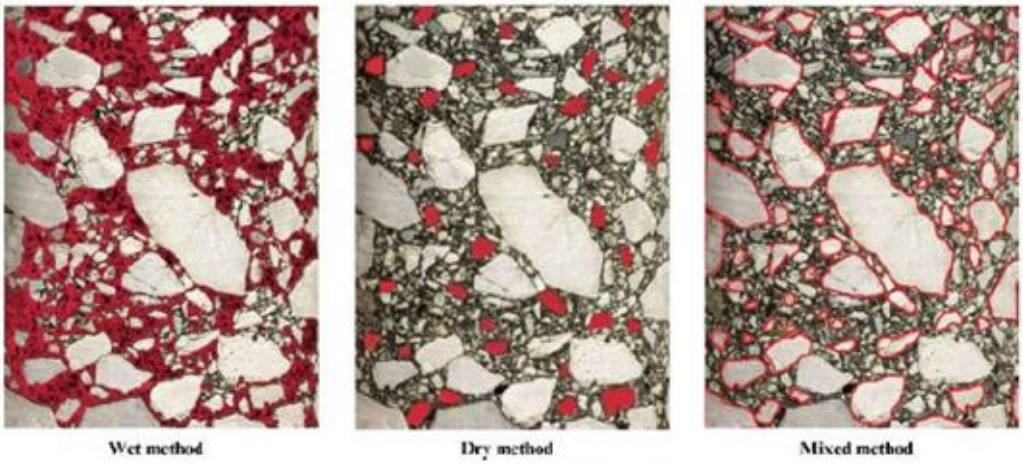

Figure 6. Role of plastics in the three mixing approaches (source: Boom et al., 2023)

1.3.4. Environmental and economic aspects

Recycling plastic waste offers several potentially significant environmental benefits. These include the conservation of non-renewable natural resources, the reduction of energy demand associated with the production of new materials, the decrease in the volume of solid waste destined for disposal or abandonment in the environment, and, not least, the mitigation of atmospheric emissions such as carbon dioxide (CO_2), sulfur dioxide (SO_2), and nitrogen oxides (NO) [27].

Despite these advantages, the introduction of recycled plastics into bituminous mixtures has raised several environmental concerns within the scientific and industrial communities. Among these, the potential release of microplastics during the service life of the pavement—or because of degradation processes caused by traffic and weathering—stands out as a major issue.

Preliminary studies suggest that the amount of particles released from pavements containing recycled plastics is influenced by various environmental and operational factors. The most relevant include temperature, the acidity of runoff water, traffic conditions and intensity, as well as the method used to incorporate the plastic into the bituminous mixture. This last aspect appears to play a decisive role in determining both the extent and timing of microplastic release.

Enfrin et al. highlighted that the wet process, which involves the direct introduction of plastic into the bituminous matrix, results in greater exposure of the material in the surface layers of the pavement. This would lead to an earlier release of microplastics compared to the dry process, in which plastic particles are physically embedded and retained among the mineral aggregates [28].

This structural difference between the two construction approaches helps explain the distinct release dynamics observed and underscores the importance of carefully evaluating the plastic-integration method when assessing the overall environmental sustainability of the material.

Life Cycle Cost Analysis (LCCA) is essential for assessing potential economic benefits. A first advantage concerns the reduction in the consumption of virgin bitumen, a costly material subject to high price volatility. Several studies show that the introduction of waste plastics can replace part of the traditional binder, helping to reduce procurement costs and decreasing dependence on non-renewable resources.

A further economic benefit is linked to the reduction of plastic-waste management costs. The use of post-consumer plastics in road infrastructure reduces the volumes destined for landfill or incineration, generating a dual advantage: on the one hand, lower disposal costs; on the other, the valorisation of a material that would otherwise have no market value. This approach aligns with the principles of the circular economy and can support the development of local recovery and transformation supply chains, with positive economic impacts on the territory.

Finally, alignment with European and international policies on sustainability and recycling can facilitate access to economic incentives and dedicated funding. Organizations such as the Federal Highway Administration emphasize that the use of recycled materials in infrastructure can generate systemic economic benefits, in addition to environmental ones, by promoting the adoption of innovative and sustainable technologies.

1.4. Rejuvenator

Bituminous mixtures are not exempt from critical issues. Among the various factors that influence their long-term performance, the interaction with the surrounding environment plays a decisive role. Temperature fluctuations, humidity and the continuous exposure to oxygen gradually alter the characteristics of the bituminous binder, triggering ageing processes that make it progressively stiffer, less elastic and ultimately more fragile.

This phenomenon becomes particularly evident when dealing with Reclaimed Asphalt Pavement. As previously discussed, RAP consists of aggregates coated with a binder that has already undergone years of oxidative ageing. When this material is reintroduced into new mixtures, the aged bitumen often proves too rigid and brittle to ensure adequate workability and performance, limiting the potential benefits of recycling.

For this reason, the scientific community has devoted increasing attention to the development of strategies capable of restoring the original properties of aged binders. Among these, rejuvenators represent one of the most effective and widely studied solutions. These additives are specifically designed to soften the oxidised binder and re-establish its binding capacity, enabling RAP to be reintegrated into new mixtures without compromising mechanical behaviour.

Understanding how rejuvenators work, how they interact with aged bitumen and how they influence the overall performance of the mixture requires a deeper look at the mechanisms underlying bitumen ageing.

1.4.1. Aging mechanisms in bitumen

The ageing of bitumen is a complex and progressive phenomenon that significantly influences the long-term performance of asphalt mixtures. In general, this process can be described through two distinct but interconnected phases.

The first, known as short-term ageing, takes place during the production cycle of the asphalt mixture (mixing, transport, laying and compaction) when the binder is exposed to high temperatures and oxygen. Under these conditions, oxidation occurs rapidly, altering the chemical structure of the binder even before the pavement enters service.

The second phase, referred to as long-term ageing, develops gradually throughout the service life of the pavement. Here, the binder is continuously subjected to environmental and operational actions: ultraviolet radiation, daily and seasonal temperature fluctuations, humidity, oxygen diffusion, as well as the mechanical action of traffic and exhaust gases. Over time, these combined effects lead to a progressive hardening of the binder and a loss of its original viscoelastic balance.

At the molecular level, ageing induces significant transformations in the chemical and physical matrix of bitumen. A widely used interpretative framework is the SARA analysis, which divides bitumen into four main components: Saturates, Aromatics, Resins and Asphaltenes. Aged binders typically show an increase in the asphaltene fraction, due to the condensation and polymerisation of polar species, and a reduction in aromatics, which are more volatile and prone to oxidation. This shift disrupts the colloidal equilibrium of the binder, resulting in higher stiffness, reduced elasticity and greater susceptibility to cracking.

As highlighted by Karlsson and Isacsson and summarised by Urbano (2023)[29], these changes arise from four principal mechanisms:

1. Oxidation, driven by the reaction between bitumen and oxygen, accelerated by heat and UV radiation. This leads to the formation of oxygenated functional groups and a progressive increase in viscosity.

2. Volatilisation of lighter components, particularly aromatics and saturates, which evaporate under high temperatures, altering the internal balance of the binder and contributing to stiffness growth.

3. Exudation, the migration of oily maltenic components toward the aggregate surface, especially in porous aggregates. This process reduces the adhesive capacity of the binder and depletes the mixture of its most ductile fractions.

4. Physical hardening, a reversible phenomenon associated with molecular rearrangements at low temperatures. Unlike the other mechanisms, it can be mitigated simply by heating and is therefore not typically considered when evaluating the effectiveness of rejuvenators.

Together, these mechanisms explain why aged bitumen becomes progressively more rigid and brittle, losing its ability to relax stresses and accommodate deformation. Understanding these processes is essential for developing effective restoration strategies, such as the use of rejuvenators, which aim to rebalance the chemical composition of the binder and recover its original performance.

1.4.2. Chemical composition

Their composition typically includes materials rich in maltenic fractions, such as aromatic extracts, bio-derived oils, or synthetic esters, selected for their ability to penetrate the oxidised binder and rebalance the chemical components that deteriorate during ageing. The production of these additives blends substances that restore the lighter, oily fractions lost through oxidation and volatilisation, allowing the bitumen to recover the viscoelastic behaviour typical of fresh material. As highlighted in several studies [11], an effective rejuvenator does more than simply soften the binder: it actively contributes to restoring the equilibrium between asphaltenes and maltenes, which is essential for long-term performance.

It is important to distinguish true rejuvenating agents from fluxing agents, as the two categories differ significantly in both purpose and effect. Real rejuvenators are specifically engineered to reverse, at least partially, the chemical consequences of ageing. They interact with the binder at a molecular level, increasing the proportion of maltenes and improving ductility, elasticity and resistance to cracking. Their action is intended to be durable, ensuring that the restored properties are maintained throughout the service life of the pavement.

Fluxing agents, on the other hand, act primarily as temporary softeners. They reduce viscosity by dilution rather than by rebalancing the chemical structure of the binder. Often based on light oils or solvent-like components, their effect tends to diminish over time due to evaporation or absorption, and excessive use may even compromise the mixture's stability, increasing the risk of rutting or premature deformation. As noted in the literature [30], fluxing agents may improve workability during production, but they do not provide a true rejuvenation of the aged binder.

Understanding this distinction is essential when designing mixtures with high RAP content, as the choice between rejuvenators and fluxing agents directly influences the mechanical behaviour and durability of the final pavement. Real rejuvenators offer a pathway to restoring the performance of aged binders, while fluxing agents merely facilitate processing without addressing the underlying chemical imbalance.

1.4.3. Environmental and economic benefits

The use of rejuvenators in asphalt mixtures is not only a technical solution for restoring the properties of aged binders but also a strategy with significant environmental and economic implications.

From an environmental perspective, rejuvenators enable the incorporation of higher percentages of Reclaimed Asphalt Pavement (RAP), thereby reducing the demand for virgin aggregates and bitumen, materials whose extraction and production are associated with considerable energy consumption and greenhouse gas emissions. Several studies [11], [30] highlight that increasing RAP utilisation through effective rejuvenation can substantially lower the carbon footprint of asphalt mixtures, contributing to more sustainable pavement construction practices.

Bio-based rejuvenators offer additional advantages, as they are derived from renewable and often biodegradable sources, further decreasing the environmental burden associated with traditional petroleum-based additives.

From an economic standpoint, rejuvenators support cost-effective pavement production by reducing the reliance on virgin binder, which represents one of the most expensive components of asphalt mixtures. The ability to incorporate larger quantities of RAP without compromising performance translates into direct savings in material costs and, in many cases, lower overall production expenses. Rother studies [11] indicate that the economic benefits become especially significant when RAP contents exceed 30–40%, a threshold at which rejuvenators play a crucial role in maintaining mixture workability and long-term durability.

Moreover, the use of rejuvenators can extend pavement service life by improving resistance to cracking and fatigue, thereby reducing maintenance interventions and associated lifecycle costs.

Overall, rejuvenators represent a key enabler for both environmental sustainability and economic efficiency in modern asphalt technology. Their capacity to restore aged binders, promote circularity in pavement materials, and reduce long-term costs positions them as essential components in the transition toward more responsible and resource-efficient road construction.

2. Fatigue

2.1. Introduction

Fatigue cracking is one of the main degradation mechanisms affecting bituminous mixtures. It is a progressive phenomenon triggered by the repeated application of traffic loads, which induces an accumulation of microstructural damage within the material, eventually leading to the formation and propagation of macroscopic cracks.

Unlike other structural distresses, fatigue is not immediately detectable: at first glance, the material may appear intact even when the internal bitumen–aggregate matrix has already undergone significant changes in its ability to transfer and dissipate stresses.

Although the individual loads generated by traffic are generally lower than the ultimate strength of the bituminous mixture, their cyclic nature leads to a cumulative damage process that progressively reduces the stiffness of the mixture and shortens its service life. When the process reaches an advanced stage, the deterioration becomes visible on the surface through a characteristic network of cracks, commonly referred to as *alligator cracking*. This pattern compromises both the functionality and structural integrity of the pavement, facilitating water infiltration and accelerating the deterioration of the underlying layers.

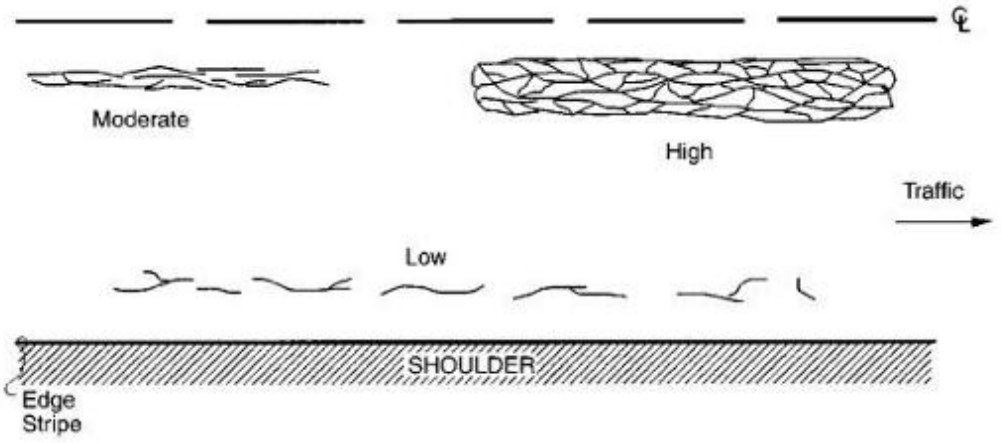

Figure 7. Fatigue cracking (source: Distress Identification Manual – FHWA, 2014)

From a mechanical standpoint, the fatigue-cracking process can be divided into three main phases: crack initiation, stable crack propagation, and unstable crack propagation [31].

A detailed analysis of these phases is provided below:

- Crack initiation: the initial stage of damage is characterized by the appearance of the first micro-discontinuities within the mixture. The repeated action of traffic loads induces localized permanent deformations at the microscopic scale, which tend to concentrate in areas where the material exhibits intrinsic weaknesses. These critical zones may correspond to air voids, the interface between aggregates and the bituminous mastic (composed of binder and filler), or the binder matrix itself. The progressive accumulation of these micro-deformations leads to the formation of microcracks, whose size is generally comparable to that of the finest aggregates.

- Stable crack propagation: during this second phase, microcracks begin to merge and extend within the mixture, gradually evolving into larger fractures. Crack growth proceeds in a relatively regular and predictable manner and is accompanied by a gradual reduction in the overall stiffness of the mixture.

- Unstable crack propagation: when the main crack reaches a size that significantly reduces the effective load-bearing section, the material can no longer sustain the applied load. At this point, propagation becomes suddenly unstable and accelerates rapidly, leading to structural failure and a sharp drop in the stiffness of the mixture.

Citing again [31], in flexible and semi-rigid pavements these phases can give rise to different types of cracking:

1. Top-down cracking: these are longitudinal cracks that originate at the pavement surface typically near the edges of the tire–pavement contact area and then propagate downward through the bituminous layers. The main causes of this propagation mode are the high shear stresses that develop at the surface due to the non-uniform pressure distribution of modern radial tires, combined with oxidative aging of the binder in the wearing course.

Figure 8. Top down cracking (source: Bessa et al., 2022)

2. Bottom-up cracking: traffic loads cause the pavement layers to bend under repeated wheel passages. This bending generates compressive stresses in the upper portion of the layer and tensile stresses in the lower portion. Since bituminous materials exhibit low tensile strength, cracks tend to form precisely in the lower part of the bound layer (typically at the bottom of the base or binder course) and then propagate vertically toward the surface. Once the crack reaches the pavement surface, it branches and interconnects with adjacent fractures, leading to the characteristic alligator-cracking pattern.

Figure 9. Bottom up cracking (source: Bessa et al., 2022)

3. Reflective cracking: although this type of crack propagation is not strictly attributable to fatigue, it is worth mentioning. It results from the reactivation and growth of a discontinuity already present in the pavement structure. This phenomenon occurs when a new wearing course is placed over an existing pavement that already contains cracks.

   Relative movements of the underlying crack edges, induced by thermal variations or traffic loads, generate stress concentrations in the new layer, promoting the formation of a new crack exactly above the original one. The crack thus initiated propagates upward, reproducing the underlying discontinuity until it eventually reaches the surface.

To achieve proper structural design of road pavements, it is essential to thoroughly understand the mechanisms described above and to analyse this phenomenon through laboratory testing.

A wide range of experimental approaches exists to evaluate fatigue resistance, all based on the application of cyclic loads until specimen failure. However, these tests may differ in several aspects, such as the temperature at which they are performed, the geometry of the specimen, the magnitude and type of applied load, and whether the test is conducted under stress or strain control.

The most used tests include the four-point bending test (4PB) and the indirect tensile test, described briefly below (they will be discussed in detail in the following chapters of this thesis):

1. Four-point bending test: this test allows the evaluation of the response of the material under controlled bending, generating a uniform strain field in the central region of the specimen. This configuration makes it possible to analyse damage evolution and stiffness reduction over time, making it particularly suitable for assessing the fatigue resistance of bound layers under conditions like those encountered in service (see the detailed description of bottom-up cracking on the previous page).

2. Indirect tensile test: this test applies cyclic diametral loads to cylindrical specimens, inducing tensile stresses perpendicular to the loading direction. It is appreciated for its operational simplicity, reproducibility, and ability to provide insight into the material's sensitivity to horizontal deformations.

Before addressing the topic from a theoretical standpoint, it is important to analyse those volumetric properties—particularly air-void content—are among the main factors governing the fatigue behaviour of bituminous mixtures.

According to Zeiada et al. (2023), variations in air-void content significantly influence fatigue performance both in laboratory testing and in long-term simulations, confirming that more compacted mixtures exhibit superior performance. Indeed, the presence of voids—considering their quantity, shape, and distribution—represents a key parameter for pavement durability.

2.2 Viscoelastic nature

Understanding fatigue mechanisms cannot be separated from the viscoelastic nature of bituminous mixtures, since the interaction between elastic response and viscous dissipation governs the evolution of damage under cyclic loading.

A material can be defined as elastic when a one-to-one relationship exists between stress and strain components. Under these conditions, the deformation induced by a load occurs instantaneously and disappears as soon as the load is removed, with full recovery of the energy stored during the deformation process. Linear elastic behaviour is described by Hooke's spring model, according to which the material response is independent of time and of the history of the applied loads.

$$\sigma = E \cdot \varepsilon \qquad \text{(Eq. 2.1)}$$

$$\tau = G \cdot \gamma \qquad \text{(Eq. 2.2)}$$

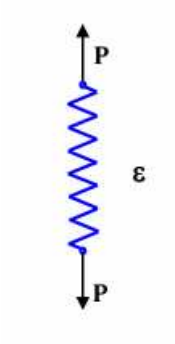

Figure 10. Hooke's spring, linear elastic behaviour

Conversely, in viscous materials deformation is not instantaneous but depends on the duration of the applied load and on the stress history. In this case, there is no longer a direct relationship between stress and strain, but rather between stress and strain rate. The theoretical model that represents this behaviour is Newton's viscous dashpot, in which stress is proportional to the strain rate through the viscosity coefficient η:

$$\tau = \eta \cdot \dot{\gamma} \qquad \text{(Eq. 2.3)}$$

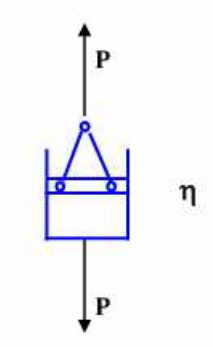

Figure 11. Newton's viscous dashpot, viscous behaviour

This model describes the typical behaviour of incompressible fluids, in which the applied energy is entirely dissipated as heat.

In the case of bituminous mixtures, the actual behaviour is neither purely elastic nor purely viscous, but a combination of the two. As mentioned earlier, this is referred to as viscoelastic behaviour, in which both components coexist.

Therefore, the behaviour of viscoelastic materials can be represented through an appropriate combination of elastic springs and viscous dashpots.

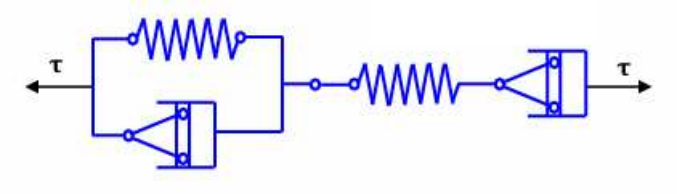

Figure 12. Burger model, viscoelastic behaviour

The mechanical behaviour of bituminous mixtures is strongly influenced by the viscoelastic nature of the binder from which they derive. Bitumen is a thermally sensitive material whose response varies over time: this means that the deformation induced by a load depends not only on its magnitude, but also on its duration, the frequency of application, and the temperature at which the material is subjected [32].

This dependency becomes particularly evident under cyclic loading, such as that generated by vehicular traffic. Under these conditions, the response of the mixture is not instantaneous: a time lag is observed between the peak applied stress and the peak resulting strain. This delay is described by the phase angle (δ), a fundamental parameter for characterizing viscoelastic behaviour.

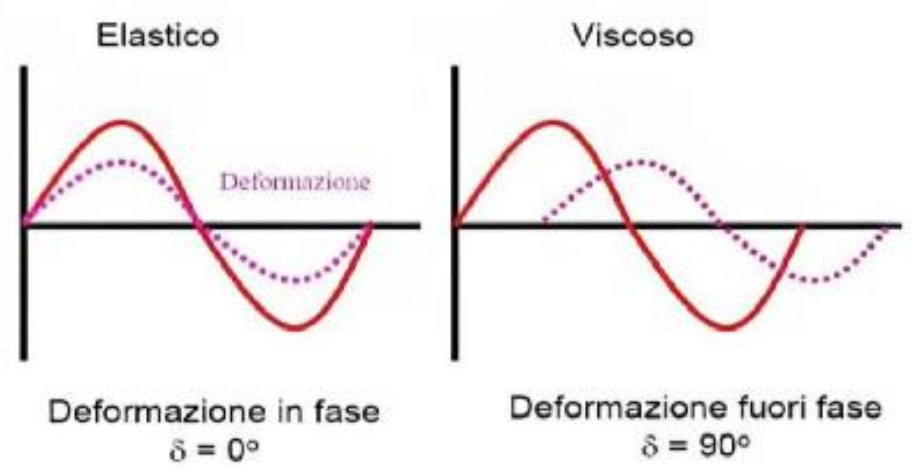

Figure 13. Difference between elastic response (left) and viscous response (right)

As can be inferred from the figure above, a phase angle δ equal to zero indicates purely elastic behaviour, while a value of 90° represents purely viscous behaviour. Bituminous mixtures fall in an intermediate condition, with δ values that vary depending on temperature and loading frequency.

The dynamic response of the material is generally described through the complex modulus E^*. To understand its meaning, consider the following example: a cylindrical specimen of bituminous mixture subjected to a sinusoidal axial stress with amplitude σ_0 and angular frequency ω:

$$\sigma(t) = \sigma_0 \sin(\omega t) \qquad \text{(Eq. 2.4)}$$

The material responds with a sinusoidal strain as well, but not perfectly in phase with the applied load. Due to the viscous component of viscoelastic behaviour, the strain is delayed with respect to the stress by the phase angle δ introduced earlier:

$$\varepsilon(t) = \varepsilon_0 \sin(\omega t - \delta) \qquad \text{(Eq. 2.5)}$$

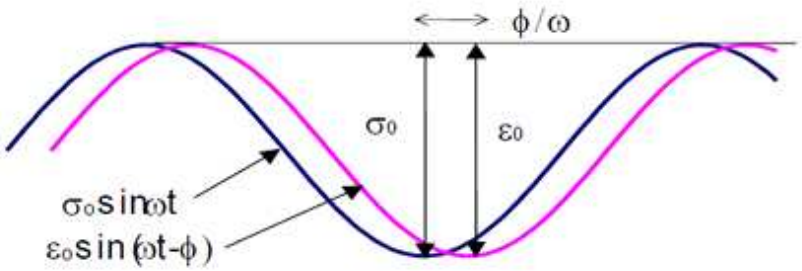

Figure 14. Stress response (blue curve) and resulting strain (purple curve) in a viscoelastic material subjected to dynamic loading

The complex modulus E^* is defined as the ratio between the applied stress and the resulting strain:

$$E^* = \frac{\sigma_0 \ \sin(\omega t)}{\varepsilon_0 \ \sin(\omega t - \delta)} \qquad \text{(Eq. 2.6)}$$

Since stress and strain are not in phase, the complex modulus cannot be represented as a simple real number. Its absolute value, obtained from the ratio between the amplitudes of the two sinusoids, is known as the dynamic modulus:

$$| \ E^* \ | = \frac{\sigma_0}{\varepsilon_0} \qquad \text{(Eq. 2.7)}$$

The dynamic modulus represents the effective stiffness of the material under cyclic loading and is a fundamental parameter in the mechanical characterization of bituminous mixtures.

This parameter can be represented as a vector in the complex plane and decomposed into two fundamental components:

$$E^* = E_{\text{el}} + i \, E_{\text{vis}} \qquad \text{(Eq. 2.8)}$$

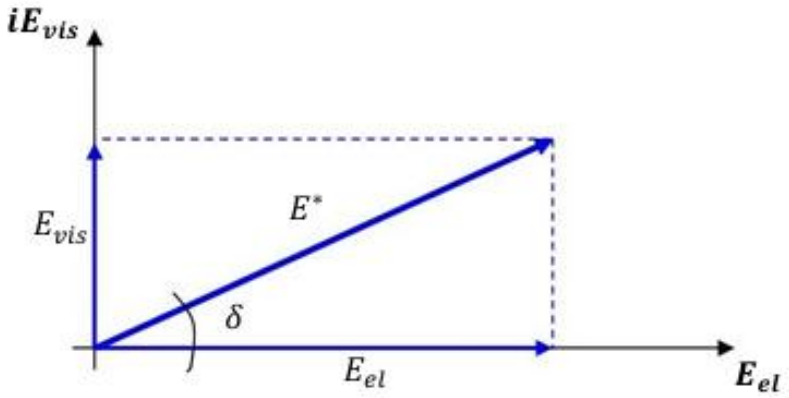

Figure 15. Representation of the complex modulus in the complex plane

They are defined as follows:

1. Storage modulus E_{el}, which represents the elastic part of the response and quantifies the energy stored and recoverable:

$$E_{\text{el}} = | \ E^* \ | \cos \ \delta = \frac{\sigma_0}{\varepsilon_0} \cos \ \delta \qquad \text{(Eq. 2.9)}$$

2. Loss modulus E_{vis}, which expresses the viscous component and measures the energy dissipated due to irreversible deformations:

$$E_{vis} = | E^* | \sin \delta = \frac{\sigma_0}{\varepsilon_0} \sin \delta \qquad \text{(Eq. 2.10)}$$

The sensitivity of bitumen to temperature makes its viscoelastic behaviour highly variable. At low temperatures, the binder tends to stiffen, increasing the elastic component and reducing the phase angle. Under these conditions, the material becomes more brittle and more susceptible to cracking. Conversely, at high temperatures the bitumen softens, the viscous component becomes predominant, and the complex modulus decreases, promoting permanent deformations and instability phenomena.

An equally important role is played by the frequency of cyclic loading. Loads applied rapidly do not allow the binder sufficient time to flow, resulting in a stiffer response dominated by the elastic component. Conversely, loads applied slowly or conditions of congested traffic favour the viscous response, with an increase in the phase angle and greater energy dissipation [33].

During each load cycle, part of the energy is not recovered but contributes to the accumulation of microstructural damage within the mixture. This dissipated energy corresponds to the area of the hysteresis loop in the stress–strain diagram. As cycles progress, this damage accumulates, promoting the nucleation and growth of microcracks that, over the long term, lead to the degradation of the mixture. Viscoelastic Continuum Damage (VECD) models, developed and refined over recent decades, have made it possible to quantitatively describe this process by linking energy dissipation to damage evolution.

2.3 Fatigue theory

The method traditionally used for the fatigue characterization of bituminous mixtures is the phenomenological approach. It focuses exclusively on the macroscopic response of the material, relating a mechanical input variable (typically the initial applied strain or stress) to the outcome, namely the number of load cycles the specimen can withstand before reaching a predefined failure criterion.

It is therefore a descriptive method that does not investigate the microscopic damage mechanisms but relies on empirical correlations derived from laboratory tests conducted at different stress levels.

The relationship between the amplitude of the initial applied strain and the fatigue life of the material is mathematically described by the Wöhler law, also known as the "fatigue law." This relationship generally takes the form of a power law:

$$N_f = k_\varepsilon \, \varepsilon_0^{-n_\varepsilon} \qquad \text{(Eq. 2.11)}$$

where N_f is the number of cycles to failure, ε_0 is the amplitude of the initial tensile strain (or alternatively the initial stress σ_0), and k_ε and n_ε are mixture-related parameters determined through regression of experimental data. By applying the logarithm to both sides, the relationship becomes linear:

$$\log N_f = \log k_\varepsilon - n_\varepsilon \log \varepsilon_0 \qquad \text{(Eq. 2.12)}$$

allowing the test results to be plotted on a bi-logarithmic diagram, where the experimental points tend to align along a straight line, commonly referred to as the fatigue line.

In this context, the parameters of the Wöhler law acquire a physical meaning: the intercept k_ε is associated with the intrinsic strength of the material (a higher line indicates a longer fatigue life for the same strain), while the slope n_ε expresses the sensitivity of the mixture to the stress level.

Lower absolute values of the slope indicate a more damage-tolerant behaviour, since even significant variations in initial strain produce relatively small reductions in fatigue life. It is well known, for example, that mixtures containing polymer-modified binders tend to exhibit flatter slopes than mixtures with conventional binders, reflecting greater ductility, improved energy-dissipation capacity, and therefore better resistance to crack propagation.

After addressing the theoretical aspect, it is useful to examine laboratory tests, which can be conducted according to two main approaches: load-controlled and strain-controlled testing. These methods reproduce different operational conditions and provide valuable information on the fatigue resistance of the mixture.

In stress-controlled tests, the amplitude of the applied stress is kept constant throughout the test. In this case, the material tends to exhibit a progressive increase in cyclic strain as damage accumulates. This increase is due to the reduction in stiffness of the mixture, which, being viscoelastic, becomes progressively more deformable under a constant load. This type of test is particularly sensitive to the crack-propagation phase: when stiffness decreases beyond a certain threshold, strain grows rapidly until failure. Load-controlled tests are considered suitable for simulating the behaviour of rigid pavements, and thus for stiff and brittle materials.

Conversely, in strain-controlled tests, the amplitude of the applied strain is kept constant. In this case, it is the stress that varies over time: as the material becomes damaged and its stiffness decreases, the stress required to maintain the imposed strain progressively decreases. This behaviour tends to slow down damage accumulation, since the material is not forced to withstand increasing strain levels as occurs in load-controlled testing.

This type of test is considered representative of the operational conditions of flexible pavements, where the deformation imposed by traffic is often limited by the overall structure of the pavement system.

The comparison between the two methods highlights significant differences in fatigue life: for the same initial stress level, strain-controlled tests tend to yield longer fatigue lives than load-controlled tests. This divergence is closely linked to the viscoelastic nature of bituminous mixtures and their ability to dissipate energy. In load-controlled testing, the energy dissipated per cycle increases as damage progresses, accelerating failure; in strain-controlled testing, the reduction in stress limits energy dissipation, slowing the evolution of damage.

However, the phenomenological method presents several intrinsic limitations that reduce its descriptive capability, especially when analysing complex materials or variable operating conditions.

Its main weakness lies in the fact that it is based solely on the observation of the macroscopic response of the material, without considering the microstructural mechanisms governing crack initiation and propagation. The empirical correlations derived from it, such as the Wöhler law, describe the relationship between stress level and fatigue life but do not provide information on the degradation process or its evolution over time.

Another limitation concerns the dependence on test conditions. The parameters of the Wöhler law are strongly influenced by temperature, loading frequency, control mode (stress or strain), specimen geometry, and the adopted failure criterion. This implies that laboratory results are not always directly transferable to real-world conditions, where the material is subjected to variable loads. Moreover, the phenomenological approach does not explicitly account for the viscoelastic nature of bituminous mixtures: time dependence, temperature effects, and loading rate are implicitly embedded in the empirical parameters, without explicit modelling of the underlying physical phenomena.

These limitations become particularly evident when analysing innovative materials, such as mixtures with high RAP content, polymer-modified binders, or other additives, where damage mechanisms may differ significantly from those of traditional mixtures [34].

2.4. Failure criteria

Failure criteria play a central role in the interpretation of fatigue tests on bituminous mixtures, as they define the point at which the material is considered to have "failed" under cyclic loading. Among the criteria most widely used at the international level (and adopted in this thesis), two are particularly relevant: the 50% initial modulus criterion and the Energy Ratio (ER) criterion.

A detailed analysis of both is provided below.

2.4.1. 50% initial modulus criterion

According to this criterion, which represents the most traditional approach, the number of cycles to failure N_f corresponds to the point at which the stiffness modulus of the specimen has decreased to half of its initial value. However, the initial modulus is not measured at the first cycle, as one might expect, but after a short conditioning phase, typically around the hundredth cycle, to eliminate the settling effects characteristic of the first load applications and to obtain a more stable and representative value of the material's behaviour.

The widespread use of this criterion is mainly due to its operational simplicity: stiffness is an easily measurable quantity during testing, and the 50% threshold provides a clear and repeatable reference point. Nevertheless, this very "strength" of the criterion also represents a major limitation, since the choice of this threshold is entirely arbitrary and lacks any scientific foundation. In fact, it does not correspond to a well-defined physical event, such as the formation of a macro-crack, but merely identifies a conventional point along the stiffness-degradation curve.

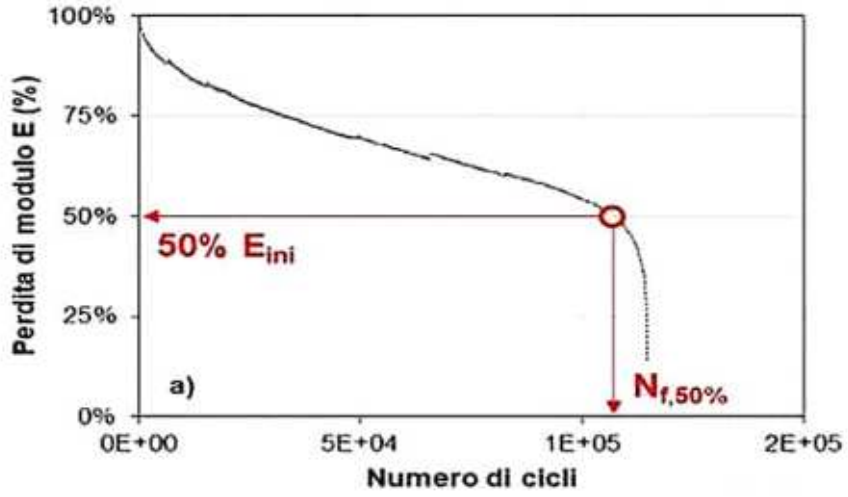

Figure 16. 50% initial modulus failure criterion (source: site www.stradeeautostrade.it)

The scientific community has shown that when the modulus has decreased to half of its initial value, the mixture has already undergone an extended phase of diffuse microcracking, although the coalescence of microcracks into a main fracture may not yet have occurred. This may lead to underestimation or overestimation of the fatigue life of the mixture under investigation [31], [35].

2.4.2. Energy Ratio criterion

The Energy Ratio (ER) criterion was developed as a response to the limitations of the 50% modulus criterion discussed above. It represents a physically based approach for defining the fatigue life of bituminous mixtures. It is founded on the idea that damage is closely related to the energy dissipated by the material during each load cycle. In viscoelastic materials, part of the mechanical energy applied is not elastically recovered but is converted into heat and microstructural damage. This dissipated energy corresponds to the area enclosed by the hysteresis loop in the stress–strain diagram and constitutes a direct indicator of the evolution of internal damage.

The Energy Ratio criterion analyses the trend of a dimensionless parameter defined as:

$$ER_n = \frac{W_0}{W_n} = \frac{\sigma_0\ \varepsilon_0 \sin\ \delta_0}{\sigma_n\ \varepsilon_n \sin\ \delta_n} \qquad \text{(Eq. 2.13)}$$

where n is the number of cycles, σ_0 and σ_n are the stresses at the first and the n-th cycle respectively, ε_0 and ε_n are the corresponding strains, and W_0 and W_n represent the dissipated energy at the first and the n-th cycle.

By analysing the trend of dissipated energy as a function of the number of cycles, a well-defined behaviour is generally observed. In the initial phase of the test, the curve exhibits an almost linear segment: in this region, the material accumulates damage gradually and in a controlled manner, without showing evident instability. This corresponds to the phase of diffuse micro-damage, during which microcracks form and slowly develop within the bituminous matrix.

As the number of load cycles increases, the curve begins to deviate from linearity, showing a more pronounced change in slope. This transition marks the shift from the stable-damage phase to the unstable propagation of the macrocrack—namely, the moment when the material loses its ability to dissipate energy uniformly and the fracture process becomes dominant.

According to the energy-based criterion, this transition point defines the true failure of the specimen, as it coincides with the onset of uncontrolled growth of the main crack.

In load-controlled tests, identifying this point is relatively straightforward. Since the amplitude of the applied stress remains constant, crack initiation leads to a rapid increase in strain, which in turn causes a significant rise in the dissipated energy per cycle. Consequently, the peak of the Energy Ratio is clearly identifiable and corresponds to the beginning of dominant crack propagation.

The situation is more complex in strain-controlled tests, where strain is imposed and stress progressively decreases as damage advances. In this case, the variation in dissipated energy does not exhibit such a distinct peak. However, as demonstrated by Rowe and Bouldin (2000), it is still possible to identify the critical point by applying the same logic used for load-controlled tests [36].

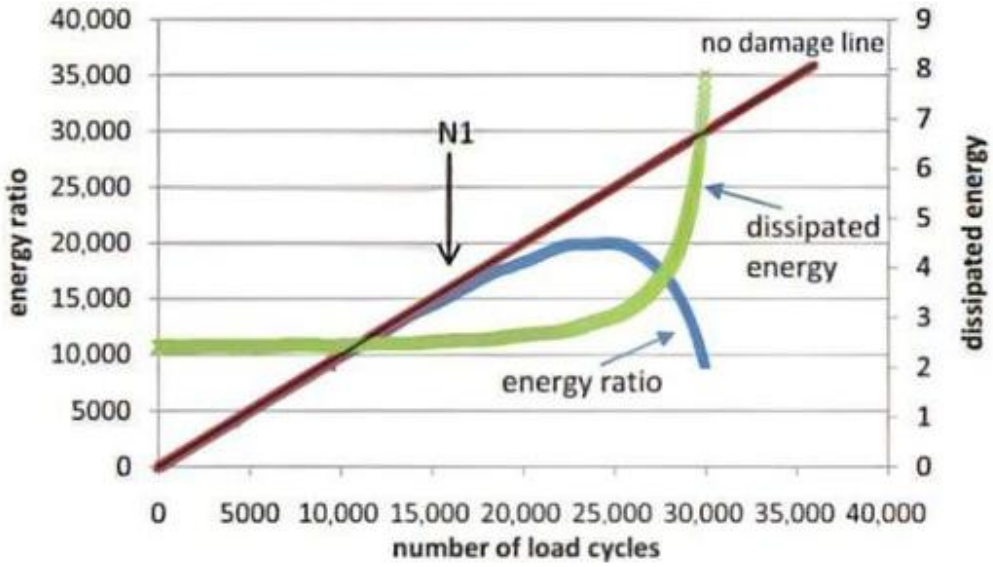

Figure 17. Energy Ratio failure criterion (source: Xu et al., 2025)

3. Experimental campaign

3.1. Objectives and framework of the work

The regulatory and technical evolution affecting the road infrastructure sector places strong attention on construction solutions oriented towards environmental sustainability. In this context, the Ministerial Decree of 5 August 2024, which introduces the new Minimum Environmental Criteria (CAM), establishes a fundamental principle: the use of recovered or recycled materials must not compromise the mechanical and functional performance of the pavement. Therefore, mixtures containing non-virgin materials must guarantee performance levels in line with those achievable with first-use materials.

This direction has been further strengthened by the update of the CAM introduced by the Ministerial Decree of 11 September 2025.

Within this regulatory framework lies the present thesis work, which aims to assess the actual technical and plant feasibility of producing bituminous mixtures containing high percentages of reclaimed asphalt pavement (RAP at 50%) and a polymeric compound obtained entirely from recycled rigid plastics, introduced into the mixture through a dry methodology with a hybrid approach. The main objective is to analyse the impact of such materials on mechanical performance, with particular attention to fatigue resistance, a key parameter for pavement durability.

To support this evaluation, a direct comparison was carried out with analogous mixtures produced in the laboratory and already studied in previous thesis works, to verify the consistency between the experimental results obtained in a controlled environment and those derived from real production at plant scale.

To achieve the above objectives, the following four types of mixtures were produced, all representative of a binder course (AC 16):

1. *MIX50 1*: containing 50% RAP (by aggregate weight) and 0.3% polymeric compound (by mixture weight), mixed with hybrid methodology.
2. *MIX50 2*: containing 50% RAP and 0.5% polymeric compound, mixed with hybrid methodology.
3. *MIX50 3*: containing 50% RAP and 0.7% polymeric compound, mixed with hybrid methodology.
4. *MIX50 REF*: still containing 50% RAP and mixed with a modified bitumen through wet methodology (PmB), without polymeric compound in order to obtain a reference mixture.

To establish the acceptance limits adopted in the mechanical and volumetric characterization phase of the above mixtures, the Special Tender Specifications ("Capitolato Speciale d'Appalto", CSA) relating to the resurfacing of the wearing course and underlying layers of the A4 motorway were taken as reference.

With regard to fatigue resistance, this was evaluated through two test configurations in accordance with the provisions of BS EN 12697-24 [37]:

- *CIT-CY*: indirect tensile test under stress control on cylindrical specimens, without rest period (frequency 10 Hz and temperature 20°C).
- *4PB-PR*: four-point bending test under strain control, performed on prismatic specimens (frequency 10 Hz and temperature 20°C).

3.2. Materials

The mixtures introduced in the previous paragraph and forming the basis of this thesis work were produced using the following materials:

- Virgin aggregates and filler.
- Reclaimed asphalt pavement (RAP).
- Neat bitumen.
- PmB bitumen.
- Rejuvenating additive, also known as rejuvenator (Iterlene ACF 2000 green).
- Polymeric compound (SuperPlastEco), supplied by the company Iterchimica S.p.A., based in Suisio (Bergamo).

These were produced directly at the company Bitux S.p.A., located in Foglizzo (Turin), a reference entity in Piedmont in the field of construction and maintenance of road and motorway pavements.

Figure 18. Production Center of Bitux S.p.A.

The mixtures were directly sampled from the production plant on 25 June 2025 and transported to the laboratory of the Department of Road Infrastructures of Politecnico di Torino for their characterization.

Figure 19. Sampling of the mixtures produced at the plant.

It should be noted that, to allow material sampling, reduced batches specifically dedicated to the experimentation were produced. This operational mode resulted in limited homogeneity of the obtained material, particularly regarding the bitumen content and the amount of rejuvenating agent introduced into each mixture.

As for the bitumen content, as will be illustrated in the following paragraphs, several determinations were carried out to quantify it precisely. However, the results showed a non-negligible variability. This non-uniformity was reflected, in the subsequent phases of the experimentation, in the production of specimens characterized by a non-uniform air void content.

Regarding the rejuvenator, an actual dosage significantly lower than that foreseen in the design recipes was detected. This shortage led to a reduction in stiffness moduli and lower workability of the prepared specimens, aspects that will be analysed in detail in the chapter dedicated to the processing of experimental results.

Another element to highlight concerns the grading of the aggregates used in the plant. As will be further discussed, the grading curves of the different mixtures show deviations, although limited, from the envelopes prescribed by the Special Tender Specifications of the A4 motorway.

Since the present work is part of a broader research project, developed within a PhD programme active for several years, an in-depth description of the materials used during the design phase and definition of the theoretical recipes of the mixtures under study is provided below. As anticipated, during the experimental campaign some deviations from the expected formulations emerged, aspects that will be analysed in detail in Chapter 4.

3.2.1. Virgin aggregates and RAP

The grading classes of the virgin aggregates used for the development of the mixture recipes, representative of an AC16 binder course, were selected in accordance with the prescriptions reported in the main Special Tender Specifications (CSA), including that of the A4 motorway. In accordance with these specifications, the fractions used and their dimensional ranges are the following:

- Sand 0/5 mm.
- Coarse aggregate 8/16 mm.
- Coarse aggregate 16/20 mm.
- Filler < 0.063 mm.

Regarding the contribution of RAP, the material used for the definition of the recipes came from the milling of a motorway section in the Aosta Valley. It is a mixed RAP, since it was obtained from the combined milling of base, binder, and wearing courses.

To ensure its homogeneity and make it suitable for use in the designed mixtures, the RAP underwent a preliminary crushing process, followed by sieving into two distinct grading fractions: RAP 0/12 and RAP 0/20.

The binder content of the two fractions was determined through ignition test, performed according to EN 12697-39 [38]. The analyses showed a bitumen content equal to 4.15% by weight on aggregate for the RAP 0/12 fraction and 5.45% for the RAP 0/20 fraction. Subsequently, the RAP samples were subjected to sieve analysis, to precisely define their grading distribution.

The following figure reports the grading curves of the virgin aggregates and RAP used in the mixtures under study.

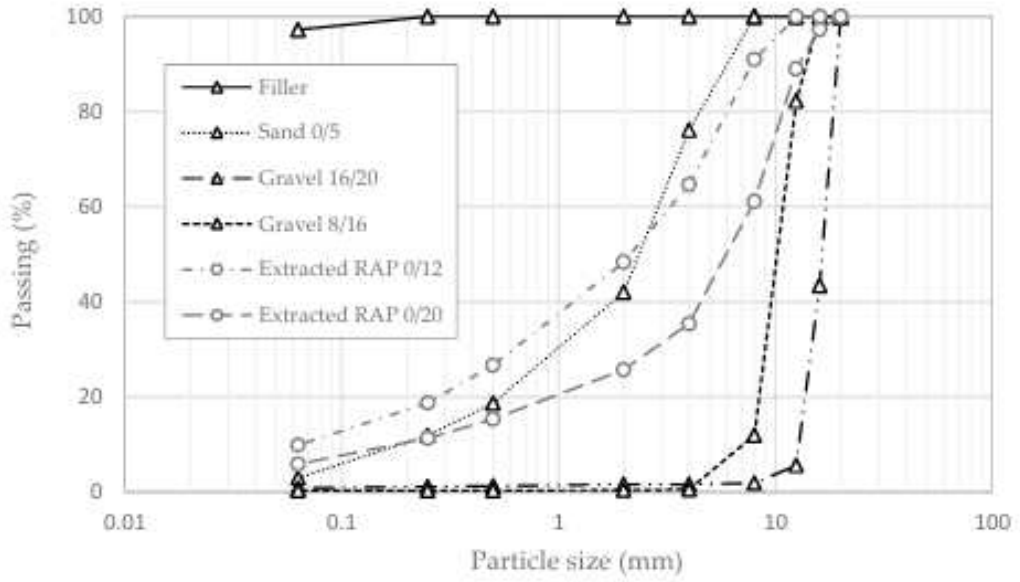

Figure 20. Particle size distributions of aggregate and RAP fractions (source: La Macchia et al, 2024 [24]).

3.2.2. Bitumen

As anticipated in the subsection 3.1 - Objectives and framework of the work, two different bituminous binders were used in the present study:

1. Neat bitumen with penetration grade 50/70, used in the mixtures in which the polymeric compound was introduced through hybrid methodology, classified according to EN 12591 [39]. In the table below, referred to as binder A.
2. Polymer-modified bitumen with SBS polymer, identified as PmB 45/80−70, compliant with the EN 14023 standard [40]. In the table below, referred to as binder B.

Both binders, within the PhD project in which this work is included, underwent complete characterization, including both performance-based and empirical tests. The following table reports their respective Performance Grades (PG), determined according to the Superpave classification system (AASHTO M323 22) [41], together with penetration values (EN 1426) [42] and softening point (EN 1427) [43].

	Performance Grade	Penetration at 25 °C (dmm)	Softening Point (°C)
Binder A	PG 46E-22	70	48.1
Binder B	PG 64E-22	55	80.3

Table 3. Characteristics of asphalt binders (source: La Macchia et al, 2024 [24]).

3.2.3. Rejuvenating additive

Bituminous mixtures present some intrinsic criticalities, including marked sensitivity to environmental conditions. Among the factors that most influence their deterioration is the ageing of the bituminous binder, a process favoured by high temperatures, the presence of oxygen, and moisture (Pyrig et al., 2022).

RAP, as already described, consists of aggregates coated with a bitumen film that has become oxidised and hardened due to long exposure to atmospheric agents and traffic loads during the pavement's service life. This ageing modifies the chemical balance of the binder, altering the ratio between asphaltenes, responsible for stiffness, and maltenes, which provide ductility and flexibility. The result is an excessively stiff and brittle binder, which reduces the workability of the mixture and increases its susceptibility to premature cracking [42], [43].

When high percentages of RAP are used, it therefore becomes necessary to employ specific rejuvenating agents capable of restoring the original properties of the aged bitumen.

These additives, commonly referred to as rejuvenators, penetrate the binder film coating the RAP aggregates and promote its diffusion within the bituminous matrix. Once absorbed, the rejuvenator reintegrates the lost maltene fraction, rebalancing the chemical composition of the binder and reducing its viscosity and stiffness. This process allows the bitumen to recover part of its flexibility, while improving the workability and durability of the final mixture [44].

The rejuvenator considered during the recipe design phase has the following properties:

Aspect	Liquid
Color	Brown–purple
Density at 80 °F (25 °C)	0.93 ± 0.1 g/cm^3
Viscosity at 80 °F (25 °C)	100 ± 50 cP
Flash point	>390 °F (200 °C)
Water content	<2%

Table 4. Properties of the rejuvenating agent (source: La Macchia et al, 2024 [24]).

3.2.4. Polymeric compound

SuperPlastEco is a polymeric compound obtained 100% from recycled rigid plastics, originating both from municipal waste and industrial scraps. It is supplied in the form of granules with dimensions between 4 and 6 mm and has been specifically developed for use in bituminous mixtures through dry methodology or hybrid approach.

Its chemical composition, protected by industrial patent, has been formulated to ensure optimal behaviour during mixing and compaction phases. In fact, it has a softening point between 160°C and 180°C, a value very close to the typical production temperatures of HMA. This characteristic allows the polymer to soften and modify its shape during mixing, an essential condition for the correct functioning of the hybrid process, in which the compound must effectively interact with the binder and the aggregate matrix.

The following table reports the main properties of this polymeric compound:

Aspect	Granules
Color	Shades of gray
Apparent density at 80 °F (25 °C)	0.4–0.6 g/cm^3
Softening point	160–180 °C

Table 5. Main characteristics of the polymeric compound additive (source: La Macchia et al, 2024 [24]).

3.2.5. Theoretical mixtures (from recipe)

The grading curve adopted for the mixtures was defined in previous research activities [24], referring to the technical prescriptions of the main Special Tender Specifications for binder courses. For the experimental investigation mentioned above, an AC16 mixture was selected, characterized by a nominal maximum aggregate size of 16 mm and by a grading distribution compliant with Italian specifications for dense bituminous mixtures intended for binder course [45].

The two RAP fractions were introduced in all formulations while maintaining a constant ratio of 3:2. Therefore, the contribution of the two sizes was respectively 30% for the 0/12 material and 20% for the 0/20 fraction.

Below are reported the dimensional distribution of the different aggregate classes, that of the RAP, and the design curve used.

Sieve	Sand 0-5	Gravel 8-16	Gravel 16-22	Filler	RAP 0-12	RAP 0-20
[mm]	[%]	[%]	[%]	[%]	[%]	[%]
31.5	100.0	100.0	100.0	100.0	100.0	100.0
20.0	100.0	100.0	100.0	100.0	100.0	100.0
16.0	100.0	100.0	43.4	100.0	100.0	97.2
12.5	100.0	82.2	5.6	100.0	100.0	89.0
8.0	100.0	12.0	1.9	100.0	91.0	61.1
4.0	76.1	0.5	1.6	100.0	64.7	35.4
2.0	42.1	0.4	1.6	100.0	48.3	25.8
0.5	18.7	0.4	1.3	100.0	26.7	15.4
0.25	12.0	0.4	1.2	100.0	18.7	11.3
0.063	3.0	0.3	0.8	97.2	9.9	5.9

Table 6. Particle-size distribution of virgin aggregates and RAP (source: La Macchia et al, 2024 [24]).

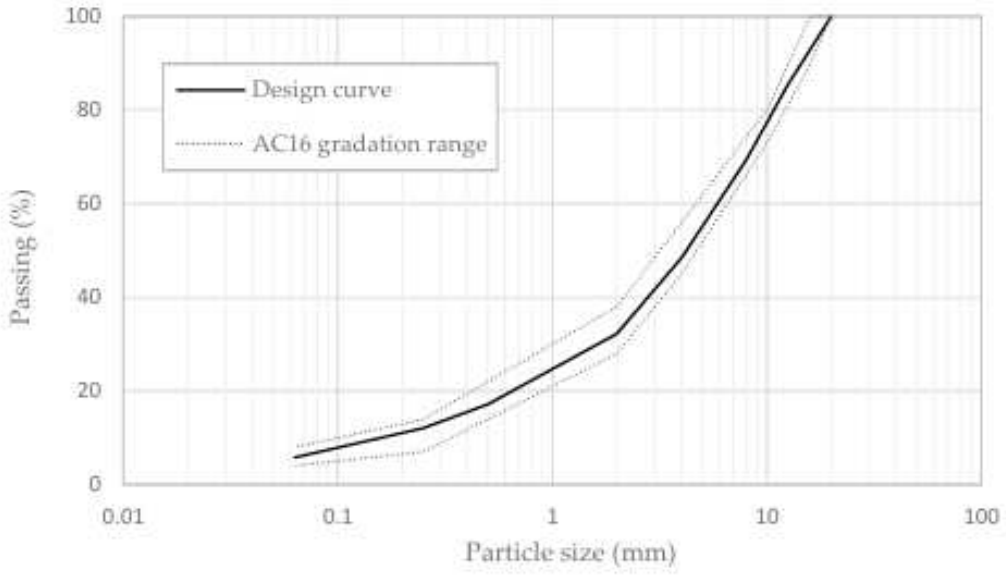

Figure 21. Gradiation limits and target gradation curve of AC mixtures (source: La Macchia et al, 2024 [24]).

Based on the results emerging from the previously illustrated PhD research and discussed in depth [24], the theoretical formulations of the mixtures to be produced at the Bitux S.p.A. mixing plant were defined.

Regarding binder content, in the reference mixture containing PmB a value of 4.5% by weight on the finished mixture was adopted. In the mixtures modified with polymeric compound, instead, the total binder content was increased considering that the compound contributes to the binder phase. For example, in the mixture named MIX50 1, the total binder content reaches 4.8%, since the 0.3% of polymeric compound (by total mixture weight) is added to the bitumen present.

Therefore, as can be deduced, the total binder content was calculated as the sum of the different components: added virgin bitumen, aged bitumen from RAP, rejuvenating additive, and polymeric compound.

The following table reports the weight percentages, referred to the finished mixture, of each component used in the different formulations.

Component	MIX50 1	MIX50 2	MIX50 3	MIX50 REF
	[%]	[%]	[%]	[%]
Sand 0/5	26.304	26.249	26.194	26.387
Gravel 8/16	9.826	9.805	9.785	9.857
Gravel 16/22	10.802	10.780	10.757	10.836
RAP 0/12 (virgin aggregates basis)	28.560	28.500	28.440	28.650
RAP 0/20 (virgin aggregates basis)	19.040	19.000	18.960	19.100
Filler	0.668	0.666	0.665	0.670
Total Binder	4.800	5.000	5.200	4.500
RAP 0/12 binder	1.557	1.553	1.550	1.561
RAP 0/20 binder	0.790	0.789	0.787	0.793
Virgin binder	2.004	2.009	2.014	1.996
Polymer	0.300	0.500	0.700	0.000
Rejuvenator	0.150	0.150	0.149	0.150
RAP 0/12 total	30.117	30.053	29.990	30.211
RAP 0/20 total	19.830	19.789	19.747	19.893
RAP total	49.947	49.842	49.737	50.104
Total	100.000	100.000	100.000	100.000

Table 7. Percentages of the components by mixture weight

3.3. The experimental campaign

In the following paragraphs, the operational procedures adopted for carrying out the experimental tests conducted at the Road Materials Laboratory of the Department of Land and Infrastructure Engineering of Politecnico di Torino will be illustrated in detail, with precise references to the applicable technical standards.

An in-depth description of the mixing phases carried out at the Bitux S.p.A. plant will also be provided, to clarify in detail the process through which the mixtures examined in this thesis work were produced.

3.3.1. Plant mixing

The production of bituminous mixtures containing Reclaimed Asphalt Pavement (RAP) in a batch plant follows a well-defined operational sequence, articulated into distinct and time-regulated phases. The introduction of RAP cold, meaning without any pre-heating, represents the simplest and most widespread method for integrating recycled material into the production cycle, but it also entails a series of technical constraints that influence both the maximum RAP percentage usable and the quality of the final mixture.

As highlighted by [1], cold addition is one of the most common techniques in traditional batch plants, but it is also the one presenting the greatest operational limitations, especially in terms of thermal balance and control of the moisture content of the recycled material.

The process begins with the management of virgin aggregates, stored in separate stockpiles and fed into the cold feeders. From here, the different grading fractions are dosed and conveyed towards the dryer drum. In this phase, the aggregates present a variable moisture content, which must be completely removed to ensure adequate adhesion of the binder. Drying takes place inside the drum, where the burner provides the necessary heat and the rotating motion ensures uniform exposure to the hot airflow.

The operating temperatures of the drum, in the presence of cold RAP, are generally higher than those of a plant producing fully virgin mixtures. In industrial practice, virgin aggregates are often heated up to 170–190°C, values required to compensate for the cooling induced by RAP introduced at ambient temperature (typically 15–25°C). This thermal increase is essential to obtain a final mixture temperature compatible with laying and compaction requirements, which for a traditional mixture generally lies between 140 and 160°C.

[1] emphasises how the impossibility of pre-heating RAP in a traditional batch plant makes this overheating of virgin aggregates necessary, with consequent increases in energy consumption and emissions.

Once heated, the aggregates are transferred to the hot tower via a bucket elevator. Here, the vibrating screen separates them into different grading classes, subsequently stored in the hot bins. This phase is particularly important when RAP is used, since the recycled material often contains a high percentage of fines, deriving from milling operations and any crushing processes.

[1] highlights that the presence of excessive fines can limit the maximum RAP percentage that can be introduced, making accurate mix design management necessary and, when possible, the fractionation of the recycled material.

In parallel with the dosing of hot aggregates, the filler and virgin bitumen—kept at the required pumping temperature (generally 150–170°C)—are weighed. RAP, instead, is not sent to the dryer drum but is stored in dedicated stockpiles, preferably covered, to limit moisture absorption. The paper notes that RAP tends to retain much more water than natural aggregates, with moisture values that may reach 7–8%, and that moisture represents one of the main critical factors in the production of mixtures with cold addition [1]. The entry of moist RAP into the mixer may in fact generate violent vaporisation phenomena, with steam emissions and potential micro-explosions.

The introduction of RAP takes place directly into the mixer, generally immediately after loading the hot aggregates. In this phase, the first thermal contact between the two materials occurs: the virgin aggregates transfer heat to the RAP, favouring the partial softening of the oxidised binder present in the recycled material.

However, the literature shows that, under cold-addition conditions, the degree of blending between virgin binder and RAP binder is limited and cannot be considered complete; part of the binder present in RAP remains encapsulated within the aggregates, behaving like a sort of "black rock" [1]. Only afterwards is the virgin bitumen introduced, completing the wet mixing phase until the desired homogeneity is reached.

At the end of the cycle, the mixture is discharged into trucks or hot storage silos, which allow temperature stabilisation before transport to the construction site. The final temperature of the mixture, in the presence of cold RAP, tends to lie between 125 and 150°C, depending on the RAP percentage introduced and the initial temperature of the virgin aggregates.

After a detailed review of the steps followed in a batch plant with cold RAP addition, such as the Bitux S.p.A. plant, the advantages and disadvantages of this plant configuration are briefly reported.

Cold addition of RAP in a batch plant presents some significant advantages. The first concerns plant simplicity: it does not require major structural modifications, such as parallel drums or dedicated pre-heating systems, and can be implemented even in older plants. This makes the technology economically accessible and easily adoptable.

Furthermore, the procedure allows the recovery of valuable materials, reducing the consumption of virgin aggregates and bitumen, with environmental and economic benefits. [1] recalls that RAP contains about 95% aggregates and 5% binder, and that its use allows a significant reduction in natural resource extraction and emissions associated with bitumen production.

Alongside the advantages, cold addition also presents important limitations. The main one concerns the maximum RAP percentage usable, which rarely exceeds 15–30% in traditional batch plants, precisely due to the strong cooling of the mixture and the difficulty of ensuring an adequate degree of blending between virgin binder and RAP binder. The thermal balance is particularly critical: aggregates must be overheated to compensate for the entry of cold RAP, with consequent increases in energy consumption. Moreover, RAP moisture represents a risk factor both for mixture quality and for process safety, as highlighted in the paper.

Finally, the variability of the recycled material, in terms of grading, binder content, and presence of contaminants, can significantly influence the consistency of the final mixture's performance, making particularly rigorous quality control necessary.

3.3.2. Determination of the Theoretical Maximum Density

For each mixture, the theoretical maximum density (MMVT or TMD) was determined, a parameter essential for establishing the amount of material required during compaction, ensuring the production of specimens with similar air void content.

TMD represents the mass per unit volume that the mixture would reach under ideal conditions, meaning in the total absence of voids: a theoretical situation in which aggregates and binder completely fill the available volume. In practice, however, bituminous mixtures always present some residual porosity, which is why this value remains a theoretical reference.

The determination of TMD was carried out according to EN 12697-5, using the volumetric procedure [46], which involves the use of a pycnometer and the application of vacuum to remove the air trapped inside the mixture.

Material sampling was performed according to EN 12697-27 [47]. For the pycnometer test, the minimum mass of the sample was defined as fifty times the nominal maximum aggregate size, expressed in millimetres.

The material was initially heated to 110 ± 5°C until reaching a workable consistency; it was then disintegrated to reduce agglomerates to a size not exceeding 6 mm.

Once prepared, the material was subjected to quartering, as illustrated in BS EN 12697-38, to obtain two homogeneous and representative portions of the mixture.

For each mixture, at least two independent determinations were carried out, and the final TMD value was calculated as the average of the two measurements.

Below is a list of the equipment used to perform the test:

1. Deaerated water, i.e., water from which dissolved gases, particularly oxygen and nitrogen, have been removed.
2. Vacuum system capable of reaching a residual pressure ≤ 4 kPa.
3. Balance with a reading precision of 0.1 g.

4. Pycnometer equipped with a calibrated-volume cap, subjected to periodic calibration checks.

After listing the necessary equipment, a detailed explanation of the procedure to be followed in accordance with the current standard is provided:

1. After preparing a material sample (with mass of approximately 1600 g) as previously described, two empty pycnometers with known calibrated volume and their respective caps are weighed, and their mass is recorded, hereafter indicated as m_1.

2. After quartering the material, the two resulting dry samples are taken and introduced into the two pycnometers.

3. The mass of the pycnometer (with cap) containing the dry sample is recorded, hereafter indicated as m_2.

4. After removing the cap, deaerated water is added to a level approximately three fingers above the surface of the dry sample, taking care not to trap air during this operation.

5. Entrapped air is removed by applying vacuum down to ≤ 4 kPa for about 30 minutes, possibly assisted by vibration or agitation of the pycnometer every 2 minutes.

6. Once deaeration is completed, the pycnometer is completely filled with deaerated water and the cap is replaced.

7. Using a pipette, the cap volume is also filled with deaerated water until a water meniscus is formed.

8. The pycnometer is dried externally to remove any water droplets and the final mass is recorded, indicated as m_3.

The theoretical relationship used to define the theoretical maximum density is the following:

$$\rho_{mw} = \frac{m_2 - m_1}{10^3 \cdot V_p - \frac{m_3 - m_2}{\rho_w}}$$

where:

- ρ_{mw} is the theoretical maximum density of the bituminous mixture, expressed in $\mathrm{Mg/m^3}$.
- m_1 is the mass of the empty pycnometer including cap, expressed in g.
- m_2 is the mass of the pycnometer, including cap, filled with the dry bituminous mixture sample, expressed in g.

- m_3 is the mass of the pycnometer, including cap, filled with the mixture sample and deaerated water, expressed in g.
- V_p is the calibrated volume of the pycnometer, expressed in m^3.
- ρ_w is the density of water at the test temperature, expressed in Mg/m^3 and calculated using the following relationship:

$$\rho_w = 1.00025205 + \frac{7.59 \cdot t - 5.32 \cdot t^2}{10^6}$$

For greater clarity, explanatory images taken during the experimental phase are provided below.

Figure 22. Disintegration of the material

Figure 23. Quartering of the material

Figure 24. Weighing of the pycnometer, with known calibrated volume, and its cap, m_1.

Figure 25. Weighing of the pycnometer, its cap and the dry material sample, m_2.

Figure 26. Air removal

Figure 27. Weighing of the pycnometer, its cap, the sample and water filled to the meniscus, m_3.

Figure 28. Detail of the water meniscus

3.3.3. Sieve Analysis

Sieve analysis represents one of the fundamental steps in the characterization of bituminous mixtures, as it makes it possible to verify whether the aggregate size distribution falls within the design curves and the regulatory tolerances. The BS EN 933-1:2012 standard defines the reference method for determining the particle size distribution of aggregates through sieving.

In the case of bituminous mixtures, the test is generally carried out on aggregates extracted from the mixture or on virgin aggregates intended for production, with the aim of checking the granulometric conformity with the specification requirements.

The procedure begins with the preparation of the test sample. Starting from a representative sample of mixture or aggregate, a test portion is obtained with a mass suitable for the nominal maximum aggregate size, in accordance with the indications of the standard. It is essential that the sample is representative of the entire batch or mixture, which is why the sampling and material reduction phase plays a crucial role. In the case of bituminous mixtures, when the aim is to analyse only the aggregate grading curve, it is necessary to first extract the bituminous binder using appropriate methods (for example, solvent extraction or centrifuge), in order to obtain a clean aggregate free of bitumen residues that could affect the sieving process.

Once the material has been prepared, it is dried in an oven at a controlled temperature, generally equal to 110 ± 5 °C, until constant mass is reached, except for particular cases in which the standard provides alternative methods for aggregates sensitive to oven drying. The purpose of drying is to eliminate moisture and ensure that the measured mass corresponds solely to the solid fraction. After cooling to room temperature, the sample is weighed using a balance of adequate precision, recording the initial mass which will serve as the reference for calculating the passing and retained percentages.

The choice of the sieve series to be used depends on the nominal maximum aggregate size and the design specifications. BS EN 933-1:2012 refers to the nominal sieve openings defined in Part 2 of the same standard series, ensuring consistency between the mesh sizes used and the granulometric classes of interest. The sieves are arranged in a stack, from the largest to the finest, with a closed pan at the bottom to collect the smallest passing fraction. Before use, it is good practice to check the condition of the sieves, ensuring that the mesh is neither deformed nor clogged, so as not to alter the test result.

The dried sample is then evenly distributed on the top sieve, and the entire stack is subjected to mechanical or manual sieving for a sufficient time to ensure that the passage of material through the mesh is complete or at least stable. The standard provides indications on the minimum sieving time and on the criteria for determining when the test can be considered complete, for example by checking that the amount of material continuing to pass through a sieve within a defined time interval is negligible. In some cases, for aggregates containing a significant fine fraction, a preliminary washing of the sample on the finest sieve involved is required, to remove adhering particles and improve the accuracy of the determination of the passing fraction.

At the end of the sieving process, the material retained on each sieve and in the pan is collected and weighed separately. It is important to avoid material losses during transfer and weighing, as any discrepancies between the sum of the retained masses and the initial sample mass must remain within the narrow tolerance limits indicated by the standard for the test to be considered valid.

The difference between the initial mass and the sum of the retained masses constitutes an internal quality check on the correctness of the procedure. The next phase consists in calculating the particle size distribution. For each sieve, the retained mass and the corresponding percentage relative to the total sample mass are determined. From these values, the cumulative retained percentage and, by difference, the passing percentage at each sieve opening are calculated. The results are generally reported in tabular form and graphically represented on a semi-logarithmic diagram, in which the x-axis shows the particle diameter (on a logarithmic scale) and the y-axis the passing percentage. BS EN 933-1:2012 provides examples of test sheets and graphical representations of results, which can be used as references for drafting test reports.

In the context of bituminous mixtures, the resulting grading curve is compared with the design curve and with the acceptance limits specified in the technical requirements. A good correspondence between the experimental and theoretical curves indicates correct aggregate dosing and controlled production. Significant deviations may instead indicate problems in dosing, material segregation, sampling errors, or variations in aggregate supply. Since particle size distribution directly affects workability, compactability, stiffness, and durability of the bituminous mixture, sieve analysis is an essential tool both in mixture design and in production control.

Finally, the test report drafted according to BS EN 933-1:2012 must clearly include all the information necessary to correctly interpret the results: sample identification and source, test sample mass, sieve series used with their nominal openings, any washing operations, drying conditions, retained masses and passing percentages for each sieve, and any observations on anomalies encountered during the test.

Accurate documentation makes it possible to track over time the quality of aggregates used in bituminous mixtures and to correlate the mechanical response of the mixtures with their particle size characteristics, closing the loop between design, quality control, and in-service performance.

Figure 29. Sieve stack for performing the sieve analysis.

Figure 30. Sieve column mounted on a vibrating plate.

3.3.4. Evaluation of Binder Content

The ignition test plays a fundamental role in verifying the actual distribution of the binder coming from RAP, a particularly relevant aspect as it directly affects the homogeneity of the mixture and, consequently, its final performance.

During the process, the bitumen is oxidised and volatilised, while the aggregates remain unchanged. The mass loss recorded between the initial weight of the sample and the final weight, once combustion is complete, makes it possible to calculate the binder content.

To determine it, the reference standard was followed, which in this case is BS EN 12697-39 [38]. In particular, method B was used.

Below is a list of the equipment used to carry out the test:

1. Oven capable of reaching the test temperature, i.e. 540 °C, equipped with a ventilation system and filters to manage the fumes produced.
2. Balance with a reading precision of 0.1 g.
3. A perforated basket for containing the material and a collection tray for the residues (images will be shown below).

For the execution of the test, the minimum sample mass was defined according to the nominal maximum aggregate size, expressed in millimetres, following the indications of the standard.

Nominal maximum aggregate size mm	Mass of sample g	Maximum constant mass limit g
4	1 000 to 1 400	0,15
5,6 or 6,3 or 8 or 10	1 000 to 1 600	0,15
11,2 or 12,5 or 14 or 16	1 000 to 1 700	0,20
20 or 22,4	1 000 to 2 400	0,25
31,5	1 000 to 3 000	0,30
40 or 45	1 000 to 4 000	0,40

Table 8. Mass quantity for the ignition test (source: BS EN 12697 39)

The material was initially heated to 110 ± 5 °C until it reached a consistency suitable for processing; afterwards, it was broken down in order to reduce the agglomerates to a size not greater than 6 mm.

After listing the necessary equipment, a detailed explanation of the procedure to be followed in accordance with the current standard is now provided:

1. First, the oven is switched on and set to the temperature of 540 °C, since reaching this temperature requires at least one hour.
2. The mass of the metal basket, consisting of a lower plate and two shelves used for placing the material, is recorded; from now on it will be referred to as W_t.
3. The bituminous mixture sample is then placed inside the basket, taking care to distribute it evenly over the two shelves.
4. The mass of the basket and the sample, generally known as the "mass before ignition", is recorded and indicated as W_{t+s}.
5. Wearing the appropriate safety devices, the basket is inserted into the oven at the temperature indicated in point 1, until no further mass losses are detected.
6. The basket is removed from the oven and allowed to cool, placing it safely behind a suitable protective screen.
7. Once cooled, the mass of the basket and the sample, known as the "mass after ignition", is recorded and indicated as W_{t+m}.

The theoretical relation used to evaluate the initial mass of the sample is the following:

$$W_s = W_{t+s} - W_t$$

where:

- W_s is the initial mass of the bituminous mixture sample, expressed in g.
- W_{t+s} is the mass of the basket and the sample before ignition, expressed in g.
- W_t is the mass of the metal basket, expressed in g.

Before introducing the relation for determining the binder content, it is necessary to report the one relating to the final mass of the sample:

$$W_a = W_{t+a} - W_t$$

where:

- W_a is the final mass of the bituminous mixture sample, expressed in g.
- W_{t+a} is the mass of the basket and the sample after ignition, expressed in g.
- W_t is the mass of the metal basket, expressed in g.

In conclusion, the theoretical relation necessary for determining the binder content is the following:

$$B = \frac{(W_s - W_a)}{W_s} \cdot 100 - C_F$$

where:

- B is the total binder content, expressed as %.
- W_s is the initial mass of the bituminous mixture sample, expressed in g.
- W_a is the final mass of the bituminous mixture sample, expressed in g.
- C_F is the calibration factor, expressed as %.

An aspect that deserves particular attention concerns the definition of the calibration factor. It allows correcting the measured binder mass by excluding the amount of volatile material present in the aggregates that evaporates at the high test temperatures. In previous research activities [24], an average volatilisation equal to 0.23% was quantified, mainly attributable to retained water and other volatile components intrinsic to the aggregate.

In the specific case of mixtures produced in the plant, however, the question arises as to whether this contribution should actually be considered. The aggregates, in fact, undergo a pre-heating process that drastically reduces, if not eliminates, the presence of retained water at the moment of mixing. Consequently, the amount of mass that could volatilise during the ignition test is, under real operating conditions, negligible.

For this reason, and from a precautionary yet production-consistent perspective, a calibration factor equal to 0% was chosen. This choice reflects the assumption that the retained water has already been eliminated in the plant and that, therefore, there is no significant contribution to mass loss attributable to the aggregates during the ignition test.

Figure 31. Oven capable of reaching the test temperature, 540 °C

Figure 32. Perforated basket for containing the material and a collection tray for the residues

Figure 33. Mass of the basket and the sample before ignition, expressed in g, W_{t+s}.

Figure 34. Introduction of the basket, with material, into the oven

Figure 35. Mass of the basket and the sample after ignition, expressed in g, W_{t+a}.

Figure 36. Protective screen suitable to allow cooling the sample safely

3.3.5. Compaction of the Specimens

The compaction of the cylindrical specimens was carried out in accordance with the EN 12697-31 standard [48], using a gyratory shear press (Gyratory Compactor).

This equipment represents one of the most effective tools for reproducing in the laboratory the compaction conditions that occur on site. The rollers used in real operations, in fact, do not apply only a vertical load, but also generate shear stresses that significantly contribute to the densification of the bituminous layer. The gyratory shear press reproduces this combined action through two simultaneous movements:

- a constant static compression;
- a rotation of the axis of the specimen, which describes a conical surface of revolution, characterised by an inclination angle equal to 1.25° (2ϕ in the traditional geometric representation, Figure 37).

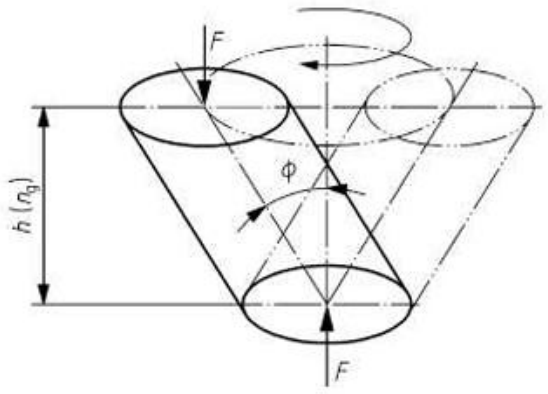

Figure 37. Representation of the action of a gyratory compactor (source: EN 12697-31)

During compaction, the machine applies a constant vertical stress equal to 600 kPa and a rotation speed of 30 revolutions/min. A dedicated software continuously records the height of the specimen at each rotation, allowing the compaction curve to be obtained, the workability of the mixture to be evaluated, and the air void content of the specimens to be determined. These data are essential for interpreting the behaviour of the mixture during the densification phase and for verifying compliance with regulatory requirements.

The diameter of the specimens was set at 150 mm, in relation to the Nmax value of the mixtures, while the maximum number of rotations was set at 200, in accordance with the indications of the Special Tender Specifications of the A4.

The compaction temperature was set at 150 ± 5 °C for mixtures containing unmodified bitumen and at 160 ± 5 °C for those with PmB, to ensure an adequate viscosity of the binder and proper workability of the mixture during the densification phase.

Below is a list of the equipment used to carry out the test:

1. Oven capable of reaching the predetermined compaction temperature.
2. Balance with a reading precision of 0.1 g.
3. Mould with appropriate metal inserts.
4. Filter paper sheets.
5. Scoop for inserting the required amount of material inside the mould.

After providing the theoretical background relating to compaction, the operational procedure is reported below, in accordance with the EN 12697-31 standard [48]:

1. The mould, with an internal diameter of 150 mm, together with its metal inserts, is placed inside the oven and brought to the compaction temperature.
2. The bituminous mixture to be compacted is placed in the oven so that it can also reach the predetermined temperature.
3. Once the compaction temperature is reached, a precise amount of bituminous mixture (the theoretical relation necessary for its determination is reported below) is placed inside the mould, positioning a filter paper sheet at the base.
4. The mould containing the material to be compacted is placed back in the oven so that the specimen can regain the temperature lost during the filling operations. The temperature of the material is checked from the outside using a calorimetric probe inserted into the core of the material.
5. Once the compaction temperature is reached, the mould is removed from the oven and a filter paper sheet and the final metal plate are placed on top of the surface of the material inside the mould using a magnet.
6. The mould is placed inside the appropriate housing of the gyratory shear press and fixed to the three clamps located inside the machine chamber. At this point, the compaction procedure is started, after setting the parameters of vertical pressure, specimen diameter and number of rotations.
7. Once the compaction operation is completed, the freshly compacted specimen is removed by extruding it from the mould using a hydraulic piston and left to cool for a sufficient time to allow handling.

Regarding the mass to be inserted into the mould, for each mixture under study, it was evaluated using the following relation:

$$M = \pi \frac{d^2}{4} \rho_{mw} \left(1 - \frac{v_{geo}}{100}\right)$$

where:

- M is the mass of mixture to be inserted inside the mould, expressed in g.
- d is the diameter of the final specimen and therefore the internal diameter of the mould, expressed in mm.
- v_{geo} is the target geometric air void content, expressed in %.

A target geometric air void content equal to 7% was set, to obtain, after compaction, an average real air void content close to 3.5%.

Figure 38. Mould with appropriate metal inserts and filter paper sheets

Figure 39. Positioning of the mould inside he appropriate housing of the gyratory shear press and fixing to the three clamps located inside the machine chamber

Figure 40. Insertion of the bituminous mixture inside the mould, positioning a filter paper sheet at the base

Figure 41. Removal of the freshly compacted specimen by extruding it from the mould using a hydraulic piston

The production of the prismatic specimens was carried out starting from slabs compacted by means of a roller compactor, in accordance with the EN 12697-33 standard [49]. The compaction operations were performed at the Iterchimica facility in Suisio (BG). The mixture, kept at the working temperature, was evenly distributed inside the mould and subsequently densified through controlled passes of the roller, adjusting the applied load and the number of passes in order to reach the predetermined level of air voids.

Once compacted, the slabs were cut to obtain prismatic specimens of the required dimensions, according to the indications of EN 12697-24 [37], using a guide manufactured at the Road Materials Laboratory of the Department of Engineering of Territory and Infrastructure of the Politecnico di Torino, an image of which is shown at the end of this paragraph. For this experimental campaign, a geometric air void content equal to 7% was imposed.

The use of the roller compactor makes it possible to reproduce in the laboratory compaction conditions very close to those that occur during laying and rolling on site, ensuring a high representativeness of the material tested in the subsequent mechanical tests.

Figure 42. Detail of a self-made guide used to properly cut the material slabs.

Figure 43. Detail of the cut

3.3.6. Determination of the Actual Dimensions of the Compacted Specimens

For the evaluation of the volumetric properties of the compacted bituminous mixtures, the actual dimensions of the specimens were determined following the procedures indicated in EN 12697-29 [50], which regulates the measurement methods for the samples.

In accordance with the provisions of the standard, cylindrical specimens were characterised by measuring the diameter at two mutually perpendicular points and the height at four positions distributed along the perimeter; the final values were obtained as the average of the respective measurements. The standard indeed requires that the measurements be carried out using instruments with a minimum precision of 0.1 mm and that the measurement points be chosen so as to capture any geometric irregularities.

About prismatic specimens, EN 12697-29 [50] prescribes that each main dimension—length, width and thickness—be obtained as the average of at least four measurements taken on opposite surfaces. This procedure makes it possible to obtain a more reliable representation of the geometry of the specimen, reducing the influence of imperfections due to cutting or compaction.

For greater clarity, some images are provided below.

Figure 44. Detail of the height measurement of a cylindrical specimen

Figure 45. Detail of the geometric dimensions measurement of a prismatic specimen

3.3.7. Determination of the Bulk Density of the Compacted Specimens

The determination of the bulk density of the specimens was carried out in accordance with the EN 12697-6 standard [51], which defines this parameter as the mass per unit volume of the sample, including air voids, measured at a known test temperature. The bulk density represents a fundamental element, together with the maximum theoretical density, for the evaluation of the air void content of compacted bituminous mixtures.

The bulk density was determined using the Saturated Surface Dry (SSD) procedure, prescribed by the standard for specimens characterised by a closed surface, dense-graded aggregate structure and low absorption capacity. This method requires the specimen to be saturated so that only the surface voids are filled with water, while the external surface must be carefully dried before weighing. EN 12697-6 [51] specifies that the SSD condition allows the exclusion from the calculation of the volume of open surface voids, thus obtaining a density value referring to an effective volume slightly smaller than the geometric one.

The use of the SSD procedure is particularly suitable for reliably estimating the effective voids of the specimens and, in the case of mixtures compacted with a gyratory press, for correlating density with the number of gyrations and deriving the corresponding compaction curve. The standard also emphasises the importance of using instruments with adequate resolution and maintaining constant temperature conditions during measurements, to ensure repeatability and comparability of results.

Below is the operational procedure, in accordance with EN 12697-6 [51]:

1. The mass of the dry specimen is recorded, hereafter referred to as m_1 and expressed in g.
2. The specimen is immersed in water for at least 30 minutes (rotating it every 5 minutes to promote the removal of air from the voids), leaving it in saturation until its mass reaches a constant value.
3. The temperature of the water is measured using an appropriate thermometer, and its density ρ_w is calculated with an approximation of 0.0001 $\mathrm{Mg/m^3}$.
4. After the saturation time has elapsed and after shaking the specimen one last time to ensure the removal of any remaining air bubbles, the mass of the specimen in water is measured, known as m_2 and expressed in g.
5. The specimen is then removed from the water, and its external surface is dried with a dry chamois cloth, to remove only the thin layer of water present on the outside without affecting the saturated voids.
6. Immediately afterwards, the mass of the saturated surface-dry specimen is recorded, known as m_3 and expressed in g.

The theoretical relation used to define the saturated surface-dry bulk density is the following:

$$\rho_{ssd} = \frac{m_1}{m_3 - m_2} \cdot \rho_w$$

where:

- ρ_{ssd} is the bulk density, expressed in $\mathrm{Mg/m^3}$.
- m_1 is the mass of the dry specimen, expressed in g.
- m_2 is the mass of the specimen immersed in water, expressed in g.
- m_3 is the mass of the saturated surface-dry specimen, expressed in g.
- ρ_w is the density of water at the test temperature, expressed in $\mathrm{Mg/m^3}$.

Images relating to the evaluation of the bulk density for both cylindrical and prismatic specimens are provided below.

Figure 46. Recording of the dry specimen mass, referred to as m_1.

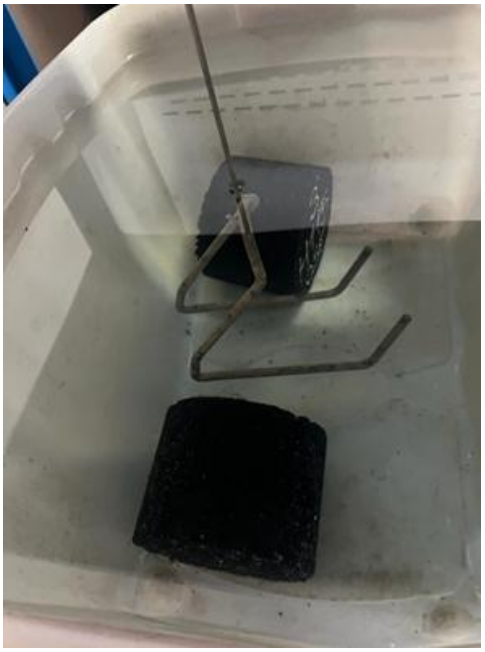

Figure 47. Immersion, in water, of the specimens

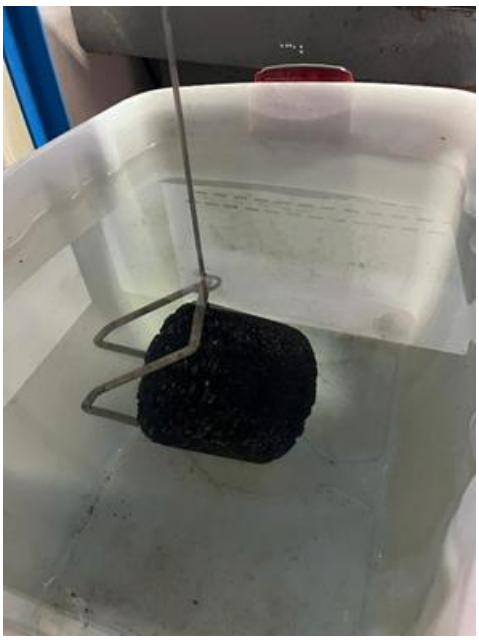

Figure 48. Recording of the specimen mass in water, known as m_2.

Figure 49. Drying of the specimen external surface with a dry chamois cloth

3.3.8. Determination of the Stiffness Moduli of the Compacted Specimens

The stiffness modulus is one of the most widely used indicators for assessing the response of the material to mechanical tensile loading and for estimating its ability to withstand elastic and viscoelastic deformations at different temperatures. The mechanical response of bituminous mixtures can be investigated through a wide range of experimental tests, which include configurations based on bending and tension, performed either in direct mode or through indirect loading.

In this thesis work, its determination was carried out according to the BS EN 12697-26 standard [52], adopting Annex C, which regulates the indirect tensile test on cylindrical specimens (IT-CY) under strain control. This methodology makes it possible to obtain consistent and comparable stiffness values, providing an effective measure of the response of the material under repeated loading conditions.

In parallel, for a more complete description of the mechanical behaviour, the complex modulus, often referred to in the literature as the dynamic modulus, was also evaluated through four-point bending tests (4PB-PR) on prismatic specimens, also conducted under deformation control.

The integration of the two experimental approaches, indirect tension and bending, makes it possible to capture more comprehensively the viscoelastic-plastic nature of the bituminous mixture, providing a complete picture of its stiffness and its evolution as loading and temperature conditions vary.

The procedures previously introduced will now be discussed in detail, first considering the Indirect Tensile Test and then Four-Point Bending Test.

The Indirect Tensile Test, carried out according to the prescriptions of EN 12697-26 [52], as previously mentioned, is based on the application of a vertical load along a diametral plane of the cylindrical specimen. Although the load is compressive in nature, the configuration induces, due to the Poisson effect, a stress state predominantly in tension along the horizontal diameter, where the displacements required for the calculation of the modulus are measured.

To ensure the proper development of mechanical properties, the cylindrical specimens are stored for 14 days before performing the test. In this thesis work, both for the volumetric samples compacted at Nmax and for the specimens compacted at Ndesign (120 gyrations) intended for fatigue tests, the counting of the days starts from the moment of cutting, which is necessary to obtain the height prescribed by the standard.

The standard also establishes an admissible height range depending on the maximum aggregate size: in the present study, specimens of 60 ± 2 mm were used. Before the test, each sample is conditioned for 4 hours at the test temperature, to stabilise the viscoelastic response.

Maximum grain size mm	Specimen diameter mm	Specimen height mm
≤ 16	100 ± 3 150 ± 3	40 to 60 ± 2
> 16 to < 32	150 ± 3	60 ± 2
≥ 32	150 ± 3	90 ± 2

Table 9. Admissible specimen heights for performing the stiffness test (source: EN 12697-26)

The execution of the test was carried out using the UTM 30 system, equipped with an actuator capable of applying load pulses with a controlled waveform and with a specific frame for indirect tension. Two LVDT displacement transducers, mounted diametrically in the horizontal position, record the recoverable diametral deformation induced by the load.

The applied pulse has a haversine shape, chosen to simulate the passage of a single wheel, and is delivered to reach the peak within a time between 50 and 125 ms, as required by the standard. The load intensity is adjusted so that the maximum imposed horizontal displacement is equal to 11.2 μm, keeping the material response within the linear viscoelastic range. Each pulse is followed by an interval of approximately 3 seconds, necessary to allow the complete recovery of the deformation.

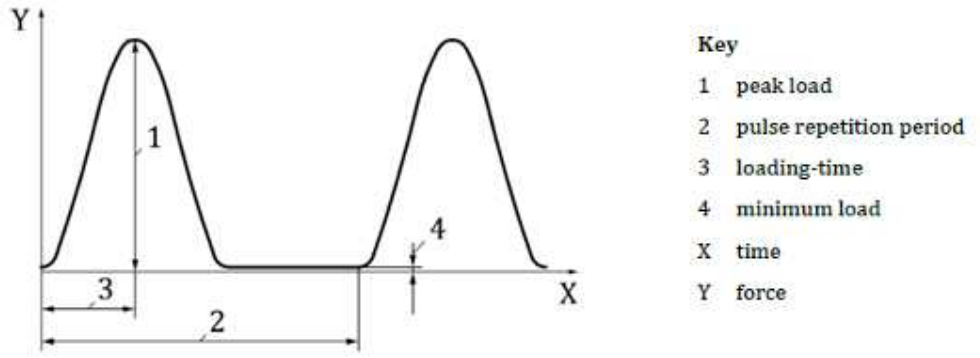

Figure 50. Shape of the applied load pulse (source: EN 12697-26)

Once the specimen has been positioned in the loading frame and symmetrically tightened using a torque wrench, the machine applies a preliminary series of 10 pulses, used to calibrate the load level required to reach the target displacement. Subsequently, 5 valid pulses are applied, from which the stiffness modulus is obtained as the average value.

Once this first phase is completed, the specimen is rotated by 90° ± 10° around its horizontal axis and the procedure is repeated. The standard requires that the average value obtained in the second series falls within +10% and −20% of the average of the first series. Only in this case is the final modulus calculated as the mean of the two results; otherwise, the test must be repeated.

After describing the test procedure, the theoretical relation used to define the stiffness modulus is reported below, derived from elasticity theory for a disc compressed diametrically:

$$E = \frac{F \cdot (\nu + 0.27)}{z \cdot h}$$

where:

- E is the stiffness modulus, expressed in MPa.
- F is the peak value of the applied vertical load, expressed in N.
- z is the amplitude of the resilient horizontal deformation obtained during the loading cycle, expressed in mm.
- h is the average of the four height measurements recorded at diametrically opposite points as described in paragraph 3.3.6, expressed in mm.
- ν is the Poisson's ratio, for which a conventional value of 0.35 is assumed for bituminous mixtures under standard test conditions.

Figure 51. The UTM-30 system

Figure 52. Execution of the test in the IC-CY configuration

The determination of the dynamic modulus of bituminous mixtures through four-point bending tests on prismatic beams represents one of the reference methods prescribed by EN 12697-26 [52], Annex B, for the characterization of stiffness in the linear viscoelastic regime.

In this configuration, the specimen is modelled as a beam supported on four supports: two external reaction supports and two internal loading supports, arranged to generate, in the region between the load application points, an almost constant bending moment field free from shear forces. It is precisely in this "pure moment" region that the vertical deformation (deflection) is measured, allowing the dynamic modulus to be derived under conditions that are well defined from both a mechanical and kinematic standpoint.

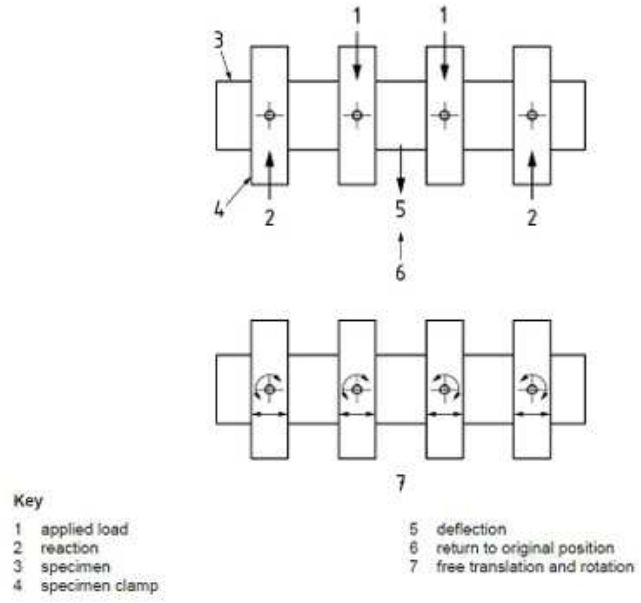

Figure 53. Configuration of the 4PB-PR test (source: EN 12697-26)

For the execution of the 4PB-PR tests, the UTM 16 system was used, equipped with a servo-pneumatic actuator capable of applying controlled sinusoidal loads. The four-point loading frame accommodates prismatic beams with a cross-section of approximately 50×50 mm and a variable length between 410 mm and 440 mm, dimensioned in accordance with the geometric requirements of the standard to ensure an adequate ratio between the test span and the height of the section.

At the centre of the beam, a high-resolution displacement transducer is positioned, which measures the vertical deflection in the constant-moment region. The entire system is placed inside a climatic chamber, which ensures the maintenance of the prescribed test temperature, an essential condition for the correct viscoelastic characterization of the material.

The beams are placed on the loading frame and cyclically loaded at the internal supports, according to a four-point bending scheme compliant with EN 12697-26 [52]. The test is conducted in deformation control, imposing a maximum flexural strain amplitude equal to 50 μm/m, chosen to keep the response of the mixture within the linear viscoelastic range and to prevent progressive damage phenomena.

The applied load has a sinusoidal waveform and is repeated over a wide range of frequencies: 0.1 Hz, 0.2 Hz, 0.5 Hz, 1 Hz, 2 Hz, 5 Hz, 10 Hz, 20 Hz and again 0.1 Hz. This sequence makes it possible to construct the stiffness curve as a function of frequency (and, by analogy, of loading time), highlighting the viscoelastic nature of the material and its sensitivity to the strain rate.

The final repetition of the test at the frequency of 0.1 Hz has a control scope: the modulus values obtained at the end of the cycle must be comparable with those measured at the beginning, to exclude the occurrence of significant damage during the test. From a theoretical point of view, the dynamic modulus $E^*$is derived from the ratio between the amplitude of the bending stress and that of the strain, considering the possible phase shift between the two quantities (phase angle), typical of viscoelastic materials. The 4PB-PR test, configured in this way, therefore makes it possible to obtain a detailed description of the dynamic behaviour of the bituminous mixture, providing fundamental data for the structural modelling of pavements and for the performance comparison between different mixture formulations.

Figure 54. The UTM-10 system

In conclusion, regardless of the test configuration adopted, the stiffness modulus provides a fundamental indicator of the ability of the mixture to withstand traffic-induced deformations. High values are generally associated with greater resistance to rutting, as they limit the accumulation of permanent deformations; however, excessively high stiffness may promote low-temperature cracking, due to the high restraint stresses that develop when thermal movements are prevented.

3.3.9. Determination of the Indirect Tensile Strength

The indirect tensile strength (ITS) represents one of the fundamental parameters for assessing the ability of a bituminous mixture to withstand tensile stresses, which are particularly relevant in thermal and fatigue cracking phenomena. In the BS EN 12697-23 standard [53], it is defined as the maximum tensile stress calculated from the maximum load applied to a cylindrical specimen loaded diametrically to failure under the specified test conditions.

The test is based on the same mechanical principle that characterises the IT-CY configuration for stiffness: a vertical compressive load applied along the diameter of the specimen generates, due to the Poisson effect, a tensile stress state in the horizontal direction. Failure therefore occurs by indirect tension, allowing the estimation of the ability of the material to resist stresses that tend to open the section of the specimen.

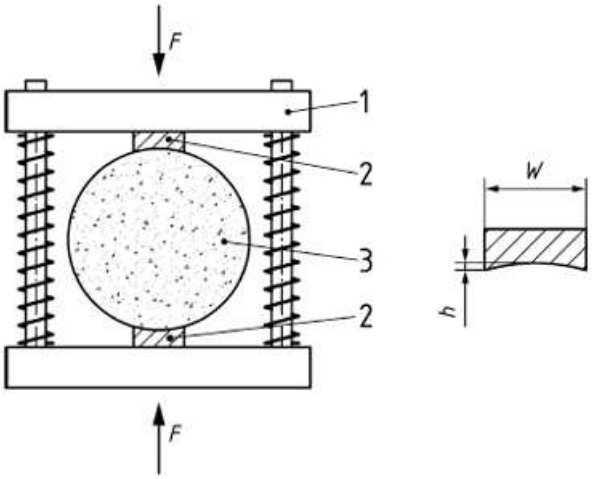

Key

1	testing head
2	loading strips
3	specimen
W	Width of the loading strip
h	Maximum height difference at the curved side of the loading strip
F	load

Figure 55. Configuration of the ITS test (source: EN 12697-23)

The standard establishes that the cylindrical specimens intended for the ITS test must have an age between 48 hours and 42 days and that, before execution, they must be kept at the test temperature, equal to 25 °C ± 2 °C, for a minimum period of four hours.

It is also required that the dimensions of the samples fall within the prescribed tolerances, to ensure a stress distribution consistent with theoretical models and guarantee the comparability of results. These geometric limits are the same as those adopted and introduced in the previous paragraph relating to the determination of the stiffness modulus.

Proper thermal conditioning represents an essential step, as it allows stabilisation of the viscoelastic response of the mixture and reduces variability linked to temperature-dependent effects.

Once the preparation phase is completed, the specimen is placed inside the loading frame in a carefully symmetrical manner, verifying that the loading strips are perfectly aligned along the vertical diameter. The sample is then positioned under the loading actuator. The deformation rate must remain constant and equal to 50 mm/min, as prescribed by BS EN 12697-23; this relatively high value allows failure to be reached in a short time, limiting the influence of viscous phenomena and enabling a clearer assessment of the tensile behaviour of the material.

During execution, the acquisition system continuously records the vertical displacement of the actuator, the applied load and the duration of the test. The maximum load value reached immediately before failure constitutes the fundamental datum for calculating the indirect tensile strength, obtained through the formula derived from elasticity theory for a disc subjected to diametral compression.

The standard also provides a classification of failure modes, useful for assessing the correctness of the test and the reliability of the result. Pure tensile failure appears as a well-defined fracture along the diameter and is considered the ideal condition. In other cases, the specimen may show diffuse deformation without a clear fracture line, indicating behaviour dominated by plastic or viscous phenomena; or it may exhibit a combined failure, characterised by a partial fracture accompanied by large deformed areas near the loading strips. Accurate identification of the failure mode is essential, as any anomalies may indicate positioning errors, specimen defects or inadequate test conditions.

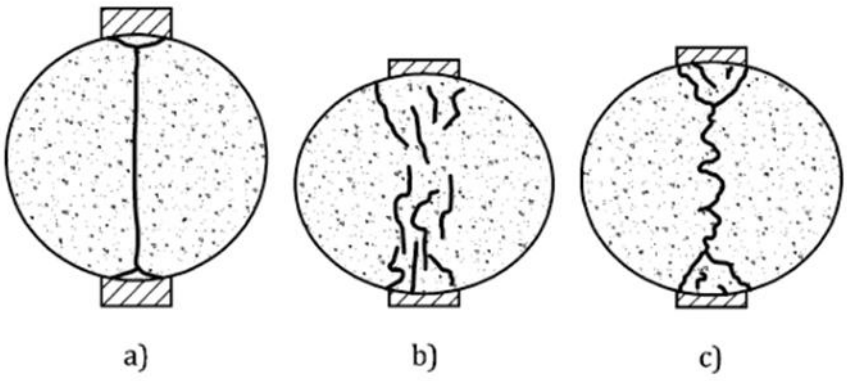

Figure 56. Failure modes of the ITS test (source: EN 12697-23)

After describing the test procedure, the theoretical relation used to define the indirect tensile strength is reported below:

$$ITS = \frac{2P}{\pi\, D\, h} \cdot 1000$$

where:

- ITS is the indirect tensile strength, expressed in kPa.
- P is the peak value of the applied vertical load, expressed in N.
- D is the average of the two diameter measurements recorded as described in paragraph 3.3.6, expressed in mm.
- h is the average of the four height measurements recorded at diametrically opposite points as described in paragraph 3.3.6, expressed in mm.

In conclusion, the indirect tensile strength thus determined provides valuable indications on the ability of the mixture to withstand stresses that tend to open the section of the material, such as those generated by low-temperature thermal contractions, repeated loading cycles that promote the formation of microcracks, or tensile stresses that develop in the lower part of flexible pavements.

High ITS values are generally associated with good internal cohesion and an effective bond between bitumen and aggregates; however, excessively high strength may reflect an overly stiff mixture, potentially more vulnerable to thermal cracking phenomena.

Figure 57. ITS testing system

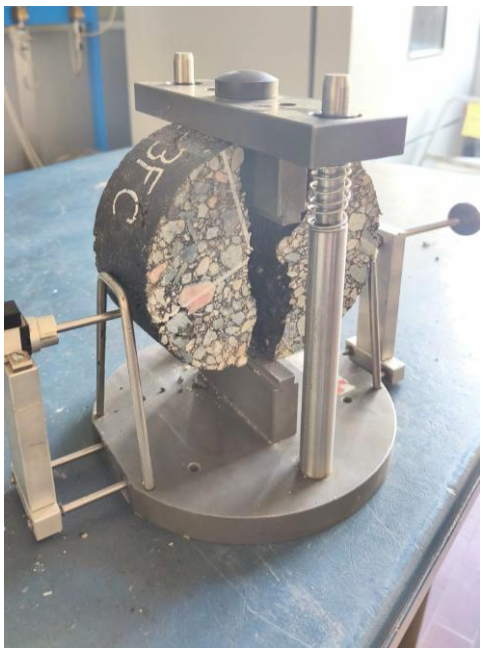

Figure 58. Failure mode of the specimen

Figure 59. Detail of the fracture of a specimen after the ITS test.

3.3.10. Determination of Fatigue Resistance

The evaluation of the fatigue resistance of bituminous mixtures represents a fundamental step for understanding their long-term behaviour and their tendency to crack under repeated loading.

BS EN 12697-24 [37] defines fatigue as the progressive reduction of the resistance capacity of a material when subjected to cyclic stresses, compared with the resistance it would exhibit under a single load. In the case of flexible pavements, this phenomenon is closely linked to the formation and propagation of microcracks induced by traffic, which over time may evolve into significant structural damage.

To fully characterise the fatigue behaviour of bituminous mixtures, the standard provides several test configurations, each capable of capturing specific aspects of the viscoelastic response and the damage mechanism. Among these, the most widespread are the four-point bending test on prismatic beams, conducted in deformation control, and the cyclic indirect tensile test on cylindrical specimens, performed in load control without rest periods. Although based on different mechanical principles, the two configurations allow the analysis of cracking resistance under stress conditions representative of the actual stress states that develop in the bituminous layers of a pavement.

In the following paragraphs, the experimental procedures adopted for both specimen types will be described in detail, highlighting the operational steps and the theoretical relations required.

The cyclic indirect tensile test on cylindrical specimens (CIT-CY) is performed in accordance with Annex F of EN 12697-24 [37]. In this configuration, the

cylindrical specimen, generally compacted at 120 gyrations (Ndesign) with a target height of 60 mm, is subjected to a cyclic sinusoidal compressive load applied along the vertical diameter, in stress control, without rest periods.

Maximum grain size mm	**Specimen diameter** Ω mm	**Specimen height** h mm
≤ 16	100 ± 3	40 ± 2
> 16 to < 32	150 ± 3	60 ± 2
≥ 32	150 ± 3	90 ± 2

Table 10. Geometric dimensions of the specimen required for the CIT-CY test (source: EN 12697-24)

Although the load is compressive in nature, the stress state that develops in the material is one of indirect tension along the horizontal diameter, with a biaxial stress field at the centre of the specimen, characterised by horizontal tension and vertical compression.

Before performing the tests, the specimens are conditioned for 4 hours at the test temperature, equal to 20 °C, in accordance with the standard. The stress level to be applied is defined starting from the stiffness modulus previously determined according to EN 12697-26 [52], to ensure that the amplitude of the initial tensile strain falls within the range between 25 and 100 μm/m and that the fatigue life lies between 10^3 and 10^6 load cycles. The loading frequency is equal to 10 Hz, chosen to simulate traffic conditions corresponding to a speed of approximately 80 km/h. The stress state is therefore calibrated as a function of the mixture stiffness and the Poisson's ratio, assumed equal to 0.35, to obtain strain–stress levels consistent with the linear viscoelastic field and with the desired fatigue-life range.

$$S_{mix,n} = \frac{\sigma_a}{\varepsilon_a} \cdot (1 + 3\nu) \cdot 10^6$$

where:

- $S_{mix,n}$ is the stiffness modulus at the n-th cycle, expressed in MPa.
- σ_a is the amplitude of the tensile stress at the centre of the specimen, expressed in kPa.
- ε_a is the amplitude of the horizontal strain at the centre of the specimen, expressed in $\mu m/m$.
- ν is the Poisson's ratio, for which a conventional value of 0.35 is assumed for bituminous mixtures under standard test conditions.

Operationally, the procedure requires the bonding of metal supports along the thickness of the specimen at two diametrically opposite points, on which the horizontal displacement transducers (LVDTs) are mounted. The sample is then

symmetrically fixed inside the loading frame and, once the transducers are calibrated, the test begins in stress control. The applied sinusoidal load generates a horizontal displacement that can be described as the sum of a mean component, a cyclic component of defined amplitude, and a time-increasing term associated with permanent viscoplastic deformations.

$$u(t) = u_m + u_a \cdot \sin(2\pi f t + \varphi) + u_d \cdot t$$

where:

- $u(t)$ is the horizontal displacement measured by the transducers over time, expressed in mm.
- u_m is the mean component of the horizontal displacement, expressed in mm.
- u_a is the maximum amplitude of the horizontal displacement induced by the sinusoidal load, expressed in mm.
- u_d is the time-increasing horizontal displacement term associated with permanent viscoplastic deformations, expressed in mm.
- f is the loading frequency, expressed in Hz.
- φ is the phase angle between load and displacement, expressed in degrees.

The maximum amplitude of the initial tensile strain is conventionally evaluated as the average value of the strains measured between the 90th and 100th cycle, to exclude primary settlement effects, and is defined by the following theoretical relation:

$$\varepsilon_a = \left(\frac{2\,u_a}{\Omega}\right) \cdot \left[\frac{1+3\nu}{4+\pi\nu-\pi}\right] \cdot 10^6$$

where:

- ε_a is the maximum amplitude of the horizontal strain at the centre of the specimen, expressed in μm/m.
- u_a is the maximum amplitude of the horizontal displacement induced by the sinusoidal load, expressed in mm.
- Ω is the specimen diameter, expressed in mm.
- ν is the Poisson's ratio, assumed equal to 0.35 for bituminous mixtures under standard test conditions.

In the CIT-CY configuration, the tensile strain at the centre of the specimen is assumed equal to twice the maximum amplitude of the cyclic strain, from which

the working point in the bi-logarithmic strain–number of cycles to failure plane is defined.

$$\Delta\varepsilon = 2\,\varepsilon_a$$

For each mixture, at least three repetitions are performed for each of the three selected strain–stress levels, to obtain a sufficiently robust distribution of experimental data.

Once the initial applied stress is known, the horizontal displacements and the corresponding strain are measured, and the number of cycles required to reach failure is recorded, it is possible to identify a series of points in the plane relating strain to fatigue life. By interpolating these points, the so-called fatigue line is obtained, which allows the performance of the mixture to be described and simulated, in particular to determine the strain corresponding to a reference life of one million cycles (ε_6).

The definition of fatigue life may be based on different criteria provided by BS EN 12697-24, including the 50% reduction of the initial modulus, the Energy Ratio, and complete specimen failure; in all cases, the initial stiffness is taken as the average of the values recorded between the 90th and 100th cycle, so as to ensure a consistent and repeatable evaluation of the long-term behaviour of the bituminous mixture.

In the four-point bending tests conducted in strain control, each mixture was tested by setting different initial strain levels, chosen to cover a fatigue-life range extending approximately from 10^4 up to about $2 \cdot 10^6$ load cycles. The loading frequency was kept constant at 10 Hz, to reproduce dynamic loading conditions consistent with those prescribed by the standard.

Before execution, the prismatic beams are stabilised at the test temperature (20 °C) inside a climatic chamber, then positioned in the loading frame, where the internal and external supports are arranged in perfectly symmetrical positions.

The load is applied through a vertical sinusoidal force at the two internal points, while the external supports remain fixed. This configuration allows the central portion of the beam to work under constant bending moment conditions, generating a uniform deformation along the section between the loading points. In this region, the specimen is subjected to pure bending: the lower fibres are in tension, while the upper fibres are compressed. This is a one-dimensional stress state that faithfully reproduces the conditions which, in flexible or semi-rigid pavements, promote bottom-up cracking.

The choice of strain control reflects the behaviour of thinner and more ductile bituminous layers, in which the strain at the base of the layer is governed mainly by the stiffness of the underlying layers. Moreover, the fact that the maximum tensile stress is not concentrated at a single point but distributed uniformly in the central region allows a more representative evaluation of the average properties of the mixture, reducing the influence of possible local heterogeneities.

During the test, the progressive reduction of the stiffness modulus as the number of applied cycles increases is monitored. The fatigue life N_f was determined by adopting two criteria provided by the standard: the 50% reduction of the initial modulus, calculated as the average of the values recorded between the 98th and 102nd cycle, so as to eliminate settlement effects, and the Energy Ratio criterion, which takes into account the evolution of the dissipated energy during damage.

4. Analysis of the experimental results

In this chapter, the results obtained within the experimental campaign will be analysed and discussed, carried out according to the operational procedures described in the previous chapter and in full compliance with the current technical standards. The aim is to critically understand the performance of the different bituminous mixtures investigated, highlighting the main trends that emerged from the laboratory tests.

For this purpose, in addition to the presentation of the experimental data, direct comparisons between the mixtures are proposed, also using statistical analysis tools, useful for assessing the significance of the observed differences and supporting a more robust interpretation of the results.

Finally, with reference to the performance limits prescribed by the Technical Specifications of the A4 motorway for each parameter considered, an attempt will be made to evaluate the actual production feasibility of mixtures containing high percentages of RAP and recycled plastics, with particular attention to performance aspects and operational implications for their possible adoption in the plant.

4.1. Maximum theoretical density

For each mixture, as illustrated in paragraph 3.3.2., the theoretical maximum density (TMD) was determined, a fundamental parameter for defining the amount of material to be used during compaction and thus ensuring the production of specimens with comparable air-voids contents. The TMD represents the mass per unit volume that the mixture would reach under ideal conditions, that is, in the complete absence of voids: a theoretical configuration in which aggregates and binder fully occupy the available volume.

In addition to the experimental determination, an analytical estimation of the TMD was also carried out, in accordance with the prescriptions of EN 12697-5 [46]and in continuity with the previous doctoral work [24]. It was obtained from the bulk densities (derived from the doctoral study [24]) and the weight percentages of the individual components of the mixture according to the mix design. The integration between experimental and analytical approaches provides a more complete framework and allows verification of the internal consistency of the data, an essential element for a correct interpretation of the results in the subsequent phases of the analysis.

From a theoretical point of view, the analytical evaluation of the TMD is performed using the following theoretical relation:

$$\rho_{mc} = \frac{100}{\sum_i \frac{p_i}{\rho_i}}$$

where:

- ρ_{mc} is the analytical form of the mixture TMD, expressed in Mg/m^3.
- p_i is the percentage of the *i-th* component with respect to the total weight of the mixture, expressed in %.
- ρ_i is the bulk density of the i-th component of the mixture, expressed in Mg/m^3.

In the following table, the analytical evaluations of the TMD for each investigated mixture are reported:

Component	ρ	MIX50 1	MIX50 2	MIX50 3	MIX50 REF
	[Mg/m^3]	[%]	[%]	[%]	[%]
Sand 0/5	2.780	26.304	26.249	26.194	26.387
Gravel 8/16	2.849	9.826	9.805	9.785	9.857
Gravel 16/22	2.813	10.802	10.780	10.757	10.836
RAP 0/12 (virgin aggregates basis)	2.765	28.560	28.500	28.440	28.650
RAP 0/20 (virgin aggregates basis)	2.774	19.040	19.000	18.960	19.100
Filler	2.730	0.668	0.666	0.665	0.670
RAP 0/12 binder	1.000	1.557	1.553	1.550	1.561
RAP 0/20 binder	1.000	0.790	0.789	0.787	0.793
Virgin binder	1.000	2.004	2.009	2.014	1.996
Polymer	0.600	0.300	0.500	0.700	0.000
Rejuvenator	1.000	0.150	0.150	0.149	0.150
ρ_{mc} [Mg/m^3]		2.552	2.535	2.518	2.578

Figure 60. Analytical TMD calculation for each investigated mixture.

After presenting the results in analytical terms of the maximum theoretical density, the TMD values obtained from the experimental campaign are reported below, following the procedure described in detail in paragraph 3.3.2.

Iteration	MIX50 1	MIX50 2	MIX50 3	MIX50 REF
Sample 1	2.572	2.549	2.556	2.577
Sample 2	2.576	2.545	2.55	2.568
Sample 3	2.568	2.548	-	2.592
Sample 4	-	-	-	2.592
Repeatability	0.008	0.004	0.006	0.009
ρ_{mw} [Mg/m^3]	2.572	2.547	2.553	2.583

Figure 61. Experimental TMD values for each mixture.

First, it should be noted that the values reported in the table represent mean values obtained from at least three repetitions for each mixture. This choice complies with the prescriptions of the reference standard BS EN 12697-5 [64], which, in addition to defining the minimum amount of material to be used for each test ("loose samples shall have a mass, expressed in grams, of at least 50 times the numerical value of the nominal maximum particle size of the aggregates in millimeters with a minimum of 250 g"), also requires an adequate level of repeatability of the data. In this specific case, considering a nominal maximum particle size of 16 mm, the minimum required mass is equal to 800 g.

The standard also states that, under same operator and same apparatus conditions, repeatability shall not exceed 0.011 Mg/m³. However, it is important to correctly interpret this requirement. With reference to the previous table, and in particular to the results related to the MIX50 REF mixture, it should be remembered that the repeatability limit applies exclusively to tests carried out under the same experimental conditions.

Consequently, it may happen that two pairs of tests, each internally characterised by a repeatability compliant with the standard, show significant differences when compared with each other, especially if performed on different days or under slightly varied operating conditions. This does not imply that such tests should be discarded: the observed variation falls within normal experimental fluctuations and does not compromise the overall validity of the results.

Compliance with this requirement ensures the reliability of the measurements and allows the use of the obtained averages as representative values of the behaviour of the different mixtures analysed.

$$r = 2.77 \cdot \sigma_r = 0.011 \text{ Mg/m}^3$$

where:

- r is the repeatability of the data, assumed equal to 0.011 Mg/m^3 when water is used.
- σ_r is the standard deviation, assumed equal to 0.007 Mg/m^3 water is used.

Below, a direct comparison is presented, in tabular form, between the analytical value of the TMD (ρ_{mc}) and the corresponding experimental value (ρ_{mw}) for each mixture.

	MIX50 1	MIX50 2	MIX50 3	MIX50 REF
ρ_{mc} [Mg/m^3]	2.552	2.535	2.518	2.578
ρ_{mw} [Mg/m^3]	2.572	2.547	2.553	2.583

Table 11. Direct comparison between the analytical and experimental TMD values for each mixture analysed.

As highlighted by the results reported in the previous table, significant differences can be observed between the analytical and experimental TMD values. It is important to underline that these differences mainly derive from the fact that the RAP used for defining the mix designs — employed years ago during the doctoral work [24] — came from the milling of a motorway section in the Valle d'Aosta, while the exact origin of the RAP actually used in the plant for producing the analysed mixtures is not precisely known.

A similar consideration applies to the virgin aggregates: it is likely that the batch used during the mix-design phase does not coincide with the one used in the current plant production. Differences in the starting materials, even if minimal, can significantly influence the bulk density of the individual components and, consequently, the analytically calculated TMD.

In light of these considerations, it is advisable to rely on the experimental TMD values, while the comparison with the analytical values should be interpreted only as an order-of-magnitude assessment and not as a precise or conclusive verification. Nevertheless, this comparison remains useful for evaluating the general consistency of the mixtures' behaviour, even though it cannot be considered strictly significant.

4.2. Sieve Analysis

In this paragraph, the experimental results of the sieve analysis carried out on each mixture are presented. For a detailed description of the adopted procedure, the underlying theoretical principles, and the related normative references [1], reference is made to paragraph 3.3.3.

It should be specified that the reported grading curves were obtained as the average of two repetitions for each mixture, in order to ensure a more stable and reliable representation of the particle-size distribution of the materials.

Below, the experimental results obtained for each mixture are reported, together with the corresponding limits prescribed by the Technical Specifications, to allow an immediate evaluation of the grading conformity with respect to the design requirements.

Starting from the analysis of the mixtures named MIX50 1, MIX50 2 and MIX50 3, all characterised by a RAP content of 50% and by the addition of polymer compound in increasing dosages (0.3%, 0.5% and 0.7%), produced through the hybrid methodology, the grading limits prescribed by the Technical Specifications of the A4 motorway are reported. These limits refer to a bituminous mixture intended for the binder layer, with neat bitumen and polymers for dry modification (PMA), as indicated on page 86 of the specifications.

Sieve size	Minimum passing	Maximum passing
[mm]	[%]	[%]
31.5	100	100
20	100	100
16	90	100
12.5	65	85
8	52	70
4	35	55
2	25	40
0.5	10	23
0.25	6	15
0.063	4	10
0	0	0

Table 12. Gradation limits prescribed by the A4 special specifications.

With specific reference to the MIX50 1 mixture, the corresponding grading curve is presented below, together with the values of the two repetitions in tabular form. The points where the experimental curve deviates from the limits imposed by the above-mentioned specification are also highlighted, to allow an immediate evaluation of the grading conformity of the mixture.

MIX50 1	Sample 1			Sample 2			Average
Sieve size	Sieve mass	Sieve+soil	Passing	Sieve mass	Sieve+soil	Passing	Passing
[mm]	[g]	[g]	[%]	[g]	[g]	[%]	[%]
31.5	1298.8	1298.8	100.0	1298.9	1298.9	100.0	100.0
20	1317.4	1350.4	96.8	1317.4	1364.9	95.5	96.2
16	1302	1425.8	85.0	1302	1352.9	90.6	87.8
12.5	1183.2	1263.2	77.4	1183.3	1329.9	76.6	77.0
8	1070.2	1174.5	67.4	1070.2	1173.6	66.8	67.1
4	1107.9	1413.9	38.1	1107.8	1424.2	36.6	37.4
2	980.1	1115	25.2	980.1	1111.1	24.1	24.7
0.5	784.3	893.4	14.8	784	886.9	14.3	14.5
0.25	726.5	765.4	11.0	726.7	764.9	10.7	10.8
0.063	767.7	816.4	6.4	767.7	815.8	6.1	6.2
0	724.4	726.4	0.0	895.2	897.3	0.0	0.0
Total	11262.5	10944.4	-	11433.3	12420.4	-	-

Table 13. Average gradation passings of the MIX50 1 mixture.

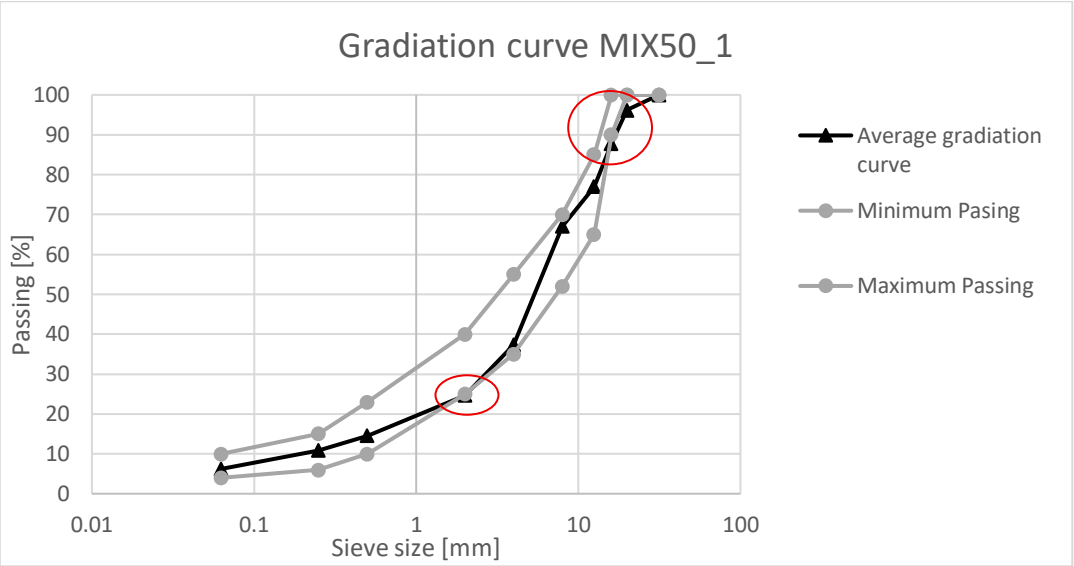

Figure 62. Gradiation curve MIX50 1

Similarly, the results obtained for the mixture named MIX50 2 are reported below.

MIX50 2	Sample 1			Sample 2			Average
Sieve size	Sieve mass	Sieve+soil	Passing	Sieve mass	Sieve+soil	Passing	Passing
[mm]	[g]	[g]	[%]	[g]	[g]	[%]	[%]
20	1317.4	1317.4	100.0	1317.4	1317.4	100.0	100.0
16	1302.1	1321.4	98.3	1302.1	1355	95.4	96.9
12.5	1183.3	1309.7	87.2	1183.3	1242.4	90.3	88.8
8	1070.1	1171.5	78.3	1070.1	1178.3	81.0	79.6
4	1107.7	1523.6	41.7	1107.8	1539.3	43.8	42.7
2	980.1	1152.2	26.6	980.4	1160.8	28.2	27.4
0.5	783.6	911.3	15.3	784	924.2	16.1	15.7
0.25	726.4	772.9	11.3	726.5	775.8	11.8	11.6
0.063	767.1	824.1	6.2	767.4	827.8	6.6	6.4
0	724.4	731.6	0.0	724.3	727.9	0.0	0.0
Total	9962.2	11035.7	-	11433.3	12420.4	-	-

Table 14. Average gradation passings of the MIX50 2 mixture.

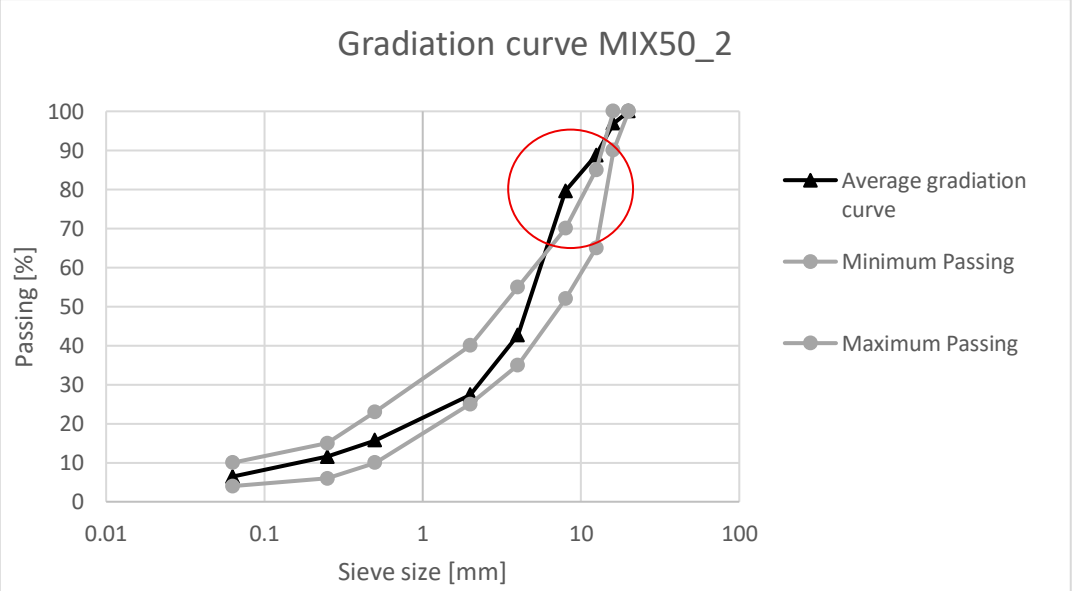

Figure 63. Gradiation curve MIX50 2

Finally, the results of the mixture named MIX50 3 are reported.

MIX50 3	Sample 1			Sample 2			Average
Sieve size	Sieve mass	Sieve+soil	Passing	Sieve mass	Sieve+soil	Passing	Passing
[mm]	[g]	[g]	[%]	[g]	[g]	[%]	[%]
31.5	1299	1299	100.0	1299	1299	100.0	100.0
20	1317.4	1370.7	94.9	1317.3	1355	96.4	95.7
16	1302	1344.2	90.9	1302	1399.8	87.2	89.1
12.5	1183.3	1294.7	80.4	1183.2	1320.3	74.2	77.3
8	1070.2	1212.6	66.8	1070.1	1188.2	63.1	65.0
4	1107.8	1422.8	36.9	1107.9	1416.2	34.0	35.4
2	980	1117.4	23.9	979.9	1099.4	22.7	23.3
0.5	783.7	885.8	14.2	783.8	880.9	13.5	13.8
0.25	726.3	764.8	10.5	726.4	763	10.0	10.3
0.063	767.5	813.8	6.1	767.6	811.4	5.9	6.0
0	724.4	728.6	0.0	895.2	899	0.0	0.0
Total	11261.6	12254.4	-	11432.4	12432.2	-	-

Table 15. Average gradation passings of the MIX50 3 mixture.

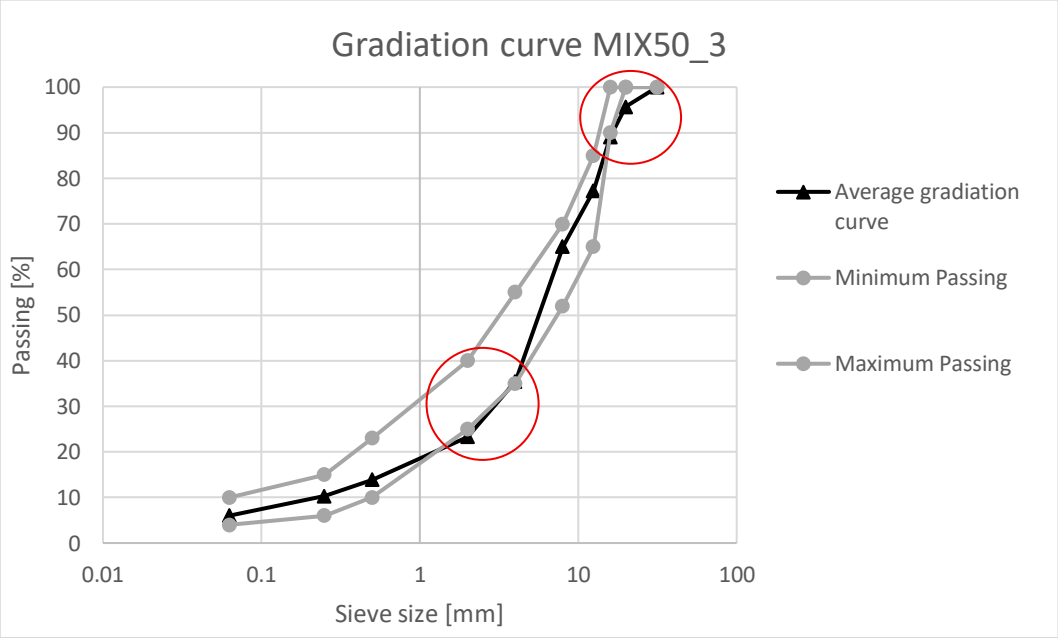

Figure 64. Gradiation curve MIX50 3.

Focusing on the analysis of the mixture named MIX50 REF, characterised by a RAP content of 50% and by the absence of polymer compound, produced through the wet methodology (PmB), the grading limits prescribed by the Special Tender Specifications of the A4 motorway are reported. These limits refer to a bituminous mixture intended for the binder layer, with polymer-modified bitumen (PMB), as indicated on page 75 of the specifications.

Sieve size	Minimum passing	Maximum passing
[mm]	[%]	[%]
31.5	100	100
20	100	100
16	90	100
12.5	75	85
8	52	70
4	35	55
2	25	40
0.5	10	23
0.25	6	15
0.063	4	10
0	0	0

Table 16. Gradation limits prescribed by the A4 special specifications.

As done previously for the PMA mixtures, the corresponding grading curve is presented below, together with the values of the two repetitions in tabular form. The points where the experimental curve deviates from the limits imposed by the above-mentioned specification are also highlighted.

MIX50 REF	Sample 1			Sample 2			Average
Sieve size	Sieve mass	Sieve+soil	Passing	Sieve mass	Sieve+soil	Passing	Passing
[mm]	[g]	[g]	[%]	[g]	[g]	[%]	[%]
31.5	1298.9	1298.9	100.0	1298.9	1298.9	100.0	100.0
20	1317.4	1343	97.6	1317.4	1341.9	97.7	97.6
16	1302	1302.1	97.5	1302.1	1321.9	95.8	96.7
12.5	1183.2	1285.2	87.8	1183.3	1306.4	84.0	85.9
8	1070.2	1250.1	70.6	1070.2	1257	66.3	68.4
4	1107.9	1452.6	37.6	1107.9	1449.9	33.7	35.6
2	980	1129.4	23.3	980	1110	21.3	22.3
0.5	783.7	883.5	13.7	784.1	873.9	12.7	13.2
0.25	726.4	760.7	10.5	726.7	759.4	9.6	10.0
0.063	767.4	811.2	6.3	767.5	808.9	5.7	6.0
0	895.1	898.3	0.0	895.1	898.7	0.0	0.0
Total	11432.2	11116.1	-	11433.2	12426.9	-	-

Table 17. Average gradation passings of the MIX50 REF mixture.

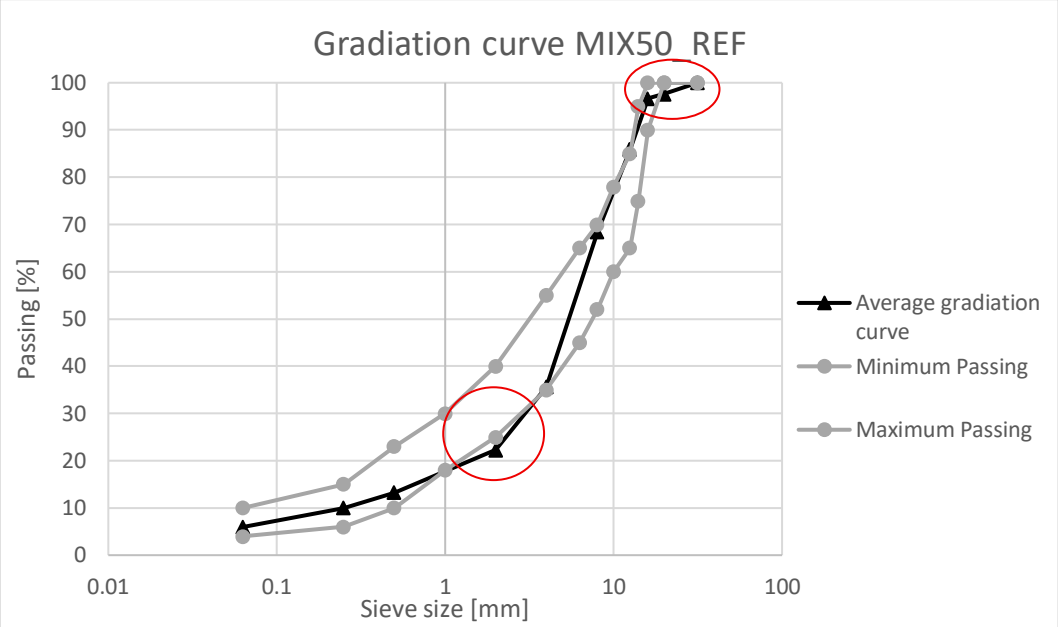

Figure 65. Gradiation curve MIX50 REF.

As can be observed from the graphs reported for each mixture, the grading curve generally shows deviations from the limits imposed by the specification, particularly at the 2 mm sieve and in the upper part of the curve (for example at the 20 mm sieve).

The causes may be multiple and often related to the nature of the materials used and to the operating conditions. In the case of the 2 mm passing, the deviation concerns the transition zone between the fine and coarse fractions, a portion that is particularly sensitive to variations in the RAP. This material, in fact, has a grading that is less controllable than that of virgin aggregates and may differ significantly from one batch to another.

Therefore, a possible cause may be the non-correspondence between the RAP batch used in the plant and the one employed during the mix-design phase: in this case, it is natural that the percentage of fine material varies, especially because additional fine particles may be generated during milling or handling.

The deviations in the upper part of the curve, such as at the 20 mm sieve, are instead linked to the coarser aggregate fraction. Here, the variability of the virgin aggregate batches supplied to the plant and segregation phenomena that may occur during transport or loading of the materials play a major role. The sampling phase of the materials may also strongly influence the deviations of the grading curve from the limits imposed by the specification.

In general, when the experimental grading curve deviates from the grading limits, this does not necessarily imply a non-conformity of the mixture but rather reflects the difference between the real material produced and the theoretical design material. The experimental curve should therefore be interpreted as the most accurate representation of the material obtained, while the design curve remains an ideal reference.

4.3. Binder content

After completing the sieve analysis, and following the order adopted in Chapter 3, the evaluation of the binder content through the ignition test is now addressed. The reader is referred to paragraph 3.3.4 for the theoretical and normative references.

The results of the ignition test carried out on each mixture are reported below. It should be specified that the values presented in the table represent the average of two repetitions, in order to ensure a more stable and representative estimate of the total binder content.

Mixture	MIX50 1 [%]	MIX50 2 [%]	MIX50 3 [%]	MIX50 REF [%]
Total binder content with respect to the mixture weight [%] according to the recipe	4.80	5.00	5.20	4.50
Total binder content with respect to the mixture weight [%] via ignition	4.83	5.46	5.25	4.83

Table 18. Comparison between the total binder content from the recipe and that determined by the ignition method.

From the analysis of the data reported in the previous table, it emerges that the bitumen content experimentally determined through the ignition test for the mixtures MIX50 1 and MIX50 3 is substantially in line with what is expected from the theoretical mix design. A similar consistency is not observed for the mixtures MIX50 2 and MIX50 REF, which show more marked deviations.

An aspect that deserves particular attention concerns the calibration factor introduced in the theoretical formulation for the determination of the binder content, illustrated in paragraph 3.3.4. This factor allows the correction of the measured binder mass by excluding the amount of volatile material present in the aggregates that evaporates at the high temperatures of the test. In previous research activities [24], an average volatilisation equal to 0.23% was quantified, mainly attributable to retained water and other volatile components intrinsic to the aggregate.

In the case of the mixtures produced in the plant, however, the question arises as to whether this contribution should actually be considered. The aggregates are in fact subjected to a pre-heating process that drastically reduces, if not completely eliminates, the presence of retained water at the moment of mixing. Consequently, the mass loss attributable to volatilisation during the ignition test is, under real operating conditions, negligible. For this reason, and in a manner consistent with the adopted production process, a calibration factor equal to 0% was chosen, assuming that the retained water has already been eliminated in the plant and that there are no significant contributions to mass loss due to the aggregates.

In addition to this methodological aspect, the observed deviations may be linked to several causes related to real production. First, the RAP used in the plant may present a residual binder content different from that assumed during the mix-design phase.

This is an intrinsically variable material, whose percentage of bitumen available depends on its origin, degree of ageing, storage conditions, and even the processing temperature.

To this, one must add the possible non-perfect representativeness of the sampled material: segregation phenomena, especially in the fine fractions and in the binder, may lead to samples that are slightly richer in bitumen compared to the average mixture produced.

4.4. Bulk density

The determination of the bulk density of the specimens was carried out in accordance with the EN 12697-6 standard [51], which defines this parameter as the mass per unit volume of the sample, including air voids, measured at a known test temperature. For the theoretical and normative references, the reader is referred to paragraph 3.3.7.

The bulk density was obtained through the Saturated Surface Dry (SSD) procedure, required by the standard for specimens with a closed surface, dense-graded particle size distribution, and low absorption capacity. The same standard also requires verifying that the relative difference between the bulk density of each specimen and the average value of the series does not exceed 1%.

To avoid overloading the discussion with continuous theoretical references, it is appropriate to specify that all results related to bulk density are reported together in this single subsection. They concern: the seven cylindrical specimens, for each mixture, compacted at Nmax (200 gyrations), used in the preliminary phase of characterising the mixtures produced in the plant to determine their actual composition; the nine cylindrical specimens for each mixture compacted at Ndesign (120 gyrations), used for the evaluation of fatigue resistance, carried out both before and after the cutting operations described in paragraph 3.3.5.; and finally the eight prismatic specimens for each mixture, also intended for fatigue characterisation.

Below, the results obtained in terms of bulk density are presented, both in tabular form and through a graphical representation, in order to provide a complete and immediate overview of the behaviour of the different mixtures.

Cylindrical specimen Nmax (200 gyrations)	MIX50 1	MIX50 2	MIX50 3	MIX50 REF
	[Mg/m^3]	[Mg/m^3]	[Mg/m^3]	[Mg/m^3]
Average value	2.514	2.417	2.481	2.467
Standard deviation	0.004	0.024	0.006	0.022

Table 19. Bulk density of the cylindrical specimens compacted at 200 gyrations.

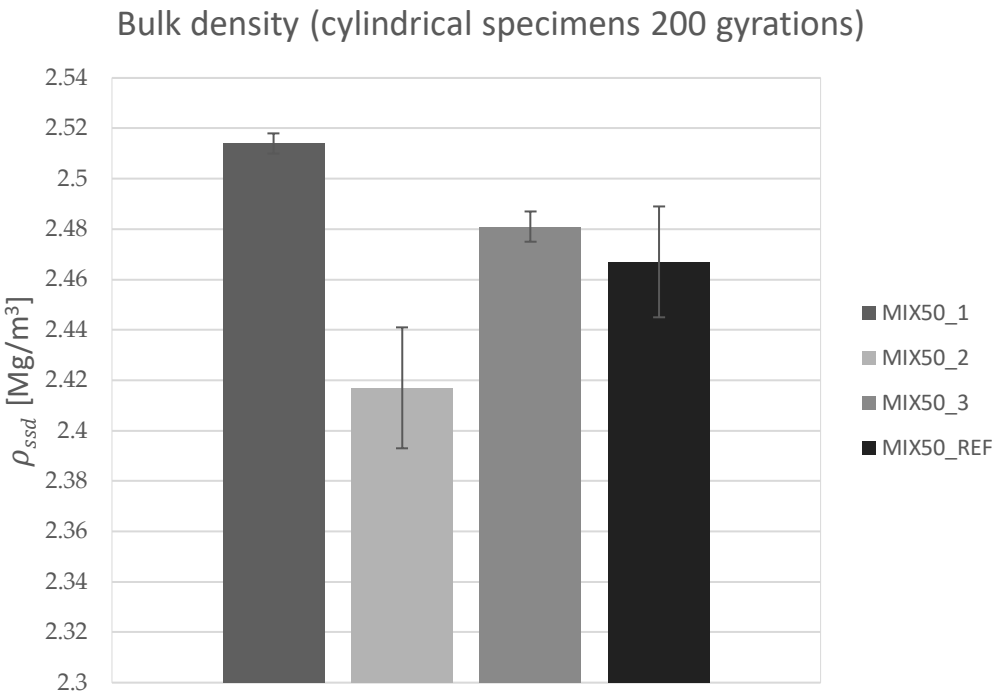

Figure 66. Bulk density of the cylindrical specimens compacted at 200 gyrations.

Cylindrical specimen Ndesign (120 gyrations) before cutting	MIX50 1	MIX50 2	MIX50 3	MIX50 REF
	[Mg/m^3]	[Mg/m^3]	[Mg/m^3]	[Mg/m^3]
Average value	2.494	2.446	2.459	2.444
Standard deviation	0.006	0.017	0.012	0.007

Table 20. Bulk density of the cylindrical specimens compacted at 120 gyrations, before cutting operations.

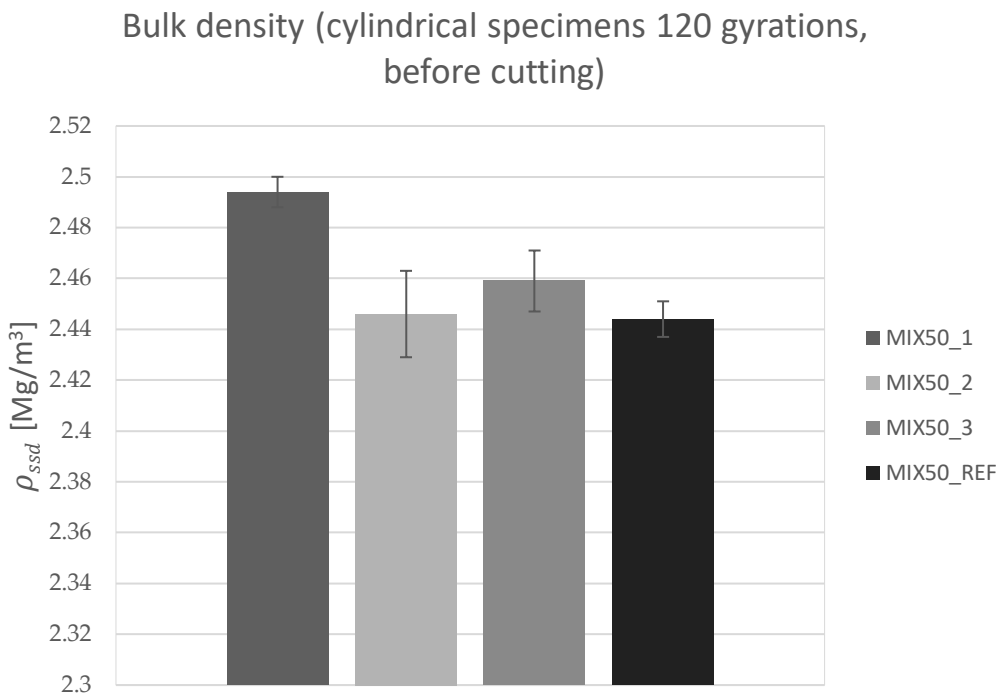

Figure 67. Bulk density of the cylindrical specimens compacted at 120 gyrations, before cutting operations.

Cylindrical specimen Ndesign (120 gyrations) after cutting	MIX50 1 [Mg/m³]	MIX50 2 [Mg/m³]	MIX50 3 [Mg/m³]	MIX50 REF [Mg/m³]
Average value	2.526	2.487	2.492	2.487
Standard deviation	0.007	0.013	0.014	0.011

Table 21. Bulk density of the cylindrical specimens compacted at 120 gyrations, after cutting operations.

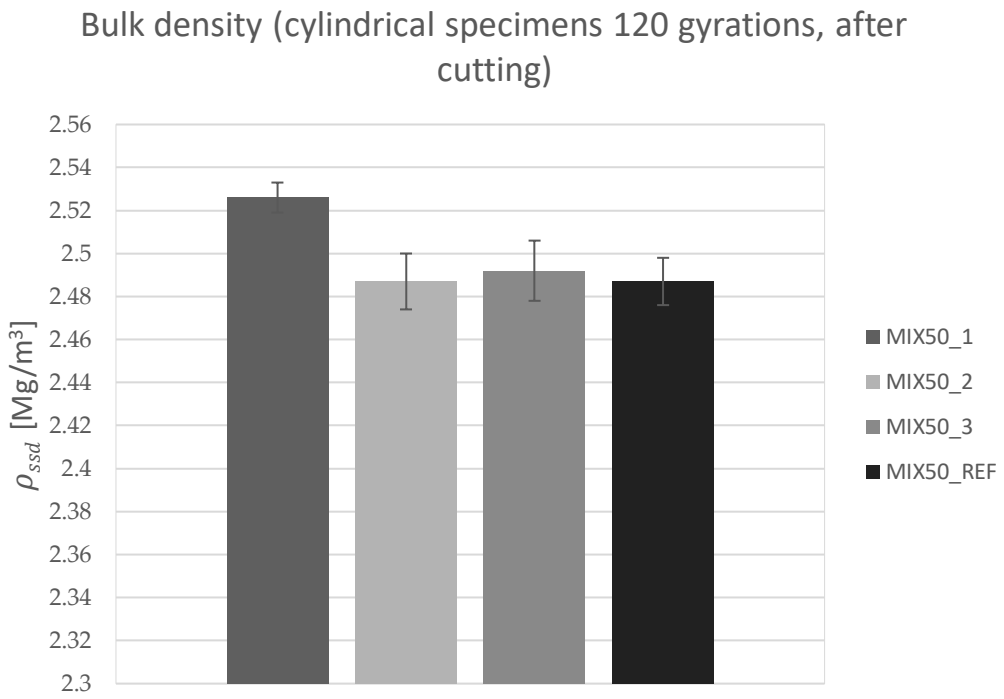

Figure 68. Bulk density of the cylindrical specimens compacted at 120 gyrations, after cutting operations.

Prismatic specimen	MIX50 1	MIX50 2	MIX50 3	MIX50 REF
	[Mg/m³]	[Mg/m³]	[Mg/m³]	[Mg/m³]
Average value	2.471	2.408	2.436	2.459
Standard deviation	0.007	0.011	0.004	0.006

Table 22. Bulk density of the prismatic specimens.

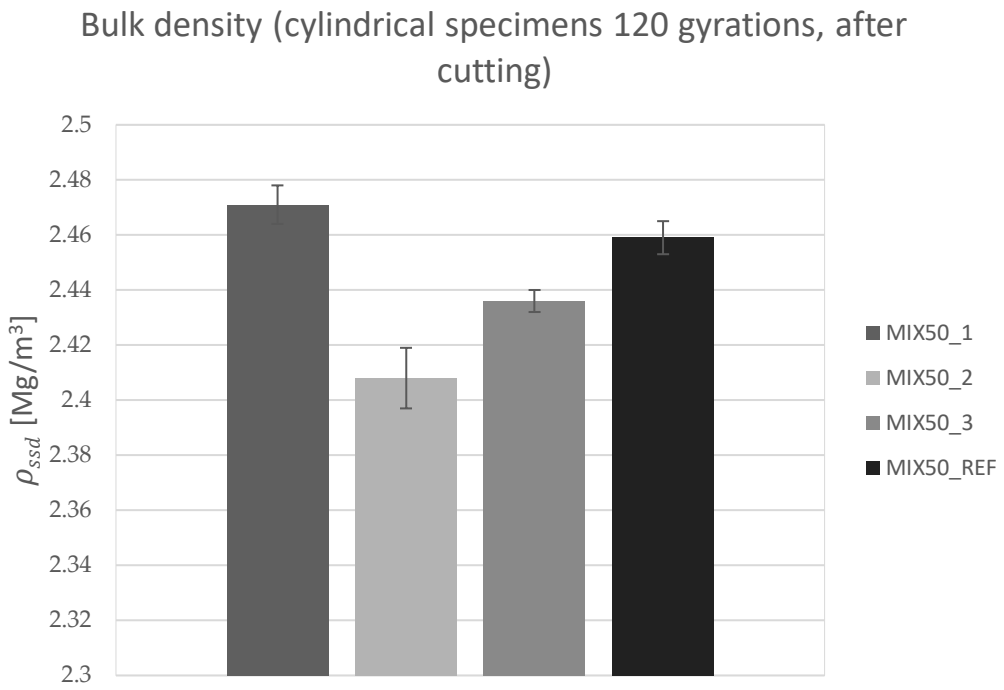

Figure 69. Bulk density of the prismatic specimens.

The analysed mixtures show a certain consistency both for the cylindrical specimens (compacted at 200 gyrations and at 120 gyrations) and for the prismatic specimens.

When evaluating the trend of the bulk density of the analysed bituminous mixtures, a behaviour emerges that is only apparently counter-intuitive. The mixture with the highest content of bitumen and plastic (MIX50 3) actually shows a lower bulk density compared to the MIX50 1 mixture, which, despite having a lower binder content (4.83% versus 5.25%, determined through the ignition test) and a smaller amount of plastic, reaches higher density values. This result can be explained by the fact that bulk density does not directly depend on the amount of bitumen present in the mixture, but rather on the ability of the granular system to compact and reduce air voids during compaction. In other words, what governs density is not the richness in binder, but the efficiency of aggregate packing and the rheological behaviour of the mixture during the compaction phase.

The presence of a higher amount of recycled plastic may indeed make the mixture stiffer already at compaction temperatures, reducing the mobility of the bitumen and hindering the rearrangement of the aggregates. A stiffer mixture tends to compact with greater difficulty, leaving a higher percentage of residual voids and therefore resulting in a lower bulk density. Even an excess of bitumen does not necessarily guarantee more effective densification: beyond a certain threshold, the

binder may behave as a film that separates the aggregates rather than promoting their contact, reducing the stability of the granular skeleton and limiting the ability of the mixture to reach a denser configuration.

To this, the role of RAP must be added, which constitutes 50% of the mixture and, with its aged binder and its actual grading, significantly influences compaction behaviour. If in the mixture with less bitumen and less plastic the RAP is finer or more "active", it may contribute to more efficient packing, favouring the reduction of voids.

Finally, the effects related to plant production should not be overlooked, such as temperature differences, variability in RAP pre-heating, the presence of residual moisture, or possible segregation phenomena during sample collection. All these factors may amplify the differences between the mixtures and explain why a mixture theoretically richer in bitumen and plastic may, in practice, compact less effectively and show a lower bulk density compared to a poorer mixture.

4.5. Evaluation of air voids and compaction parameters

As already mentioned in the previous chapter, the compaction of the cylindrical specimens was carried out in accordance with the EN 12697-31 standard [48], using a gyratory shear press (Gyratory Compactor). The reader is referred to paragraph 3.3.8 for further information.

Compaction by means of a gyratory press makes it possible to analyse in detail the evolution of the densification of a bituminous mixture through the determination of the voids present in the specimen. During the process, the acquisition system records the variation in the height of the sample as a function of the number of gyrations, h(n). The progressive reduction in height leads to a decrease in volume and a consequent increase in bulk density, allowing the number of gyrations to be correlated with the degree of densification achievable on site.

The percentage of voids inside the compacted specimen is defined as the ratio between the volume of air voids and the total volume of the sample:

$$\%\mathrm{v} = \frac{V_v}{V_{tot}} \cdot 100$$

where:

- V_v as mentioned, is the volume of air voids inside the compacted specimen.
- V_{tot} is the total volume of the sample.

Based on this definition, it is possible to express the voids as a function of the bulk density (MV) and the maximum theoretical density (TMD), which represents the ideal condition of absence of voids:

$$\%v = \left(1 - \frac{MV}{TMD}\right) \cdot 100$$

Since the TMD is an intrinsic property of the mixture, the relationship makes it possible to describe the decreasing trend of the voids as the number of gyrations increases. From it, the degree of compaction is obtained:

$$C(n) = 1 - v(n)$$

which, when represented on a semi-logarithmic scale with respect to the number of gyrations, gives rise to the compaction curve or workability line:

$$C(n) = C_1 + k \cdot \log(n)$$

where C_1 represents the initial compaction due to the self-weight of the mixture, known as self-densification, and k expresses the workability (also referred to as densification gradient), that is, the ability of the mixture to densify under the action of the applied load.

Alongside the parameters derived from the compaction curve, the Construction Densification Index (CDI) was also considered, a dimensionless indicator that makes it possible to evaluate the amount of energy required for the mixture to reach adequate levels of densification during the construction phase. The CDI is determined as the area under the compaction curve starting from the eighth gyration of the press, to reproduce the initial action exerted by the paver during laying, up to the achievement of a densification equal to 92% of the maximum theoretical density.

This parameter is particularly relevant because it allows a direct comparison of the response of the different mixtures to the compaction process. A curve that rapidly tends towards high density values generates a reduced CDI, indicating a mixture that requires a limited energy input to reach the service condition. Conversely, a higher CDI indicates the need to apply greater compaction energies, highlighting lower workability.

In operational terms, the CDI represents the work that the rollers must perform on site to bring the mixture to the threshold of 8% air voids, a condition generally associated with traffic opening. It is therefore a synthetic but highly effective parameter for assessing the compactability of the mixture and its suitability for the expected operating conditions.

To avoid overloading the discussion, it is appropriate to specify that all results related to the evaluation of voids are reported together in this single subsection. They concern: the seven cylindrical specimens, for each mixture, compacted at Nmax (200 gyrations), used in the preliminary phase of characterising the mixtures produced in the plant to determine their actual composition; the nine cylindrical

specimens for each mixture compacted at Ndesign (120 gyrations), used for the evaluation of fatigue resistance, carried out both before and after the cutting operations described in paragraph 3.3.5.; and finally the eight prismatic specimens for each mixture, also intended for fatigue characterisation.

To ensure completeness and transparency in the presentation, the entire set of experimental data is fully reported in the appendix, allowing the reader to consult every numerical detail. In the main text, instead, the most significant results related to the different types of specimens mentioned above are summarised and discussed. In particular, attention is focused on the voids recorded at 10, 120 and 200 gyrations, on the self-densification parameter C_1 and the workability parameter k, as well as on the CDI value associated with each mixture.

As a complement to the interpretation of the results, the prescriptive requirements of the Special Tender Specifications of the A4 Motorway, which constitute the normative reference, are also recalled.

4.5.1. Cylindrical specimens compacted at N_{max} (200 gyrations)

The cylindrical specimens used for the characterisation of the mixtures are considered first. The values obtained for each mixture are summarised in tabular form, to provide an immediate and comparable overview of the main quantities of interest. It should be specified that the reported data represent the average of the seven specimens compacted for each mixture, in order to ensure a more robust and representative evaluation of the actual behaviour of the material.

Mix code	$V_{10\,gyrations}$ [%]	$V_{120\,gyrations}$ [%]	$V_{200\,gyrations}$ [%]	C_1 [-]	k [-]	CDI [-]	Dev. St. CDI [-]
MIX50 1	12.3	3.59	2.26	80.61	7.81	71.97	12.63
MIX50 2	15.49	6.56	5.13	77.24	7.9	411.79	144.52
MIX50 3	12.96	4.14	2.79	80.03	7.7	107.13	22.33
MIX50 REF	14.93	6.12	4.47	77.83	8.21	331.94	133.12

Table 23. Average values of air voids and compaction parameters for each mixture – 200 gyration cylindrical specimens.

As mentioned earlier, the limits imposed by the Special Tender Specifications of the A4 motorway are reported below:

Miscela bituminosa		
Condizioni di prova (UNI EN 12697-31/13108-20)	Unità di misura	Limiti (UNI EN 13108-1)
Angolo di rotazione	°	1,25 ± 0,02
Velocità di rotazione	Giri/min	30
Pressione verticale	kPa	600 ± 3
Diametro del provino	mm	100
Rotazioni N1	---	10
Rotazioni N2	---	120
Rotazioni N3	---	200

Risultati richiesti	Unità di misura	Limiti (UNI EN 13108-1)
Affinità bitume-aggregato – Spogliamento (UNI EN 12697-11)	%	≥ 5
Vuoti a N1 (UNI EN 12697-8)	%	≤ 14 (V_{max14})
Vuoti a N2 (UNI EN 12697-8)	%	3 ÷ 6 (V_{min3}-V_{max6})
Vuoti a N3 (UNI EN 12697-8)	%	≥ 2 (V_{min2})
Resistenza a Trazione Indiretta a 25°C (UNI EN 12697-23)	N/mm²	1,20 ÷ 2,20
Coefficiente di Trazione Indiretta a 25°C	N/mm²	60 ÷ 250
Perdita di Resistenza a Trazione Indiretta a 25°C (UNI EN 12697-12)	%	≥ 90 ($ITSR_{90}$)
Rigidezza (UNI EN 12697-26 – Annesso C)		
T= 5°C, Def.= 7µm, Freq.= 2Hz, Coeff.P.= 0,35	N/mm²	18.000 ÷ 27.000
T= 20°C, Def.= 7µm, Freq.= 2Hz, Coeff.P.= 0,35	N/mm²	8.000 ÷ 15.000
T= 40°C, Def.= 7µm, Freq.= 2Hz, Coeff.P.= 0,35	N/mm²	900 ÷ 6.000

Table 24. Voids limits prescribed by the CSA.

To facilitate the interpretation of the voids measured at 10, 120 and 200 gyrations, the data reported in the previous table have also been represented in graphical form. In the graphs, the prescriptive limits established by the CSA have been included through red reference lines, to make the comparison between the performance of the different mixtures and the normative requirements immediate. For each mixture, the standard deviations are also indicated, in order to highlight the variability of the results and their statistical reliability.

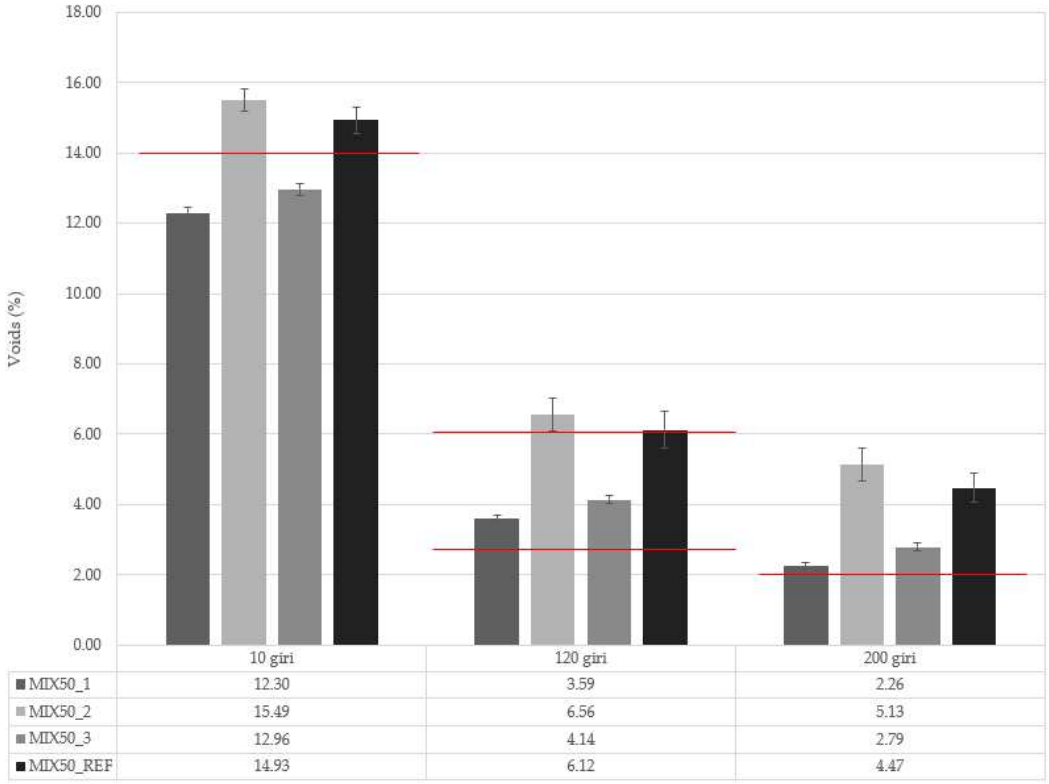

Figure 70. Trend of air void content for the analysed mixtures and prescribed limits – Cylindrical specimens compacted at 200 gyrations.

In continuity with what was illustrated for the voids values, a dedicated graph showing the trend of the CDI for the different mixtures has also been produced. The representation allows a visual comparison of the behaviour of the analysed formulations, including for each of them the corresponding standard deviations, so as to highlight the variability of the data and their statistical reliability.

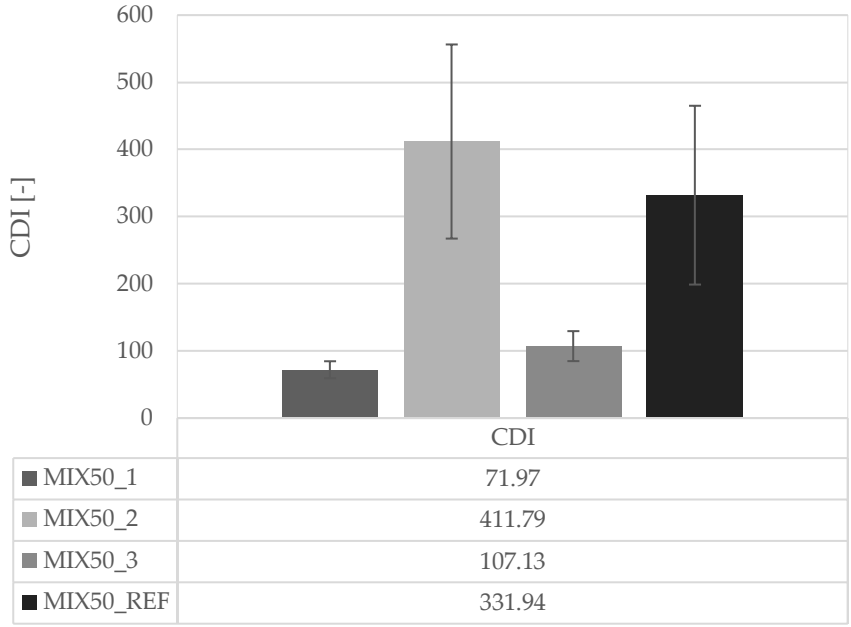

Figure 71. Trend of CDI for the analysed mixtures – Cylindrical specimens compacted at 200 gyrations.

4.5.2. Cylindrical specimens compacted at N_{design} (120 gyrations), before cutting

In continuity with what was presented in the previous paragraph for the cylindrical specimens compacted at N_{max} (200 gyrations), the results obtained on the specimens compacted at N_{design} (120 gyrations), used for the fatigue characterisation of the analysed mixtures prior to the cutting operation, are illustrated here. Also in this case, the reported values represent the average of the nine specimens produced for each mixture, to ensure a statistically more robust evaluation of the material's behaviour. The prescriptive reference limits remain those already recalled in the previous subsection.

Mix code	$V_{10\ gyrations}$ [%]	$V_{120\ gyrations}$ [%]	C_1 [-]	k [-]	CDI [-]	Dev. St. CDI [-]
MIX50 1	11.98	3.07	80.11	8.2	57.58	8.27
MIX50 2	13.37	4.17	78.52	8.39	130.71	51.02
MIX50 3	12.45	3.65	79.65	8.15	87.33	26.84
MIX50 REF	14.54	5.35	77.95	8.32	236.68	36.02

Table 25. Average values of air voids and compaction parameters for each mixture – 120 gyration cylindrical specimens before cutting operations.

To facilitate the interpretation of the voids measured at 10 and 120 gyrations, the data reported in the previous table have also been represented in graphical form. In the graphs, the prescriptive limits established by the CSA have been included through red reference lines.

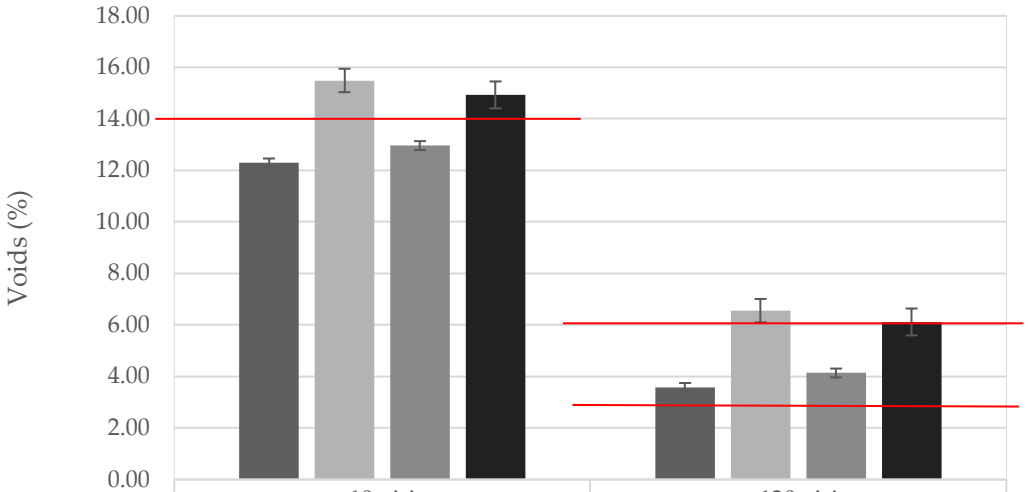

	10 giri	120 giri
MIX50_1	12.30	3.59
MIX50_2	15.49	6.56
MIX50_3	12.96	4.14
MIX50_REF	14.93	6.12

Figure 72. Trend of air void content for the analysed mixtures and prescribed limits – Cylindrical specimens compacted at 120 gyrations, before cutting operations.

In continuity with what was illustrated for the voids values, a dedicated graph showing the trend of the CDI for the different mixtures has also been produced.

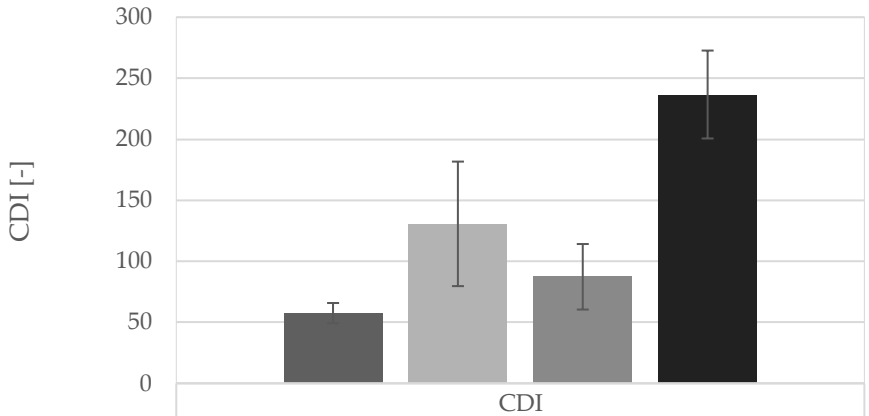

	CDI
MIX50_1	57.58
MIX50_2	130.71
MIX50_3	87.33
MIX50_REF	236.68

Figure 73. Trend of CDI for the analysed mixtures – Cylindrical specimens compacted at 120 gyrations, before cutting operations.

4.5.3. Cylindrical specimens compacted at N_{design} (120 gyrations), after cutting

Regarding the cylindrical specimens compacted at N_{design}(120 gyrations) and intended for fatigue characterisation, the percentage of voids was also evaluated after the cutting operations required to obtain specimens with a height compliant with the normative prescriptions. For a detailed description of the adopted procedure, the reader is referred to paragraph 3.3.10.1.

Mix code	v [%]	Dev. St. v [-]
MIX50 1	1.97	0.43
MIX50 2	2.6	0.62
MIX50 3	2.37	0.46
MIX50 REF	3.85	0.41

Figure 74. Average values of air voids and compaction parameters for each mixture – 120 gyration cylindrical specimens after cutting operations.

The data reported in the previous table have also been represented in graphical form, including a red reference line indicating the prescriptive limit established by the CSA. This visualisation makes it possible to immediately compare the performance of the different mixtures with respect to the normative requirement.

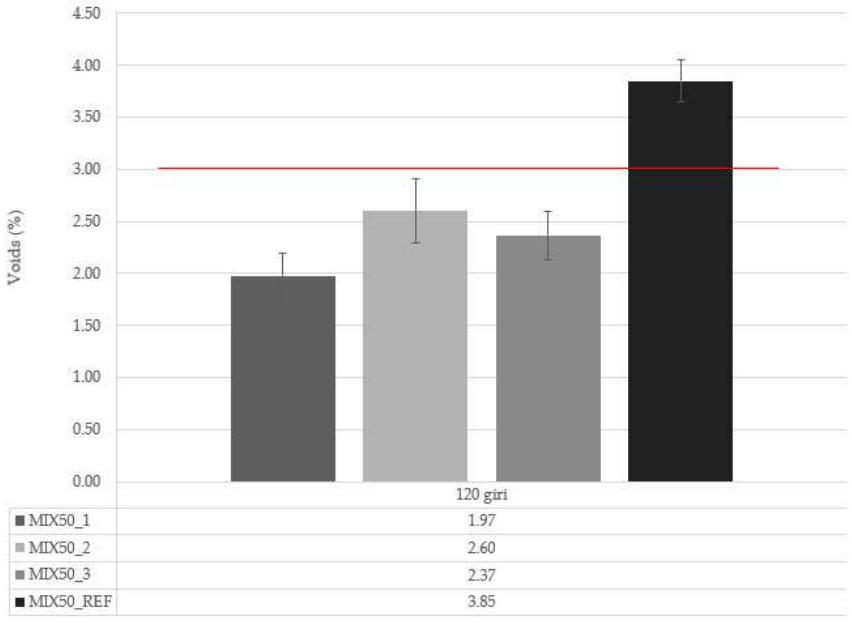

Figure 75. Trend of air void content for the analysed mixtures and prescribed limits – Cylindrical specimens compacted at 120 gyrations, after cutting operations.

From the previous graph it emerges that, after the cutting operations, only the MIX50 REF mixture falls within the void limits prescribed by the Special Tender Specifications of the A4 motorway (>3% at 120 gyrations). It is, however, important to consider the very nature of the cutting process: the cylindrical specimen is trimmed both at the top and at the bottom, generally according to a ratio of about 2:3. This results in the removal of a larger portion from the upper surface, which is typically less compacted than the base. Consequently, the apparent decrease in voids is an expected effect intrinsic to the procedure, and the resulting specimens can still be considered compliant for the purposes of mechanical characterisation.

From the analysis of the voids trend, both for the specimens compacted at N_{max}(200 gyrations) and for those compacted at N_{design}(120 gyrations), before and after trimming, an overall consistent behaviour emerges among the different mixtures. In particular, the MIX50 2 and MIX50 REF formulations show, on average, a higher void content compared to the others. The behaviour of the mixtures containing the polymeric compound is also particularly interesting, as they exhibit a distinct evolution of voids that deserves specific attention.

The trend of air voids in the mixtures containing different percentages of plastic (0.3%, 0.5% and 0.7%) shows a non-monotonic behaviour: the mixture with 0.3% exhibits fewer voids than the one with 0.5%, which in turn shows more voids than the mixture with 0.7%. It is therefore a bell-shaped trend, in which the intermediate condition (0.5%) proves to be the most unfavourable in terms of compaction.

In parallel, the bulk density shows an opposite trend: the mixture with 0.5% plastic exhibits the lowest apparent density, forming a “downward cusp”. This mirrored behaviour is entirely consistent, since an increase in voids inevitably corresponds to a decrease in bulk density.

To correctly interpret this phenomenon, it is necessary to consider the mechanisms governing the compaction of bituminous mixtures. This result can be explained by the fact that bulk density does not directly depend on the amount of bitumen present in the mixture, but rather on the ability of the granular system to compact and reduce air voids during compaction. In other words, what governs density is not the richness in binder, but the efficiency of aggregate packing and the rheological behaviour of the mixture during the compaction phase.

The presence of a higher amount of recycled plastic may indeed make the mixture stiffer already at compaction temperatures, reducing the mobility of the bitumen and hindering the rearrangement of the aggregates. A stiffer mixture tends to compact with greater difficulty, leaving a higher percentage of residual voids and therefore resulting in a lower bulk density.

The bell-shaped trend of voids (and the inverted bell-shaped trend of bulk density) suggests that there exists an optimal plastic content beyond which the mixture begins to compact less effectively. At low percentages (0.3%), the plastic may slightly improve the viscosity of the binder without excessively stiffening the mixture. The granular system can still rearrange efficiently, and the voids remain relatively low. At intermediate percentages (0.5%), the stiffening effect becomes more pronounced: the mixture loses mobility, the aggregates cannot compact adequately, and the voids increase. This is the point at which the mixture is most difficult to densify. At higher percentages (0.7%), the mixture may exhibit a more complex behaviour: the increase in plastic may lead to greater surface cohesion or to a different behaviour of the modified binder, which in some cases may favour a slight improvement in compaction compared to the intermediate condition. However, the mixture remains stiffer and less workable than the formulation with 0.3%.

The result is a bell-shaped curve, with a maximum of voids (and a minimum of bulk density) corresponding to the intermediate percentage.

Nevertheless, it remains advisable to expand the laboratory activity in order to experimentally confirm the validity of the considerations emerging from the results just discussed.

4.5.4. Prismatic specimens

After discussing the results related to the cylindrical specimens prepared as part of the laboratory activity, the values of air voids measured on the prismatic specimens are now presented. As before, the reported data correspond to the average of the eight specimens produced for each mixture.

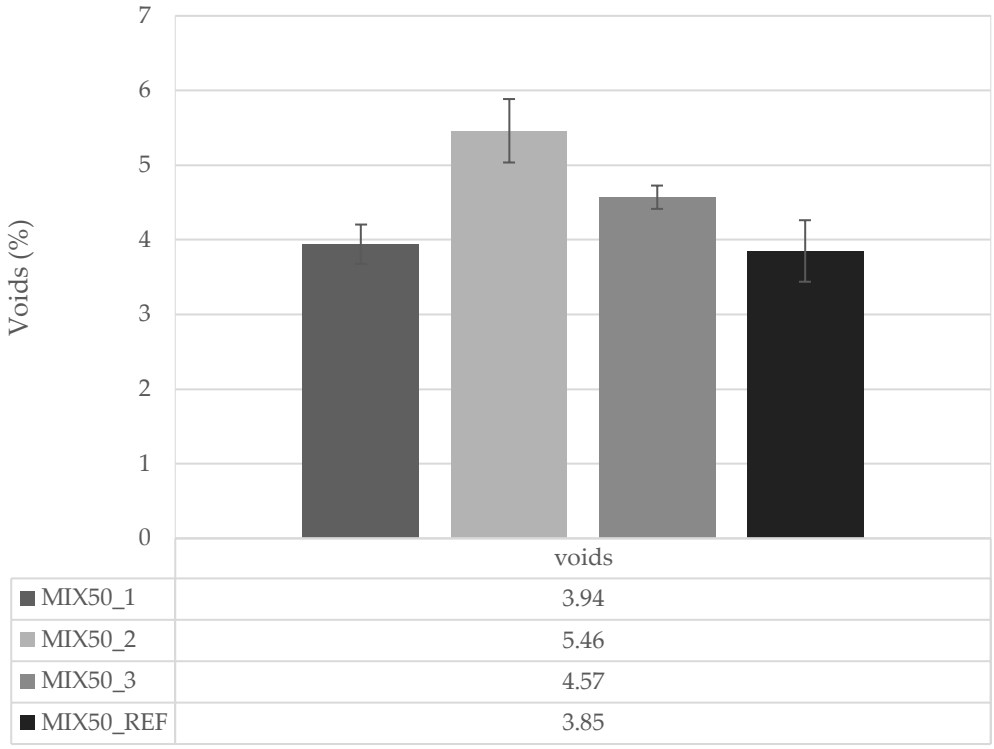

Figure 76. Trend of air void content for the analysed mixtures – Prismatic specimens.

In conclusion, the results related to the voids of the prismatic specimens show a trend consistent with what was observed for the cylindrical specimens, confirming a substantial uniformity of behaviour among the analysed mixtures, regardless of the type of specimen prepared.

Before proceeding with the evaluation of the stiffness moduli, it is appropriate to analyse the volumetric parameters VMA (Voids in Mineral Aggregate) and VFB (Voids Filled with Bitumen), which play a central role in the design and control of bituminous mixtures. The VMA depends on how the mixture has been compacted and is therefore a function of the binder content. To determine this parameter, the binder must ideally be removed from the mixture after compaction. It constitutes a direct indicator of the granular structure and of the ability of the mixture to accommodate an adequate amount of bitumen. The VFB, defined as the percentage of these voids that is actually filled by the binder, instead makes it possible to assess the degree of aggregate coating and the balance between residual air voids and bitumen content. The combined analysis of these two parameters allows verification

of the correct compromise between stability, durability, and workability of the mixture, helping to prevent phenomena such as excessive stiffness, susceptibility to cracking, hot instability, or premature degradation. In the present study, VMA and VFB were determined on the cylindrical specimens compacted at Nmax (200 revolutions) used for the characterization of the mixtures, by means of the theoretical expressions reported below.

$$\text{VMA} = v_{120} \cdot \frac{B \cdot \rho_{mb}}{\rho_b}$$

$$\text{VFB} = \frac{(B \cdot \rho_{mb} \cdot 100)}{\rho_b \cdot VMA}$$

where:

- VMA is the volumetric parameter voids in mineral aggregates, expressed in %.
- VFB is the volumetric parameter voids filled with bitumen, expressed in %.
- v_{120} is the percentage of voids at 120 revolutions, expressed in %.
- B is the total binder content, expressed in %.
- ρ_{mb} is the bulk density of the mixture, expressed in Mg/m³.
- ρ_b is the density of the bituminous binder, expressed in Mg/m³.

The results obtained for the investigated mixtures are reported below in tabular form, together with the corresponding standard deviations. It should be noted that the values shown represent the averages calculated on the seven specimens produced for each mixture, thus ensuring a statistically more robust assessment of the measured properties.

Mix code	VMA [%]	Dev. St. VMA [-]	VFB [%]	Dev. St. VFB [-]
MIX50 1	15.62	0.18	77.04	1.01
MIX50 2	19.63	0.78	66.72	3.39
MIX50 3	17.04	0.22	75.74	1.14
MIX50 REF	17.68	0.95	65.58	4.05

Table 26. Mean values and standard deviations of the investigated mixtures – 200 gyration cylindrical specimens.

To verify the statistical significance of the differences observed between the mean values of VMA and VFB obtained for the different mixtures, a one-way ANOVA test (one-way analysis of variance) was carried out. This analysis makes it possible to assess whether the differences observed between the means of several groups are statistically significant, or whether, at the current stage, there is no

evidence to consider them as such, by comparing the variability within the groups with the variability between the groups themselves.

ANOVA a una via (Fisher)

	F	gdl1	gdl2	p
VMA	49.2	3	24	< .001

Table 27. Results of the one way ANOVA test on VMA of cylindrical specimens compacted at 200 gyrations.

Descrittive Gruppo

	Mix code	N	Media	SD	SE
VMA	MIX50_1	7	15.6	0.182	0.0688
	MIX50_2	7	19.6	0.778	0.2940
	MIX50_3	7	17.0	0.218	0.0824
	MIX50_REF	7	17.7	0.946	0.3576

Table 28. Descriptive parameters of the mixture for the purpose of the test – cylindrical specimens compacted at 200 gyrations.

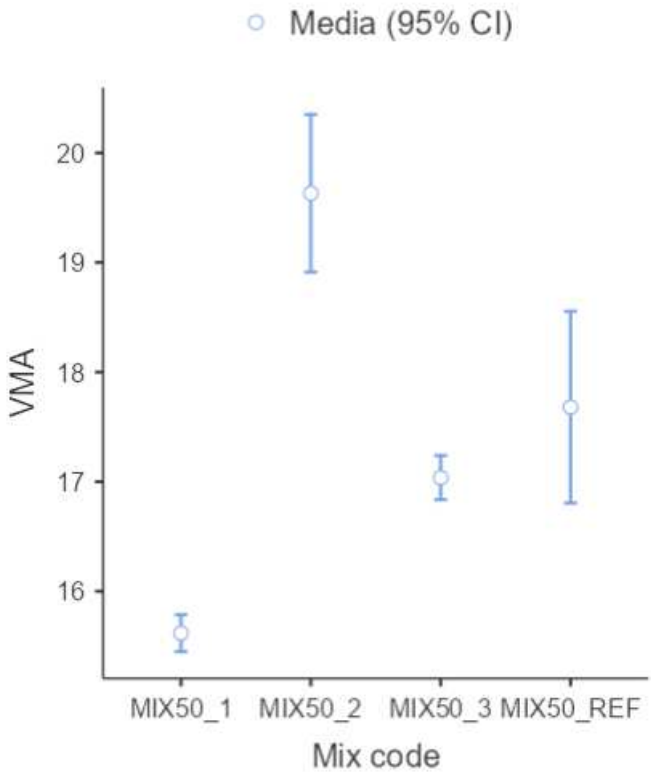

Figure 77. Mean VMA values for each mixture, with corresponding 95% confidence intervals– cylindrical specimens compacted at 200 gyrations.

Test Post-Hoc di Tukey – VMA

		MIX50_1	MIX50_2	MIX50_3	MIX50_REF
MIX50_1	Differenza media	—	−4.01 ***	−1.42 **	−2.061 ***
	valore p	—	< .001	.002	< .001
MIX50_2	Differenza media		—	2.59 ***	1.951 ***
	valore p		—	< .001	< .001
MIX50_3	Differenza media			—	−0.643
	valore p			—	.249
MIX50_REF	Differenza media				—
	valore p				—

Nota. * p < .05, ** p < .01, *** p < .001

Table 29. Results of the post hoc test performed on the VMA values– cylindrical specimens compacted at 200 gyrations.

ANOVA a una via (Fisher)

	F	gdl1	gdl2	p
VFB	32.8	3	24	< .001

Table 30. Results of the one way ANOVA test on VFB of cylindrical specimens compacted at 200 gyrations.

Descrittive Gruppo

	Mix code	N	Media	SD	SE
VFB	MIX50_1	7	77.0	1.01	0.382
	MIX50_2	7	66.7	3.39	1.282
	MIX50_3	7	75.7	1.14	0.430
	MIX50_REF	7	65.6	4.05	1.531

Table 31. Descriptive parameters of the mixture for the purpose of the test – cylindrical specimens compacted at 200 gyrations.

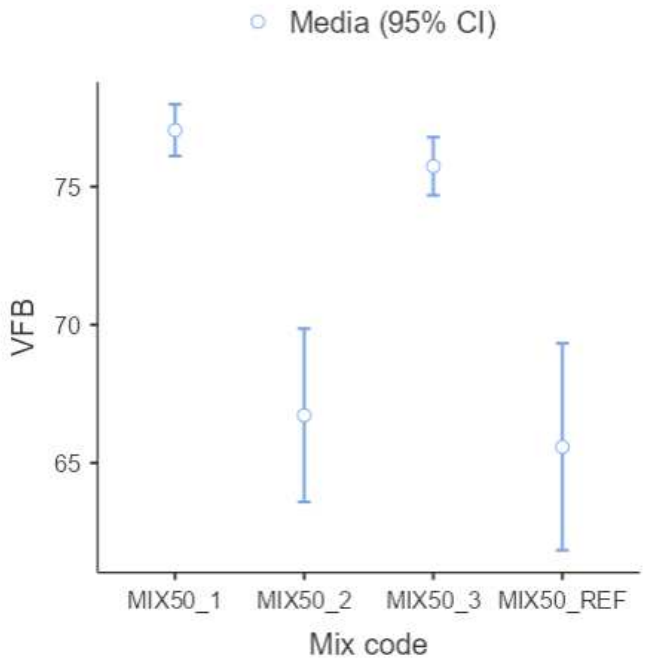

Figure 78. Mean VFB values for each mixture, with corresponding 95% confidence intervals– cylindrical specimens compacted at 200 gyrations.

Test Post-Hoc di Tukey – VFB

		MIX50_1	MIX50_2	MIX50_3	MIX50_REF
MIX50_1	Differenza media	—	10.3 ***	1.31	11.46 ***
	valore p	—	< .001	.811	< .001
MIX50_2	Differenza media		—	−9.01 ***	1.14
	valore p		—	< .001	.865
MIX50_3	Differenza media			—	10.15 ***
	valore p			—	< .001
MIX50_REF	Differenza media				—
	valore p				—

Nota. * p < .05, ** p < .01, *** p < .001

Table 32. Results of the post hoc test performed on the VFB values– cylindrical specimens compacted at 200 gyrations.

By closely examining the data related to the Post-Hoc tests concerning the VMA and VFB values, no statistically significant differences emerge between the mixtures named MIX50 1 and MIX50 3, and likewise between the mixtures MIX50 2 and MIX50 REF.

4.6. Stiffness moduli

The stiffness of a bituminous mixture is a fundamental parameter for describing its stress–strain response, as it makes it possible to assess its ability to resist tensile stresses over a wide range of temperatures. This quantity provides direct indications of the mechanical behaviour of the material and of its suitability to withstand the service conditions typical of road pavements. The normative reference for the determination of the stiffness modulus is BS EN 12697-26, with particular attention to Annex C, to which the reader is referred for a detailed description of the theoretical principles and the experimental procedure adopted (see paragraph 3.3.8.1).

The tests were carried out according to two distinct configurations, selected on the basis of the specimen geometry and the objectives of the investigation. For the cylindrical specimens, both those compacted at N_{max} and those compacted at N_{design}, the IT-CY configuration was adopted, imposing a maximum horizontal displacement of 11.2 μm. The prismatic specimens, on the other hand, were tested using the 4PB-PR configuration, applying a constant maximum flexural strain amplitude of 50 μm/m, to remain within the linear viscoelastic range. This distinction makes it possible to capture the mechanical behaviour of the mixtures more comprehensively, exploiting the specific potential of each test configuration.

With regard to the test temperature, the standard prescribes that the stiffness modulus be determined, in order, at 20°C, 10°C and 40°C, to characterise the mixture under thermal conditions representative of different service states. However, during the preliminary tests it emerged that the cylindrical specimens compacted at N_{max} tended to break during the determination of the modulus at 40°C, compromising the possibility of obtaining reliable measurements. To avoid this issue, the highest temperature was reduced to 30°C, a choice that made it possible to correctly complete the test sequence without altering the significance of the results. Further details on this operational decision are provided later in the paragraph.

A different approach was adopted for the cylindrical specimens compacted at N_{design} (120 gyrations) and for the prismatic specimens intended for fatigue characterisation: in this case, since the objective was to define the behaviour of the material under conditions consistent with the fatigue resistance tests, the samples were tested exclusively at the reference temperature for this type of investigation, equal to 20°C.

In continuity with the approach adopted for presenting the results related to bulk density and air void content, the data will again be presented by distinguishing the different types of specimens prepared. This structure makes it possible to highlight more clearly the specific features of each configuration, followed by a detailed and accurate analysis of the results obtained.

As a complement to the interpretation of the results, the prescriptive requirements of the Special Tender Specifications of the A4 Motorway, which constitute the normative reference, are also recalled.

4.6.1. Cylindrical specimens compacted at N_{max} (200 gyrations)

The cylindrical specimens used for the mechanical characterisation of the mixtures are analysed first. The values obtained for each formulation are reported in tabular form. It should be specified that the presented data represent the average of the seven specimens compacted for each mixture.

As already illustrated in Chapter 3, the stiffness modulus of each cylindrical specimen is determined as the average of two consecutive measurements. Between one repetition and the next, the specimen is rotated by 90° ± 10° around its horizontal axis, so as to assess any anisotropy induced by the compaction process. The standard also establishes that the mean value obtained in the second series must fall within the interval between +10% and −20% with respect to the mean of the first series, a requirement necessary to ensure the reliability and repeatability of the measurement.

After performing this check, excluding results where necessary, the average modulus values obtained are reported.

Mix code	$E_{10°C}$ [MPa]	Dev. St. $E_{10°C}$ [-]	$E_{20°C}$ [MPa]	Dev. St. $E_{20°C}$ [-]	$E_{30°C}$ [MPa]	Dev. St. $E_{30°C}$ [-]
MIX50 1	22357.7	1104.9	13360.0	1466.0	6606.8	904.4
MIX50 2	20947.2	1764.2	11121.2	1340.5	5146.4	1163.6
MIX50 3	21992.8	1294.2	13305.1	932.6	6727.0	877.2
MIX50 REF	14174.5	2250.6	8928.9	2064.6	4349.3	338.1

Table 33. Average values of stiffness modulus for each mixture – 200 gyration cylindrical specimens.

As anticipated, the acceptability limits established by the Special Tender Specifications of the A4 motorway are reported below. For the purposes of the analysis, however, only the value prescribed at the temperature of 20 °C must be considered.

Risultati richiesti	Unità di misura	Limiti (UNI EN 13108-1)
Affinità bitume-aggregato – Spogliamento (UNI EN 12697-11)	%	≥ 5
Vuoti a N1 (UNI EN 12697-8)	%	≤ 14 (V_{max14})
Vuoti a N2 (UNI EN 12697-8)	%	3 ÷ 6 (V_{min3}-V_{max6})
Vuoti a N3 (UNI EN 12697-8)	%	≥ 2 (V_{min2})
Resistenza a Trazione Indiretta a 25°C (UNI EN 12697-23)	N/mm²	1,20 ÷ 2,20
Coefficiente di Trazione Indiretta a 25°C	N/mm²	60 ÷ 250
Perdita di Resistenza a Trazione Indiretta a 25°C (UNI EN 12697-12)	%	≥ 90 ($ITSR_{90}$)
Rigidezza (UNI EN 12697-26 – Annesso C)		
T= 5°C, Def.= 7µm, Freq.= 2Hz, Coeff.P.= 0,35	N/mm²	18.000 ÷ 27.000
T= 20°C, Def.= 7µm, Freq.= 2Hz, Coeff.P.= 0,35	N/mm²	8.000 ÷ 15.000
T= 40°C, Def.= 7µm, Freq.= 2Hz, Coeff.P.= 0,35	N/mm²	900 ÷ 6.000

Table 34. Acceptability limits for stiffness moduli (source: A4 motorway Special Contract Specifications).

To facilitate the interpretation of the stiffness values, the data reported in the previous table have also been represented in graphical form. In the graphs, the prescriptive limits established by the CSA have been included through red reference lines, thus making it possible to immediately compare the performance of the different mixtures with the normative requirements, for the temperature of 20 °C only.

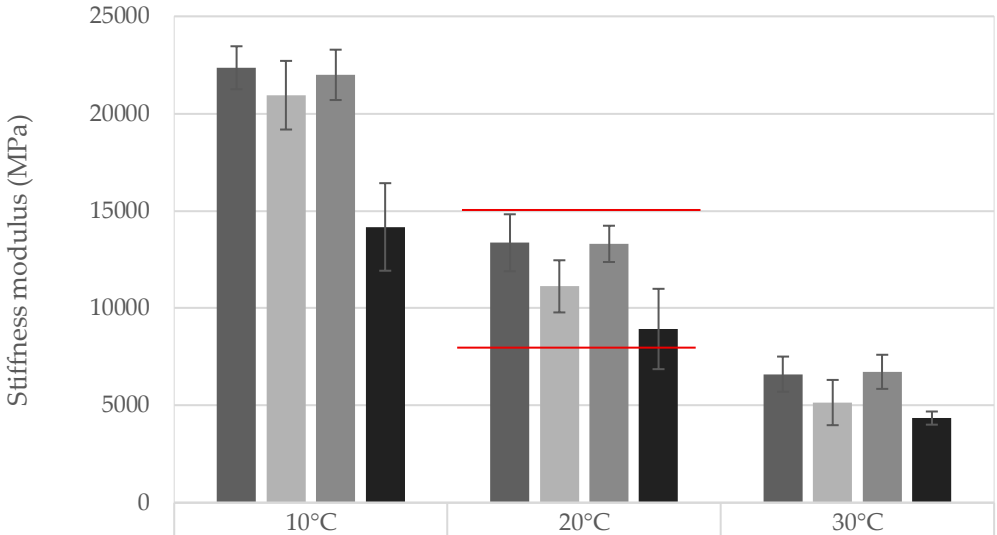

	10°C	20°C	30°C
MIX50_1	22358	13360	6607
MIX50_2	20947	11121	5146
MIX50_3	21993	13305	6727
MIX50_REF	14175	8929	4349

Figure 79. Trend of stiffness modulus for the analysed mixtures and prescribed limits – Cylindrical specimens compacted at 200 gyrations.

4.6.2. Cylindrical specimens compacted at N_{design} (120 gyrations), after cutting

Regarding the cylindrical specimens compacted at N_{design} (120 gyrations) and intended for fatigue characterisation, the stiffness modulus was evaluated after the cutting operations. As already anticipated, in this case the stiffness modulus was assessed exclusively at the temperature of 20 °C. The results obtained are reported below in tabular form.

Mix code	$E_{20°C}$ [MPa]	Dev. St. $E_{20°C}$ [-]
MIX50 1	14278.4	498.9
MIX50 2	12895.4	1020.1
MIX50 3	14977.1	1519.9
MIX50 REF	8963.0	420.4

Table 35. Average values of stiffness modulus for each mixture – 120 gyration cylindrical specimens.

For completeness, the data are also presented in graphical form, highlighting the specification limits set by the technical standards.

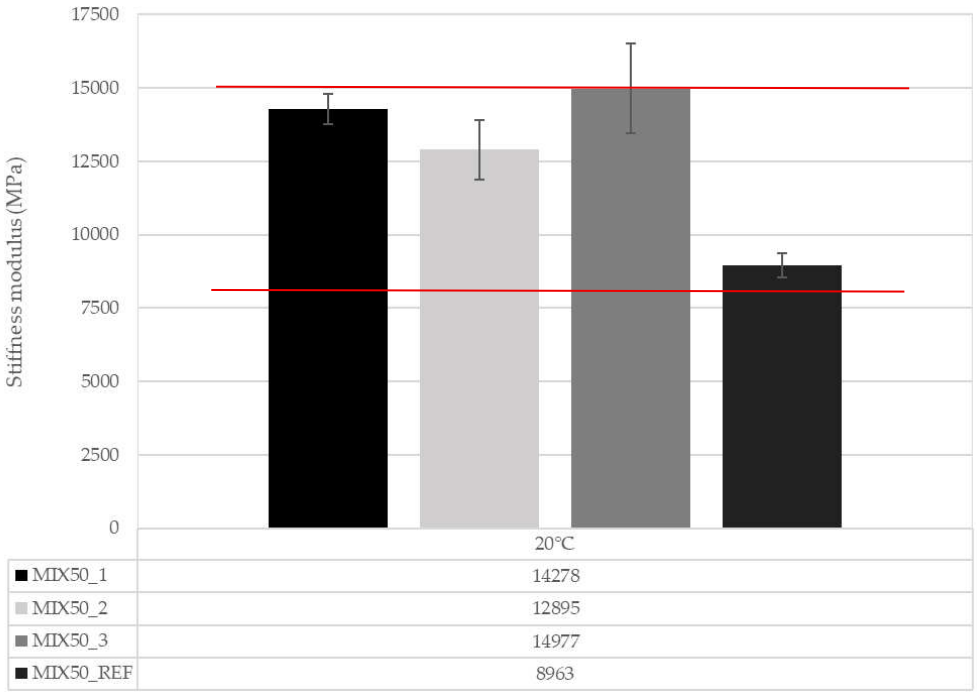

Figure 80. Trend of stiffness modulus for the analysed mixtures and prescribed limits – Cylindrical specimens compacted at 120 gyrations.

It is important to note that both the cylindrical specimens compacted at N_{max} (200 gyrations) and those compacted at N_{design} (120 gyrations) exhibit stiffness moduli at 20 °C that are compatible with the acceptability limits imposed by the Specifications.

As repeatedly highlighted throughout this work, both RAP and recycled plastics exert, when properly dosed and dispersed within the bituminous matrix, a marked stiffening effect on the mixture. This is attributable, on the one hand, to the presence of the aged binder contained in the RAP, characterised by a higher viscosity compared to virgin bitumen, and, on the other hand, to the contribution of the polymeric compound, which tends to stiffen the binder phase and improve the interaction with the aggregate skeleton.

In this context, the MIX50 REF mixture represents the "least stiff" reference among those investigated. It is in fact the only one without polymeric compound and has a total binder content equal to that of MIX50 1 (4.83%, see paragraph 4.3). With the same binder content, the absence of plastic means that the binder does not exhibit the additional stiffening induced by the polymeric component, resulting in a lower stiffness modulus compared to the modified mixtures.

Turning to the mixtures containing polymeric compound, if one were to consider only the plastic and RAP content from a purely theoretical standpoint—ideally assuming a constant total binder content—one might expect a monotonic (ideally quasi-linear) increase in stiffness modulus with increasing polymer content, from 0.3% to 0.7%. In other words, a progressive increase in the polymer fraction within the binder should translate into an increase in the overall stiffness of the mixture, due to the higher viscosity and the improved ability of the modified binder to transfer loads to the aggregate skeleton.

However, the experimental results do not follow this simplified trend. The stiffness modulus of a bituminous mixture does not depend solely on the nature and content of the binder (virgin, aged, modified), but is also strongly influenced by volumetric parameters, particularly the air-voids content. To correctly interpret the stiffness values, it is therefore necessary to recall what was previously discussed regarding bulk density and void content.

The MIX50 2 mixture, despite having an intermediate plastic content and a higher total binder contribution compared to the other mixtures, shows a lower average stiffness modulus at all temperatures considered. This apparently counterintuitive behaviour can be explained precisely in light of the volumetric parameters: MIX50 2 is the mixture with the highest void content. A higher void content implies lower compaction density and reduced continuity of both the binder phase and the aggregate skeleton, leading to a reduced ability of the mixture to distribute loads and, consequently, to a lower stiffness modulus. In other words, the stiffening effect of the polymeric compound is partly "offset" by the loss of compaction and the increase in voids.

This suggests the existence of a threshold plastic content beyond which the effect of the polymeric compound is no longer solely stiffening, but begins to interfere with the compaction process, worsening the volumetric structure of the mixture. Up to a certain limit, the addition of plastic contributes to stiffening the binder and improving the mechanical response; beyond that limit, an excess of polymeric component may make the binder too viscous or less lubricating during compaction, hindering proper aggregate rearrangement and increasing the void content.

In the case under examination, the addition of 0.3% plastic leads to an increase in the overall stiffness of the mixture, as the polymeric compound stiffens the binder without significantly compromising compaction. At 0.5%, however, the effect of the polymeric compound appears to result in reduced compactability: the mixture tends to compact less, voids increase, and the stiffness modulus decreases despite the higher plastic content. At 0.7% plastic, finally, the behaviour changes again: the plastic appears to exert a filling effect, occupying part of the voids and contributing to a new reduction in air-void content. This results in an increase in bulk density and, consequently, in the overall stiffness of the mixture. A non-linear behaviour thus emerges, in which the effect of the polymeric compound results from the interaction between rheological modifications of the binder and changes in the volumetric structure of the mixture.

In addition to the role of the polymeric compound, it is plausible that this behaviour is further influenced by the characteristics of the RAP used, particularly for the MIX50 2 mixture. RAP is not a perfectly homogeneous material: its mechanical performance may vary depending on its origin, the degree of binder ageing, the gradation, and possible segregation phenomena. Since it is produced in large quantities at the plant, local differences in the properties of the RAP incorporated into the mixtures cannot be excluded, nor can sampling errors or segregation during collection. A RAP that is locally stiffer or more brittle, or with a less favourable gradation, could modify the mechanical response of the mixture, amplifying or attenuating the effects of the polymeric compound and the void content.

A further relevant aspect is the absence of rejuvenator in the mixtures considered. The rejuvenator is an additive specifically used to “rejuvenate” the aged binder present in RAP, partially restoring its original rheological properties. In simplified terms, the rejuvenator tends to reduce the viscosity of the aged binder, improving its ductility and its ability to deform without cracking, and promoting better miscibility between virgin and aged bitumen. Its presence generally helps mitigate the excessive stiffening caused by high RAP contents, improving plant workability, field compaction, and fatigue performance.

In the present case, the absence of rejuvenator implies that the binder from the RAP retains a high degree of ageing, with higher viscosity and lower ability to dissipate deformations. This further stiffens the mixture, making it potentially more sensitive to cracking phenomena and less tolerant to variations in void content. In other words, in a system already stiffened by the presence of RAP and polymeric compound, the lack of rejuvenator amplifies the role of volumetric parameters: small variations in void content or compaction can translate into significant differences in stiffness modulus and in the overall mechanical behaviour.

4.6.3. Prismatic specimens

After discussing the results related to the cylindrical specimens prepared as part of the laboratory activity, the stiffness moduli measured on the prismatic specimens are now presented. As before, the reported data correspond to the average of the eight specimens produced for each mixture.

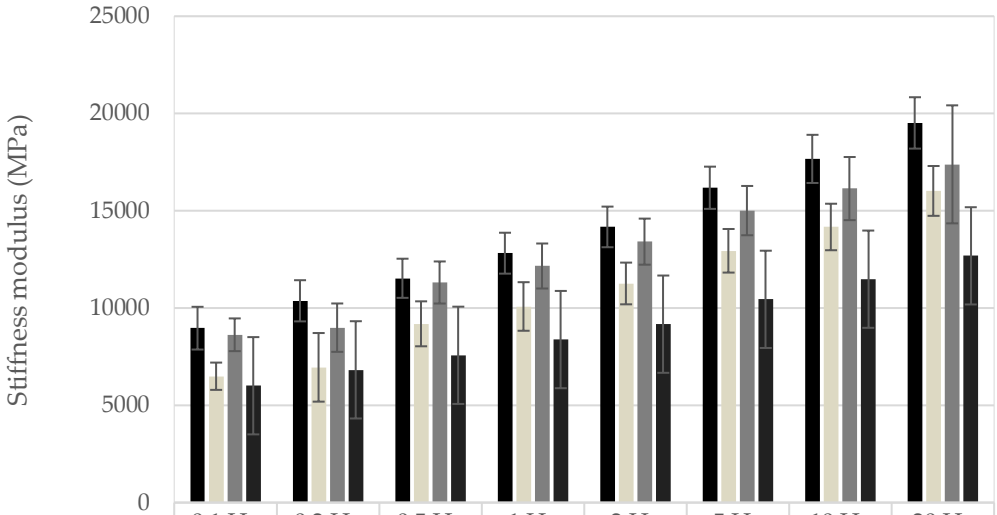

	0.1 Hz	0.2 Hz	0.5 Hz	1 Hz	2 Hz	5 Hz	10 Hz	20 Hz
MIX50_1	8966	10374	11531	12822	14171	16185	17668	19518
MIX50_2	6496	6953	9190	10082	11265	12945	14169	16022
MIX50_3	8627	8993	11315	12162	13414	15010	16143	17388
MIX50_REF	6007	6824	7571	8381	9172	10448	11484	12685

Figure 81. Trend of stiffness modulus for the analysed mixtures – Prismatic specimens.

In conclusion, the results related to the stiffness moduli of the prismatic specimens show a trend consistent with what was observed for the cylindrical specimens, confirming a substantial uniformity of behaviour among the analysed mixtures, regardless of the type of specimen prepared.

4.6.4. Statistical analysis of the results

To gain a deeper understanding of the differences observed in the stiffness values of the mixtures, it was necessary to carry out a statistical evaluation. A one-way analysis of variance (one-way ANOVA) was performed, a tool that makes it possible to determine whether the variations observed among the mean values of the different groups are attributable to a real effect or whether they may be ascribed to normal experimental variability.

The ANOVA approach compares the dispersion of the data within each group with the variability observed between the group means: when the latter is significantly greater than the former, it can be concluded that the differences between the mixtures are not random but statistically significant. Conversely, the analysis suggests that, based on the available data, there is insufficient evidence to state that the mixtures exhibit genuinely distinct mechanical behaviours in terms of stiffness.

The outcomes of the statistical analysis are presented below, organised according to the same sequence adopted for the presentation of the experimental results: first the cylindrical specimens compacted at N_{max}, then those compacted at N_{design}, and finally the prismatic specimens.

To complement the analysis, a post hoc test was also carried out, with the aim of precisely identifying which pairs of mixtures exhibited statistically significant differences.

1. Cylindrical specimens compacted at Nmax (200 gyrations)

ANOVA a una via (Fisher)

	F	gdl1	gdl2	p
Stiffness modulus	4.08	3	24	.018

Table 36. Results of the one way ANOVA test on the stiffness moduli of cylindrical specimens compacted at 200 gyrations.

Descrittive Gruppo

	Mix code	N	Media	SD	SE
Stiffness modulus	MIX50_1	7	13360	1466	554
	MIX50_2	7	11121	1224	463
	MIX50_3	7	13305	933	352
	MIX50_REF	7	11719	2065	780

Table 37. Descriptive parameters of the mixture for the purpose of the test – cylindrical specimens compacted at 200 gyrations.

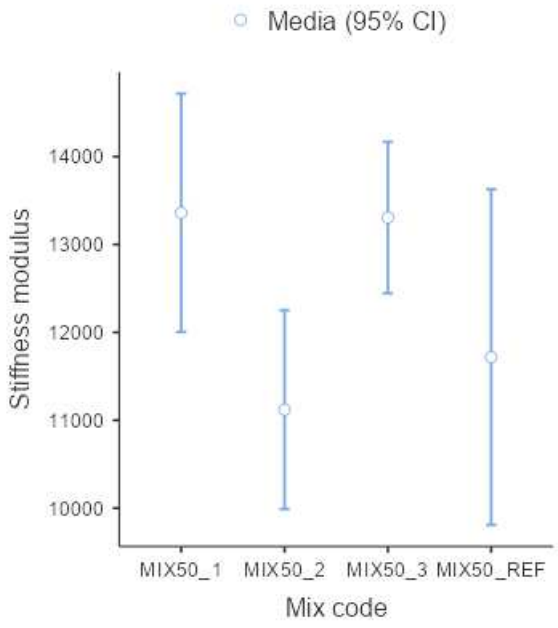

Figure 82. Mean stiffness values for each mixture, with corresponding 95% confidence intervals– cylindrical specimens compacted at 200 gyrations.

Test Post-Hoc di Tukey – Stiffness modulus

		MIX50_1	MIX50_2	MIX50_3	MIX50_REF
MIX50_1	Differenza media	—	2239 *	54.9	1641
	valore p	—	.043	1.000	.191
MIX50_2	Differenza media		—	−2183.9	−597
	valore p		—	.050	.874
MIX50_3	Differenza media			—	1586
	valore p			—	.215
MIX50_REF	Differenza media				—
	valore p				—

Nota. * p < .05, ** p < .01, *** p < .001

Table 38. Results of the post hoc test performed on the stiffness values– cylindrical specimens compacted at 200 gyrations.

2. Cylindrical specimens compacted at Ndesign (120 gyrations), after cutting

ANOVA a una via (Fisher)

	F	gdl1	gdl2	p
Stiffness modulus	9.65	3	32	< .001

Table 39. Results of the one way ANOVA test on the stiffness moduli of cylindrical specimens compacted at 120 gyrations.

Descrittive Gruppo

	Mix code	N	Media	SD	SE
Stiffness modulus	MIX50_1	9	14278	499	166
	MIX50_2	9	12895	1020	340
	MIX50_3	9	14977	1520	507
	MIX50_REF	9	13023	420	140

Table 40. Descriptive parameters of the mixture for the purpose of the test – cylindrical specimens compacted at 120 gyrations.

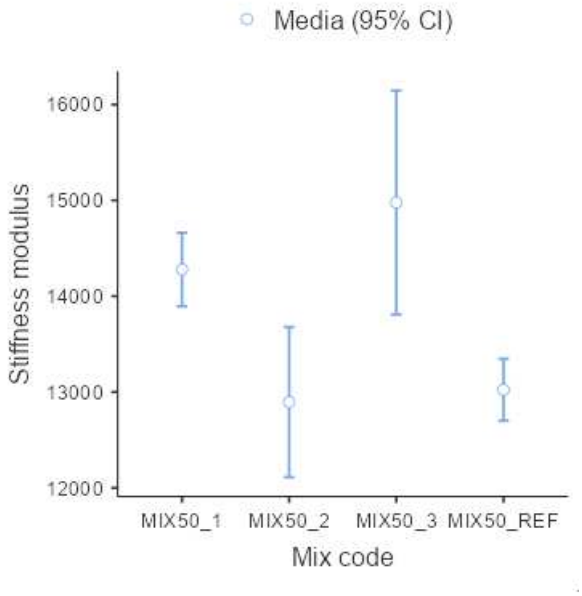

Figure 83. Mean stiffness values for each mixture, with corresponding 95% confidence intervals– cylindrical specimens compacted at 120 gyrations.

Test Post-Hoc di Tukey – Stiffness modulus

		MIX50_1	MIX50_2	MIX50_3	MIX50_REF
MIX50_1	Differenza media	—	1383*	−699	1255*
	valore p	—	.024	.435	.047
MIX50_2	Differenza media		—	−2082***	−128
	valore p		—	< .001	.992
MIX50_3	Differenza media			—	1954***
	valore p			—	< .001
MIX50_REF	Differenza media				—
	valore p				—

Nota. * p < .05, ** p < .01, *** p < .001

Table 41. Results of the post hoc test performed on the stiffness values– cylindrical specimens compacted at 120 gyrations.

3. Prismatic specimens

ANOVA a una via (Fisher)

	F	gdl1	gdl2	p
Stiffness modulus	9.12	3	28	< .001

Table 42. Results of the one way ANOVA test on the stiffness moduli of prismatic specimens.

Descrittive Gruppo

	Mix code	N	Media	SD	SE
Stiffness modulus	MIX50_1	8	17671	1146	405
	MIX50_2	8	14169	1195	422
	MIX50_3	8	16143	1622	574
	MIX50_REF	8	16896	1596	564

Table 43. Descriptive parameters of the mixture for the purpose of the test – prismatic specimens.

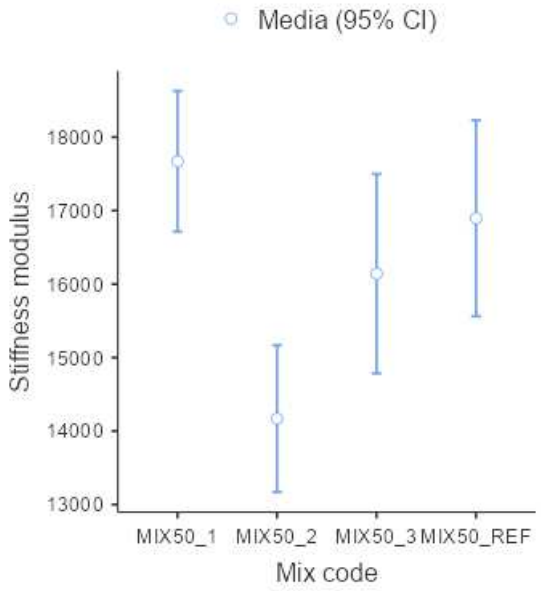

Figure 84. Mean stiffness values for each mixture, with corresponding 95% confidence intervals– prismatic specimens.

Test Post-Hoc di Tukey – Stiffness modulus

		MIX50_1	MIX50_2	MIX50_3	MIX50_REF
MIX50_1	Differenza media	—	3502***	1528	775
	valore p	—	< .001	.156	.692
MIX50_2	Differenza media		—	−1974*	−2727**
	valore p		—	.042	.003
MIX50_3	Differenza media			—	−754
	valore p			—	.710
MIX50_REF	Differenza media				—
	valore p				—

Nota. * p < .05, ** p < .01, *** p < .001

Table 44. Results of the post hoc test performed on the stiffness values– prismatic specimens.

The outcome of this in-depth assessment confirmed what had already been suggested by the experimental evidence, highlighting the combinations of mixtures that exhibit significant deviations in stiffness values. In particular, as shown by the three post-hoc tests performed, there are statistically significant differences between the mixtures referred to as MIX50 1 and MIX50 2, as well as between the mixtures MIX50 3 and MIX50 REF.

4.7. Indirect tensile strength

The indirect tensile strength (ITS) is a key parameter for assessing the response of a bituminous mixture to tensile stresses, which are particularly relevant in thermal and fatigue cracking phenomena. According to BS EN 12697-23, this quantity is obtained by applying a diametral load to a cylindrical specimen until failure, thus determining the maximum tensile stress under the prescribed test conditions.

In continuity with the approach adopted in the previous sections, the results obtained for the cylindrical specimens compacted at N_{max} (200 gyrations) are first presented in tabular form; subsequently, after introducing the prescriptive limits set by the Special Tender Specifications of the A4 motorway, they are also represented graphically.

Mix code	ITS [N/mm^2]	Dev. St. ITS [-]
MIX50 1	2.29	0.07
MIX50 2	1.87	0.28
MIX50 3	2.25	0.18
MIX50 REF	1.72	0.22

Table 45. Average values of indirect tensile strength for each mixture – 200 gyration cylindrical specimens.

The performance requirements set by the Special Tender Specifications differ between mixtures modified with polymeric compound and those containing hard bitumen. For completeness, the prescriptive values relating to binder layers produced with unmodified bitumen and with polymers introduced through the dry technology are reported below, as indicated in the CSA of the A4 motorway (page 92, article 5.6.9).

Risultati richiesti	Unità di misura	Limiti (UNI EN 13108-1)
Affinità bitume-aggregato – Spogliamento (UNI EN 12697-11)	%	≥ 5
Vuoti a N1 (UNI EN 12697-8)	%	≤ 14 (V_{max14})
Vuoti a N2 (UNI EN 12697-8)	%	3 ÷ 6 (V_{min3}-V_{max6})
Vuoti a N3 (UNI EN 12697-8)	%	≥ 2 (V_{min2})
Resistenza a Trazione Indiretta a 25°C (UNI EN 12697-23)	N/mm²	1,20 ÷ 2,20
Coefficiente di Trazione Indiretta a 25°C	N/mm²	60 ÷ 250
Perdita di Resistenza a Trazione Indiretta a 25°C (UNI EN 12697-12)	%	≥ 90 ($ITSR_{90}$)
Rigidezza (UNI EN 12697-26 – Annesso C)		
T= 5°C, Def.= 7µm, Freq.= 2Hz, Coeff.P.= 0,35	N/mm²	18.000 ÷ 27.000
T= 20°C, Def.= 7µm, Freq.= 2Hz, Coeff.P.= 0,35	N/mm²	8.000 ÷ 15.000
T= 40°C, Def.= 7µm, Freq.= 2Hz, Coeff.P.= 0,35	N/mm²	900 ÷ 6.000

Table 46. Performance limits for bituminous mixtures with unmodified binder and with polymers introduced through the dry process technology (source: CSA – A4 Motorway).

Meanwhile, the prescriptive values relating to the binder layers made with hard-modified bitumen, as indicated in the CSA of the A4 motorway (page 81, article 5.5.10), are as follows:

Risultati richiesti	Unità di misura	Limiti (UNI EN 13108-1)
Affinità bitume-aggregato – Spogliamento (UNI EN 12697-11)	%	≥ 5
Vuoti a N1 (UNI EN 12697-8)	%	≤ 14 (V_{max14})
Vuoti a N2 (UNI EN 12697-8)	%	3 ÷ 6 (V_{min3}-V_{max6})
Vuoti a N3 (UNI EN 12697-8)	%	≥ 2 (V_{min2})
Resistenza a Trazione Indiretta a 25°C (UNI EN 12697-23)	N/mm²	0,95 ÷ 1,70
Coefficiente di Trazione Indiretta a 25°C	N/mm²	60 ÷ 250
Perdita di Resistenza a Trazione Indiretta a 25°C (UNI EN 12697-12)	%	≥ 90 ($ITSR_{90}$)
Rigidezza (UNI EN 12697-26 – Annesso C)		
T= 5°C, Def.= 7µm, Freq.= 2Hz, Coeff.P.= 0,35	N/mm²	14.000 ÷ 20.000
T= 20°C, Def.= 7µm, Freq.= 2Hz, Coeff.P.= 0,35	N/mm²	5.000 ÷ 8.000
T= 40°C, Def.= 7µm, Freq.= 2Hz, Coeff.P.= 0,35	N/mm²	700 ÷ 2.500

Table 47. Performance limits for bituminous mixtures with hard grade modified binder (source: CSA – A4 Motorway).

The data reported in the previous table have also been represented in graphical form. In the graphs, the prescriptive limits established by the CSA have been included through red reference lines, depending on the mixture considered.

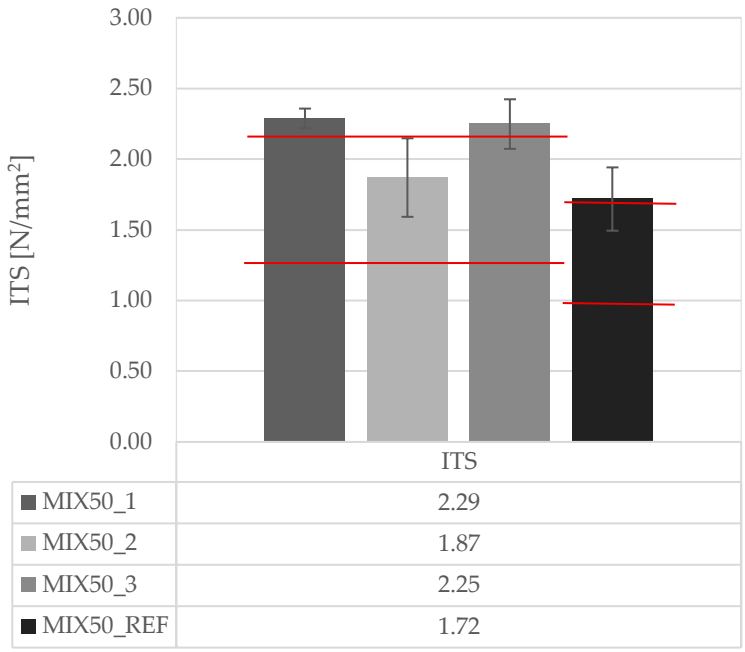

Figure 85. Trend of ITS for the analysed mixtures and prescribed limits – 200 gyration cylindrical specimens.

The analysis of the histogram shows that, except for the mixture referred to as MIX50 2, none of the formulations examined fall within the limits required by the specifications. The indirect tensile strength (ITS) tends to increase when the mixture exhibits good internal cohesion and an effective bond between bitumen and aggregates. However, particularly high values may indicate an excessively stiff behaviour, which makes the material more susceptible to cracking phenomena, especially under severe thermal conditions.

This picture is consistent with the results related to the stiffness moduli: the MIX50 1 and MIX50 3 mixtures, which show ITS values above the prescriptive limits, are also those characterised by higher stiffness compared to MIX50 2. This association suggests that, in the specific case, the increase in stiffness does not translate into an improvement in tensile strength, but rather into a reduced ability of the mixture to deform without breaking, confirming the brittle nature of the stiffer formulations.

Furthermore, within the framework of this thesis, the Indirect Tensile Coefficient (CTI) was also evaluated. This parameter, introduced by Italian technical standards, is used to assess the quality and durability of bituminous mixtures through the indirect tensile strength (ITS) test.

The CTI does not represent an absolute mechanical value, but a performance index that relates the indirect tensile strength of the mixture to the minimum requirements established by the specifications. It is defined by the following relation:

$$CTI = \frac{\pi\, D\, ITS}{2\, dv}$$

where:

- CTI is the indirect tensile coefficient, expressed in MPa.
- ITS is the indirect tensile strength, expressed in MPa.
- D is the average of the two diameter measurements recorded as described in paragraph 3.3.6, expressed in mm.
- dv is the deformation of the specimen, expressed in mm.

The values obtained from this calculation for each of the mixtures analysed are presented below.

Mix code	CTI [N/mm^2]	Dev. St. CTI [-]
MIX50 1	239.87	121.85
MIX50 2	203.67	48.68
MIX50 3	256.53	82.06
MIX50 REF	188.07	56.41

Table 48. Average values of CTI for each mixture – 200 gyration cylindrical specimens

.

Unlike what was observed for the indirect tensile strength, the performance requirements established by the Special Tender Specifications are identical for mixtures modified with polymeric compound and for those containing hard bitumen. The reference prescriptive values are reported in the following table, where they have been appropriately highlighted to facilitate consultation.

Risultati richiesti	Unità di misura	Limiti (UNI EN 13108-1)
Affinità bitume-aggregato – Spogliamento (UNI EN 12697-11)	%	≥ 5
Vuoti a N1 (UNI EN 12697-8)	%	≤ 14 (V_{max14})
Vuoti a N2 (UNI EN 12697-8)	%	3 ÷ 6 (V_{min3}-V_{max6})
Vuoti a N3 (UNI EN 12697-8)	%	≥ 2 (V_{min2})
Resistenza a Trazione Indiretta a 25°C (UNI EN 12697-23)	N/mm^2	1,20 ÷ 2,20
Coefficiente di Trazione Indiretta a 25°C	N/mm^2	60 ÷ 250
Perdita di Resistenza a Trazione Indiretta a 25°C (UNI EN 12697-12)	%	≥ 90 ($ITSR_{90}$)
Rigidezza (UNI EN 12697-26 – Annesso C)		
T= 5°C, Def.= 7µm, Freq.= 2Hz, Coeff.P.= 0,35	N/mm^2	18.000 ÷ 27.000
T= 20°C, Def.= 7µm, Freq.= 2Hz, Coeff.P.= 0,35	N/mm^2	8.000 ÷ 15.000
T= 40°C, Def.= 7µm, Freq.= 2Hz, Coeff.P.= 0,35	N/mm^2	900 ÷ 6.000

Table 49. Performance limits for bituminous mixtures (source: CSA – A4 Motorway).

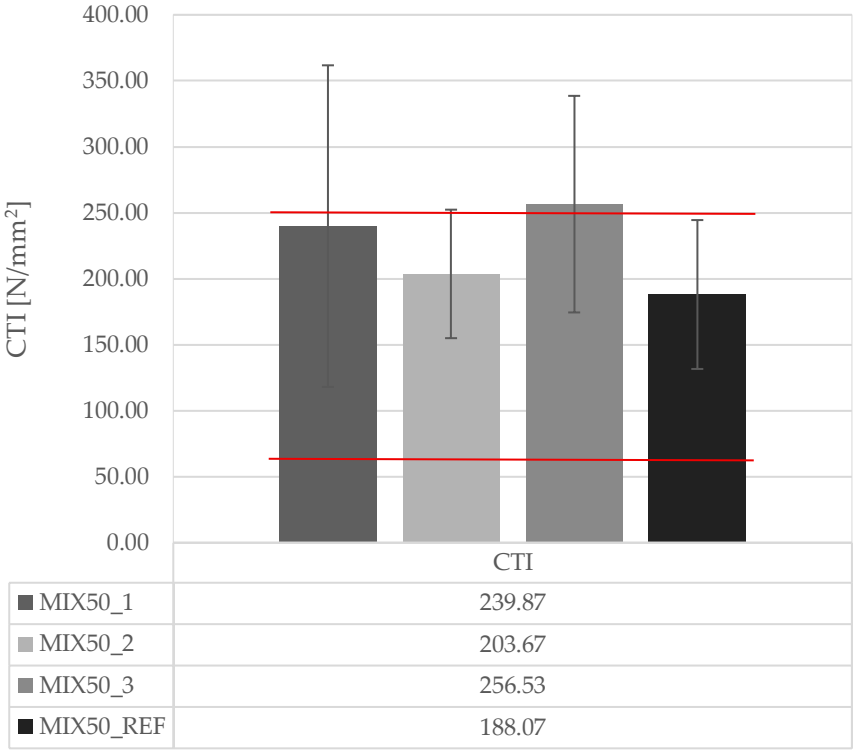

Figure 86. Trend of CTI for the analysed mixtures and prescribed limits – 200 gyration cylindrical specimens.

4.8. Fatigue performance

To conclude the experimental programme, the results related to the fatigue characterisation of the analysed mixtures are presented, a central theme of the entire work. For a broader theoretical and procedural framework, reference is made to paragraph 3.3.10, where the methodologies adopted for the execution of the tests are described in detail.

Before proceeding with the analysis of the results, it is appropriate to clarify the criterion adopted for their presentation, both for the cylindrical and the prismatic specimens, and to illustrate the preliminary process carried out to verify the quality of the experimental data. In particular, a careful statistical evaluation was conducted to identify any anomalous values, ensuring that the fatigue curves and subsequent elaborations are based exclusively on reliable measurements.

The analysis of the experimental results makes it possible to derive, through regression of the fatigue curves, the value of horizontal strain associated with a failure life of $N_f = 10^6$ cycles. This parameter, indicated as $\varepsilon_6$and expressed in μm/m, represents a synthetic indicator of the mixture's ability to withstand repeated loads over time. High ε_6 values are generally associated with more ductile materials capable of dissipating energy, and therefore less prone to fatigue cracking. Conversely, a lower value suggests a more brittle behaviour and a reduced tolerance to deformation, resulting in a shorter service life of the material.

To ensure the statistical reliability of the above regressions, a preliminary verification of the data was carried out to identify any anomalous values. For this purpose, the interquartile range (IQR) method was adopted, which is particularly effective in recognising significant deviations from the central distribution of the data. The approach involved calculating the residuals of each experimental point with respect to the regression line and subsequently determining the quartiles Q_1 and Q_3, from which the interquartile range was obtained as $IQR = Q_3 - Q_1$. Based on these values, the acceptability limits were defined:

$$\text{Upper limit} = Q_3 + 1.5 \cdot IQR$$

$$\text{Lower limit} = Q_1 - 1.5 \cdot IQR$$

Points with residuals falling outside this interval were classified as outliers and excluded from the subsequent analyses. In the paragraphs dedicated respectively to the cylindrical and prismatic specimens, an indication is also provided, for each specimen type of the samples excluded from the analysis following the identification of anomalous values.

4.8.1. Cylindrical specimens

As anticipated in Chapter 3, the tests on the cylindrical specimens were carried out using the CIT CY configuration, in accordance with the requirements of EN 12697-24. This procedure involves the application of cyclic loads along the diameter of the specimen, generating a tensile field in the direction perpendicular to the loading line. The load is applied under load-controlled conditions through a continuous sinusoidal wave at 10 Hz, without rest periods.

For each mixture, at least three repetitions were performed for each of the three stress levels considered, for a total of nine specimens tested per mixture and, overall, thirty-six tests. The preliminary statistical analysis identified a single anomalous value, related to the MIX50 3 mixture, which was subsequently excluded from the elaborations.

In continuity with the approach adopted throughout the work, the results are first presented in tabular form. The following table reports the regression parameters of the fatigue law (intercept k_ε and slope n_ε), together with the coefficient of determination R^2, which indicates the degree of agreement between the model and the experimental data, and the extrapolated ε_6 values for each mixture, calculated according to the two failure criteria described in Chapter 2.

Mix code	Failure Criteria	k_ε [-]	n_ε [-]	R^2 [-]	ε_6 [μm/m]
MIX50_1	50%	7.71E+13	-4.871	0.911	44
	ER	1.26E+13	-4.508	0.995	40
MIX50_2	50%	6.53E+10	-3.418	0.905	29
	ER	3.03E+10	-3.284	0.916	25
MIX50_3	50%	3.08E+10	-3.216	0.986	25
	ER	2.83E+10	-3.222	0.946	25
MIX50_REF	50%	2.89E+09	-2.808	0.984	18
	ER	3.34E+09	-2.864	0.981	18

Table 50. Regression parameters and ε_6 values for each mixture and for the different failure criteria – cylindrical specimens.

From the examination of the ε_6 values reported in the previous table, it clearly emerges that the MIX50 1 mixture exhibits the best fatigue resistance among the formulations considered. As discussed in the introductory paragraph of this chapter, high ε_6 values are indicative of a more ductile material capable of effectively dissipating the energy induced by repeated loads, with a lower tendency to initiate and propagate cracks. Conversely, lower values suggest a more brittle behaviour and a reduced ability to withstand cyclic deformations, ultimately leading to a shorter service life.

This evidence is confirmed by comparing the average air-void contents obtained after trimming, as reported in paragraph 4.5.3. The MIX50 1 mixture is indeed the one with the lowest average void content among all the mixtures analysed. This result is fully consistent with the well-known relationship between porosity and fatigue behaviour: a high void content introduces internal discontinuities that promote stress concentration and the initiation of microcracks, whereas a denser structure enhances material cohesion and its ability to transfer stresses between aggregates and bituminous binder.

The trend observed for the MIX50 REF mixture further supports this behaviour, showing a lower fatigue life associated with a higher void content. Conversely, more compact mixtures tend to develop larger deformations before failure, making them less susceptible to cracking. Within this framework, the MIX50 2 and MIX50 3 mixtures exhibit intermediate and substantially similar performance.

Overall, the results suggest that, under the loading conditions considered, the hybrid polymer-modification approach can provide superior fatigue performance compared to the wet modification.

The fatigue curves for the different mixtures analysed are presented below, providing a graphical representation of the observations discussed above. For completeness, two separate graphs are shown: the first refers to the failure criterion based on a 50% reduction of the initial modulus, while the second uses the Energy Ratio criterion.

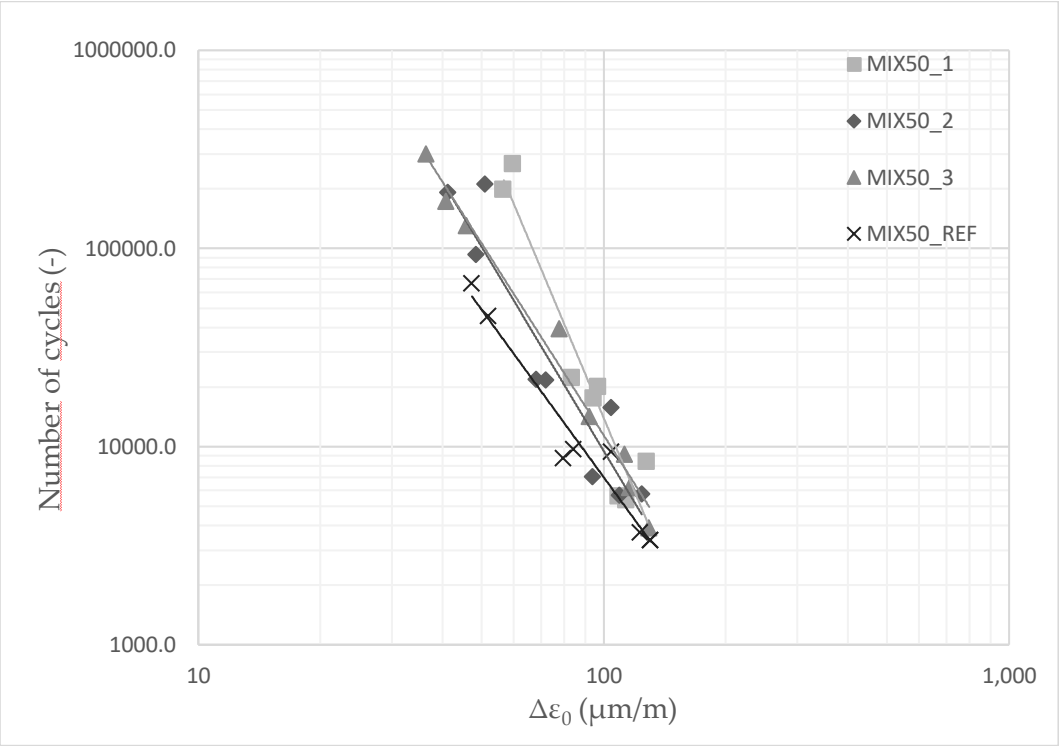

Figure 87. Fatigue lines for the different mixtures, cylindrical specimens – 50% initial modulus criterion.

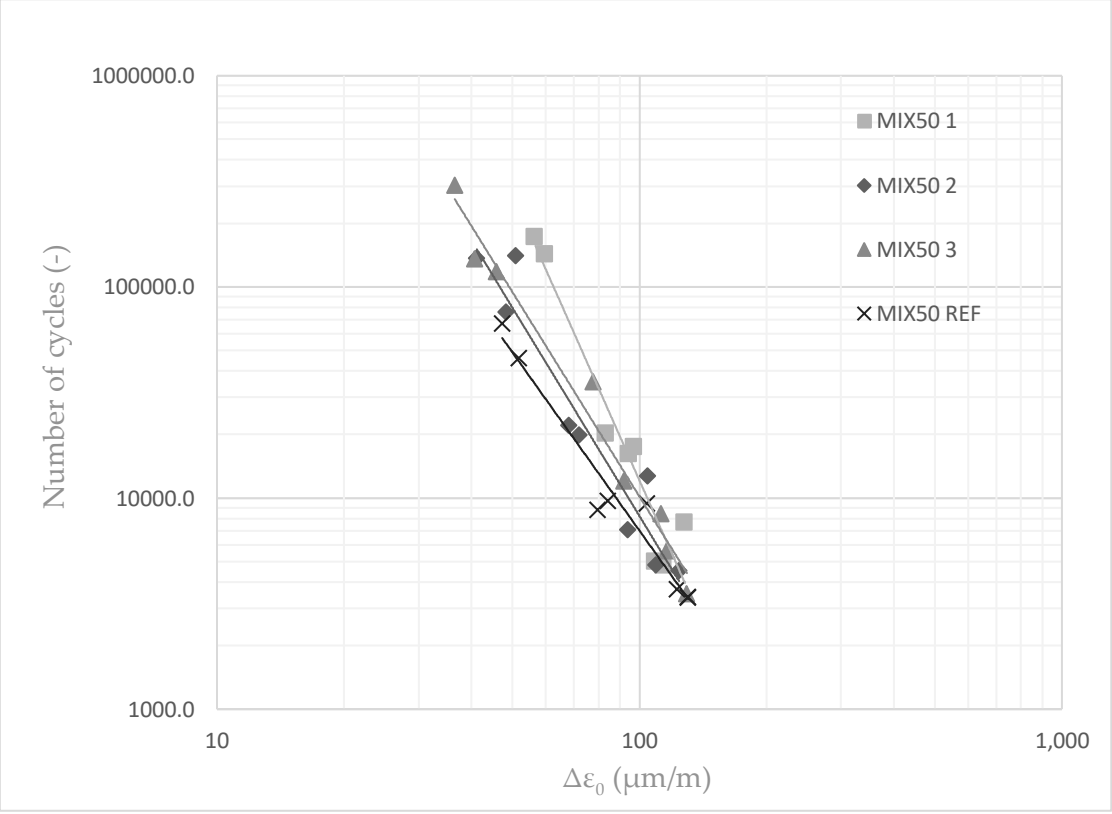

Figure 88. Fatigue lines for the different mixtures, cylindrical specimens – Energy Ratio criterion.

4.8.2. Prismatic specimens

As anticipated in Chapter 3, the tests on the prismatic specimens were carried out using the 4PB-PR configuration, in accordance with the requirements of EN 12697-24. The strain-controlled test performed on prismatic specimens involves subjecting the beams to periodic flexural loading through the application of a sinusoidal load at a frequency of 10 Hz. This configuration makes it possible to generate, in the central region of the beam, a condition of constant bending moment (and therefore constant deformation). For this configuration, eight specimens were used for each mixture.

The preliminary statistical analysis identified three anomalous values, related to the MIX50 2, MIX50 3 and MIX50 REF mixtures (one for each mixture), which were subsequently excluded from the elaborations.

In continuity with the approach adopted for the cylindrical specimens, the results are first presented in tabular form. The following table reports the regression parameters of the fatigue law (intercept k_ε and slope n_ε), together with the coefficient of determination R^2, which indicates the agreement between the model and the experimental data, and the extrapolated ε_6 values for each mixture, calculated according to the two failure criteria described in Chapter 2.

Mix code	Failure Criteria	k_ε [-]	n_ε [-]	R^2 [-]	ε_6 [μm/m]
MIX50_1	50%	7.42E+25	-9.640	0.955	116
	ER	2.52E+20	-7.052	0.927	116
MIX50_2	50%	9.22E+16	-5.427	0.561	124
	ER	2.28E+15	-4.674	0.453	126
MIX50_3	50%	6.14E+13	-4.118	0.430	108
	ER	1.47E+19	-6.599	0.451	109
MIX50_REF	50%	2.87E+18	-6.298	0.760	103
	ER	4.67E+20	-7.321	0.795	106

Table 51. Regression parameters and ε_6 values for each mixture and for the different failure criteria – prismatic specimens.

The results obtained with this testing configuration show a greater data dispersion than expected and significantly higher than that observed in the other experimental setups, as also suggested by the values of the coefficient of determination R^2. This variability made both the interpretation of the fatigue behaviour and the definition of a sufficiently reliable fatigue law less straightforward. For this reason, the assessment of the mixtures' performance was carried out using a cautious approach, aimed at capturing only the main trends.

From an initial analysis, the MIX50 2 mixture appears to exhibit the most favourable performance; however, this is only a preliminary indication, which would require further investigation to be confirmed with greater robustness. Despite the data dispersion, a signal consistent with what was observed in the other testing configurations still emerges: the hybrid polymer-modification approach appears capable of providing overall superior fatigue resistance compared to the wet modification.

The fatigue curves for the different mixtures analysed are presented below, providing a graphical representation of the observations discussed above. For completeness, two separate graphs are shown: the first refers to the failure criterion based on a 50% reduction of the initial modulus, while the second uses the Energy Ratio criterion.

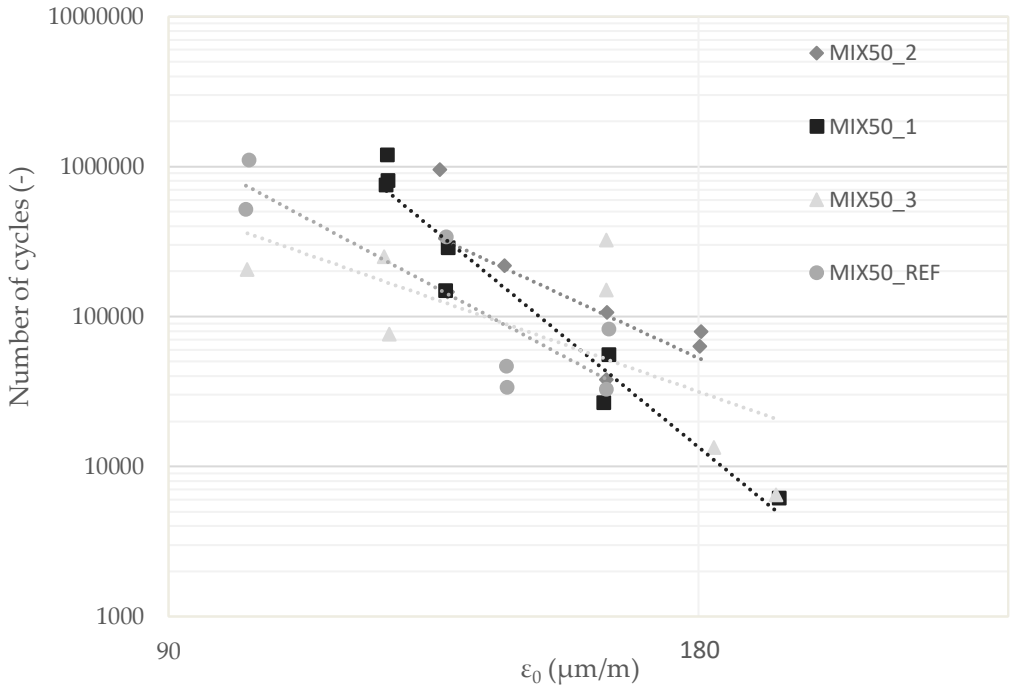

Figure 89. Fatigue lines for the different mixtures, prismatic specimens – 50% initial modulus criterion.

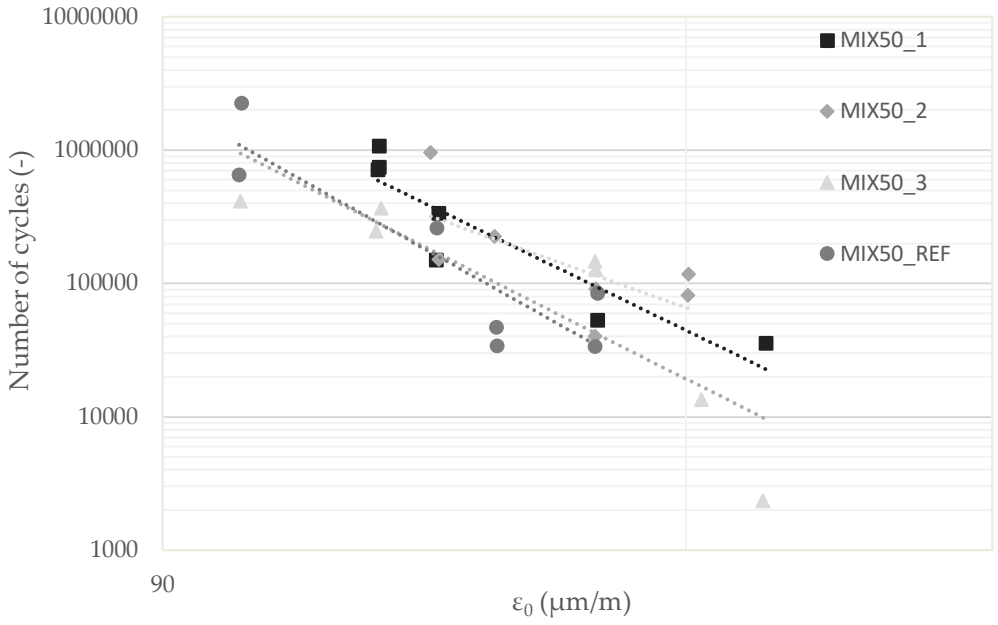

Figure 90. Fatigue lines for the different mixtures, prismatic specimens – Energy Ratio criterion.

5. *Comparison between plant-produced and laboratory-produced mixtures*

The analysis developed in this chapter focuses on the systematic comparison between the asphalt mixtures produced in the plant within the current study and a set of mixtures prepared in the laboratory during previous research activities. After having thoroughly presented the results of the plant-produced mixtures in the previous chapter, the aim is now to outline any performance correspondences or deviations with the analogous mixtures produced in the laboratory.

The comparison focuses specifically on stiffness moduli and fatigue response, which are fundamental parameters for assessing the durability and reliability of the analysed solutions.

5.1. Laboratory produced mixtures

To ensure a complete interpretative framework, a detailed description of the laboratory procedures adopted for the preparation of the reference mixtures will also be provided, with particular attention to the operational and methodological aspects that guided their production.

The laboratory-prepared mixtures considered as reference terms are the following:

- *SP1 4.8%*: composed of 50% virgin aggregates, 50% RAP by aggregate weight, 0.3% rejuvenator by RAP weight, 0.3% polymer compound by mixture weight, and 2% neat bitumen by total mixture weight.
- *SP2 5.0%*: composed of 50% virgin aggregates, 50% RAP by aggregate weight, 0.3% rejuvenator by RAP weight, 0.5% polymer compound by mixture weight, and 2% neat bitumen by total mixture weight.
- *PMB 4.5%*: composed of 50% virgin aggregates, 50% RAP by aggregate weight, 0.3% rejuvenator by RAP weight, and 2% polymer-modified bitumen by total mixture weight.

These formulations are directly comparable with the mixtures named MIX50 1, MIX50 2 and MIX50 REF analysed in the present work, allowing for a coherent and in-depth evaluation of the mechanical performance obtained in the plant with respect to those observed in the laboratory.

The preparation of the asphalt mixtures followed a laboratory protocol designed to reproduce the conditions of an industrial plant and to activate the aged binder contained in the RAP. Once the composition was defined, the virgin aggregates were weighed and heated up to approximately 280 °C, to ensure an adequate thermal gradient during mixing. The RAP was instead brought to 70 °C and treated with a predetermined amount of rejuvenator, promoting the softening of the oxidised binder and the breakdown of agglomerates.

Filler and bitumen were also prepared beforehand: the former dried and kept at 160 °C, the latter heated to the same temperature to ensure workability. Mixing was carried out in a mechanical mixer maintained at 170 °C. The heated aggregates were introduced first, from the coarsest to the finest fraction, and briefly mixed. The treated RAP was then added, generating a thermal shock that quickly brought the material to the working temperature without prolonged direct heating. After about one minute, the polymer compound was incorporated, exploiting the high temperature of the mixture to promote its softening and uniform distribution. The virgin bitumen and filler were added in two separate stages, each followed by short periods of low-speed mixing to ensure gradual integration.

Once all components had been added, the mixture underwent high-speed mixing and was then left to rest for about fifteen minutes at the working temperature, simulating transport from the plant to the construction site. Finally, a short final mixing phase was performed, first at low speed and then at high speed, to reproduce the action of the paver and obtain characteristics representative of real laying conditions.

5.2. Stiffness moduli

This paragraph presents the comparison between the mixtures produced in the plant and those prepared in the laboratory, with reference to stiffness modulus values. For ease of reading, the results for mixtures MIX50 1, MIX50 2 and MIX50 REF, obtained on cylindrical specimens compacted at N_{design} (120 gyrations) and used for the fatigue characterisation of the plant-produced mixtures, are reported again. The values shown in the graph and table correspond to the averages of the nine specimens prepared for each mixture.

As previously described, the stiffness modulus of each specimen is calculated as the average of two consecutive measurements. Between one measurement and the next, the specimen is rotated by 90° ± 10° around its horizontal axis, to assess any anisotropy introduced by the compaction process. The standard also requires that the average of the second set of measurements falls within the +10% / −20% range relative to the average of the first set, a necessary condition to ensure data reliability and repeatability.

Once this verification has been carried out and any non-compliant measurements excluded, the average modulus values used for the comparison between the different mixtures are finally reported.

Mix code	$E_{20°C}$ [MPa]	Dev. St. $E_{20°C}$ [-]
MIX50 1	14278.4	498.9
MIX50 2	12895.4	1020.1
MIX50 REF	8963.0	420.4

Table 52. Average values of stiffness modulus for each mixture produced in plant – 120 gyration cylindrical specimens.

As anticipated in paragraph 4.6.1, the values obtained comply with the prescriptive limits established by the Special Tender Specifications of the A4 motorway. To make the interpretation of the stiffness modulus results more immediate, the data reported in the previous table have also been represented graphically, to highlight more clearly the differences between the mixtures considered.

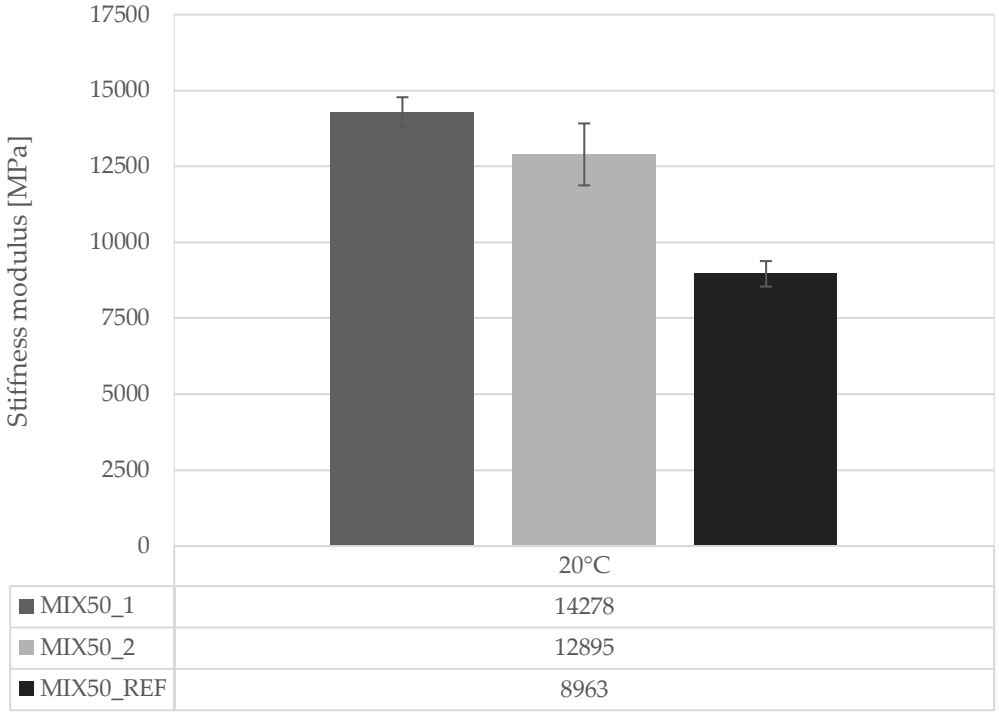

Figure 91. Trend of stiffness modulus for the analysed mixtures (produced in plant) and prescribed limits – Cylindrical specimens compacted at 120 gyrations.

Similarly to what was illustrated for the plant-produced mixtures, the stiffness moduli of the mixtures mentioned in the introductory paragraph of this chapter are reported below. In this case as well, the acceptance procedure for the results follows the same criteria adopted throughout the entire work, ensuring consistency and comparability of the data. The values presented represent the averages of the six specimens prepared for each mixture, obtained after verifying the requirements necessary for the acceptance of the measurements.

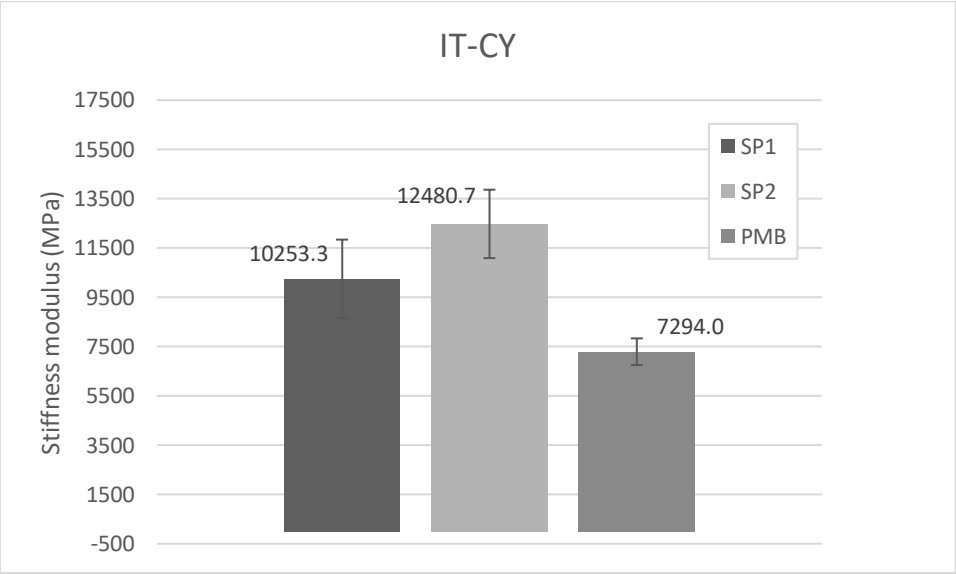

Figure 92. Trend of stiffness modulus for the analysed mixtures produced in laboratory – Cylindrical specimens compacted at 120 gyrations (source: thesis [54]).

To facilitate the comparison between the different mixtures, a cartesian plane structured as follows is used: on the x-axis, the average stiffness modulus values at 20 °C of the laboratory-produced mixtures are reported, while on the y-axis the corresponding values of the plant-produced mixtures appear. The bisector represents the condition of perfect coincidence between the two data sets: if the points related to the same mixture lie along this line, it means that the behaviour of the plant-produced mixtures and that of the laboratory-produced ones is essentially identical. Consequently, the distance of the points from the bisector indicates the degree of deviation between the two production conditions, highlighting any differences in the mechanical behaviour of the mixtures.

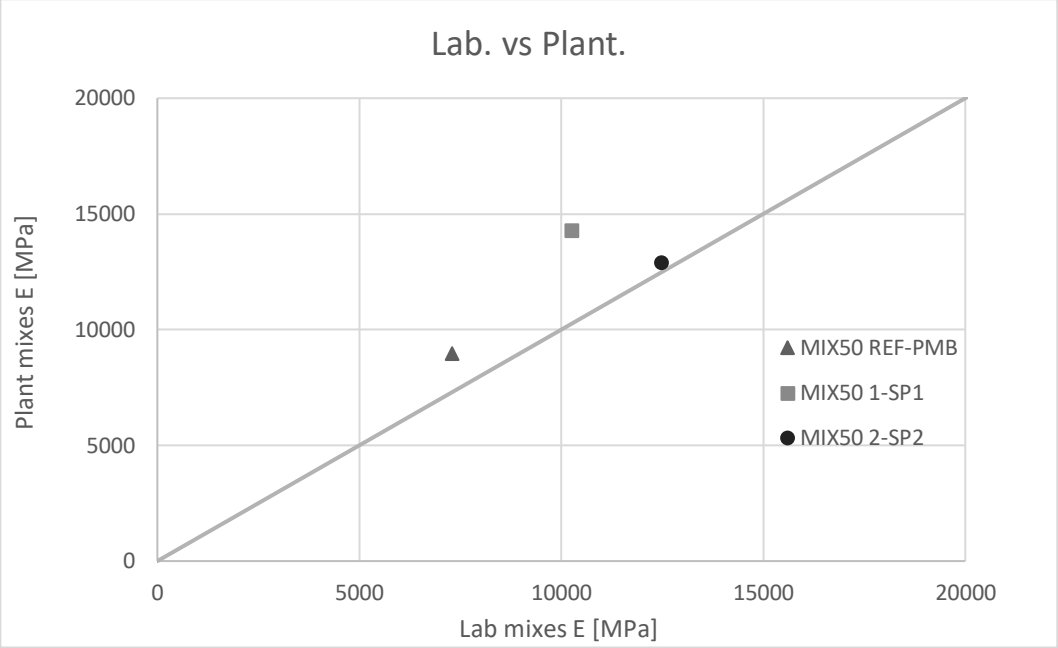

Figure 93. Direct comparison between plant produced and laboratory produced mixtures – 120 gyration cylindrical specimens, stiffness moduli.

The trend shown by the graph highlights that the points do not lie along the bisector, indicating the absence of a perfect correspondence between the mixtures produced in the laboratory and those manufactured in the plant. In all the mixtures analysed, the stiffness moduli of the compacted specimens are systematically higher for the mixtures coming from the plant, suggesting a stiffer mechanical behaviour compared to the corresponding laboratory samples.

A first interpretation can be attributed to the differences in rejuvenator content: the laboratory mixtures contain 0.3% by RAP weight, whereas in the plant a significantly lower amount was introduced compared to the planned mix designs. The absence or reduced dosage of rejuvenator limits the reactivation of the aged RAP binder, which maintains a stiffer and more brittle structure and, consequently, increases the overall stiffness of the mixture, directly influencing its mechanical response.

In addition to compositional differences, the intrinsic uncertainties associated with plant production must be considered. Unlike the laboratory environment, characterised by controlled conditions, extremely accurate dosages and reproducible thermal cycles, the plant introduces variabilities that are difficult to eliminate. Among the main sources of uncertainty are:

1. Thermal fluctuations during the heating of aggregates and RAP, which may influence binder viscosity and mixing efficiency.

2. Limited accuracy in dosages, especially for components present in small quantities such as additives and rejuvenator.

3. Heterogeneity of the RAP, which may show variability in residual binder content, degree of oxidation and particle size distribution.

4. Mixing times and operating conditions that cannot be perfectly replicated, affecting additive dispersion and the final homogeneity of the mixture.

5. Effects of production scale, since mixing large volumes may generate zones with different levels of RAP binder activation.

In conclusion, the combination of these factors makes it plausible that the mixtures produced in the plant show higher stiffness values compared to those prepared in the laboratory.

Continuing the comparison between the different mixtures, attention can now be directed to the prismatic specimens analysed in the second thesis work, with the aim of extending the comparative evaluation of mechanical properties. In continuity with the approach adopted for the cylindrical specimens, the results of the two studies are first presented separately, to clearly highlight the performance of each mixture, and then directly compared.

For ease of consultation, the values relating to mixtures MIX50 1, MIX50 2 and MIX50 REF, obtained on the prismatic specimens also used for the fatigue characterisation of the plant-produced mixtures, are reported again. As already illustrated previously, the data shown represent the average of the eight specimens produced for each mixture, ensuring an adequate statistical basis for the interpretation of the results.

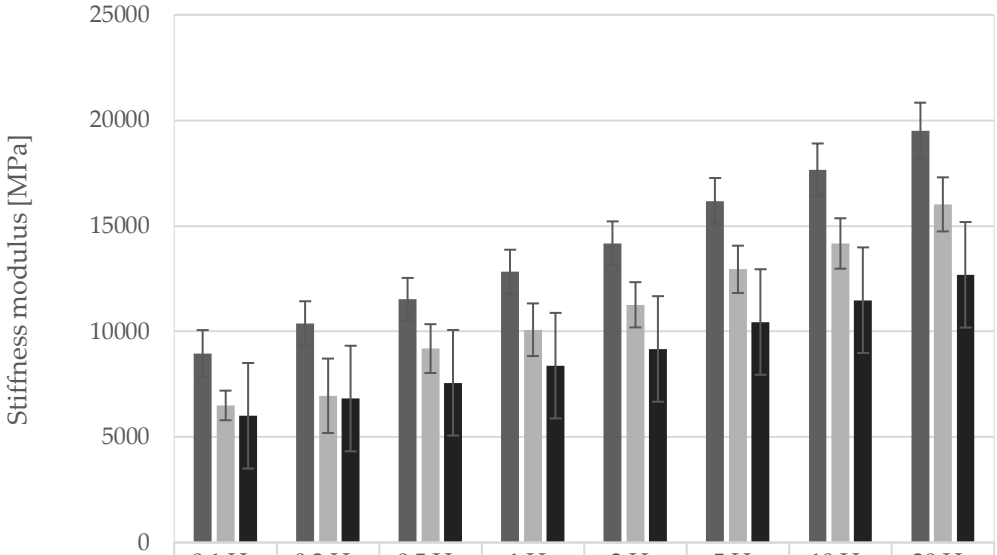

	0.1 Hz	0.2 Hz	0.5 Hz	1 Hz	2 Hz	5 Hz	10 Hz	20 Hz
MIX50_1	8966	10374	11531	12822	14171	16185	17668	19518
MIX50_2	6496	6953	9190	10082	11265	12945	14169	16022
MIX50_REF	6007	6824	7571	8381	9172	10448	11484	12685

Figure 94. Trend of stiffness modulus for the analysed mixtures produced in plant – Prismatic specimens.

Similarly to what was shown for the plant-produced mixtures, the stiffness moduli of the mixtures mentioned in the introductory paragraph of this chapter are provided below.

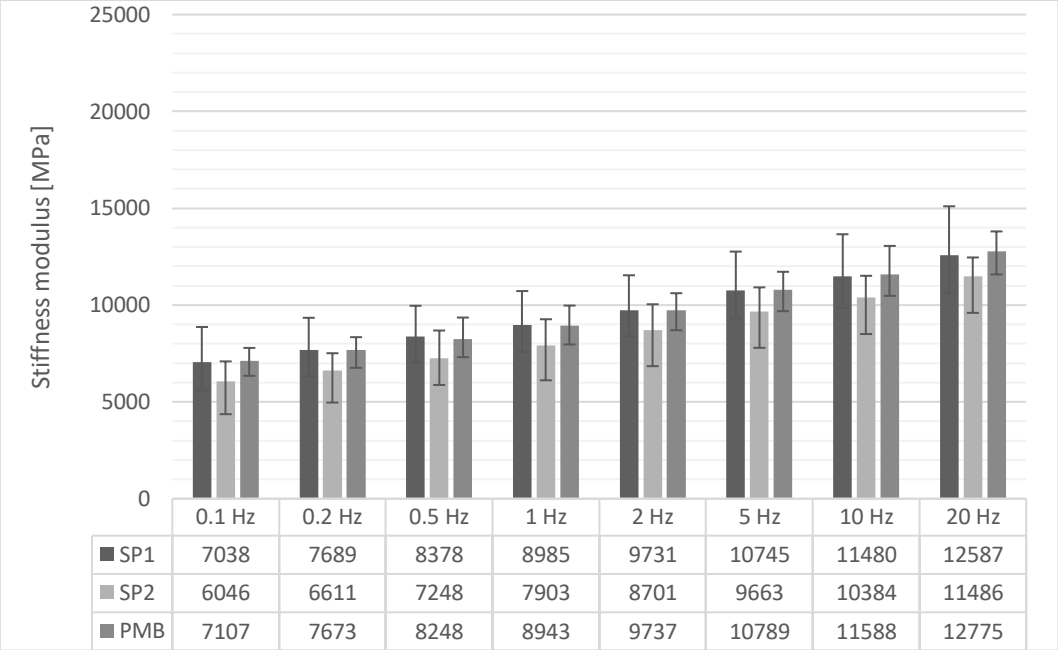

	0.1 Hz	0.2 Hz	0.5 Hz	1 Hz	2 Hz	5 Hz	10 Hz	20 Hz
SP1	7038	7689	8378	8985	9731	10745	11480	12587
SP2	6046	6611	7248	7903	8701	9663	10384	11486
PMB	7107	7673	8248	8943	9737	10789	11588	12775

Figure 95. Trend of stiffness modulus for the analysed mixtures produced in laboratory – Prismatic specimens (source: thesis [55]).

The comparison between the mixtures is presented below using a cartesian plane arranged according to the same criteria adopted for the cylindrical specimens (for a detailed description of the representation method, see Figure 93). For readability and to provide a more immediate representation of the results, the comparison is shown only for the moduli determined at the frequency of 10 Hz.

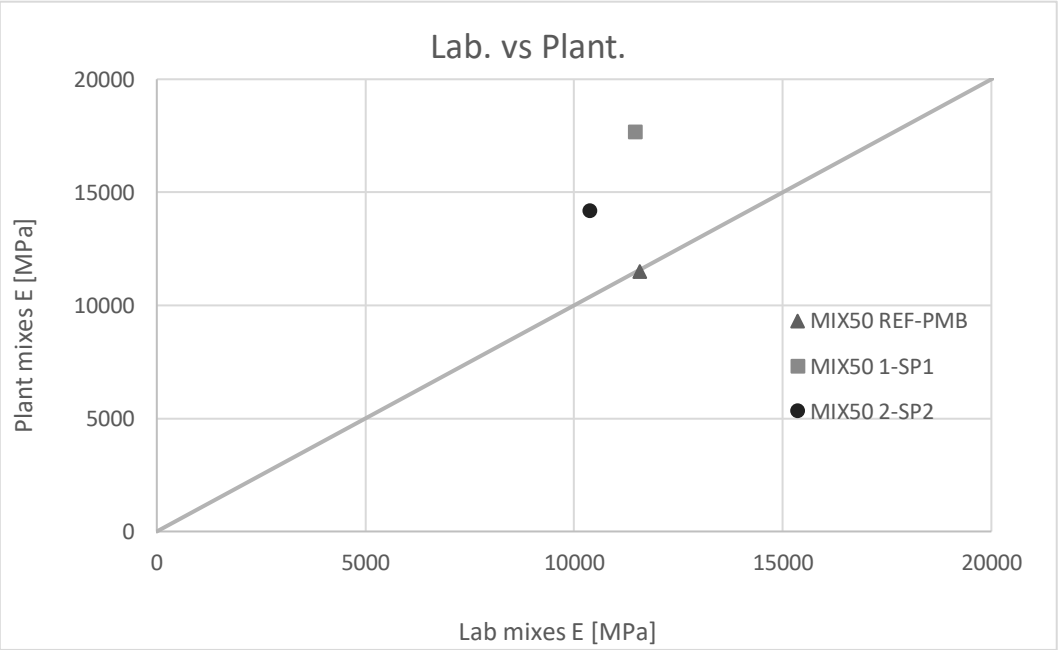

Figure 96. Direct comparison between plant produced and laboratory produced mixtures – prismatic specimens, stiffness moduli.

As shown in the graph, except for mixtures MIX50 REF and PMB, which display an almost identical behaviour, all the other formulations confirm what was already observed on the cylindrical specimens: the plant-produced mixtures are systematically stiffer than their corresponding laboratory-prepared mixtures.

5.3. Fatigue performance

After examining the behaviour of the stiffness moduli of the mixtures produced in the plant and in the laboratory, the focus now shifts to the comparison of their fatigue life, as previously recalled in this thesis. In line with the structure adopted in the previous section, the results obtained on the cylindrical specimens compacted at N_{design} (120 revolutions) are presented first, followed by the discussion of the data obtained from the prismatic specimens, in order to provide a complete and consistent picture of the fatigue behaviour of the mixtures under study. To support readability and ensure continuity with the structure used throughout the work, the results already discussed in Chapter 4 are presented again in tabular form. The table reports the extrapolated ε_6 values for each mixture, determined according to the failure criterion based on a 50% reduction of the initial modulus, as described in Chapter 2.

Mix code	Failure Criteria	ε_6 [μm/m]
MIX50_1	50%	44
MIX50_2	50%	29
MIX50_REF	50%	18

Table 53. ε_6 values for each mixture (produced in plant) and for the failure criteria of 50% of the initial stiffness modulus – cylindrical specimens.

For the sake of completeness, the fatigue curves for the various mixtures analysed are also presented below.

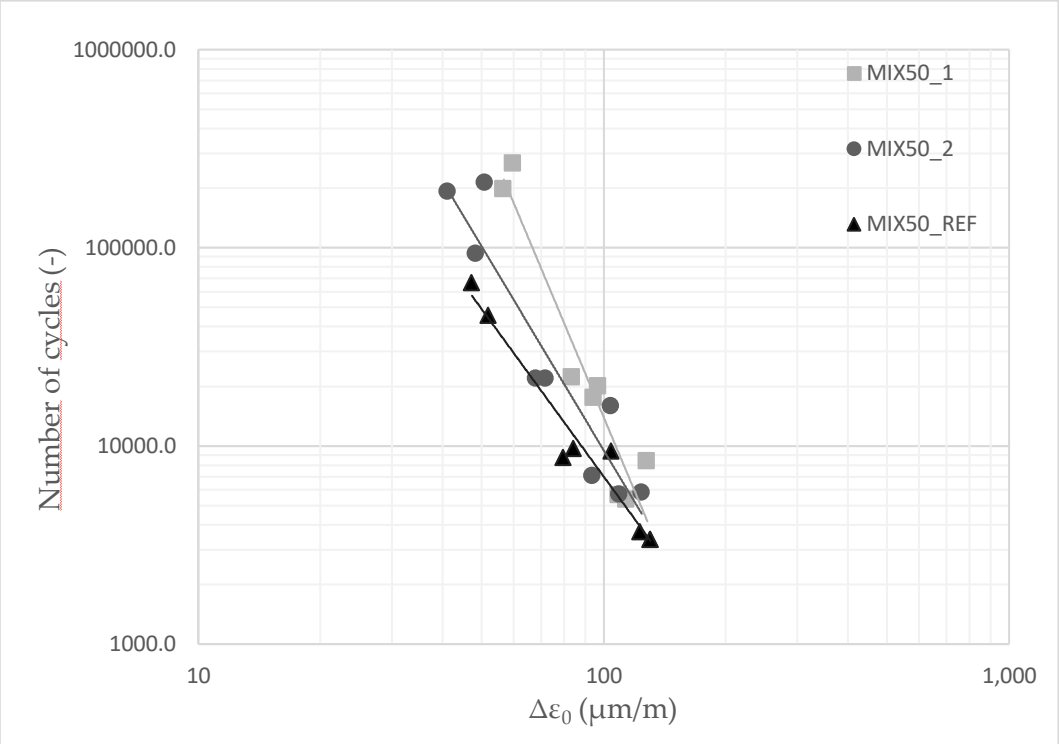

Figure 97. Fatigue lines for the different mixtures (produced in plant), cylindrical specimens – 50% initial modulus criterion.

Similarly to what was shown for the plant-produced mixtures, the ε_6 values of the mixtures referred to in the introductory paragraph of this chapter are presented below.

Mix code	Failure Criteria	ε_6 [μm/m]
SP1	50%	35
SP2	50%	40
PMB	50%	38

Table 54. ε_6 values for each mixture (produced in laboratory) and for the failure criteria of 50% of the initial stiffness modulus – cylindrical specimens (source: thesis [54]).

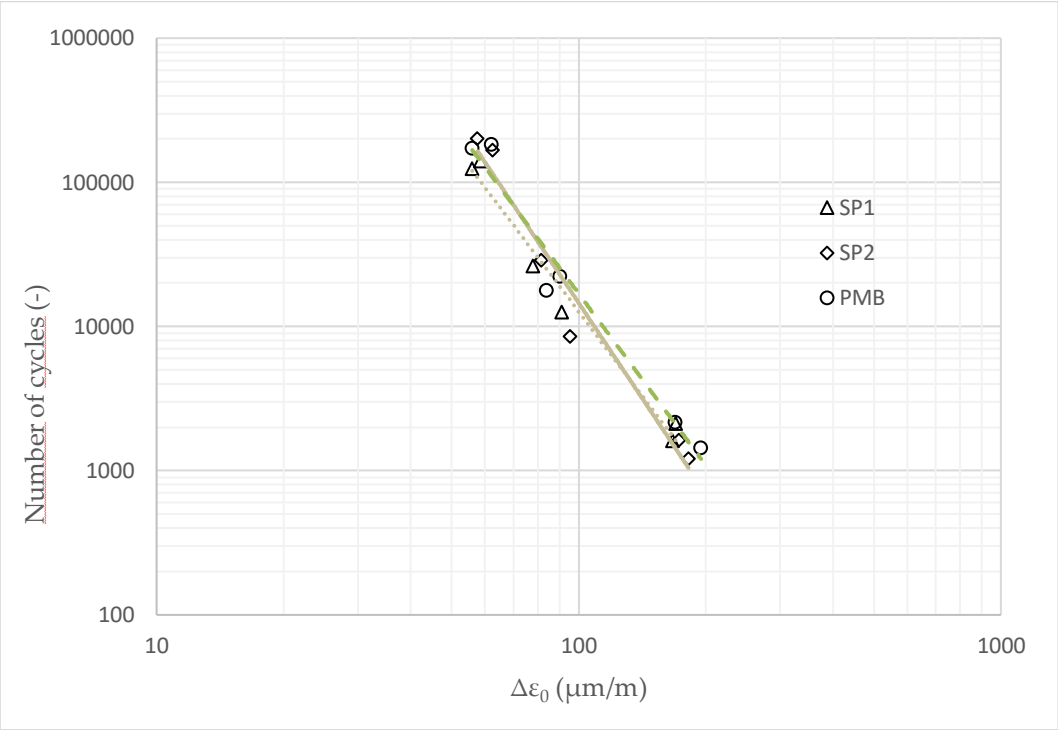

Figure 98. Fatigue lines for the different mixtures (produced in laboratory), cylindrical specimens – 50% initial modulus criterion (source: thesis [54]).

In line with what was shown in the previous paragraph, the cartesian plane used for the direct comparison of the different mixtures is now presented, following the same graphical and interpretative layout already applied to the analysis of the cylindrical specimens.

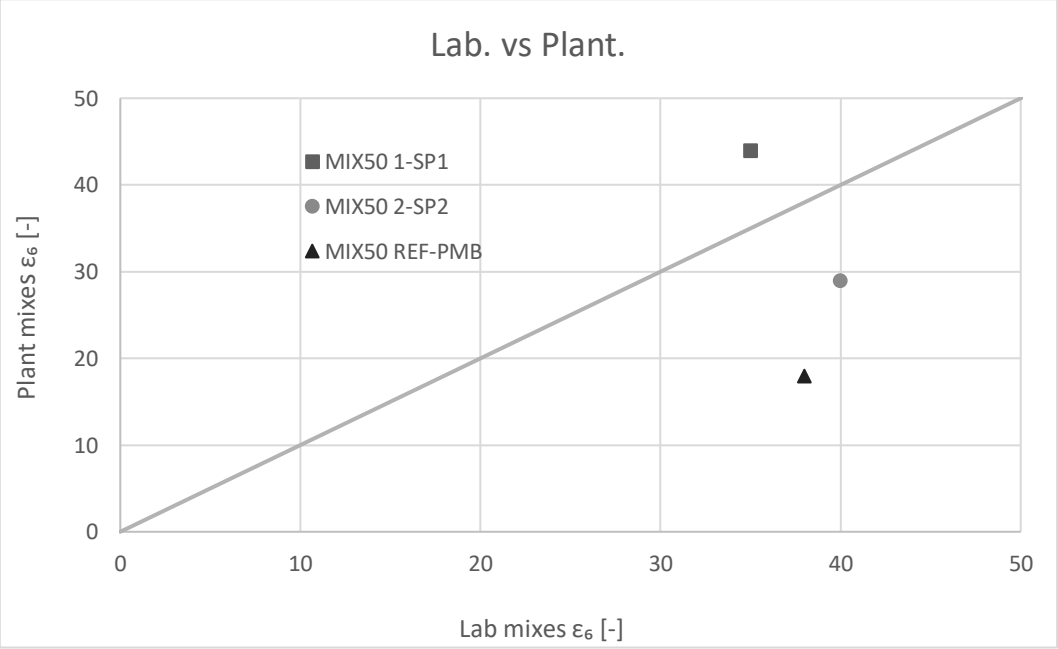

Figure 99. Direct comparison between plant produced and laboratory produced mixtures – 120 gyration cylindrical specimens, ε_6 values.

The trend shown in the graph indicates that the points do not align along the bisector, revealing the lack of a perfect correspondence between the laboratory-produced mixtures and those manufactured in the plant.

With the exception of mixture MIX50 1, which displays an ε_6 value higher than that of the corresponding laboratory SP1, the other mixtures confirm what had already emerged from the comparison of the stiffness moduli: the SP2 and PMB mixtures produced in the laboratory have lower moduli than their plant-produced counterparts, which translates into higher ε_6 values. Higher ε_6 values indicate a more ductile material, able to dissipate more effectively the energy associated with repeated loads and less prone to crack formation and propagation, whereas lower values suggest a more brittle behaviour and a reduced capacity to withstand cyclic deformations, ultimately shortening the service life of the mixture.

Moving forward with the comparison among the different mixtures, attention can now shift to the prismatic specimens analysed in the second thesis work. Consistent with the approach adopted for the cylindrical specimens, the results of the two works are first presented separately, to clearly highlight the performance of each mixture, and then directly compared.

Mix code	Failure Criteria	ε_6 [μm/m]
MIX50_1	50%	116
MIX50_2	50%	124
MIX50_REF	50%	103

Table 55. ε_6 values for each mixture (produced in plant) and for the failure criteria of 50% of the initial stiffness modulus – prismatic specimens.

Similarly to what was shown for the plant-produced mixtures, the ε_6 values of the mixtures referred to in the introductory paragraph of this chapter are presented below.

Mix code	Failure Criteria	ε_6 [μm/m]
SP1	50%	139
SP2	50%	164
PMB	50%	160

Table 56. ε_6 values for each mixture (produced in laboratory) and for the failure criteria of 50% of the initial stiffness modulus – prismatic specimens (source: thesis [55]).

The cartesian plane used for the direct comparison of the different mixtures is now presented.

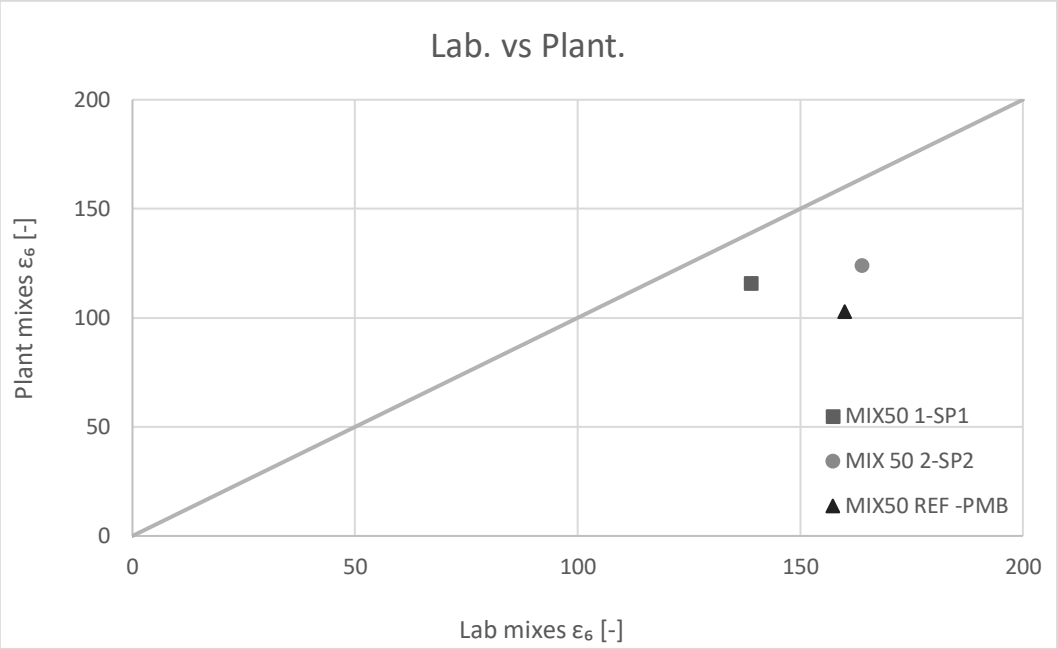

Figure 100. Direct comparison between plant produced and laboratory produced mixtures – prismatic specimens, ε_6 values.

In this case, mixture MIX50 1 also exhibits an ε_6 value lower than that of its corresponding plant-produced mixture. When the results obtained on both cylindrical and prismatic specimens are considered together, a coherent picture emerges: the mixtures produced in the plant show an overall shorter fatigue life than those prepared in the laboratory. This behaviour can be linked to the factors already discussed in the stiffness modulus comparison—differences in dosage, less control over operating conditions, and the inherent variability of the plant production process—which will be revisited and summarised in the conclusions.

6. Summary, conclusions and future developments

The recent evolution of the road sector shows how environmental sustainability has now become an essential criterion in the design and construction of infrastructures. The growing attention toward more responsible production models has led to a reconsideration of traditional techniques, encouraging the use of recovered and recycled materials also in bituminous pavements. In this context, the Ministerial Decree of 05/08/2024 introduced the new Minimum Environmental Criteria for public contracts related to road works: a regulatory framework that not only promotes the adoption of more sustainable practices but also establishes mandatory minimum percentages of materials coming from recovery, recycling, or by-products to be used in new mixtures.

These requirements, however, do not represent a mere formal obligation: they demand that the increase in sustainability does not compromise the mechanical and functional performance of pavements. This leads to a more conscious and scientifically grounded approach to mixture design, in which materials such as reclaimed asphalt pavement (RAP) and recycled plastics play an increasingly central role. Their growing use demonstrates not only the technological maturity reached by the sector, but also the ability to combine environmental, economic, and performance-related objectives.

The analysis carried out in this work aimed to evaluate the mechanical behaviour of sustainable mixtures produced in an asphalt plant, characterized by a RAP content of 50% and using different dosages of a polymeric compound obtained from recycled hard plastics, introduced through a hybrid modification technique. Four mixtures were produced: three hybrid variants, differentiated by the percentage of polymeric additive (0.3%, 0.5% and 0.7% by total mixture weight, named MIX50 1, MIX50 2 and MIX50 3), and a wet-modified reference mixture containing a polymer-modified binder (PmB, named MIX50 REF).

The prescriptive limits used for the validation and acceptance of the experimental results obtained in this thesis derive from the Special Tender Specifications of the A4 Motorway.

The mixtures modified with the hybrid methodology (MIX50 1, MIX50 2 and MIX50 3) showed better workability compared to the reference mixture (MIX50 REF). This result emerges from the analysis of the Construction Densification Index (CDI), a dimensionless parameter expressing the energy required to achieve an adequate level of densification during paving. Lower CDI values indicate a mixture that is easier to compact, while higher values signal the need for greater compaction energy and therefore lower workability. In practice, the CDI quantifies the work required by rollers to bring the mixture to 8% air voids, a threshold commonly

associated with traffic opening, making it an effective synthetic indicator of compactability and operational suitability.

Focusing on stiffness moduli, the IT-CY and 4PB-PR tests confirm a consistent behaviour: the wet-modified reference mixture is the least stiff, while the hybrid mixtures show higher values due to the contribution of the polymeric compound. However, increasing the plastic content does not produce a linear increase in stiffness. Three distinct effects emerge: with 0.3% plastic, stiffness increases due to binder stiffening; with 0.5%, the loss of compactability prevails, increasing voids and reducing the modulus; with 0.7%, the plastic also acts as a filler, helping to close the structure and bringing stiffness back to higher values.

The fatigue analysis showed that the response of the mixtures strongly depends on the test configuration, based on the value of ε_6, used as a synthetic indicator of their ability to withstand cyclic loads. Higher values of this parameter, expressed in μm/m, correspond to more ductile materials less prone to cracking, while lower values indicate greater fragility. In this framework, considering the CIT-CY configuration, the MIX50 1 mixture showed the best performance, consistent with its lower air-void content; conversely, MIX50 REF, characterised by a higher void percentage, exhibited a shorter fatigue life. MIX50 2 and MIX50 3 occupy an intermediate position, with similar behaviours.

Considering the 4PB-PR configuration, the results show greater dispersion, requiring a cautious interpretation limited to the most robust trends. Despite these uncertainties, MIX50 2 appears to express the most favourable performance, although this indication remains preliminary and requires further verification. Despite data variability, a trend consistent with the other configuration emerges: mixtures modified with the hybrid approach tend to ensure higher fatigue resistance compared to the wet modification, confirming the key role of more compact and ductile formulations in improving the response to cyclic loads.

The comparison between mixtures produced in an asphalt plant and those prepared in the laboratory in previous research activities highlights significant differences in stiffness and fatigue behaviour. The specimens produced with plant mixtures show systematically higher moduli, mainly due to the lower rejuvenator content, which limits the reactivation of the aged RAP binder and results in a stiffer and more fragile mixture. Added to this are the typical variabilities of real-scale production — thermal fluctuations, less accurate dosing, RAP heterogeneity, non-replicable operating conditions, and scale effects — which contribute to increasing stiffness and reducing material homogeneity. Considering together the results obtained on cylindrical and prismatic specimens, a coherent picture emerges: plant-produced mixtures show higher ε_6 values and an overall shorter fatigue life compared to laboratory mixtures. This evidence confirms the decisive role of compositional choices and operating conditions in defining the mechanical response of RAP-containing mixtures.

Overall, the evidence gathered throughout this work highlights how crucial it is to strictly adhere to the prescribed mix designs, avoiding any deviations from them. The results obtained indeed confirm, indirectly but unequivocally, the decisive role played by the rejuvenating additive in mixtures characterized by high RAP contents, emphasizing that its proper integration is essential to ensure reliable and reproducible performance.

The results of the experimental campaign can be summarized as follows:

1. Mixtures containing polymeric compound and modified with the hybrid methodology show better workability than the wet-modified reference mixture.
2. With the same total RAP content, increasing the polymeric compound does not lead to a proportional increase in stiffness, suggesting the existence of a threshold beyond which additional plastic does not provide further benefits.
3. Mixtures modified with the hybrid approach show higher fatigue resistance than the wet modification, confirming the importance of more compact and ductile formulations in the response to cyclic loads.
4. Laboratory-produced mixtures exhibit a longer fatigue life compared to the corresponding plant-produced mixtures.

The experimental work therefore demonstrates the concrete feasibility of producing sustainable mixtures with high RAP and recycled plastic contents; however, to consolidate these findings and more precisely define their application limits, further investigations are required. In particular:

1. Analyse more thoroughly the bell-shaped trend observed in mixtures containing polymeric compound, increasing the number of samples and introducing new test configurations.
2. Strengthen fatigue characterization by increasing the sample size, varying test temperatures, and adopting different experimental configurations, to build a more robust database.
3. Produce plant mixtures with a rejuvenator content comparable to that used in laboratory mixtures, enabling a more balanced comparison.
4. Assess the future recyclability of the investigated mixtures, with the aim of promoting an increasingly efficient circular-economy model.

Bibliography

[1] G. Tarsi, P. Tataranni, and C. Sangiorgi, 'The Challenges of Using Reclaimed Asphalt Pavement for New Asphalt Mixtures: A Review', *Materials*, vol. 13, no. 18, p. 4052, Sep. 2020, doi: 10.3390/ma13184052.

[2] SABITA, *Southern African Bitumen Association – SABITA (2019). Use of Reclaimed Asphalt in the Production of Asphalt.*

[3] West, C.R.; Copeland, A., *West, C.R.; Copeland, A. High RAP Asphalt Pavements—Japan Practice—Lessons Learned—NAPA, Information Series 139; National Asphalt Pavement Association (NAPA): Lanham, MD, USA, 2015; pp. 1–62.*

[4] Brett, A.W.; Willis, J.R.; Ross, T.C., *Brett, A.W.; Willis, J.R.; Ross, T.C. Asphalt Pavement Industry Survey on Recycled Materials and Warm-Mix Asphalt Usage: 2018, 9th ed.; IS 138; National Asphalt Pavement Association: Greenbelt, MD, USA, 2019.*

[5] MARINI—FayatGroup., *MARINI—FayatGroup. Orientarsi Fra Impianto Continuo e Discontinuo. Available online: https://marini.fayat. com/it/tecnologia/orientarsi-fra-impianto-continuo-e-discontinuo*.

[6] West, R. C., Willis, J. R., & Marasteanu, M. O., *West, R. C., Willis, J. R., & Marasteanu, M. O. (2013). Improved mix design, evaluation, and materials management practices for hot mix asphalt with high reclaimed asphalt pavement content (Vol. 752). Transportation Research Board.*

[7] Liu, S.; Shukla, A.; Nandra, T., *Liu, S.; Shukla, A.; Nandra, T. Technological, environmental and economic aspects of Asphalt recycling for road construction. Renew. Sustain. Energy Rev. 2017, 75, 879–893.*

[8] Kandhal, P. S., & Mallick, R. B., *Kandhal, P. S., & Mallick, R. B. (1998). Pavement Recycling Guidelines for State and Local Governments: Participant's Reference Book (No. FHWA-SA-98-042)*.

[9] Copeland, A., *Copeland, A. (2011). Reclaimed asphalt pavement in asphalt mixtures: State of the practice (No. FHWA-HRT-11-021). United States. Federal Highway Administration. Office of Research, Development, and Technology.*

[10] West, C.R.; Copeland, A., *West, C.R.; Copeland, A. (2015). High RAP Asphalt Pavements - Japan Practice - Lessons Learned - NAPA, Information Series 139; National Asphalt Pavement Association (NAPA).*

[11] Zaumanis, M., Mallick, R. B., & Frank, R., *Zaumanis, M., Mallick, R. B., & Frank, R. (2014). 100% recycled hot mix asphalt: A review and analysis. Resources, Conservation and Recycling, 92, 230-245.*

[12] Al-Qadi, I. L., Elseifi, M., & Carpenter, S. H., *Al-Qadi, I. L., Elseifi, M., & Carpenter, S. H. (2007). Reclaimed asphalt pavement–a literature review.*

[13] Willis, J.R.; Marasteanu, M., *Willis, J.R.; Marasteanu, M. National Cooperative Highway Research Program; Transportation Research Board; National Academies of Sciences, Engineering, and Medicine. In Improved Mix Design, Evaluation, and Materials Management Practices for Hot Mix Asphalt with High Reclaimed Asphalt Pavement Content; The National Academies Press: Washington, DC, USA, 2013.*

[14] Brett, A.W.; Willis, J.R.; Ross, T.C., *Brett, A.W.; Willis, J.R.; Ross, T.C. (2018). Asphalt Pavement Industry Survey on Recycled Materials and Warm-Mix Asphalt Usage.*

[15] Ma,F.; Sha, A.; Lin, R.; Huang, Y.; Wang, C., *Ma,F.; Sha, A.; Lin, R.; Huang, Y.; Wang, C. Greenhouse gas emissions from asphalt pavement construction: Acase study in China. Int. J. Environ. Res. Public Health. 2016, 13, 351.*

[16] Vidal, R.; Moliner, E.; Martínez, G.; Rubio, M.C., *Vidal, R.; Moliner, E.; Martínez, G.; Rubio, M.C. (2013). Life cycle assessment of hot mix asphalt and zeolite-based warm mix asphalt with reclaimed asphalt pavement.*

[17] Brooks, A.L., Wang, S., Jambeck, J.R., *Brooks, A.L., Wang, S., Jambeck, J.R. (2018). The Chinese import ban and its impact on global plastic waste trade, Science Advances. doi: 10.1126/sciadv. aat0131*.
[18] Geyer, R., Jambeck, J.R., Law, K.L., *Geyer, R., Jambeck, J.R., Law, K.L. (2017). Production, use, and fate of all plastics ever made, Science Advances, 3.*
[19] Jambeck, J.R., Andrady, A., Geyer, R., Narayan, R., Perryman, M., Siegler, T., Wilcox, C., Law, K.L., *Jambeck, J.R., Andrady, A., Geyer, R., Narayan, R., Perryman, M., Siegler, T., Wilcox, C., Law, K.L. (2015). Plastic waste inputs from land into the ocean, Science, 347, 768-771.*
[20] National Academies of Sciences, Engineering, and Medicine, *National Academies of Sciences, Engineering, and Medicine (2020). Evaluating the effects of recycling agents on asphalt mixtures with high RAS and RAP binder ratios.*
[21] Mehta, D., Saboo, N., Abraham, S. M., & Diwaker, U., *Mehta, D., Saboo, N., Abraham, S. M., & Diwaker, U. (2023). A review on the use of waste plastics in hot mix asphalt. Mechanics of Time-Dependent Materials, 1-44.*
[22] Liang, M., Xin, X., Fan, W., Zhang, J., Jiang, H., & Yao, Z., *Liang, M., Xin, X., Fan, W., Zhang, J., Jiang, H., & Yao, Z. (2021). Comparison of rheological properties and compatibility of asphalt modified with various polyethylene. International Journal of Pavement Engineering, 22(1), 11-20.*
[23] Audy, R., Enfrin, M., Boom, Y. J., & Giustozzi, F., *Audy, R., Enfrin, M., Boom, Y. J., & Giustozzi, F. (2022). Selection of recycled waste plastic for incorporation in sustainable asphalt pavements: A novel multi-criteria screening tool based on 31 sources of plastic. Science of the Total Environment, 829, 154604.*
[24] J. N. La Macchia, O. Baglieri, D. Dalmazzo, and E. Santagata, 'Engineering Properties of Road Paving Mixtures with High Content of Reclaimed Asphalt and Recycled Waste Plastics', *Materials*, vol. 17, no. 23, p. 5681, Nov. 2024, doi: 10.3390/ma17235681.
[25] Willis, R., Yin, F., & Moraes, R., *Willis, R., Yin, F., & Moraes, R. (2020). Recycled plastics in asphalt part A: state of the knowledge.*
[26] F. Giustozzi and S. Nizamuddin, *F. Giustozzi and S. Nizamuddin (eds.), Plastic waste for sustainable asphalt roads. in Woodhead publishing series in civil and structural engineering. Cambridge, MA Kidlington, OX: WP Woodhead Publishing, an imprint of Elsevier, 2022.*
[27] R. Willis, F. Yin, and R. Moraes, 'RECYCLED PLASTICS IN ASPHALT PARTA':.
[28] M. Enfrin, R. Myszka and F. Giustozzi, *M. Enfrin, R. Myszka and F. Giustozzi, «Paving roads with recycled plastics: Microplastic pollution or Eco-friendly solution?», J. Hazard. Mater., vol. 437, p. 129334, giu. 2022, doi: 10.1016/j.jhazmat.2022.129334.*
[29] Leonardo Urbano. "The role of additives in the rejuvenation of Reclaimed, Asphalt: Tools, modelling and perspectives". Doctoral Program in Civil and, Environmental Engineering (34th Cycle). Ph.D. thesis. Torino, Italy: Politecnico, and di Torino, 2022., *Leonardo Urbano. "The role of additives in the rejuvenation of Reclaimed Asphalt: Tools, modelling and perspectives". Doctoral Program in Civil and Environmental Engineering (34th Cycle). Ph.D. thesis. Torino, Italy: Politecnico di Torino, 2022.*
[30] Huang, B., Shu, X., & Dong, Q., *Huang, B., Shu, X., & Dong, Q. (2020). Rejuvenators and softening agents for asphalt mixtures with high RAP content: A review.*
[31] M. Elseifi, J. Baek and N. Dhakal, *M. Elseifi, J. Baek and N. Dhakal, «Review of modelling crack initiation and propagation in flexible pavements using the finite element method», Int. J. Pavement Eng., vol. 19, 10.1080/10298436.2017.1345555.*
[32] M. Rochlani, G. Canon Falla, S. Caro, S. Leischner and F. Wellner, *«Understanding the influence of temperature and frequency on the fatigue resistance of bitumen», Constr. Build. Mater., vol. 296, giu. 2021, doi: 10.1016/j.conbuildmat.2021.123754.*
[33] M. Rochlani, G. Canon Falla, S. Caro, S. Leischner and F. Wellner, *M. Rochlani, G. Canon Falla, S. Caro, S. Leischner and F. Wellner, «Understanding the influence of*

temperature and frequency on the fatigue resistance of bitumen», Constr. Build. Mater., vol. 296, giu. 2021, doi: 10.1016/j.conbuildmat.2021.123754.
[34] H. Di Benedetto, C. De La Roche, H. Baaj, A. Pronk and R. Lundström, *H. Di Benedetto, C. De La Roche, H. Baaj, A. Pronk and R. Lundström, «Fatigue of bituminous mixtures», Mater. Struct. Constr., vol. 37, fasc. 267, pp. 202–216, 2004, doi: 10.1007/bf02481620.*
[35] J. T. Harvey and B.-W. Tsai, *J. T. Harvey and B.-W. Tsai, «Effects of asphalt content and air void content on mix fatigue and stiffness», Transp. Res. Rec., fasc. 1543, pp. 38–45, 1996, doi: 10.3141/1543-05.*
[36] G. Rowe and M. G. Bouldin, *G. Rowe and M. G. Bouldin, «Improved techniques to evaluate the fatigue resistance of asphaltic mixtures», pp. 754–763, gen. 2000.*
[37] European Committee for Standardization: Brussels, Belgium, «EN 1269 24, *Bituminous mixtures - Test methods; Part 24: Resistance to fatigue». 2018.*
[38] European Committee for Standardization: Brussels, Belgium, «EN 12697 39;, *Bituminous Mixtures—Test Methods—Part 39: Binder Content by Ignition». 2020.*
[39] European Committee for Standardization: Brussels, Belgium, «N 12591;, *Bitumen and Bituminous Binders—Specifications for Paving Grade Bitumens». 2009.*
[40] European Committee for Standardization: Brussels, Belgium, «EN 14023;, *Bitumen and Bituminous Binders—Specification Framework for Polymer Modified Bitumens». 2010.*
[41] American Association of State and Highway Transportation Officials: Washington, DC, USA, «AASHTO M323-22;, *American Association of State and Highway Transportation Officials: Washington, DC, USA, «AASHTO M323-22; Standard Specification for Superpave Volumetric Mix Design». 2022.*
[42] European Committee for Standardization: Brussels, Belgium, «EN 1426;, *Bitumen and Bituminous Binders—Determination of Needle Penetration». 2015.*
[43] European Committee for Standardization: Brussels, Belgium, «EN 1427;, *Bitumen and Bituminous Binders—Determination of the Softening Point—Ring and Ball Method». 2015.*
[44] Al-Saffar, Z. H., Yaacob, H., Katman, H. Y., Mohd Satar, M. K. I., Bilema, M., Putra Jaya, R., Eltwati, A. S., & Radeef, H. R., *Al-Saffar, Z. H., Yaacob, H., Katman, H. Y., Mohd Satar, M. K. I., Bilema, M., Putra Jaya, R., Eltwati, A. S., & Radeef, H. R., «A Review on the Durability of Recycled Asphalt Mixtures Embraced with Rejuvenators», Sustainability, vol. 13, fasc. 16, p. 8970, gen. 2021, doi: 10.3390/su13168970.*
[45] CIRS., *Performance-Related Technical Specification for the Construction and Maintenance of Road Pavements; Inter-University Road Research Center: Ancona, Italy, 2021.*
[46] European Committee for Standardization: Brussels, Belgium, «EN 12697-5;, *Bituminous mixtures - Test methods; Part 5: Determination of the maximum density». 2018.*
[47] European Committee for Standardization: Brussels, Belgium, «EN and 12697-27;, *Bituminous mixtures — Test methods; Part 27: Sampling». 2017.*
[48] European Committee for Standardization: Brussels, Belgium, EN 12697-31;, *Bituminous mixtures – Test methods Part 31: Specimen preparation by gyratory compactor. 2109.*
[49] European Committee for Standardization: Brussels, Belgium, «EN 12697 and 33;, *Bituminous mixtures — Test methods for hot mix asphalt — Part 33: Specimen prepared by roller compactor». 2003.*
[50] European Committee for Standardization: Brussels, Belgium, «EN and 12697-29;, *Bituminous mixtures – Test methods Part 29: Determination of the dimensions of a bituminous specimen». 2020.*

[51] European Committee for Standardization: Brussels, Belgium, «EN 12697 and 6;, *Bituminous mixtures — Test methods Part 6: Determination of bulk density of bituminous specimens». 2020.*
[52] European Committee for Standardization: Brussels, Belgium, «EN 12697 and 26;, *Bituminous mixtures — Test methods for hot mix asphalt Part 26: Stiffness». 2012.*
[53] European Committee for Standardization: Brussels, Belgium, «EN 12697-23;, *Bituminous mixtures — Test methods;*
[54] L. Rigassio, 'Studio del comportamento prestazionale di miscele bituminose ad alto contenuto di fresato addizionate con co con compound polimerico', 2024.
[55] C. Kemal, 'Sustainable asphalt mixes with RAP and waste plastics'.

Appendix

Volumetric properties and compaction parameters

MIX50 1

Test date	01/07/2025	time	11:27

Q+A			
T	Water temperature	27.9	[°C]
ρ_w	Water density	0.996	[Mg/m^3]
m_1	Mass of pyknometer + head	917	[g]
m_2	Mass of pyknometer + head + mixture	1719.3	[g]
m_3	Mass of pyknometer + head + mixture + water	2751.7	[g]
V_p	Volume of the pyknometer	0.001348	[m^3]
ρ_{mm}	Maximum density	2.572	[Mg/m^3]

Test date	21/07/2025	time	12:42

Q+A			
T	Water temperature	27.9	[°C]
ρ_w	Water density	0.996	[Mg/m^3]
m_1	Mass of pyknometer + head	917	[g]
m_2	Mass of pyknometer + head + mixture	1723.7	[g]
m_3	Mass of pyknometer + head + mixture + water	2754.8	[g]
V_p	Volume of the pyknometer	0.001348	[m^3]
ρ_{mm}	Maximum density	2.576	[Mg/m^3]

6+R			
T	Water temperature	27.9	[°C]
ρ_w	Water density	0.996	[Mg/m^3]
m_1	Mass of pyknometer + head	992.7	[g]
m_2	Mass of pyknometer + head + mixture	1782.6	[g]
m_3	Mass of pyknometer + head + mixture + water	2703.3	[g]
V_p	Volume of the pyknometer	0.001232	[m^3]
ρ_{mm}	Maximum density	2.568	[Mg/m^3]

r	**Repeatability**	0.008	[Mg/m^3]

ρmm	**Average**	2.572	[Mg/m^3]

Test date **01/07/2025** **time** **13:05**

Wt	Mass of sample basket and catch pan	2842.1	[g]
Wt+m, BI	Mass of sample basket+ catch pan + mixture, Before Ignition	3941.6	[g]
Wt+a, AI	Mass of sample basket+ catch pan + mixture, After Ignition	3888.2	[g]
Wm,BI	Mass of mixture, Before Ignition	1099.5	[g]
Wa,AI	Mass of aggregate, After Ignition	1046.1	[g]
Bm	Corrected binder content of bituminous mixture	4.86	[%]
Ba	Corrected binder content on aggregate weight	4.89	[%]
Corr Bm		4.86	[%]

Test date **01/07/2025** **time** **14:25**

Wt	Mass of sample basket and catch pan	2832.3	[g]
Wt+m, BI	Mass of sample basket+ catch pan + mixture, Before Ignition	3935.2	[g]
Wt+a, AI	Mass of sample basket+ catch pan + mixture, After Ignition	3881.8	[g]
Wm,BI	Mass of mixture, Before Ignition	1102.9	[g]
Wa,AI	Mass of aggregate, After Ignition	1049.5	[g]
Bm	Corrected binder content of bituminous mixture	4.84	[%]
Ba	Corrected binder content on aggregate weight	4.87	[%]
Corr Bm		4.84	[%]

MIX50_1 1 **Test date** **01/07/2025** **time** **14:53**

Wt	tray mass	1039.5	[g]
Wt	tray mass	1039.7	[g]
Wt+a,AI	tray mass + aggregates after ignition	2085.1	[g]
Wt+a,AI	tray mass + aggregates after ignition	2020	[g]
Wt+a,AI	tray mass + aggregates after ignition	2019.8	[g]
Wt+a,AI	tray mass + aggregates after ignition	2020.3	[g]

Sieve size [mm]	Sieve mass [g]	Sieve+soil [g]	Retained [g]	Cumulative [g]	Passing [g]	Passing [%]
31.5	1298.8	1298.8	0	0	1045.5	100
20	1317.4	1350.4	33	33	1012.5	96.8
16	1302	1425.8	123.8	156.8	888.7	85.0
12.5	1183.2	1263.2	80	236.8	808.7	77.4
8	1070.2	1174.5	104.3	341.1	704.4	67.4
4	1107.9	1413.9	306	647.1	398.4	38.1
2	980.1	1115	134.9	782	263.5	25.2
0.5	784.3	893.4	109.1	891.1	154.4	14.8
0.25	726.5	765.4	38.9	930	115.5	11.0
0.063	767.7	816.4	48.7	978.7	66.8	6.4
0	724.4	726.4	2	1045.5	0	0.0
Total	11432.2	11116.1	980.7			

MIX50_1 2 **Test date** **14/07/2025** **time** **14:29**

Wt	tray mass	1023.7	[g]
Wt	tray mass	1024.4	[g]
Wt+a,AI	tray mass + aggregates after ignition	2072.9	[g]
Wt+a,AI	tray mass + aggregates after ignition	2011.4	[g]
Wt+a,AI	tray mass + aggregates after ignition	2011.4	[g]
Wt+a,AI	tray mass + aggregates after ignition	2011.4	[g]

Sieve size [mm]	Sieve mass [g]	Sieve+soil [g]	Retained [g]	Cumulative [g]	Passing [g]	Passing [%]
31.5	1298.9	1298.9	0	0	1048.6	100
20	1317.4	1364.9	47.5	47.5	1001.1	95.5
16	1302	1352.9	50.9	98.4	950.2	90.6
12.5	1183.3	1329.9	146.6	245	803.6	76.6
8	1070.2	1173.6	103.4	348.4	700.2	66.8
4	1107.8	1424.2	316.4	664.8	383.8	36.6
2	980.1	1111.1	131	795.8	252.8	24.1
0.5	784	886.9	102.9	898.7	149.9	14.3
0.25	726.7	764.9	38.2	936.9	111.7	10.7
0.063	767.7	815.8	48.1	985	63.6	6.1
0	895.2	897.3	2.1	1048.6	0	0.0
Total	11433.3	12420.4	987.1			

Cylindrical specimens compacted at N_{max} (200 gyrations)

Specimen Code	M1 [g]	M2 [g]	M3 [g]	T [°C]	ρ_w [Mg/m^3]	ρ_{mb} [Mg/m^3]	ρ_{mv} [Mg/m^3]	v [%]
MIX50_1 1	4700.2	2840.1	4707.2	26.8	0.9966	2.509	2.572	2.46
MIX50_1 2	4659.5	2819.0	4665.9	26.8	0.9966	2.514	2.572	2.24
MIX50_1 3	4820.4	2919.6	4834.9	26.5	0.9967	2.509	2.572	2.47
MIX50_1 4	4798.9	2907.6	4807.5	23.8	0.9974	2.519	2.572	2.05
MIX50_1 5	4816.6	2922.2	4829.7	23.8	0.9974	2.519	2.572	2.08
MIX50_1 6	4803.4	2906.5	4810.1	24.5	0.9972	2.516	2.572	2.17
MIX50_1 7	4813.1	2911.8	4822.4	24.5	0.9972	2.512	2.572	2.33

Specimen Code	Date	D_{mold} [mm]	v_{real} [%]	v_{geo} [%]	Δv [%]	C1 [%]	k [-]	CDI [-]
MIX50_1 1	02/07/2025	150	2.46	4.95	2.49	80.32	7.65	78.99
MIX50_1 2	02/07/2025	150	2.24	4.37	2.13	80.26	7.78	71.54
MIX50_1 3	21/07/2025	150	2.47	5.48	3.01	80.19	7.66	82.56
MIX50_1 4	16/09/2025	150	2.05	4.36	2.32	81.36	7.38	49.78
MIX50_1 5	16/09/2025	150	2.08	5.89	3.81	80.25	7.80	70.55
MIX50_1 6	22/09/2025	150	2.17	5.13	2.97	80.59	7.65	63.34
MIX50_1 7	22/09/2025	150	2.33	5.20	2.87	79.97	7.81	87.01

Cylindrical specimens compacted at N_{design} (120 gyrations), before cutting

Specimen Code	M1 [g]	M2 [g]	M3 [g]	T [°C]	ρ_w [Mg/m^3]	ρ_{mb} [Mg/m^3]	ρ_{mv} [Mg/m^3]	v [%]
MIX50_1 1FC	4795.2	2890.4	4810	20	0.9983	2.494	2.572	3.05
MIX50_1 2FC	4791.8	2889.4	4814.9	18.9	0.9985	2.485	2.572	3.39
MIX50_1 3FC	4803.3	2892.1	4808.2	18.9	0.9985	2.503	2.572	2.68
MIX50_1 4FC	4801.4	2889.5	4812.2	18.9	0.9985	2.493	2.572	3.06
MIX50_1 5FC	4803.4	2898.8	4817.9	18.9	0.9985	2.499	2.572	2.83
MIX50_1 6FC	4813.3	2896.1	4820.3	19.1	0.9985	2.498	2.572	2.90
MIX50_1 7FC	4826.7	2903.1	4839.4	19.1	0.9985	2.489	2.572	3.23
MIX50_1 8FC	4806.4	2892.4	4824.5	19.8	0.9983	2.483	2.572	3.44
MIX50_1 9FC	4814.3	2896.4	4823.2	19.8	0.9983	2.494	2.572	3.02

Specimen Code	Date	D_{mold} [mm]	v_{real} [%]	v_{geo} [%]	Δv [%]	C1 [%]	k [-]	CDI [-]
MIX50_1 1FC	27/11/2025	150	3.05	5.80	2.76	79.92	8.28	60.63
MIX50_1 2FC	09/12/2025	150	3.39	5.95	2.56	80.31	7.93	59.14
MIX50_1 3FC	09/12/2025	150	2.68	6.06	3.38	79.96	8.45	51.95
MIX50_1 4FC	09/12/2025	150	3.06	6.10	3.04	80.34	8.14	50.90
MIX50_1 5FC	09/12/2025	150	2.83	6.64	3.81	80.54	8.07	49.69
MIX50_1 6FC	09/12/2025	150	2.90	5.28	2.38	80.20	8.25	52.06
MIX50_1 7FC	09/12/2025	150	3.23	6.68	3.45	79.84	8.26	66.93
MIX50_1 8FC	09/12/2025	150	3.44	6.58	3.14	79.57	8.29	71.24
MIX50_1 9FC	09/12/2025	150	3.02	5.93	2.91	80.34	8.14	50.21

Cylindrical specimens compacted at N_{design} (120 gyrations), after cutting

Specimen Code	M1 [g]	M2 [g]	M3 [g]	T [°C]	ρ_w [Mg/m^3]	ρ_{mb} [Mg/m^3]	ρ_{mv} [Mg/m^3]	v [%]
MIX50_1 1FC	2690.7	1632.2	2694.2	23.1	0.9976	2.528	2.572	1.73
MIX50_1 2FC	2596	1576.9	2599.8	21	0.9981	2.533	2.572	1.52
MIX50_1 3FC	2873.4	1736.5	2877.2	23.1	0.9976	2.513	2.572	2.30
MIX50_1 4FC	2516.1	1526	2518.7	21	0.9981	2.530	2.572	1.65
MIX50_1 5FC	2663.7	1617.4	2667.7	21	0.9981	2.531	2.572	1.59
MIX50_1 6FC	2690.5	1629.9	2693	21	0.9981	2.526	2.572	1.79
MIX50_1 7FC	2721.9	1647.4	2725.5	23.1	0.9976	2.519	2.572	2.08
MIX50_1 8FC	2667.6	1614.4	2673.2	23.1	0.9976	2.513	2.572	2.28
MIX50_1 9FC	2720.4	1646.4	2732.2	23.1	0.9976	2.499	2.572	2.83

Prismatic specimens

Specimen Code	M1 [g]	M2 [g]	M3 [g]	T [°C]	ρ_w [Mg/m^3]	ρ_{mb} [Mg/m^3]	ρ_{mv} [Mg/m^3]	v [%]
MIX50_1 1FP	2717.3	1624	2725.4	19.8	0.9983	2.463	2.572	4.24
MIX50_1 2FP	2784.7	1668.1	2791	19.8	0.9983	2.476	2.572	3.75
MIX50_1 3FP	2815.3	1679.4	2821.7	19.8	0.9983	2.460	2.572	4.34
MIX50_1 4FP	2995.4	1795.9	3005.1	19.8	0.9983	2.473	2.572	3.85
MIX50_1 5FP	2793	1672.8	2797.6	21	0.9981	2.478	2.572	3.65
MIX50_1 6FP	2735.5	1638.5	2740.9	21	0.9981	2.477	2.572	3.71
MIX50_1 7FP	2603.4	1554.4	2608.4	21	0.9981	2.465	2.572	4.15
MIX50_1 8FP	2851.5	1705	2855.8	21	0.9981	2.473	2.572	3.85

MIX50 2

Test date **01/07/2025** **time** **14:30**

6+R			
T	Water temperature	25.9	[°C]
ρ_w	Water density	0.997	[Mg/m^3]
m_1	Mass of pyknometer + head	992.5	[g]
m_2	Mass of pyknometer + head + mixture	1792.6	[g]
m_3	Mass of pyknometer + head + mixture + water	2707.5	[g]
V_p	Volume of the pyknometer	0.001232	[m^3]
ρ_{mm}	Maximum density	2.549	[Mg/m^3]

Test date **01/07/2025** **time** **14:30**

Q+A			
T	Water temperature	23.6	[°C]
ρ_w	Water density	0.997	[Mg/m^3]
m_1	Mass of pyknometer + head	916.9	[g]
m_2	Mass of pyknometer + head + mixture	1725	[g]
m_3	Mass of pyknometer + head + mixture + water	2752.9	[g]
V_p	Volume of the pyknometer	0.001348	[m^3]
ρ_{mm}	Maximum density	2.545	[Mg/m^3]

6+R			
T	Water temperature	23.6	[°C]
ρ_w	Water density	0.997	[Mg/m^3]
m_1	Mass of pyknometer + head	992.7	[g]
m_2	Mass of pyknometer + head + mixture	1801.3	[g]
m_3	Mass of pyknometer + head + mixture + water	2713.4	[g]
V_p	Volume of the pyknometer	0.001232	[m^3]
ρ_{mm}	Maximum density	2.548	[Mg/m^3]

r	**Repeatability**	0.004	[Mg/m^3]

ρmm	**Average**	2.547	[Mg/m^3]

Test date **14/07/2025** **time** **11:50**

Wt	Mass of sample basket and catch pan	2832.34	[g]
Wt+m, BI	Mass of sample basket+ catch pan + mixture, Before Ignition	4036.7	[g]
Wt+a, AI	Mass of sample basket+ catch pan + mixture, After Ignition	3971.5	[g]
Wm,BI	Mass of mixture, Before Ignition	1204.36	[g]
Wa,AI	Mass of aggregate, After Ignition	1139.16	[g]
Bm	Corrected binder content of bituminous mixture	5.41	[%]
Ba	Corrected binder content on aggregate weight	5.51	[%]
Corr Bm		5.41	[%]

Test date **14/07/2025** **time** **14:34**

Wt	Mass of sample basket and catch pan	2841.6	[g]
Wt+m, BI	Mass of sample basket+ catch pan + mixture, Before Ignition	4069.9	[g]
Wt+a, AI	Mass of sample basket+ catch pan + mixture, After Ignition	4001.8	[g]
Wm,BI	Mass of mixture, Before Ignition	1228.3	[g]
Wa,AI	Mass of aggregate, After Ignition	1160.2	[g]
Bm	Corrected binder content of bituminous mixture	5.54	[%]
Ba	Corrected binder content on aggregate weight	5.66	[%]
Corr Bm		5.54	[%]

MIX50_2 1 **Test date** **01/07/2025** **time** **14:53**

Wt	tray mass	407.9	[g]
Wt	tray mass	408.3	[g]
Wt+a,AI	tray mass + aggregates after ignition	1545.6	[g]
Wt+a,AI	tray mass + aggregates after ignition	1481.4	[g]
Wt+a,AI	tray mass + aggregates after ignition	1481.3	[g]
Wt+a,AI	tray mass + aggregates after ignition	1481.8	[g]

Sieve size [mm]	Sieve mass [g]	Sieve+soil [g]	Retained [g]	Cumulative [g]	Passing [g]	Passing [%]
20	1317.4	1317.4	0	0	1137.3	100.0
16	1302.1	1321.4	19.3	19.3	1118	98.3
12.5	1183.3	1309.7	126.4	145.7	991.6	87.2
8	1070.1	1171.5	101.4	247.1	890.2	78.3
4	1107.7	1523.6	415.9	663	474.3	41.7
2	980.1	1152.2	172.1	835.1	302.2	26.6
0.5	783.6	911.3	127.7	962.8	174.5	15.3
0.25	726.4	772.9	46.5	1009.3	128	11.3
0.063	767.1	824.1	57	1066.3	71	6.2
0	724.4	731.6	7.2	1137.3	0	0.0
Total	9962.2	11035.7	1073.5			

MIX50_2 2 **Test date** **14/07/2025** **time** **14:29**

Wt	tray mass	424.1	[g]
Wt	tray mass	424.5	[g]
Wt+a,AI	tray mass + aggregates after ignition	1583.1	[g]
Wt+a,AI	tray mass + aggregates after ignition	1509.5	[g]
Wt+a,AI	tray mass + aggregates after ignition	1509.4	[g]
Wt+a,AI	tray mass + aggregates after ignition	1509.8	[g]

Sieve size [mm]	Sieve mass [g]	Sieve+soil [g]	Retained [g]	Cumulative [g]	Passing [g]	Passing [%]
20	1317.4	1317.4	0	0	1158.9	100.0
16	1302.1	1355	52.9	52.9	1106	95.4
12.5	1183.3	1242.4	59.1	112	1046.9	90.3
8	1070.1	1178.3	108.2	220.2	938.7	81.0
4	1107.8	1539.3	431.5	651.7	507.2	43.8
2	980.4	1160.8	180.4	832.1	326.8	28.2
0.5	784	924.2	140.2	972.3	186.6	16.1
0.25	726.5	775.8	49.3	1021.6	137.3	11.8
0.063	767.4	827.8	60.4	1082	76.9	6.6
0	724.3	727.9	3.6	1158.9	0	0.0
Total	9963.3	11048.9	1085.6			

Cylindrical specimens compacted at N_{max} (200 gyrations)

Specimen Code	M1 [g]	M2 [g]	M3 [g]	T [°C]	ρ_w [Mg/m^3]	ρ_{mb} [Mg/m^3]	ρ_{mv} [Mg/m^3]	v [%]
MIX50_2 1	4803.9	2841.4	4825.6	26.6	0.9967	2.413	2.547	5.27
MIX50_2 2	4802.6	2832.4	4825.6	26.6	0.9967	2.402	2.547	5.72
MIX50_2 3	4821.0	2852.2	4844.4	26.5	0.9967	2.412	2.547	5.31
MIX50_2 4	4810.2	2846.4	4850.5	22.9	0.9976	2.395	2.547	6.00
MIX50_2 5	4832.0	2858.8	4871.4	22.9	0.9976	2.395	2.547	5.97
MIX50_2 6	4800.4	2864.3	4819.9	24.5	0.9972	2.448	2.547	3.90
MIX50_2 7	4803.9	2875.7	4829.2	24.5	0.9972	2.452	2.547	3.72

Specimen Code	Date	D_{mold} [mm]	v_{real} [%]	v_{geo} [%]	Δv [%]	C1 [%]	k [-]	CDI [-]
MIX50_2 1	02/07/2025	150	5.27	7.76	2.49	76.66	7.97	429.03
MIX50_2 2	02/07/2025	150	5.72	8.50	2.78	76.59	7.78	527.99
MIX50_2 3	21/07/2025	150	5.31	5.55	0.24	77.05	7.82	387.43
MIX50_2 4	15/09/2025	150	6.00	9.52	3.52	76.73	7.61	555.91
MIX50_2 5	15/09/2025	150	5.97	9.03	3.06	76.78	7.60	541.54
MIX50_2 6	22/09/2025	150	3.90	7.02	3.13	77.65	8.13	221.91
MIX50_2 7	22/09/2025	150	3.72	6.63	2.91	77.05	7.82	218.75

Cylindrical specimens compacted at N_{design} (120 gyrations), before cutting

Specimen Code	M1 [g]	M2 [g]	M3 [g]	T [°C]	ρ_w [Mg/m^3]	ρ_{mb} [Mg/m^3]	ρ_{mv} [Mg/m^3]	v [%]
MIX50_2 1FC	4798.1	2849.8	4833.1	20	0.9983	2.415	2.547	5.19
MIX50_2 2FC	4802.7	2874.6	4821.2	20.5	0.9982	2.463	2.547	3.32
MIX50_2 3FC	4798.7	2862.3	4814	20.5	0.9982	2.454	2.547	3.65
MIX50_2 4FC	4796.1	2871.1	4813.3	20.5	0.9982	2.465	2.547	3.23
MIX50_2 5FC	4803.9	2865.1	4826.1	19.1	0.9985	2.446	2.547	3.98
MIX50_2 6FC	4808.7	2862.1	4833.6	19.1	0.9985	2.435	2.547	4.39
MIX50_2 7FC	4798.1	2855	4813.5	19.9	0.9983	2.446	2.547	3.99
MIX50_2 8FC	4804.7	2840.5	4826.1	19.8	0.9983	2.416	2.547	5.16
MIX50_2 9FC	4802.5	2851.4	4825.2	19.8	0.9983	2.429	2.547	4.64

Specimen Code	Date	D_{mold} [mm]	v_{real} [%]	v_{geo} [%]	Δv [%]	C1 [%]	k [-]	CDI [-]
MIX50_2 1FC	27/11/2025	150	5.19	8.43	3.24	77.89	8.17	201.99
MIX50_2 2FC	28/11/2025	150	3.32	6.08	2.76	79.18	8.49	78.83
MIX50_2 3FC	28/11/2025	150	3.65	6.40	2.75	78.96	8.46	94.45
MIX50_2 4FC	28/11/2025	150	3.23	6.70	3.47	79.36	8.47	72.30
MIX50_2 5FC	09/12/2025	150	3.98	7.20	3.22	78.69	8.40	109.22
MIX50_2 6FC	09/12/2025	150	4.39	8.06	3.67	78.59	8.23	132.66
MIX50_2 7FC	10/12/2025	150	3.99	6.91	2.92	78.39	8.54	118.65
MIX50_2 8FC	12/12/2025	150	5.16	7.90	2.74	77.49	8.38	215.79
MIX50_2 9FC	12/12/2025	150	4.64	7.87	3.23	78.17	8.32	152.49

Cylindrical specimens compacted at N_{design} (120 gyrations), after cutting

Specimen Code	M1 [g]	M2 [g]	M3 [g]	T [°C]	ρ_w [Mg/m^3]	ρ_{mb} [Mg/m^3]	ρ_{mv} [Mg/m^3]	v [%]
MIX50_2 1FC	2515.5	1505.2	2523.2	21	0.9981	2.466	2.547	3.18
MIX50_2 2FC	2816.5	1696.8	2820.4	23.1	0.9976	2.501	2.547	1.83
MIX50_2 3FC	2755.5	1656.2	2760	21	0.9981	2.492	2.547	2.19
MIX50_2 4FC	2723.8	1640.4	2727.9	21	0.9981	2.500	2.547	1.86
MIX50_2 5FC	2628.3	1579.4	2633.9	21	0.9981	2.488	2.547	2.34
MIX50_2 6FC	2667.8	1600.6	2675.7	23.1	0.9976	2.475	2.547	2.82
MIX50_2 7FC	2650.1	1590.3	2654.4	23.1	0.9976	2.484	2.547	2.46
MIX50_2 8FC	2593	1545.5	2598.5	23.1	0.9976	2.457	2.547	3.56
MIX50_2 9FC	2597.3	1551.3	2601.9	23.1	0.9976	2.466	2.547	3.18

Prismatic specimens

Specimen Code	M1 [g]	M2 [g]	M3 [g]	T [°C]	ρ_w [Mg/m^3]	ρ_{mb} [Mg/m^3]	ρ_{mv} [Mg/m^3]	v [%]
MIX50_2 1FP	2700	1596.7	2712.2	19.8	0.9983	2.416	2.547	5.14
MIX50_2 2FP	2513	1491.1	2528.1	18.1	0.9986	2.420	2.547	4.99
MIX50_2 3FP	2510.4	1483.1	2518	18.4	0.9986	2.422	2.547	4.90
MIX50_2 4FP	2678.5	1584.6	2695.6	18.4	0.9986	2.407	2.547	5.49
MIX50_2 5FP	2587.9	1519.3	2599.2	19.2	0.9984	2.393	2.547	6.07
MIX50_2 6FP	2563.6	1505.6	2574	19.2	0.9984	2.396	2.547	5.95
MIX50_2 7FP	2651.9	1562.7	2663.1	19.2	0.9984	2.406	2.547	5.54
MIX50_2 8FP	2648.6	1561.5	2661.1	19.2	0.9984	2.405	2.547	5.59

MIX50 3

Test date **23/07/2025** **time** **17:00**

Q+A			
T	Water temperature	29.3	[°C]
ρ_w	Water density	0.996	[Mg/m^3]
m_1	Mass of pyknometer + head	917	[g]
m_2	Mass of pyknometer + head + mixture	1728.1	[g]
m_3	Mass of pyknometer + head + mixture + water	2754.6	[g]
V_p	Volume of the pyknometer	0.001348	[m^3]
ρ_{mm}	Maximum density	2.556	[Mg/m^3]

6+R			
T	Water temperature	29.3	[°C]
ρ_w	Water density	0.996	[Mg/m^3]
m_1	Mass of pyknometer + head	992.7	[g]
m_2	Mass of pyknometer + head + mixture	1790.6	[g]
m_3	Mass of pyknometer + head + mixture + water	2705.6	[g]
V_p	Volume of the pyknometer	0.001232	[m^3]
ρ_{mm}	Maximum density	2.550	[Mg/m^3]

r	**Repeatability**	0.006	[Mg/m^3]

ρmm	**Average**	2.553	[Mg/m^3]

Test date **23/07/2025** **time** **14:44**

Wt	Mass of sample basket and catch pan	2835	[g]
Wt+m, BI	Mass of sample basket+ catch pan + mixture, Before Ignition	3947.8	[g]
Wt+a, AI	Mass of sample basket+ catch pan + mixture, After Ignition	3889.6	[g]
Wm,BI	Mass of mixture, Before Ignition	1112.8	[g]
Wa,AI	Mass of aggregate, After Ignition	1054.6	[g]
CF	Calibration Factor		
Bm	Corrected binder content of bituminous mixture	5.23	[%]
Ba	Corrected binder content on aggregate weight	5.30	[%]
Corr Bm		5.23	[%]

Test date **03/11/2025** **time** **16:35**

Wt	Mass of sample basket and catch pan	2837	[g]
Wt+m, BI	Mass of sample basket+ catch pan + mixture, Before Ignition	3939.8	[g]
Wt+a, AI	Mass of sample basket+ catch pan + mixture, After Ignition	3881.8	[g]
Wm,BI	Mass of mixture, Before Ignition	1102.8	[g]
Wa,AI	Mass of aggregate, After Ignition	1044.8	[g]
Bm	Corrected binder content of bituminous mixture	5.26	[%]
Ba	Corrected binder content on aggregate weight	5.34	[%]
Corr Bm		5.26	[%]

Test date 03/11/2025 **time** 17:10

Wt	Mass of sample basket and catch pan	2844.9	[g]
Wt+m, BI	Mass of sample basket+ catch pan + mixture, Before Ignition	3946.6	[g]
Wt+a, AI	Mass of sample basket+ catch pan + mixture, After Ignition	3888.1	[g]
Wm,BI	Mass of mixture, Before Ignition	1101.7	[g]
Wa,AI	Mass of aggregate, After Ignition	1043.2	[g]
Bm	Corrected binder content of bituminous mixture	5.31	[%]
Ba	Corrected binder content on aggregate weight	5.39	[%]
Corr Bm		5.10	[%]

MIX50_3 1 **Test date** 23/07/2025 **time** 15:30

Wt	tray mass	398.1	[g]
Wt	tray mass	398.3	[g]
Wt+a,AI	tray mass + aggregates after ignition	1451.8	[g]
Wt+a,AI	tray mass + aggregates after ignition	1391.2	[g]
Wt+a,AI	tray mass + aggregates after ignition	1391.2	[g]
Wt+a,AI	tray mass + aggregates after ignition	1391.4	[g]

Sieve size [mm]	Sieve mass [g]	Sieve+soil [g]	Retained [g]	Cumulative [g]	Passing [g]	Passing [%]
31.5	1299	1299	0	0	1053.2	100
20	1317.4	1370.7	53.3	53.3	999.9	94.9
16	1302	1344.2	42.2	95.5	957.7	90.9
12.5	1183.3	1294.7	111.4	206.9	846.3	80.4
8	1070.2	1212.6	142.4	349.3	703.9	66.8
4	1107.8	1422.8	315	664.3	388.9	36.9
2	980	1117.4	137.4	801.7	251.5	23.9
0.5	783.7	885.8	102.1	903.8	149.4	14.2
0.25	726.3	764.8	38.5	942.3	110.9	10.5
0.063	767.5	813.8	46.3	988.6	64.6	6.1
0	724.4	728.6	4.2	1053.2	0	0.0
Total	11261.6	12254.4	992.8			

MIX50_3 2 **Test date** 23/07/2025 **time** 18:23

Wt	tray mass	408.2	[g]
Wt	tray mass	408.1	[g]
Wt+a,AI	tray mass + aggregates after ignition	1466.1	[g]
Wt+a,AI	tray mass + aggregates after ignition	1407.3	[g]
Wt+a,AI	tray mass + aggregates after ignition	1407.3	[g]
Wt+a,AI	tray mass + aggregates after ignition	1407.5	[g]

Sieve size [mm]	Sieve mass [g]	Sieve+soil [g]	Retained [g]	Cumulative [g]	Passing [g]	Passing [%]
31.5	1299	1299	0	0	1058.4	100
20	1317.3	1355	37.7	37.7	1020.7	96.4
16	1302	1399.8	97.8	135.5	922.9	87.2
12.5	1183.2	1320.3	137.1	272.6	785.8	74.2
8	1070.1	1188.2	118.1	390.7	667.7	63.1
4	1107.9	1416.2	308.3	699	359.4	34.0
2	979.9	1099.4	119.5	818.5	239.9	22.7
0.5	783.8	880.9	97.1	915.6	142.8	13.5
0.25	726.4	763	36.6	952.2	106.2	10.0
0.063	767.6	811.4	43.8	996	62.4	5.9
0	895.2	899	3.8	1058.4	0	0.0
Total	11432.4	12432.2	999.8			

Cylindrical specimens compacted at N_{max} (200 gyrations)

Specimen Code	M1 [g]	M2 [g]	M3 [g]	T [°C]	ρ_w [Mg/m^3]	ρ_{mb} [Mg/m^3]	ρ_{mv} [Mg/m^3]	v [%]
MIX50_3 1	4797.0	2893.2	4812.4	25.6	0.9970	2.492	2.553	2.38
MIX50_3 2	4796.1	2884.4	4809.9	25.6	0.9970	2.483	2.553	2.72
MIX50_3 3	4797.9	2875.7	4804.0	25.9	0.9969	2.480	2.553	2.83
MIX50_3 4	4826.4	2901.4	4841.9	23.8	0.9974	2.481	2.553	2.82
MIX50_3 5	4817.7	2902.1	4843.2	23.8	0.9974	2.476	2.553	3.02
MIX50_3 6	4803.0	2892.2	4827.2	24.5	0.9972	2.475	2.553	3.03
MIX50_3 7	4804.9	2891.2	4821.2	24.5	0.9972	2.483	2.553	2.74

Specimen Code	Date	D_{mold} [mm]	v_{real} [%]	v_{geo} [%]	Δv [%]	C1 [%]	k [-]	CDI [-]
MIX50_3 1	02/07/2025	150	2.38	4.71	2.33	79.60	7.99	93.40
MIX50_3 2	02/07/2025	150	2.72	5.58	2.86	80.18	7.60	89.32
MIX50_3 3	21/07/2025	150	2.83	5.20	2.37	80.30	7.52	84.59
MIX50_3 4	16/09/2025	150	2.82	5.40	2.58	79.46	7.85	107.57
MIX50_3 5	16/09/2025	150	3.02	6.64	3.62	79.04	7.91	138.57
MIX50_3 6	22/09/2025	150	3.03	6.77	3.74	78.94	7.97	137.50
MIX50_3 7	22/09/2025	150	2.74	5.99	3.25	79.86	7.68	98.96

Cylindrical specimens compacted at N_{design} (120 gyrations), before cutting

Specimen Code	M1 [g]	M2 [g]	M3 [g]	T [°C]	ρ_w [Mg/m^3]	ρ_{mb} [Mg/m^3]	ρ_{mv} [Mg/m^3]	v [%]
MIX50_3 1FC	4790.1	2867.2	4830	19.6	0.9984	2.436	2.553	4.55
MIX50_3 2FC	4785.6	2859.3	4801	19.6	0.9984	2.461	2.553	3.61
MIX50_3 3FC	4785.7	2861.9	4804.4	19.6	0.9984	2.460	2.553	3.65
MIX50_3 4FC	4805.6	2875.9	4831.7	19.8	0.9983	2.453	2.553	3.91
MIX50_3 5FC	4799.7	2871.3	4810.7	19.8	0.9983	2.471	2.553	3.21
MIX50_3 6FC	4799.2	2879.4	4817.9	20.1	0.9983	2.471	2.553	3.18
MIX50_3 7FC	4808	2880.1	4828	20.1	0.9983	2.464	2.553	3.47
MIX50_3 8FC	4801.9	2869.9	4821.5	20.1	0.9983	2.456	2.553	3.78
MIX50_3 9FC	4802.3	2873	4818.4	19.8	0.9983	2.464	2.553	3.46

Specimen Code	Date	D_{mold} [mm]	v_{real} [%]	v_{geo} [%]	Δv [%]	C1 [%]	k [-]	CDI [-]
MIX50_3 1FC	26/11/2025	150	4.55	8.93	4.38	78.68	8.15	137.45
MIX50_3 2FC	26/11/2025	150	3.61	6.20	2.59	79.82	8.12	71.79
MIX50_3 3FC	26/11/2025	150	3.65	6.78	3.13	79.25	8.33	89.30
MIX50_3 4FC	10/12/2025	150	3.91	7.28	3.38	79.32	8.17	92.39
MIX50_3 5FC	10/12/2025	150	3.21	6.17	2.96	80.81	7.82	45.72
MIX50_3 6FC	11/12/2025	150	3.18	6.26	3.08	79.72	8.30	65.68
MIX50_3 7FC	11/12/2025	150	3.47	6.75	3.28	79.88	8.13	66.11
MIX50_3 8FC	11/12/2025	150	3.78	6.71	2.93	78.96	8.40	92.04
MIX50_3 9FC	12/12/2025	150	3.46	6.62	3.16	80.38	7.90	59.08

Cylindrical specimens compacted at N_{design} (120 gyrations), after cutting

Specimen Code	M1 [g]	M2 [g]	M3 [g]	T [°C]	ρ_w [Mg/m^3]	ρ_{mb} [Mg/m^3]	ρ_{mv} [Mg/m^3]	v [%]
MIX50_3 1FC	2362.9	1422.9	2378.9	22.5	0.9977	2.466	2.553	3.39
MIX50_3 2FC	2621	1577.3	2624.1	22.5	0.9977	2.498	2.553	2.14
MIX50_3 3FC	2697.7	1627.7	2704.8	22.5	0.9977	2.499	2.553	2.11
MIX50_3 4FC	2671.5	1605.9	2679.2	22.5	0.9977	2.483	2.553	2.71
MIX50_3 5FC	2656.5	1596.9	2660	22.5	0.9977	2.493	2.553	2.33
MIX50_3 6FC	2699.4	1632.4	2706.5	22.5	0.9977	2.507	2.553	1.77
MIX50_3 7FC	2680.6	1614.3	2685.3	22.5	0.9977	2.497	2.553	2.17
MIX50_3 8FC	2618.8	1573.6	2623.1	22.5	0.9977	2.490	2.553	2.47
MIX50_3 9FC	2658.8	1599.7	2662.4	22.5	0.9977	2.496	2.553	2.21

Prismatic specimens

Specimen Code	M1 [g]	M2 [g]	M3 [g]	T [°C]	ρ_w [Mg/m^3]	ρ_{mb} [Mg/m^3]	ρ_{mv} [Mg/m^3]	v [%]
MIX50_3 1FP	2512.3	1494.8	2526.3	19.8	0.9983	2.431	2.553	4.75
MIX50_3 2FP	2571.4	1526.8	2582.9	18.1	0.9986	2.432	2.553	4.75
MIX50_3 3FP	2706.4	1607.5	2715.8	18.1	0.9986	2.439	2.553	4.47
MIX50_3 4FP	2768.3	1640.2	2775.7	18.1	0.9986	2.435	2.553	4.62
MIX50_3 5FP	2646.5	1579.7	2662.4	20.7	0.9981	2.440	2.553	4.42
MIX50_3 6FP	2761	1641.4	2774.4	20.7	0.9981	2.432	2.553	4.71
MIX50_3 7FP	2849	1692.2	2858.4	20.7	0.9981	2.438	2.553	4.48
MIX50_3 8FP	2699.1	1601.7	2705.2	20.7	0.9981	2.441	2.553	4.36

MIX50 REF

Test date	14/07/2025	time	11:30

Q+A			
T	Water temperature	25.8	[°C]
ρ_w	Water density	0.997	[Mg/m^3]
m_1	Mass of pyknometer + head	917	[g]
m_2	Mass of pyknometer + head + mixture	1751.9	[g]
m_3	Mass of pyknometer + head + mixture + water	2772.9	[g]
V_p	Volume of the pyknometer	0.001348	[m^3]
ρ_{mm}	Maximum density	2.577	[Mg/m^3]

6+R			
T	Water temperature	25.8	[°C]
ρ_w	Water density	0.997	[Mg/m^3]
m_1	Mass of pyknometer + head	992.6	[g]
m_2	Mass of pyknometer + head + mixture	1775.3	[g]
m_3	Mass of pyknometer + head + mixture + water	2699.4	[g]
V_p	Volume of the pyknometer	0.001232	[m^3]
ρ_{mm}	Maximum density	2.568	[Mg/m^3]

r	**Repeatability**	0.009	[Mg/m^3]

Test date	15/07/2025	time	16:40

Q+A			
T	Water temperature	26.5	[°C]
ρ_w	Water density	0.997	[Mg/m^3]
m_1	Mass of pyknometer + head	917	[g]
m_2	Mass of pyknometer + head + mixture	1746.9	[g]
m_3	Mass of pyknometer + head + mixture + water	2771.4	[g]
V_p	Volume of the pyknometer	0.001348	[m^3]
ρ_{mm}	Maximum density	2.592	[Mg/m^3]

6+R			
T	Water temperature	26.4	[°C]
ρ_w	Water density	0.997	[Mg/m^3]
m_1	Mass of pyknometer + head	992.6	[g]
m_2	Mass of pyknometer + head + mixture	1767.4	[g]
m_3	Mass of pyknometer + head + mixture + water	2697.2	[g]
V_p	Volume of the pyknometer	0.001232	[m^3]
ρ_{mm}	Maximum density	2.592	[Mg/m^3]

r	**Repeatability**	0.001	[Mg/m^3]

ρmm	**Average**	2.583	[Mg/m^3]

Test date **14/07/2025** **time** **14:34**

Wt	Mass of sample basket and catch pan	2844.4	[g]
Wt+m, BI	Mass of sample basket+ catch pan + mixture, Before Ignition	3947.5	[g]
Wt+a, AI	Mass of sample basket+ catch pan + mixture, After Ignition	3894.8	[g]
Wm,BI	Mass of mixture, Before Ignition	1103.1	[g]
Wa,AI	Mass of aggregate, After Ignition	1050.4	[g]
Bm	Corrected binder content of bituminous mixture	4.78	[%]
Ba	Corrected binder content on aggregate weight	4.80	[%]
Corr Bm		4.78	[%]

Test date **15/07/2025** **time** **15:29**

Wt	Mass of sample basket and catch pan	2844.4	[g]
Wt+m, BI	Mass of sample basket+ catch pan + mixture, Before Ignition	3952	[g]
Wt+a, AI	Mass of sample basket+ catch pan + mixture, After Ignition	3899.7	[g]
Wm,BI	Mass of mixture, Before Ignition	1107.6	[g]
Wa,AI	Mass of aggregate, After Ignition	1055.3	[g]
Bm	Corrected binder content of bituminous mixture	4.72	[%]
Ba	Corrected binder content on aggregate weight	4.74	[%]
Corr Bm		4.72	[%]

MIX50_REF 1 **Test date** **14/07/2025** **time** **14:29**

Wt	tray mass	930.8	[g]
Wt	tray mass	930.8	[g]
Wt+a,AI	tray mass + aggregates after ignition	1975.8	[g]
Wt+a,AI	tray mass + aggregates after ignition	1913.3	[g]
Wt+a,AI	tray mass + aggregates after ignition	1913.5	[g]
Wt+a,AI	tray mass + aggregates after ignition	1913.5	[g]

Sieve size [mm]	Sieve mass [g]	Sieve+soil [g]	Retained [g]	Cumulative [g]	Passing [g]	Passing [%]
31.5	1298.9	1298.9	0	0	1045.1	100
20	1317.4	1343	25.6	25.6	1019.5	97.6
16	1302	1302.1	0.1	25.7	1019.4	97.5
12.5	1183.2	1285.2	102	127.7	917.4	87.8
8	1070.2	1250.1	179.9	307.6	737.5	70.6
4	1107.9	1452.6	344.7	652.3	392.8	37.6
2	980	1129.4	149.4	801.7	243.4	23.3
0.5	783.7	883.5	99.8	901.5	143.6	13.7
0.25	726.4	760.7	34.3	935.8	109.3	10.5
0.063	767.4	811.2	43.8	979.6	65.5	6.3
0	895.1	898.3	3.2	1045.1	0	0.0
Total	11432.2	11116.1	982.8			

MIX50_REF 2 **Test date** **14/07/2025** **time** **14:29**

Wt	tray mass	488.7	[g]
Wt	tray mass	488.6	[g]
Wt+a,AI	tray mass + aggregates after ignition	1538.1	[g]
Wt+a,AI	tray mass + aggregates after ignition	1482	[g]
Wt+a,AI	tray mass + aggregates after ignition	1482	[g]
Wt+a,AI	tray mass + aggregates after ignition	1482.3	[g]

Sieve size [mm]	Sieve mass [g]	Sieve+soil [g]	Retained [g]	Cumulative [g]	Passing [g]	Passing [%]
31.5	1298.9	1298.9	0	0	1049.5	100
20	1317.4	1341.9	24.5	24.5	1025	97.7
16	1302.1	1321.9	19.8	44.3	1005.2	95.8
12.5	1183.3	1306.4	123.1	167.4	882.1	84.0
8	1070.2	1257	186.8	354.2	695.3	66.3
4	1107.9	1449.9	342	696.2	353.3	33.7
2	980	1110	130	826.2	223.3	21.3
0.5	784.1	873.9	89.8	916	133.5	12.7
0.25	726.7	759.4	32.7	948.7	100.8	9.6
0.063	767.5	808.9	41.4	990.1	59.4	5.7
0	895.1	898.7	3.6	1049.5	0	0.0
Total	11432.2	11116.1	993.7			

Cylindrical specimens compacted at N_{max} (200 gyrations)

Specimen Code	M1 [g]	M2 [g]	M3 [g]	T [°C]	ρ_w [Mg/m^3]	ρ_{mb} [Mg/m^3]	ρ_{mv} [Mg/m^3]	v [%]
MIX50_REF 1	4799	2893.8	4813.8	25	0.9971	2.492	2.583	3.50
MIX50_REF 2	4798.4	2892.1	4813.9	25	0.9971	2.490	2.583	3.60
MIX50_REF 3	4797	2891.5	4813.9	25.6	0.9970	2.488	2.583	3.67
MIX50_REF 4	4812.4	2884.5	4845.4	22.8	0.9977	2.448	2.583	5.19
MIX50_REF 5	4816.5	2892.9	4848	22.9	0.9976	2.458	2.583	4.83
MIX50_REF 6	4807.4	2894.3	4853.3	24.5	0.9972	2.447	2.583	5.24
MIX50_REF 7	4796.9	2872.4	4828.1	24.5	0.9972	2.446	2.583	5.29

Specimen Code	Date	D_{mold} [mm]	v_{real} [%]	v_{geo} [%]	Δv [%]	C1 [%]	k [-]	CDI [-]
MIX50_REF 1	02/07/2025	150	3.50	6.94	3.45	78.30	8.03	176.07
MIX50_REF 2	02/07/2025	150	3.60	6.79	3.19	78.26	8.01	191.10
MIX50_REF 3	21/07/2025	150	3.67	8.84	5.17	77.26	8.37	229.84
MIX50_REF 4	15/09/2025	150	5.19	9.25	4.06	77.26	8.37	423.08
MIX50_REF 5	15/09/2025	150	4.83	9.41	4.58	76.94	7.99	355.37
MIX50_REF 6	22/09/2025	150	5.24	10.96	5.72	76.64	7.94	438.56
MIX50_REF 7	22/09/2025	150	5.29	9.78	4.49	78.68	6.53	509.55

Cylindrical specimens compacted at N_{design} (120 gyrations), before cutting

Specimen Code	M1 [g]	M2 [g]	M3 [g]	T [°C]	ρ_w [Mg/m^3]	ρ_{mb} [Mg/m^3]	ρ_{mv} [Mg/m^3]	v [%]
MIX50_REF 1FC	4797.5	2875.2	4834.6	20	0.9983	2.444	2.583	5.36
MIX50_REF 2FC	4809.3	2867.9	4839.3	19.8	0.9983	2.435	2.583	5.70
MIX50_REF 3FC	4801.8	2868.9	4834.9	19.8	0.9983	2.438	2.583	5.58
MIX50_REF 4FC	4809.1	2876.1	4841.2	19.8	0.9983	2.443	2.583	5.40
MIX50_REF 5FC	4797.9	2859.4	4815.5	19.8	0.9983	2.449	2.583	5.18
MIX50_REF 6FC	4814.1	2872.6	4829.5	19.8	0.9983	2.456	2.583	4.90
MIX50_REF 7FC	4805.0	2870.0	4832.5	19.8	0.9983	2.444	2.583	5.35
MIX50_REF 8FC	4805.0	2870.0	4832.5	19.8	0.9983	2.444	2.583	5.35
MIX50_REF 9FC	4805.0	2870.0	4832.5	19.8	0.9983	2.444	2.583	5.35

Specimen Code	Date	D_{mold} [mm]	v_{real} [%]	v_{geo} [%]	Δv [%]	C1 [%]	k [-]	CDI [-]
MIX50_REF 1FC	27/11/2025	150	5.36	9.22	3.87	77.89	8.17	223.45
MIX50_REF 2FC	28/11/2025	150	5.70	9.85	4.16	79.18	8.49	269.03
MIX50_REF 3FC	28/11/2025	150	5.58	9.84	4.26	78.96	8.46	263.04
MIX50_REF 4FC	28/11/2025	150	5.40	9.47	4.07	79.36	8.47	231.76
MIX50_REF 5FC	09/12/2025	150	5.18	9.21	4.03	78.69	8.40	196.11
MIX50_REF 6FC	09/12/2025	150	4.90	8.27	3.37	78.59	8.23	177.68
MIX50_REF 7FC	10/12/2025	150	4.90	8.27	3.37	78.39	8.54	177.68
MIX50_REF 8FC	12/12/2025	150	4.90	8.27	3.37	77.49	8.38	177.68
MIX50_REF 9FC	12/12/2025	150	4.90	8.27	3.37	78.17	8.32	177.68

Cylindrical specimens compacted at N_{design} (120 gyrations), after cutting

Specimen Code	M1 [g]	M2 [g]	M3 [g]	T [°C]	ρ_w [Mg/m^3]	ρ_{mb} [Mg/m^3]	ρ_{mv} [Mg/m^3]	v [%]
MIX50_REF 1FC	2684.6	1618.4	2693	18.8	0.9985	2.495	2.583	3.41
MIX50_REF 2FC	2576.1	1543.5	2585.4	18.8	0.9985	2.469	2.583	4.40
MIX50_REF 3FC	2674.4	1607	2683.2	18.8	0.9985	2.481	2.583	3.92
MIX50_REF 4FC	2628.2	1583.8	2636.3	18.8	0.9985	2.493	2.583	3.45
MIX50_REF 5FC	2626.5	1575.2	2630.8	18.8	0.9985	2.484	2.583	3.80
MIX50_REF 6FC	2662.2	1603.9	2667.6	18.8	0.9985	2.499	2.583	3.23
MIX50_REF 7FC	2644.5	1588.8	2653.6	18.8	0.9985	2.480	2.583	3.98
MIX50_REF 8FC	2590.6	1555.3	2601.4	18.8	0.9985	2.473	2.583	4.25
MIX50_REF 9FC	2539.7	1521.3	2546.5	18.8	0.9985	2.474	2.583	4.22

Prismatic specimens

Specimen Code	M1 [g]	M2 [g]	M3 [g]	T [°C]	ρ_w [Mg/m^3]	ρ_{mb} [Mg/m^3]	ρ_{mv} [Mg/m^3]	v [%]
MIX50_REF 1FP	3010.9	1798.8	3018.2	18.3	0.9986	2.466	2.583	4.52
MIX50_REF 2FP	3001.4	1793.2	3009.5	18.3	0.9986	2.464	2.583	4.58
MIX50_REF 3FP	2912.7	1744.3	2923.5	22.1	0.9978	2.465	2.583	4.56
MIX50_REF 4FP	2878.7	1726.2	2893.4	22.1	0.9978	2.461	2.583	4.71
MIX50_REF 5FP	2707.9	1618.2	2721.1	18.1	0.9986	2.452	2.583	5.06
MIX50_REF 6FP	2609.2	1558.8	2622.6	18.1	0.9986	2.449	2.583	5.16
MIX50_REF 7FP	2589.3	1550.4	2600.6	18.1	0.9986	2.462	2.583	4.66
MIX50_REF 8FP	2658.9	1591.5	2672.8	18.1	0.9986	2.456	2.583	4.91

Stiffness moduli

MIX50 1

Cylindrical specimens compacted at N_{max} (200 gyrations) – 10°C

Specimen Code	Mix	E_1 [MPa]	E_2 [MPa]	Δ_{rel} [%]	E_{av} [MPa]
MIX50_1 1	**MIX50_1**	21791.0	19667.0	9.75	20729.0
MIX50_1 2	**MIX50_1**	22927.0	20439.0	10.85	21683.0
MIX50_1 3	**MIX50_1**	21619.0	21115.0	2.33	21367.0
MIX50_1 4	**MIX50_1**	23478.6	22962.6	2.20	23220.6
MIX50_1 5	**MIX50_1**	23853.2	23561.4	1.22	23707.3
MIX50_1 6	**MIX50_1**	23098.2	23109.3	-0.05	23103.8
MIX50_1 7	**MIX50_1**	23037.6	22348.3	2.99	22693.0

Cylindrical specimens compacted at N_{max} (200 gyrations) – 20°C

Specimen Code	Mix	E_1 [MPa]	E_2 [MPa]	Δ_{rel} [%]	E_{av} [MPa]
MIX50_1 1	**MIX50_1**	12504.0	12227.0	2.22	12365.5
MIX50_1 2	**MIX50_1**	12120.0	11860.0	2.15	11990.0
MIX50_1 3	**MIX50_1**	11918.0	11668.0	2.10	11793.0
MIX50_1 4	**MIX50_1**	15206.6	14765.9	2.90	14986.3
MIX50_1 5	**MIX50_1**	15400.9	15529.2	-0.83	15465.1
MIX50_1 6	**MIX50_1**	12897.6	13045.6	-1.15	12971.6
MIX50_1 7	**MIX50_1**	14183.4	13713.3	3.31	13948.4

Cylindrical specimens compacted at N_{max} (200 gyrations) – 30°C

Specimen Code	Mix	E_1 [MPa]	E_2 [MPa]	Δ_{rel} [%]	E_{av} [MPa]
MIX50_1 1	**MIX50_1**	5703.0	4915.0	13.82	5309.0
MIX50_1 2	**MIX50_1**	-	-	-	-
MIX50_1 3	**MIX50_1**	4947.0	5823.0	-17.71	5385.0
MIX50_1 4	**MIX50_1**	7623.7	7123.3	6.56	7373.5
MIX50_1 5	**MIX50_1**	7317.3	7266.0	0.70	7291.7
MIX50_1 6	**MIX50_1**	5990.5	6050.6	-1.00	6020.6
MIX50_1 7	**MIX50_1**	7002.0	7076.2	-1.06	7039.1

Cylindrical specimens compacted at N_{design} (120 gyrations), after cutting – 20°C

Specimen Code	Mix	E_1 [MPa]	E_2 [MPa]	Δ_{rel} [%]	E_{av} [MPa]
MIX50_1 1FC	**MIX50_1**	14279.9	15362.0	-7.58	14821.0
MIX50_1 2FC	**MIX50_1**	14549.8	14429.7	0.83	14489.8
MIX50_1 3FC	**MIX50_1**	13730.5	13142.6	4.28	13436.6
MIX50_1 4FC	**MIX50_1**	14455.8	14682.6	-1.57	14569.2
MIX50_1 5FC	**MIX50_1**	14585.0	13997.3	4.03	14291.2
MIX50_1 6FC	**MIX50_1**	14552.7	14994.0	-3.03	14773.4
MIX50_1 7FC	**MIX50_1**	14619.4	14412.5	1.42	14516.0
MIX50_1 8FC	**MIX50_1**	13586.4	13557.5	0.21	13572.0
MIX50_1 9FC	**MIX50_1**	13913.2	14159.5	-1.77	14036.4

MIX50 2

Cylindrical specimens compacted at N_{max} (200 gyrations) – 10°C

Specimen Code	Mix	E_1 [MPa]	E_2 [MPa]	Δ_{rel} [%]	E_{av} [MPa]
MIX50_2 1	**MIX50_2**	18584.0	17942.0	3.45	18263.0
MIX50_2 2	**MIX50_2**	20801.0	18537.0	10.88	19669.0
MIX50_2 3	**MIX50_2**	23360.0	22127.0	5.28	22743.5
MIX50_2 4	**MIX50_2**	-	-	-	-
MIX50_2 5	**MIX50_2**	20914.7	20353.7	2.68	20634.2
MIX50_2 6	**MIX50_2**	21126.4	22440.0	-6.22	21783.2
MIX50_2 7	**MIX50_2**	22561.5	22619.3	-0.26	22590.4

Cylindrical specimens compacted at N_{max} (200 gyrations) – 20°C

Specimen Code	Mix	E_1 [MPa]	E_2 [MPa]	Δ_{rel} [%]	E_{av} [MPa]
MIX50_2 1	**MIX50_2**	9513.0	8943.0	5.99	9228.0
MIX50_2 2	**MIX50_2**	9619.0	9754.0	-1.40	9686.5
MIX50_2 3	**MIX50_2**	12501.0	12294.0	1.66	12397.5
MIX50_2 4	**MIX50_2**	-	-	-	-
MIX50_2 5	**MIX50_2**	11640.3	11222.3	3.59	11431.3
MIX50_2 6	**MIX50_2**	12075.2	12356.0	-2.33	12215.6
MIX50_2 7	**MIX50_2**	11237.9	12298.8	-9.44	11768.4

Cylindrical specimens compacted at N_{max} (200 gyrations) – 30°C

Specimen Code	Mix	E_1 [MPa]	E_2 [MPa]	Δ_{rel} [%]	E_{av} [MPa]
MIX50_2 1	**MIX50_2**	3265.0	3034.0	7.08	3149.5
MIX50_2 2	**MIX50_2**	3875.0	2360.0	39.10	3117.5
MIX50_2 3	**MIX50_2**	5629.0	5571.0	1.03	5600.0
MIX50_2 4	**MIX50_2**	-	-	-	-
MIX50_2 5	**MIX50_2**	5408.6	5363.0	0.84	5385.8
MIX50_2 6	**MIX50_2**	5333.0	5469.8	-2.57	5401.4
MIX50_2 7	**MIX50_2**	6383.9	6006.3	5.91	6195.1

Cylindrical specimens compacted at N_{design} (120 gyrations), after cutting – 20°C

Specimen Code	Mix	E_1 [MPa]	E_2 [MPa]	Δ_{rel} [%]	E_{av} [MPa]
MIX50_2 1FC	**MIX50_2**	12592.6	12734.3	-1.13	12663.5
MIX50_2 2FC	**MIX50_2**	12839.0	12905.6	-0.52	12872.3
MIX50_2 3FC	**MIX50_2**	12322.6	12821.9	-4.05	12572.3
MIX50_2 4FC	**MIX50_2**	14444.1	13823.8	4.29	14134.0
MIX50_2 5FC	**MIX50_2**	13462.2	13371.8	0.67	13417.0
MIX50_2 6FC	**MIX50_2**	13994.6	13729.9	1.89	13862.3
MIX50_2 7FC	**MIX50_2**	13960.3	13552.7	2.92	13756.5
MIX50_2 8FC	**MIX50_2**	11421.0	10804.0	5.40	11112.5
MIX50_2 9FC	**MIX50_2**	11814.4	11522.4	2.47	11668.4

MIX50 3

Cylindrical specimens compacted at N_{max} (200 gyrations) – 10°C

Specimen Code	Mix	E_1 [MPa]	E_2 [MPa]	Δ_{rel} [%]	E_{av} [MPa]
MIX50_3 1	**MIX50_3**	21214.0	18552.0	12.55	19883.0
MIX50_3 2	**MIX50_3**	21340.0	19730.0	7.54	20535.0
MIX50_3 3	**MIX50_3**	23079.0	21849.0	5.33	22464.0
MIX50_3 4	**MIX50_3**	23335.4	23674.8	-1.45	23505.1
MIX50_3 5	**MIX50_3**	22466.3	23144.0	-3.02	22805.2
MIX50_3 6	**MIX50_3**	22341.6	22530.6	-0.85	22436.1
MIX50_3 7	**MIX50_3**	22512.5	22130.1	1.70	22321.3

Cylindrical specimens compacted at N_{max} (200 gyrations) – 20°C

Specimen Code	Mix	E_1 [MPa]	E_2 [MPa]	Δ_{rel} [%]	E_{av} [MPa]
MIX50_3 1	**MIX50_3**	11876.0	11308.0	4.78	11592.0
MIX50_3 2	**MIX50_3**	13487.0	13438.0	0.36	13462.5
MIX50_3 3	**MIX50_3**	12841.0	13150.0	-2.41	12995.5
MIX50_3 4	**MIX50_3**	14740.7	14722.4	0.12	14731.6
MIX50_3 5	**MIX50_3**	13946.1	13365.0	4.17	13655.6
MIX50_3 6	**MIX50_3**	13673.9	13083.6	4.32	13378.8
MIX50_3 7	**MIX50_3**	13815.1	12823.9	7.17	13319.5

Cylindrical specimens compacted at N_{max} (200 gyrations) – 30°C

Specimen Code	Mix	E_1 [MPa]	E_2 [MPa]	Δ_{rel} [%]	E_{av} [MPa]
MIX50_3 1	**MIX50_3**	5113.0	5129.0	-0.31	5121.0
MIX50_3 2	**MIX50_3**	6274.0	6362.0	-1.40	6318.0
MIX50_3 3	**MIX50_3**	2452.0	-	-	-
MIX50_3 4	**MIX50_3**	7562.8	7349.2	2.82	7456.0
MIX50_3 5	**MIX50_3**	7639.7	6806.3	10.91	7223.0
MIX50_3 6	**MIX50_3**	6938.4	7454.6	-7.44	7196.5
MIX50_3 7	**MIX50_3**	7001.9	7092.9	-1.30	7047.4

Cylindrical specimens compacted at N_{design} (120 gyrations), after cutting – 20°C

Specimen Code	Mix	E_1 [MPa]	E_2 [MPa]	Δ_{rel} [%]	E_{av} [MPa]
MIX50_3 1FC	**MIX50_3**	13740.7	14259.4	-3.77	14000.1
MIX50_3 2FC	**MIX50_3**	13619.7	13527.9	0.67	13573.8
MIX50_3 3FC	**MIX50_3**	17713.8	16872.0	4.75	17292.9
MIX50_3 4FC	**MIX50_3**	15637.8	15484.9	0.98	15561.4
MIX50_3 5FC	**MIX50_3**	15264.1	14298.3	6.33	14781.2
MIX50_3 6FC	**MIX50_3**	17718.0	17313.0	2.29	17515.5
MIX50_3 7FC	**MIX50_3**	13413.1	15555.1	-15.97	14484.1
MIX50_3 8FC	**MIX50_3**	14609.9	13776.6	5.70	14193.3
MIX50_3 9FC	**MIX50_3**	13654.5	13128.8	3.85	13391.7

MIX50 REF

Cylindrical specimens compacted at N_{max} (200 gyrations) – 10°C

Specimen Code	Mix	E_1 [MPa]	E_2 [MPa]	Δ_{rel} [%]	E_{av} [MPa]
MIX50_REF 1	**MIX50_REF**	20771.0	20598.0	0.83	20684.5
MIX50_REF 2	**MIX50_REF**	21363.0	20093.0	5.94	20728.0
MIX50_REF 3	**MIX50_REF**	16478.0	14850.0	9.88	15664.0
MIX50_REF 4	**MIX50_REF**	21996.9	21356.0	2.91	21676.4
MIX50_REF 5	**MIX50_REF**	22805.1	21691.9	4.88	22248.5
MIX50_REF 6	**MIX50_REF**	22477.6	21668.2	3.60	22072.9
MIX50_REF 7	**MIX50_REF**	20304.7	20866.4	-2.77	20585.6

Cylindrical specimens compacted at N_{max} (200 gyrations) – 20°C

Specimen Code	Mix	E_1 [MPa]	E_2 [MPa]	Δ_{rel} [%]	E_{av} [MPa]
MIX50_REF 1	**MIX50_REF**	11788.0	11977.0	-1.60	11882.5
MIX50_REF 2	**MIX50_REF**	11325.0	11064.0	2.30	11194.5
MIX50_REF 3	**MIX50_REF**	7782.0	6953.0	10.65	7367.5
MIX50_REF 4	**MIX50_REF**	13467.7	12661.4	5.99	13064.6
MIX50_REF 5	**MIX50_REF**	13493.1	13184.3	2.29	13338.7
MIX50_REF 6	**MIX50_REF**	12868.6	13187.2	-2.48	13027.9
MIX50_REF 7	**MIX50_REF**	12572.1	11737.8	6.64	12155.0

Cylindrical specimens compacted at N_{max} (200 gyrations) – 30°C

Specimen Code	Mix	E_1 [MPa]	E_2 [MPa]	Δ_{rel} [%]	E_{av} [MPa]
MIX50_REF 1	**MIX50_REF**	5712.0	5534.0	3.12	5623.0
MIX50_REF 2	**MIX50_REF**	-	-	-	-
MIX50_REF 3	**MIX50_REF**	2025.0	0.0	100.00	1012.5
MIX50_REF 4	**MIX50_REF**	6012.6	6269.6	-4.27	6141.1
MIX50_REF 5	**MIX50_REF**	6566.6	6461.9	1.59	6514.3
MIX50_REF 6	**MIX50_REF**	6265.4	6408.4	-2.28	6336.9
MIX50_REF 7	**MIX50_REF**	6004.8	6057.9	-0.88	6031.4

Cylindrical specimens compacted at N_{design} (120 gyrations), after cutting – 20°C

Specimen Code	Mix	E_1 [MPa]	E_2 [MPa]	Δ_{rel} [%]	E_{av} [MPa]
MIX50_REF 1FC	**MIX50_REF**	13447.4	13950.8	-3.74	13699.1
MIX50_REF 2FC	**MIX50_REF**	13147.0	13656.1	-3.87	13401.6
MIX50_REF 3FC	**MIX50_REF**	13036.7	13112.7	-0.58	13074.7
MIX50_REF 4FC	**MIX50_REF**	13202.8	12864.7	2.56	13033.8
MIX50_REF 5FC	**MIX50_REF**	12748.7	12132.9	4.83	12440.8
MIX50_REF 6FC	**MIX50_REF**	13544.4	12808.4	5.43	13176.4
MIX50_REF 7FC	**MIX50_REF**	12182.4	12573.4	-3.21	12377.9
MIX50_REF 8FC	**MIX50_REF**	12773.3	13480.3	-5.53	13126.8
MIX50_REF 9FC	**MIX50_REF**	12831.6	12923.6	-0.72	12877.6

Fatigue performance

MIX50 1

Cylindrical specimens compacted at N_{design} (120 gyrations)

ID	E_0	σ_a	ε_a	$\Delta\varepsilon$	$N_{f,50\%}$	$N_{f,ER}$	$\log_{10}\Delta\varepsilon$	$\log_{10} N_{f,50\%}$	$\log_{10} N_{f,ER}$
	[MPa]	[MPa]	[µm/m]	[MPa]	[-]	[-]	[µm/m]	[-]	[-]
MIX50_1 1FC	20653	549	54.6	109.2	5630	4970	2.038	3.751	3.696
MIX50_1 2FC	16871	414	48.6	97.2	20050	17420	1.988	4.302	4.241
MIX50_1 3FC	15990	505	64.1	128.2	8400	7630	2.108	3.924	3.883
MIX50_1 4FC	18072	416	28.4	56.7	197330	171160	1.754	5.295	5.233
MIX50_1 5FC	19061	532	57.0	114.0	5380	4770	2.057	3.731	3.679
MIX50_1 6FC	17146	421	29.9	59.8	265760	141800	1.776	5.424	5.152
MIX50_1 8FC	17361	391	47.2	94.5	17490	16050	1.975	4.243	4.205
MIX50_1 9FC	19647	403	41.7	83.5	22270	20070	1.922	4.348	4.303

MIX50 1	$N_{f,50\%}$	$N_{f,ER}$
$\log_{10} k_\varepsilon$ [-]	13.887	13.100
k_ε [-]	7.71E+13	1.26E+13
n_ε [-]	-4.871	-4.508
ε_6 [µm/m]	44	40

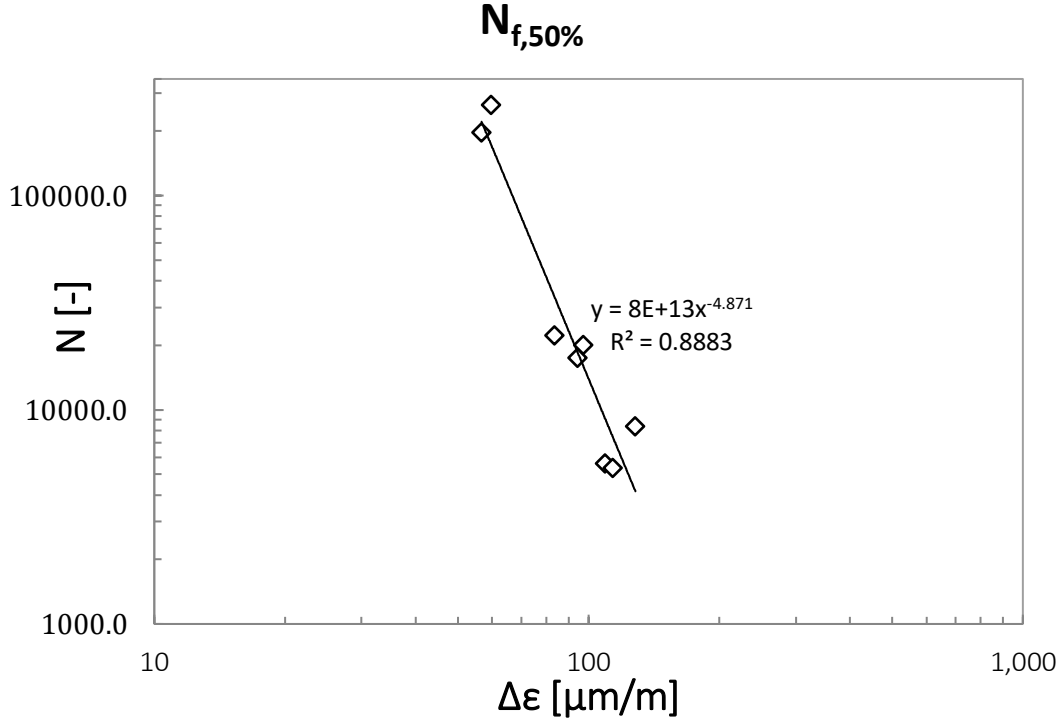

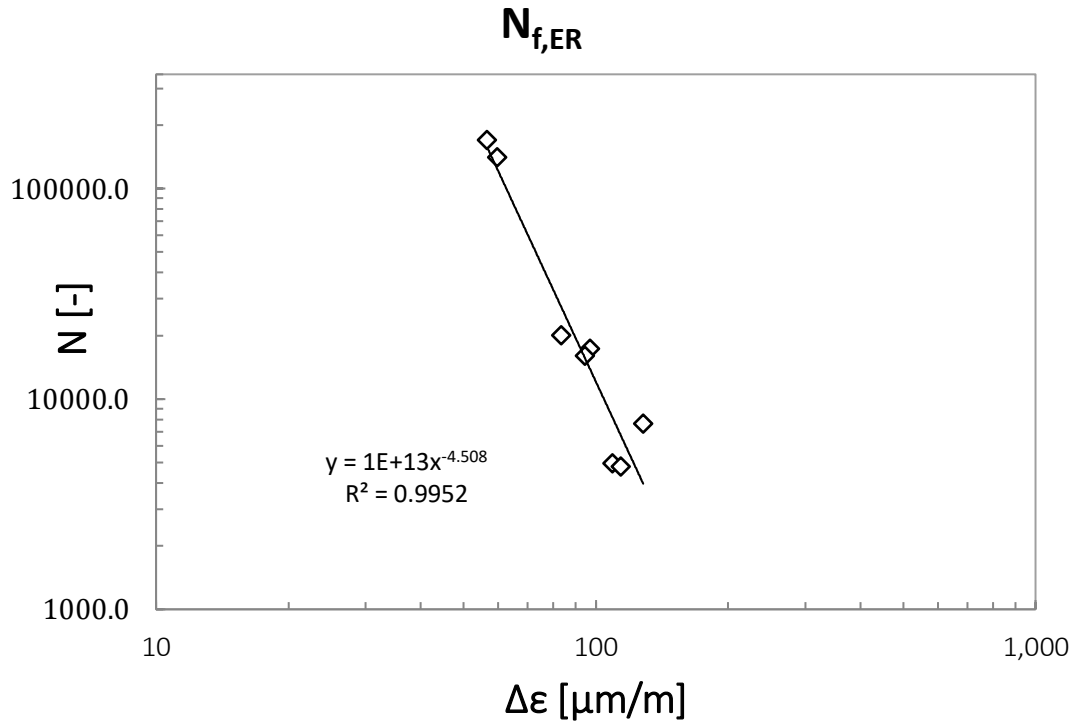

Prismatic specimens

ID	σ_0	ε_0	E_0	$N_{f,50\%}$	$N_{f,ER}$	$\log_{10} \varepsilon_0$	$\log_{10} N_{f,50\%}$	$\log_{10} N_{f,ER}$
	[MPa]	[μm/m]	[MPa]	[-]	[-]	[μm/m]	[-]	[-]
MIX50_1_ 1FP	3.438	200.2	17175	6166	35893	2.301	3.790	4.555
MIX50_1_ 2FP	2.695	160.2	16827	55805	52886	2.205	4.747	4.723
MIX50_1_ 3FP	2.389	129.3	18474	148290	149816	2.112	5.171	5.176
MIX50_1_ 4FP	2.127	129.8	16389	288404	337979	2.113	5.460	5.529
MIX50_1_ 5FP	2.023	119.7	16899	754706	713401	2.078	5.878	5.853
MIX50_1_ 6FP	2.743	159.2	17234	26710	24832	2.202	4.427	4.395
MIX50_1_ 7FP	1.968	119.9	16413	1196129	1079776	2.079	6.078	6.033
MIX50_1_ 8FP	2.379	119.9	19835	810754	743210	2.079	5.909	5.871

MIX50 1	$N_{f,50\%}$	$N_{f,ER}$
$\log_{10} k_\varepsilon$ [-]	25.870	20.402
k_ε [-]	7.42E+25	2.52E+20
n_ε [-]	-9.640	-7.052
ε_6 [μm/m]	116	116

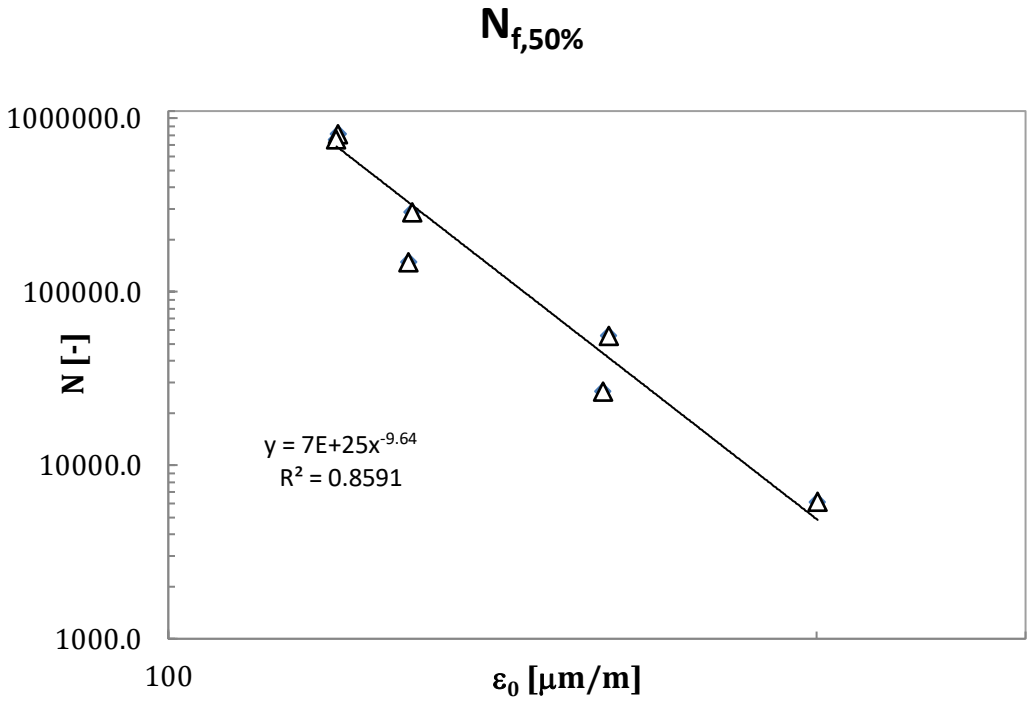
$N_{f,50\%}$
1000000.0
100000.0
10000.0
1000.0
N [-]
y = 7E+25x^-9.64
R² = 0.8591
100
ε_0 [μm/m]

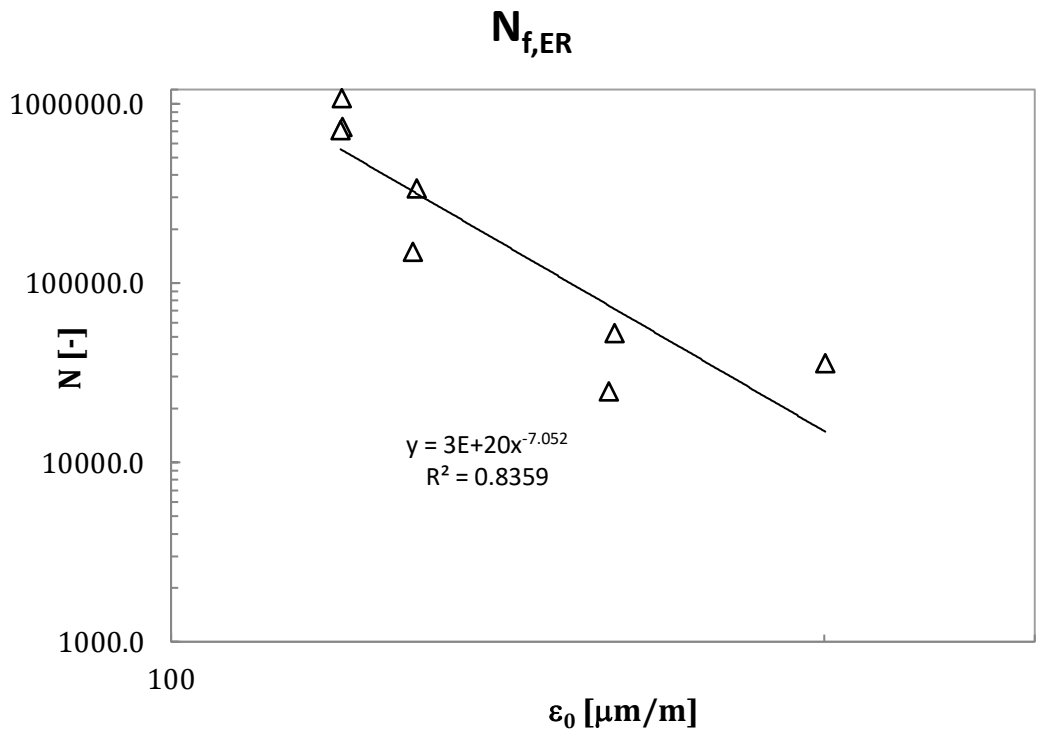
$N_{f,ER}$
1000000.0
100000.0
10000.0
1000.0
N [-]
y = 3E+20x^-7.052
R² = 0.8359
100
ε_0 [μm/m]

MIX50 2

Cylindrical specimens compacted at N_{design} (120 gyrations)

ID	E_0	σ_a	ε_a	$\Delta\varepsilon$	$N_{f,50\%}$	$N_{f,ER}$	$\log_{10}\Delta\varepsilon$	$\log_{10} N_{f,50\%}$	$\log_{10} N_{f,ER}$
	[MPa]	[MPa]	[µm/m]	[MPa]	[-]	[-]	[µm/m]	[-]	[-]
MIX50_2 1FC	18618	221	24.2	48.4	93100	75930	1.685	4.969	4.880
MIX50_2 2FC	22266	375	34.1	68.1	21910	22040	1.833	4.341	4.343
MIX50_2 3FC	20553	478	46.9	93.9	7060	7060	1.972	3.849	3.849
MIX50_2 4FC	21052	406	36.0	72.0	21800	19860	1.857	4.338	4.298
MIX50_2 5FC	22867	233	20.6	41.2	191810	136380	1.615	5.283	5.135
MIX50_2 6FC	19297	399	25.5	51.0	212520	140120	1.708	5.327	5.147
MIX50_2 7FC	15682	397	52.3	104.6	15830	12690	2.019	4.199	4.103
MIX50_2 8FC	14202	431	62.1	124.1	5800	4510	2.094	3.763	3.654
MIX50_2 9FC	16828	449	54.8	109.6	5690	4800	2.040	3.755	3.681

MIX50 2	$N_{f,50\%}$	$N_{f,ER}$
$\log_{10} k_\varepsilon$ [-]	10.815	10.482
k_ε [-]	6.53E+10	3.03E+10
n_ε [-]	-3.418	-3.284
ε_6 [µm/m]	29	25

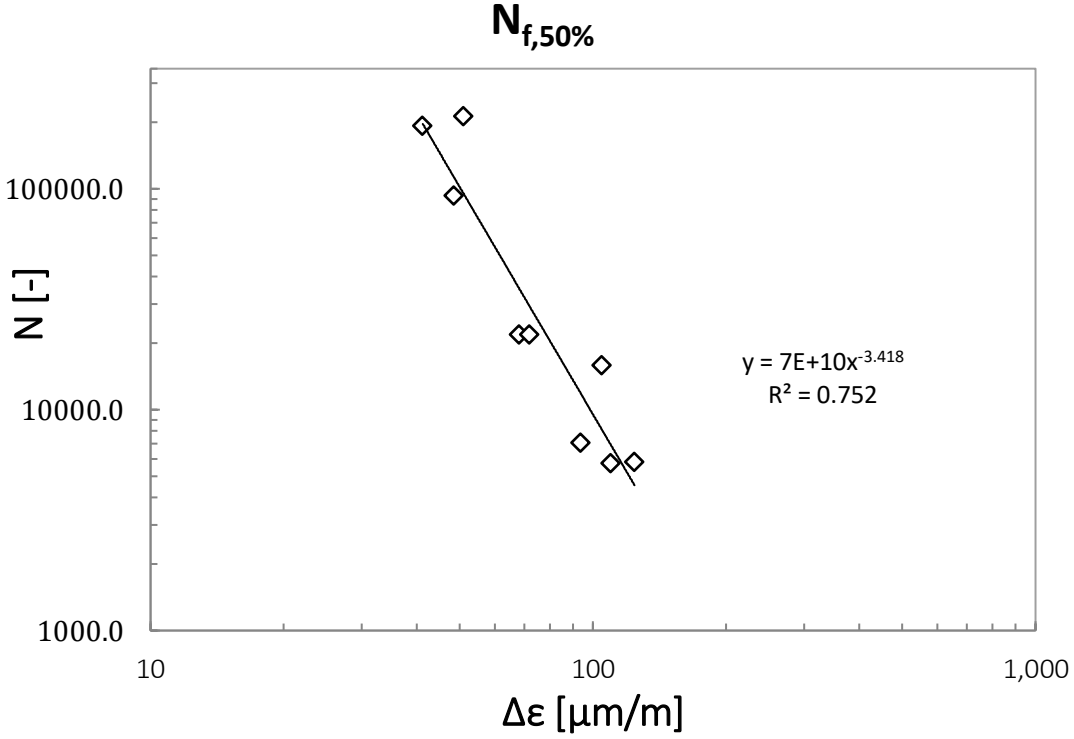

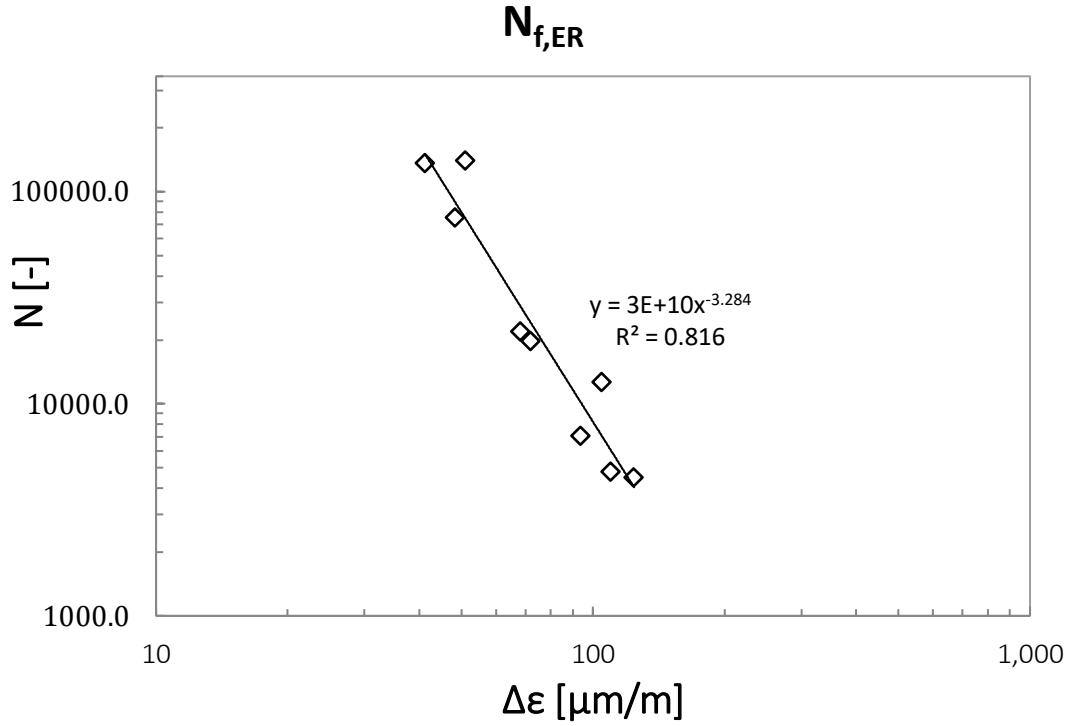

Prismatic specimens

ID	σ_0	ε_0	E_0	$N_{f,50\%}$	$N_{f,ER}$	$\log_{10} \varepsilon_0$	$\log_{10} N_{f,50\%}$	$\log_{10} N_{f,ER}$
	[MPa]	[μm/m]	[MPa]	[-]	[-]	[μm/m]	[-]	[-]
MIX50_2_ 1FP	2.575	159.7	16120	106333	91202	2.203	5.027	4.960
MIX50_2_ 2FP	2.219	159.6	13905	38019	40118	2.203	4.580	4.603
MIX50_2_ 3FP	1.661	128.4	12938	950119	959892	2.108	5.978	5.982
MIX50_2_ 4FP	1.787	129.7	13777	146031	151357	2.113	5.164	5.180
MIX50_2_ 5FP	1.860	139.8	13313	217660	225598	2.145	5.338	5.353
MIX50_2_ 6FP	2.546	180.5	14109	63096	81596	2.256	4.800	4.912
MIX50_2_ 7FP	2.391	180.7	13234	79433	117791	2.257	4.900	5.071
MIX50_2_ 8FP	1.827	139.4	13105	37874	40427	2.144	4.578	4.607

MIX50 2	$N_{f,50\%}$	$N_{f,ER}$
$\log_{10} k_\varepsilon$ [-]	16.965	15.358
k_ε [-]	9.22E+16	2.28E+15
n_ε [-]	-5.427	-4.674
ε_6 [μm/m]	124	126

$N_{f,50\%}$

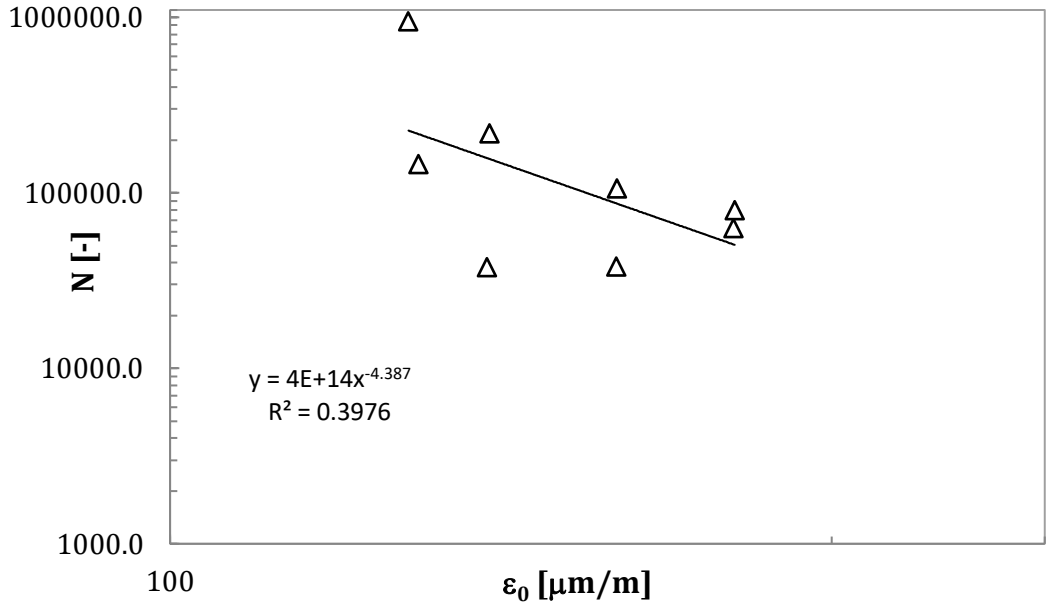
1000000.0
100000.0
10000.0
1000.0
N [-]
100
ε_0 [μm/m]
y = 4E+14x^-4.387
R² = 0.3976

$N_{f,ER}$

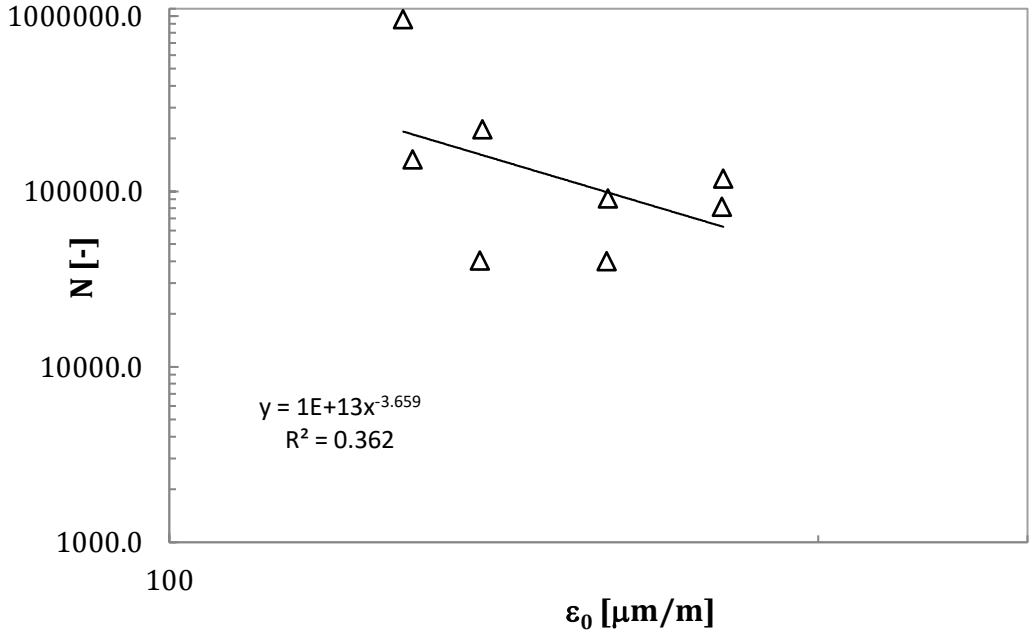
1000000.0
100000.0
10000.0
1000.0
N [-]
100
ε_0 [μm/m]
y = 1E+13x^-3.659
R² = 0.362

MIX50 3

Cylindrical specimens compacted at N_{design} (120 gyrations)

ID	E_0	σ_a	ε_a	$\Delta\varepsilon$	$N_{f,50\%}$	$N_{f,ER}$	$\log_{10}\Delta\varepsilon$	$\log_{10} N_{f,50\%}$	$\log_{10} N_{f,ER}$
	[MPa]	[MPa]	[µm/m]	[MPa]	[-]	[-]	[µm/m]	[-]	[-]
MIX50_3 1FC	26366	402	31.1	62.2	8700	8700	1.794	3.940	3.940
MIX50_3 2FC	18190	509	56.3	112.7	9170	8390	2.052	3.962	3.924
MIX50_3 3FC	28129	290	20.4	40.8	173530	135520	1.611	5.239	5.132
MIX50_3 4FC	19293	617	64.8	129.6	3910	3520	2.112	3.592	3.547
MIX50_3 5FC	18693	421	46.1	92.1	14200	12000	1.964	4.152	4.079
MIX50_3 6FC	20031	488	38.9	77.8	39550	35360	1.891	4.597	4.549
MIX50_3 7FC	26786	249	23.0	45.9	130140	118170	1.662	5.114	5.073
MIX50_3 8FC	18353	529	58.1	116.1	6250	5610	2.065	3.796	3.749
MIX50_3 9FC	25811	233	18.3	36.5	299380	303170	1.563	5.476	5.482

MIX50 3	$N_{f,50\%}$	$N_{f,ER}$
$\log_{10} k_\varepsilon$ [-]	10.489	10.451
k_ε [-]	3.08E+10	2.83E+10
n_ε [-]	-3.216	-3.222
ε_6 [µm/m]	25	25

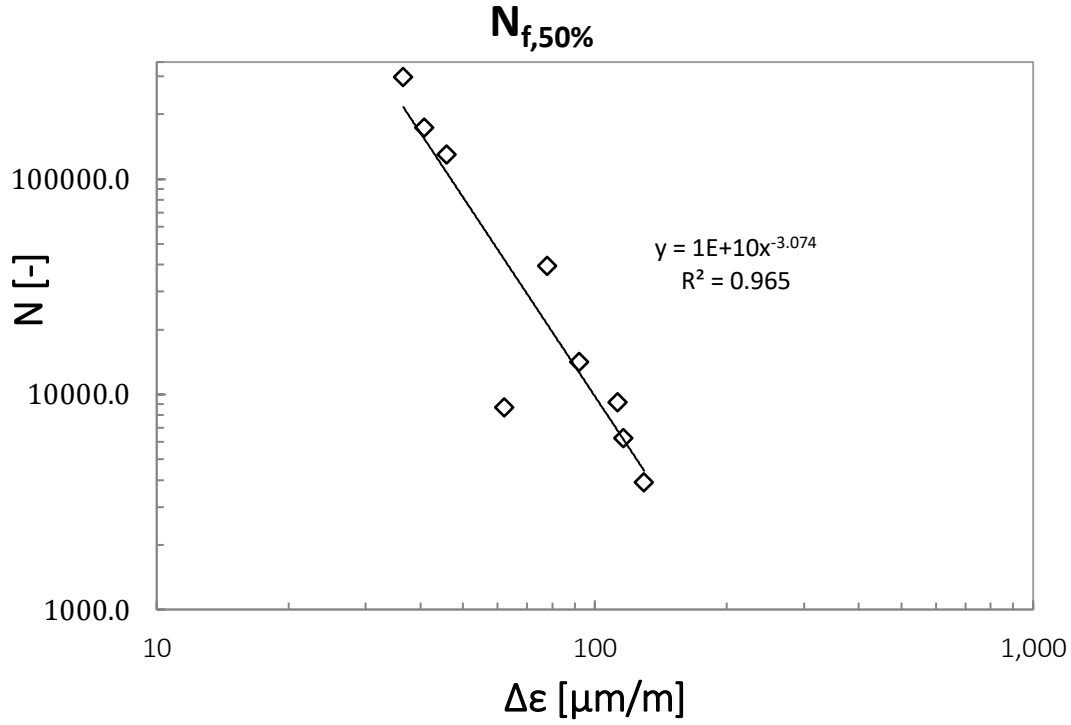

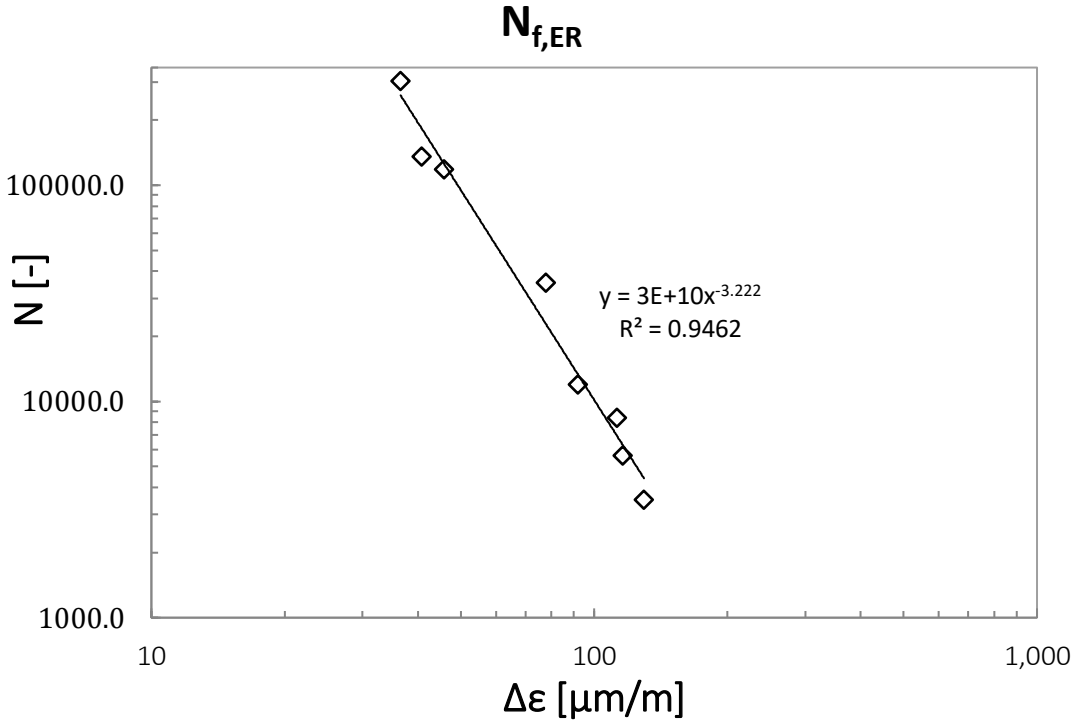

Prismatic specimens

ID	σ_0	ε_0	E_0	$N_{f,50\%}$	$N_{f,ER}$	$\log_{10} \varepsilon_0$	$\log_{10} N_{f,50\%}$	$\log_{10} N_{f,ER}$
	[MPa]	[μm/m]	[MPa]	[-]	[-]	[μm/m]	[-]	[-]
MIX50_3_ 1FP	2.349	159.6	14716	322767	146780	2.203	5.509	5.167
MIX50_3_ 2FP	2.442	159.7	15292	149816	127188	2.203	5.176	5.104
MIX50_3_ 3FP	2.352	199.4	11798	6441	2345	2.300	3.809	3.370
MIX50_3_ 4FP	3.122	183.8	16988	13387	13490	2.264	4.127	4.130
MIX50_3_ 5FP	1.590	99.8	15936	206803	414742	1.999	5.316	5.618
MIX50_3_ 6FP	2.308	145.1	15901	45709	11307	2.162	4.660	4.053
MIX50_3_ 7FP	2.042	120.2	16987	76443	368695	2.080	4.883	5.567
MIX50_3_ 8FP	2.092	119.4	17520	251189	248632	2.077	5.400	5.396

MIX50 3	$N_{f,50\%}$	$N_{f,ER}$
$\log_{10} k_\varepsilon$ [-]	13.788	19.168
k_ε [-]	6.14E+13	1.47E+19
n_ε [-]	-4.118	-6.599
ε_6 [μm/m]	108	109

$N_{f,50\%}$

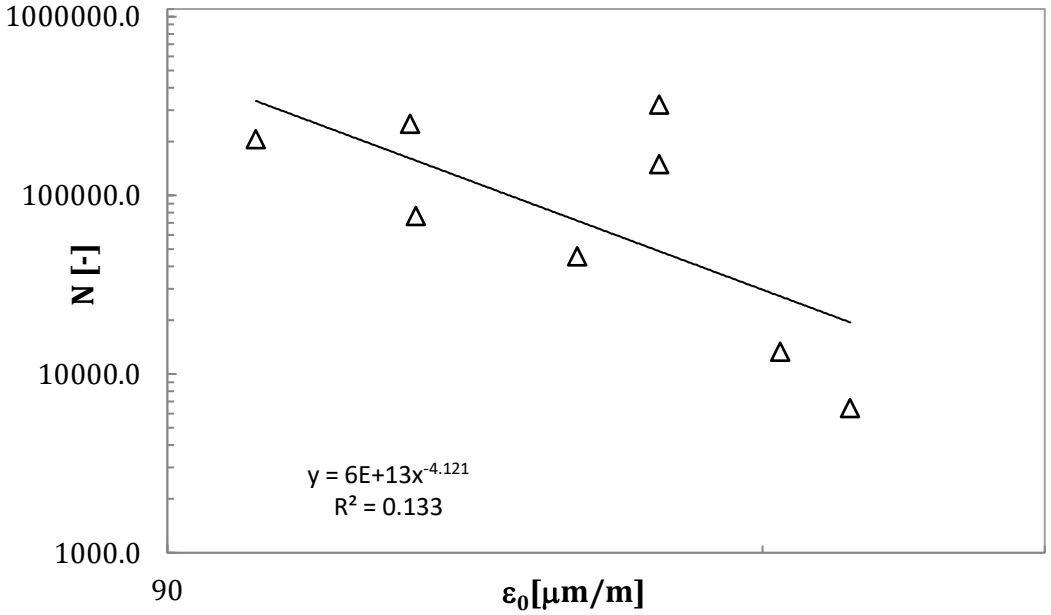
1000000.0
100000.0
10000.0
1000.0
N [-]
90
ε_0[μm/m]
y = 6E+13x^-4.121
R² = 0.133

$N_{f,ER}$

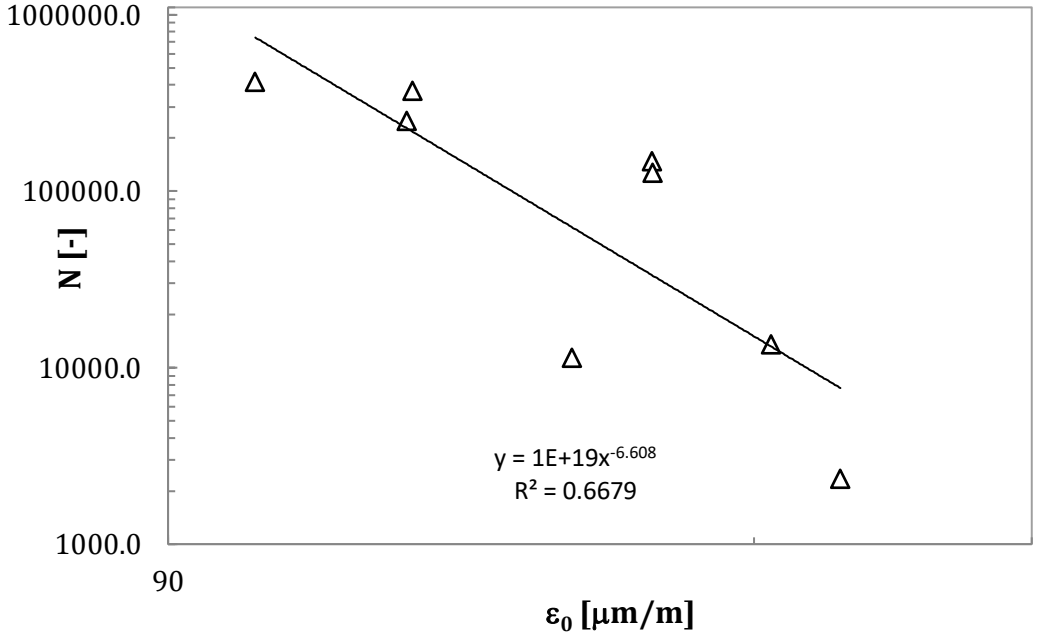
1000000.0
100000.0
10000.0
1000.0
N [-]
90
ε_0 [μm/m]
y = 1E+19x^-6.608
R² = 0.6679

MIX50 REF

Cylindrical specimens compacted at N_{design} (120 gyrations)

ID	E_0	σ_a	ε_a	$\Delta\varepsilon$	$N_{f,50\%}$	$N_{f,ER}$	$\log_{10}\Delta\varepsilon$	$\log_{10} N_{f,50\%}$	$\log_{10} N_{f,ER}$
	[MPa]	[MPa]	[µm/m]	[MPa]	[-]	[-]	[µm/m]	[-]	[-]
MIX50_REF 1FC	18998	395	42.1	84.2	9700	9700	1.925	3.987	3.987
MIX50_REF 2FC	19928	233	23.7	47.3	66740	66740	1.675	4.824	4.824
MIX50_REF 3FC	15392	494	65.2	130.5	3380	3380	2.116	3.529	3.529
MIX50_REF 5FC	14784	474	65.2	130.3	3390	3390	2.115	3.530	3.530
MIX50_REF 6FC	16356	497	61.4	122.8	3690	3690	2.089	3.567	3.567
MIX50_REF 7FC	18537	363	39.8	79.6	8760	8760	1.901	3.943	3.943
MIX50_REF 8FC	18190	381	25.9	51.8	45850	45850	1.715	4.661	4.661
MIX50_REF 9FC	14539	375	52.2	104.3	9430	9430	2.018	3.975	3.975

MIX50 REF	$N_{f,50\%}$	$N_{f,ER}$
$\log_{10} k_\varepsilon$ [-]	9.461	9.524
k_ε [-]	2.89E+09	3.34E+09
n_ε [-]	-2.808	-2.864
ε_6 [µm/m]	18	18

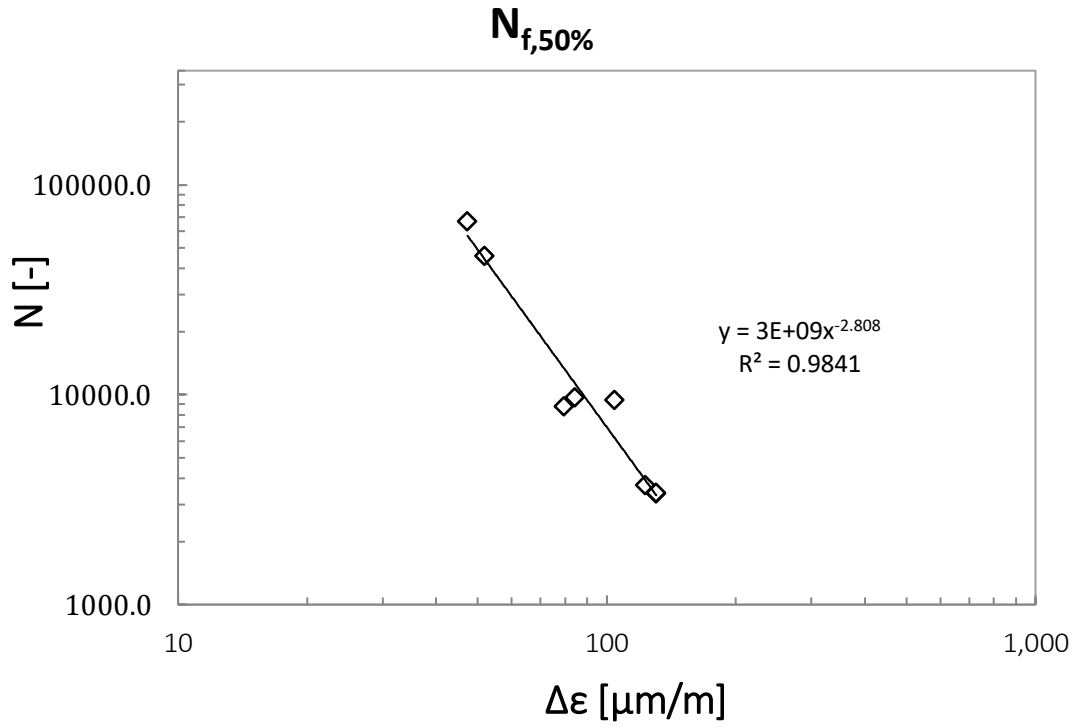

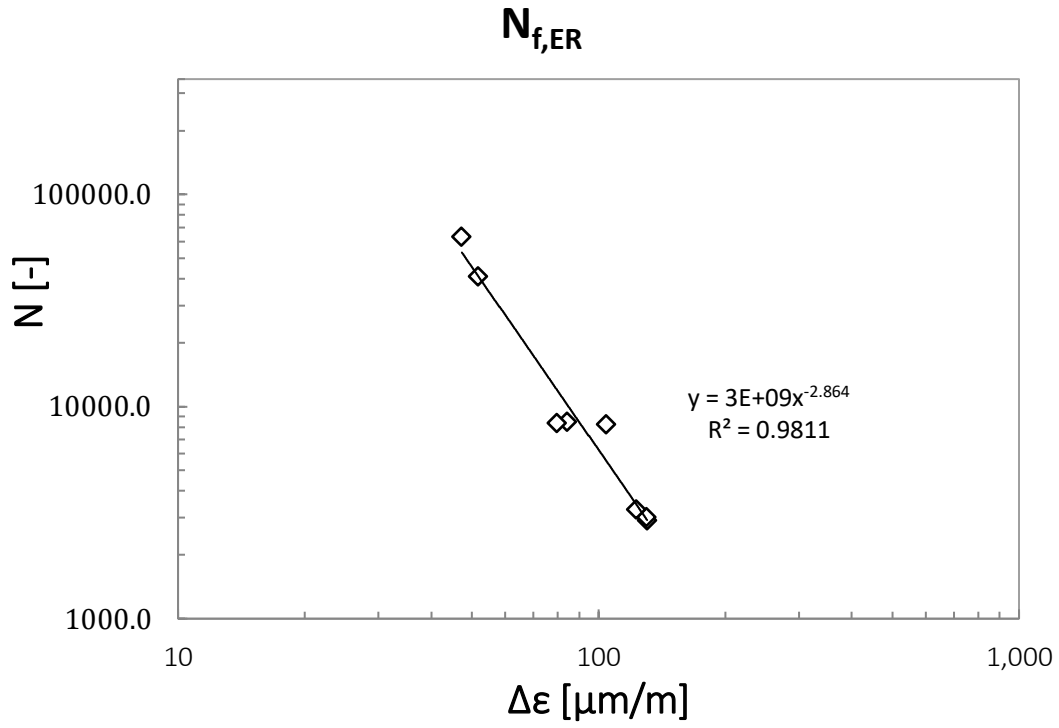

Prismatic specimens

ID	σ_0	ε_0	E_0	$N_{f,50\%}$	$N_{f,ER}$	$\log_{10} \varepsilon_0$	$\log_{10} N_{f,50\%}$	$\log_{10} N_{f,ER}$
	[MPa]	[µm/m]	[MPa]	[-]	[-]	[µm/m]	[-]	[-]
MIX50_REF_ 1FP	2.334	159.6	14623	32609	33626	2.203	4.513	4.527
MIX50_REF_ 2FP	2.618	160.2	16343	82541	84464	2.205	4.917	4.927
MIX50_REF_ 3FP	2.114	129.5	16325	339713	261685	2.112	5.531	5.418
MIX50_REF_ 4FP	1.766	99.6	17736	519465	657322	1.998	5.716	5.818
MIX50_REF_ 5FP	1.971	140.2	14062	33885	34277	2.147	4.530	4.535
MIX50_REF_ 6FP	1.582	100.0	15817	1100695	2267544	2.000	6.042	6.356
MIX50_REF_ 7FP	2.082	119.6	17402	47864	51881	2.078	4.680	4.715
MIX50_REF_ 8FP	2.643	140.1	18860	46774	47134	2.147	4.670	4.673

MIX50 REF	$N_{f,50\%}$	$N_{f,ER}$
$\log_{10} k_\varepsilon$ [-]	18.458	20.670
k_ε [-]	2.87E+18	4.67E+20
n_ε [-]	-6.298	-7.321
ε_6 [µm/m]	103	106

$N_{f,50\%}$

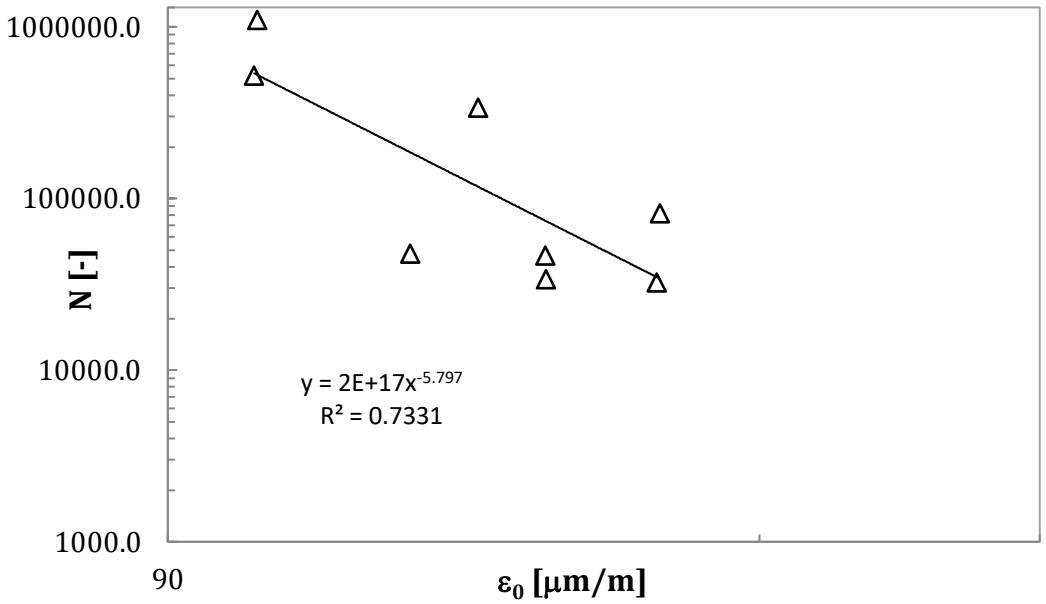
1000000.0
100000.0
10000.0
1000.0
N [-]
90
y = 2E+17x-5.797
R² = 0.7331
ε0 [μm/m]

$N_{f,ER}$

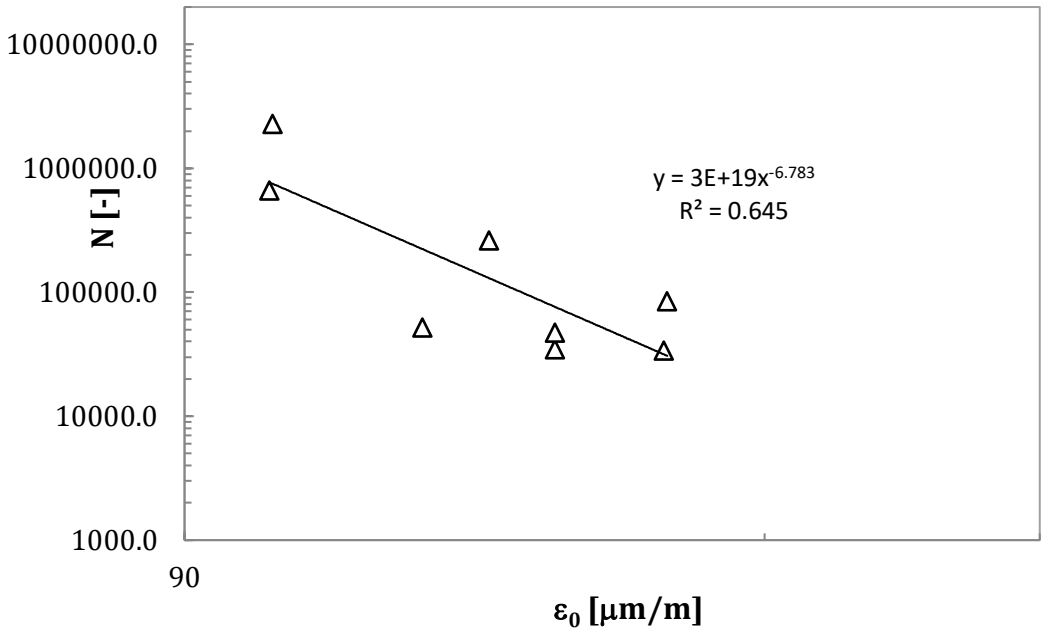
10000000.0
1000000.0
100000.0
10000.0
1000.0
N [-]
90
y = 3E+19x-6.783
R² = 0.645
ε0 [μm/m]

Desidero concludere esprimendo la mia più sincera e profonda gratitudine nei riguardi dei professori Baglieri e Dalmazzo, la cui costante e inesorabile disponibilità e dedizione verso la loro professione hanno rappresentato per me un riferimento imprescindibile. Grazie ai loro preziosi consigli, mi sono avvicinato con rinnovata curiosità a tematiche che, in un primo momento, percepivo come lontane ma che desideravo approfondire.

Un ruolo determinante nel conseguimento di questo traguardo è sicuramente quello svolto da Joseph, al quale devo molto. Persona di grande generosità, sempre pronta ad aiutare e a riporre estrema fiducia negli altri. Grazie alla sua costanza e vicinanza, non ho provato momenti di sconforto in questo percorso per me inusuale.

Infine, non posso non ringraziare il mio compagno di avventura e caro amico, Alessandro. La tua presenza ha reso leggere e piacevoli le giornate trascorse dentro il laboratorio, aiutandomi a ritrovare il sorriso in momenti non così spensierati della mia vita privata.

Un sentito grazie è rivolto anche a Davide, Enrico e Mattia che, con la loro collaborazione e simpatia, hanno contribuito ad arricchire e rendere ancor più significativa questa esperienza.

Il primo pensiero è rivolto ai miei genitori, al loro incrollabile impegno affinché questo traguardo potesse diventare realtà. Spero che questo momento di felicità possa farli sentire ripagati di tutti i sacrifici compiuti.

Ringrazio tutta la mia famiglia e, in particolare, mia nonna Ines. Nonostante i chilometri che ci separano nella quotidianità, avverto sempre la vostra vicinanza e il vostro sostegno. Siete sempre nei miei pensieri.

Parlando di famiglia, non posso non ricordare la mia seconda famiglia, quella siciliana. Ringrazio Concetta, Salvo, Gemma, nonna Dina e tutti coloro che ho avuto la fortuna di incontrare lì. Mi avete fatto sentire fin da subito parte di voi e ve ne sarò sempre grato.

Un sincero grazie lo rivolgo al mio compagno di mille avventure, Michele. Sono stato immensamente fortunato ad averti incontrato tra i banchi di scuola, e lo sono ancora di più pensando al legame che ci unisce.

Ringrazio Martina e Davide, persone di grande cuore, sempre capaci di offrire aiuto nei momenti difficili e di farti sentire parte di qualcosa di importante. Spero che questa nostra amicizia possa crescere sempre più.

Giulia e Lorenzo, avete saputo prendermi per mano in uno dei momenti più difficili della mia vita e ve ne sarò per sempre grato. Anche se non condividiamo la quotidianità, ogni volta che ci rivediamo è come se l'ultima risata insieme fosse stata ieri.

Pur essendoci persi di vista per alcuni anni delle nostre vite, ringrazio Micaela per la sua vicinanza. Sono così grato di aver ritrovato un'amicizia sincera e genuina come la nostra.

Ringrazio la mia cuginetta romana, Martina, per tutti i momenti di gioia e spensieratezza condivisi, con l'augurio che non finiscano mai.

Infine, desidero ringraziare una persona che è stata per me un punto di riferimento, capace di sostenermi nei momenti di difficoltà lungo questo percorso ma soprattutto di avermi accompagnato nella vita oltre lo studio. Nonostante le nostre vite abbiano preso purtroppo strade diverse, a tratti dolorose, vorrei dirti grazie, Enrica.

E anche se oggi è una giornata in cui sarò io a ricevere gli auguri, vorrei augurare a tutti voi di realizzare i vostri sogni e, soprattutto, di essere felici.